

Optimization of pH-Responsive Polymersomes for Enzyme Reactions

DISSERTATION

zur Erlangung des akademischen Grades

Doctor rerum naturalium

(Dr. rer. nat.)

vorgelegt

dem Bereich Mathematik und Naturwissenschaften

der Technischen Universität Dresden

von

M.Sc. Peng Wang

geboren am 7. November 1992 in Henan, VR China

Eingereicht am 23.03.2022

Die Dissertation wurde in der Zeit von 10/2017 bis 03/2022 am Leibniz-Institut für
Polymerforschung Dresden e.V. angefertigt.

“I don't measure a man's success by how high he climbs but how high he bounces when he hits bottom.”

-George S. Patton

Contents

Part I Fundamentals.....	1
1 Theoretical Background	2
1.1 Polymersomes	2
1.1.1 Polymersomes Formation.....	2
1.1.2 Self-Assembly Principles of Amphiphilic Block Copolymers (BCPs).....	5
1.1.3 Preparation Methods of Polymersomes.....	6
1.1.4 Cargo Loading in Polymersomes	8
1.2 Clustering Methods of Synthetic Vesicle.....	9
1.2.1 Host-Guest Interaction	9
1.2.2 DNA Hybridization	11
1.2.3 Copper-Free Click Chemistry	13
1.3 Stimuli-Responsive Polymersomes with Controllable Membrane Permeability	16
1.3.1 pH-Responsive Polymersomes.....	16
1.3.2 Light-Responsive Polymersomes.....	18
2 Motivation and Aim	25
Part II Experiments.....	28
3 Materials and Methods	29
3.1 Materials.....	29
3.2 Analytical Methods	32
4 Clustered pH-Responsive Polymersomes for Enzymatic Cascade Reaction.....	38
4.1 Synthetic Methods and Characterization of Block Copolymer (BCP) for Self- Assembly of Polymersomes	38
4.1.1 Synthesis of Poly(Ethylene Glycol) (PEG) Macroinitiator.....	38
4.1.2 Synthesis of Photo-Crosslinker	39
4.1.3 Synthesis of BCP with Different Terminal Groups	40
4.1.4 Synthesis of Bis-BCN Poly(ethylene glycol) Crosslinker (BisBCN-PEG)	42
4.2 Formation of Empty and Loaded Psomes-N ₃	44
4.2.1 Formation and Photo-Crosslinking of Empty-Psomes-N ₃	44
4.2.2 Preparation of Cy5 Labeled BSA (BSA-Cy5)	44
4.2.3 Preparation of RhB Labeled Myo (Myo-RhB)	44
4.2.4 Preparation of Cy5 Labeled GOx (GOx-Cy5)	45
4.2.5 Formation and Photo-Crosslinking of Loaded Psomes-N ₃	45
4.3 Preparation and Purification of Clustered Empty-Psomes-N ₃	46

4.3.1	Preparation of Clustered Empty-Psomes-N ₃ at Different Conditions	46
4.3.2	Optimized Preparation of Clustered Empty-Psomes-N ₃	49
4.3.3	Purification Method of Clustered Empty-Psomes-N ₃	49
4.3.4	DLS Measurement of the Empty-Psomes-N ₃ in the Supernatant	50
4.3.5	Quantification of Removed Psomes-N ₃ after Centrifugal Purification	50
4.4	Preparation and Purification of Clustered Enzyme-Psomes-N ₃ : Enzymatic Cascade Reaction.....	51
4.4.1	Preparation of Clustered GOx or Myo Loaded Psomes-N ₃ (GOx-Psomes-N ₃ or Myo-Psomes-N ₃)	51
4.4.2	Enzyme Activity of Myo Samples	51
4.4.3	Enzyme Activity of GOx Samples	52
4.5	Preparation and Purification of Co-Clustered Enzyme-Psomes-N ₃ : Enzymatic Cascade Reaction	52
4.5.1	Preparation of Co-Clustered Myo/GOx-Psomes-N ₃	52
4.5.2	Enzyme Activity of Co-Clustered Myo/GOx-Psomes-N ₃ Samples	53
5	Light-Driven Enzyme Reaction Based on pH-Responsive Polymersomes	54
5.1	Synthetic Methods and Characterization of Block Copolymers with Single Azobenzene Unit	54
5.1.1	Synthesis of Block Copolymer with Donor-Acceptor-Substituted Azobenzene Linkage between Hydrophilic and Hydrophobic Segments (BCP-DA-Azo)	54
5.1.2	Synthesis of Block Copolymer with Ether Substituted Azobenzene Linkage between Hydrophilic and Hydrophobic Segments (BCP-Azo).....	58
5.2	Photo-Isomerization of Macroinitiator and Block Copolymer with Azobenzene Linkage.....	62
5.2.1	Photo-Isomerization of PEG-DA-Azo Macroinitiator Based on Blue Light Irradiation or UV Irradiation	62
5.2.2	Photo-Isomerization of PEG-Azo Macroinitiator Based on Blue Light Irradiation or UV Irradiation	62
5.2.3	Photo-Isomerization of BCP-DA-Azo (-) Based on Blue Light Irradiation or UV Irradiation	62
5.2.4	Photo-Isomerization of BCP-Azo (-) Based on Blue Light Irradiation or UV Irradiation	63
5.3	Formation and Characterization of Polymersomes with Azobenzene	63
5.3.1	Self-Assembly of Polymersomes with Azobenzene	63

5.3.2	Photo-Isomerization of Psomes-DA-Azo (-) Based on Blue Light Irradiation or UV Irradiation	63
5.3.3	Photo-Isomerization of Psomes-Azo (-) Based on Blue Light Irradiation or UV Irradiation	64
5.3.4	Photo-Crosslinking of Polymersomes with Azobenzene	64
5.3.5	DLS Measurement of Photo-Crosslinked Polymersomes with Azobenzene through pH Titration.....	64
5.3.6	Photo-Stability of Polymersomes with Azobenzene	64
5.3.7	In-Situ Loaded Nile Red in Non-Photo-Crosslinked Polymersomes with Azobenzene (NR-Psomes-DA-Azo (+) or NR-Psomes-Azo (+))	65
5.3.8	In-Situ Loaded Myo in Photo-Crosslinked Polymersomes with Azobenzene (Myo-Psomes-DA-Azo (+) or Myo-Psomes-Azo (+)).....	65
5.4	Light-Induced Dye Release from Polymersomes with Azobenzene.....	65
5.4.1	Fluorescence Photobleaching of Nile Red under Blue Light or UV Irradiation ..	65
5.4.2	Nile Red Release under Blue Light or UV Irradiation.....	66
5.5	Light-Driven Enzyme Reaction Based on Polymersomes with Azobenzene	66
Part III Results and Discussions		67
6	Clustered pH-Responsive Polymersomes for Enzymatic Cascade Reaction	68
6.1	Aim and Strategy	68
6.2	Photo-Crosslinked and pH-Responsive Polymersomes	69
6.2.1	Synthesis and Characterization of Block Copolymers (BCPs)	70
6.2.2	Formation and Characterization of Polymersomes	72
6.3	Preparation and Purification of Clustered Empty-Psomes-N ₃	74
6.3.1	Key Parameters of Clustering Process	74
6.3.2	Purification Methods of Clustered Empty-Psomes-N ₃	86
6.4	Preparation and Purification of Clustered Empty-Psomes-N ₃ and Enzyme-Psomes-N ₃	90
6.4.1	Formation and Characterization of Enzyme in-Situ Loaded Psomes-N ₃ (Enzyme-Psomes-N ₃).....	90
6.4.2	Enzyme Location in Polymersomes	93
6.4.3	Deeper Characterization of Clustered Empty-Psomes-N ₃ and Clustered Enzyme-Psomes-N ₃	95
6.5	Clustered Enzyme-Psomes-N ₃ for Enzymatic Cascade Reaction	107
6.5.1	Influence of Enzyme Activity on Clustering Condition.....	107

6.5.2	Mixed Enzyme-Psomes-N ₃ for Enzymatic Cascade Reaction.....	109
6.5.3	Co-Clustered Enzyme-Psomes-N ₃ for Enzymatic Cascade Reaction	111
6.6	Summary	113
7	Light-Driven Enzyme Reaction Based on pH-Responsive Polymersomes	115
7.1	Aim and Strategy.....	115
7.2	Preparation and Characterization of Light-Responsive Polymersomes.....	117
7.2.1	Synthesis and Characterization of BCP with Different Types of Azobenzene Unit 118	
7.2.2	Self-Assembly and Photo-Crosslinking of Light-Responsive Polymersomes...	121
7.2.3	Characterization of Photo-Crosslinked Light-Responsive Polymersomes	123
7.3	Photo-Isomerization of Azobenzene Containing Polymeric Macromolecules and Vesicles	124
7.3.1	Photo-Isomerization of Azobenzene Containing PEG Macroinitiators	125
7.3.2	Photo-Isomerization of Azobenzene Containing BCPs and Polymersomes.....	127
7.4	Light-Driven Dye Release from Polymersomes with Azobenzene at Simulated Physiological Conditions.....	130
7.4.1	Characterization of In-Situ Nile Red Loaded Polymersomes	130
7.4.2	Light-Driven Dye Release from Polymersomes at Simulated Physiological Conditions	131
7.5	Light-Induced Enzyme Reaction in Polymersomes with Azobenzene at Simulated Physiological Conditions.....	134
7.5.1	Characterization of Polymersomes in-Situ Loaded Myoglobin.....	134
7.5.2	Light-Induced Enzyme Reaction in Polymersomes at Simulated Physiological Conditions	135
7.6	Summary	137
8	Conclusion and Outlook.....	139
	Reference.....	148
	List of Figures	158
	List of Tables.....	170
	List of Abbreviations and Symbols.....	171
	Appendix	175
	Acknowledgements	199
	Versicherung	201

Part I Fundamentals

1 Theoretical Background

1.1 Polymersomes

Polymersomes are hollow vesicles with an aqueous lumen surrounded by a bilayer polymer membrane, fabricated by self-assembly of amphiphilic block copolymers (BCPs).¹⁻⁴ The BCPs are highly versatile and the polymersomes display colloidal stability in the specific physiological ionic strength.^{5,6} Due to the high molecular weight of BCPs, the thick and tough membrane endow the polymersomes with high retention even for small molecules.³ However, effective delivery of cargos necessitates careful design of polymersomes.⁷⁻¹² One of the most commonly approach is to insert or encapsulate stimulus-responsive fragment into the amphiphilic block copolymers or polymersomes to response internal or external stimuli (such as light, pH, redox, magnetic field, and temperature) to achieve on-demand release of cargos through regulating the membrane permeability of polymersomes.¹³⁻³³ In addition, polymersomes show prominent advantages in loading gene, drug, protein, enzyme, and nanoparticles.³⁴⁻⁴⁰ The controllable membrane permeability, the loading capacity of the cavity, significant biocompatibility, high colloidal stability as well as easy functional modification have enabled polymersomes as artificial organelles to simulate biological behaviors such as drug release, gene expression, and enzyme reaction.

1.1.1 Polymersomes Formation

Synthetic Methods of Amphiphilic Block Copolymers (BCPs)

Firstly, the formation of polymersomes needs the fabrication of amphiphilic BCPs possessing hydrophilic and hydrophobic segments. The amphiphilic BCPs can self-assemble into multiple morphologies in solution, like spherical micelles, rods, and vesicles (polymersomes). There is a crucial ingredient in the self-assembly process: the block ratio between the hydrophilic and hydrophobic segment. Moreover, the structure, molecular weight and polarity of BCPs are also important factors which effects their size and morphology.

For this reason, well-defined BCPs with relatively low dispersity (\mathcal{D}) is required to obtain the desired size and morphology. Herein, controllable polymerization technique, like controlled radical polymerization (CRP), is a promising way to achieve the aims.^{41,42} So far, atom transfer radical polymerization (ATRP) and reversible addition-fragmentation chain transfer (RAFT)

polymerization are most popular polymerization techniques in the synthesis of amphiphilic BCPs.

Atom Transfer Radical Polymerization (ATRP)

ATRP is mechanistically related to transition metal mediated atom transfer radical addition reactions and indeed this relationship was the reason this transition metal mediated controlled radical polymerization process was named ATRP.^{43, 44} Nowadays, ATRP as among the most effective and most widely used methods of CRP shows promising prospective in designing well-defined polymeric materials.⁴⁵⁻⁴⁷ Many polymers can be synthesized by ATRP in a controlled method, for examples, polystyrene, polyacrylate, polymethacrylate, polyacrylonitrile, et.al.⁴⁸⁻⁵¹

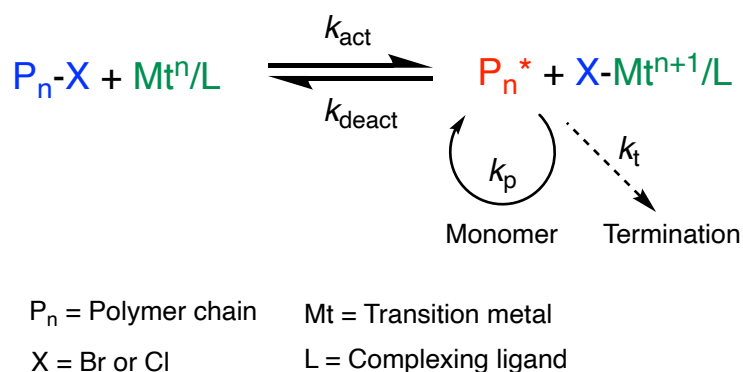


Figure 1.1 The mechanism of the transition metal catalyzed ATRP. The active radicals form at a rate constant of activation (k_{act}), subsequently propagate with a rate constant (k_p) and reversibly deactivate (k_{deact}), but also terminate (k_t).⁴³ (Reproduced with permission from ref. 43. Copyright (2001) American Chemical Society).

Generally, there are 3 indispensable components in the ATRP process including initiator, transition metal complexes and ligands. (i) Alkane-halides (R-X , X = chloride or bromide) as most common initiator molecules are because the substituents around the atom containing halogen play an important role at which stabilizing the initiating radicals (R^\cdot).⁵² (ii) In addition, the transition metal complexes, such as iron, ruthenium, palladium, molybdenum, etc., as catalyst in ATRP process.⁵³⁻⁵⁶ Among them, copper-halides are the most common catalyst in the ATRP system.^{57, 58} (iii) The primary roles of the ligand in an ATRP catalyst complex are to solubilize the transition metal salts in the polymerization medium and to adjust the redox potential of the metal center to provide appropriate activity and dynamics for the repetitive halogen exchange reaction.⁵⁹ So far, many ligands based on above principle have been

developed to improve the solubility, selectivity and reactivity of those catalysts, such as 2,2'-bipyridines, aliphatic amines or phosphines.⁵⁹⁻⁶² As shown in Figure 1.1, the essential characteristic of ATRP is the equilibrium between propagating radicals and dormant species, predominately in the form of initiating alkyl halides/macromolecular species (P_n-X).⁴³

Reversible Addition-Fragmentation Chain Transfer (RAFT) Polymerization

Unlike ATRP, RAFT polymerization has grown into one of the most versatile and powerful polymerization techniques due to its excellent compatibility with extensive range of monomers even including functional monomers containing acid and amino groups.⁶³⁻⁶⁶ RAFT polymerization enables the synthesis of polymeric architectures exhibiting predictable molecular weight, low molar mass dispersity (\mathcal{D}), high end-group fidelity, and capacity for continued chain growth.⁶⁷

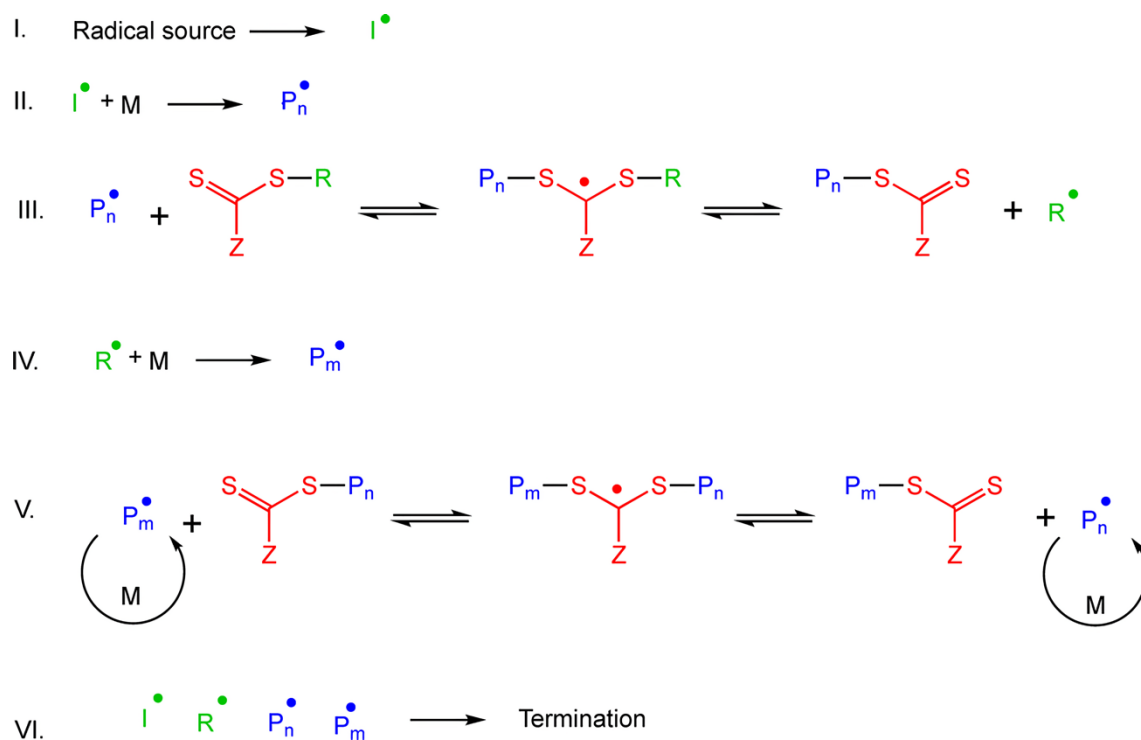


Figure 1.2 General mechanism of the RAFT polymerization.⁶³ (Reproduced with permission from ref. 63. Copyright (2017) American Chemical Society).

The RAFT mechanism is depicted in Figure 1.2. Following activation (Step I), the propagating radical (Step II) add to the RAFT agent (chain transfer agent, CTA) to enter equilibrium between active and dormant species (Steps III and V). The chain transfers steps that form the basis of the RAFT mechanism are degenerate as they involve a reversible transfer of the

functional chain end-group (typically a thiocarbonylthio group, Z-C(=S)S-R) between the dormant chains macroCTA) and the propagating radicals. In an effective process, the rate of the rate of addition/fragmentation equilibrium is higher than that of the propagation, so there should be less than one monomer unit added per activation cycle; therefore, all chains will have a similar degree of polymerization at a given time. The overall process is comprised of the insertion of monomers between the R- and Z-C(=S)S-groups of a RAFT agent, which form the α and ω end-group of the majority of the resulting polymeric chains. Once the polymerization is complete or stopped, most of the chains retain the thiocarbonylthio end-group and can be separated as stable polymer.

1.1.2 Self-Assembly Principles of Amphiphilic Block Copolymers (BCPs)

In general, self-assembly of amphiphilic BCPs is dependent on the block ratio between hydrophilic and hydrophobic segments and their relative size, which leads to various morphologies like spherical and cylindrical micelles or vesicular structures are formed preferably.

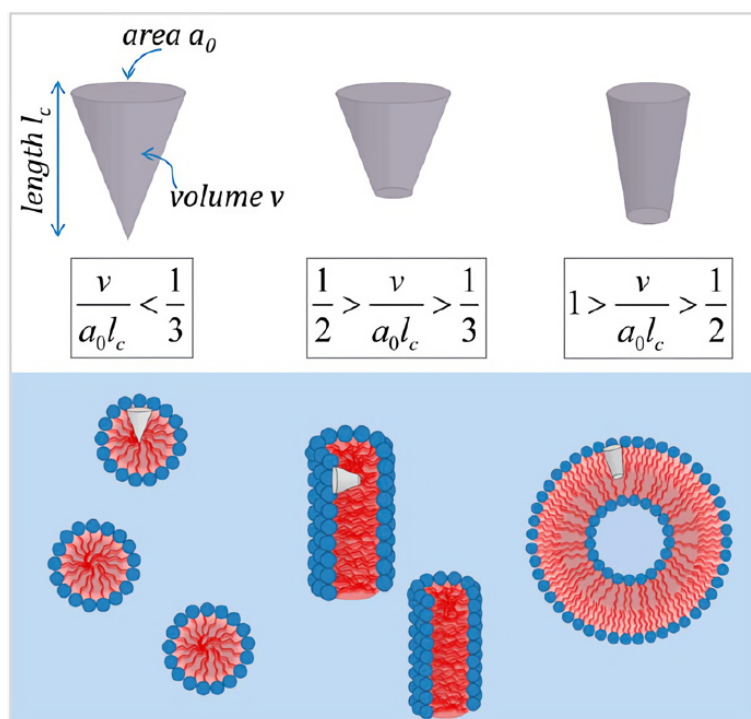


Figure 1.3 The critical packing parameter P_c and the resulting morphologies of self-assembled amphiphilic BCPs. v : volume of the hydrophobic chain; a_0 : area occupied by the hydrophilic headgroup; l_c : length of the molecule.⁶⁸ (Reproduced with permission from ref. 68. Copyright (2015) American Chemical Society).

The self-assembled morphologies of the amphiphilic BCPs can be predicted by the critical packing parameter (P_c) which is defined as $P_c = v/a_0l_c$ as shown in Figure 1.3.^{68,69} For example, the spherical micelles ($P_c < 1/3$) and worm-like micelles ($1/3 < P_c < 1/2$) occur when the P_c value is below 0.5. However, when the P_c value is close to 1 ($1/2 < P_c < 1$), polymersomes with bilayer membrane is favored. Due to the packing parameter (P_c) is fully based on geometrical consideration, it is not enough to explain the self-assembly behaviors of amphiphilic BCPs. Besides, the system's free energy, including the entropy loss during the self-assembly process and the interfacial energy of the hydrophobic-hydrophilic interface as enthalpic contribution, plays an important role in the vesicular and micellar formation.

Hence, another parameter as the hydrophilic weight fraction (f) is also used to predict the expected morphology of self-assembled structures.⁴ It is observed that polymeric vesicles (polymersomes) form at $f = 10-40\%$ in most cases. Amphiphilic BCPs with $f = 55-70\%$ can be expected to self-assemble the spherical micelles, however, cylindrical micelles are predominantly formed at $f = 45-55\%$. Although these above-mentioned parameters can to some extent be translated to the self-assembly behavior of BCPs, the resulting structure can also be determined by other factors, such as the preparation method, the concentration of amphiphilic BCPs, temperature, the property of solvent, ratio of organic solvent/water, etc.

1.1.3 Preparation Methods of Polymersomes

There are some techniques to prepare the polymersomes, such as solvent inversion, film rehydration, electroformation, direct dissolution and stimuli-induced assembly method which is indeed utilized in this study. In fact, the selection of appropriate preparation method is mainly dominated by the composition of BCPs and the desired application. It is worthy mentioned that the preparation strategy of polymersomes carries significant impact on the resulting size of polymersomes from nanometer to micrometer scale. Herein, there are four main preparation methods are simplified introduced as below.

For solvent inversion the whole BCPs need to be dissolved completely in a relatively small volume of organic solvent such as THF, chloroform, DCM or ethanol.⁷⁰⁻⁷² The organic solvent should be miscible with water in any ratio without forcing phase separation between the solvents. Subsequently, the hydration can be done by either slowly adding water to the organic polymer solution or by injecting the organic solution into water under vigorous stirring. This procedure renders the hydrophobic blocks insoluble, triggering copolymer self-assembly into

polymersomes as a result of increasing interfacial tension between the hydrophobic blocks and water. Finally, the pure polymersomes solution are obtained after removing the organic solvent by dialysis against water or ultrafiltration. However, the use of organic solvent not only bring some drawbacks, for example, the morphology change of the resulting self-assembled structures during the prolonged dialysis period, but also restricts the application of polymersomes in the biological field.⁷³

For film rehydration the amphiphilic BCPs are first dissolved in an organic solvent and slowly evaporation of the organic solvent to form a thin film on a solid surface.⁷⁴⁻⁷⁶ Next, the film is hydrated by the addition of aqueous solution to form the polymersomes. The steps in the formation of polymersomes by the hydration procedure are water permeation through defects in the polymer layers driven by hydration forces, inflation of polymer layers and formation of bulges, which finally yield vesicles upon separation from the surface. In contrast to solvent inversion, this method combines with an extrusion step to obtain polymersomes with a narrow size distribution.

For electroformation, similar to the film hydration method, the BCPs should be deposited on the electrodes, followed by a rehydration step in the presence of an alternating current.⁷⁷ The vesicles eventually detach from the surface to yield micrometer-sized giant polymersomes. The device needs a wire electrode setup and compatibility only to the self-assembly of low molecular weight BCPs restrict the development and application of electroformation technique.

For the direct dissolution method, the amphiphilic BCPs directly self-assemble in water or aqueous buffer solutions under vigorous stirring without any organic solvents.⁹ The aqueous environment without any organic solvents for self-assembly of BCPs provides a variety of possibilities for further biological application. Besides, stimuli-induced assembly method affords the possibility to form polymersomes without any organic solvents. Until now, various stimuli-responsive polymersomes have been successful prepared by the self-assembly of BCPs that bear stimuli-responsive side chains in pure water. Upon exposure to an external stimulus (e.g. pH, light or temperature) these BCPs can typically undergo some conformational or chemical changes that cause an non-equilibrium state between the hydrophobic and hydrophilic segments which subsequently initiates the self-assembly process of polymersomes.^{29, 78-83} Among all the stimuli-responsive polymersomes, undoubtedly, pH-responsive polymersomes are the easiest to prepare since the self-assembly process is driven by the pH change of the aqueous solution. The pH-sensitive groups, such as 2-(diisopropylamino)ethyl methacrylate

(DPAEMA), 2-(diethylamino)ethyl methacrylate (DEAEMA) and 2-(dimethylamino)ethyl methacrylate (DMAEMA), enable the direct dissolution of the BCPs in an acidic solution by means of protonation.^{80, 84, 85} And then, the self-assembly process is triggered by increasing the pH to basic value by means of deprotonation of the amino groups. In this thesis, all the pH-responsive polymersomes are prepared through the direct dissolution method.

1.1.4 Cargo Loading in Polymersomes

Polymersomes as artificial organelles play an essential role in cargo encapsulation and delivery. Benefit from the inherent structure, polymersomes are ideal nanocarriers to load the hydrophilic molecules in their aqueous lumen and the hydrophobic molecules in the bilayer membrane, in principle. Besides, the synthetic polymer chemistry provides flexible structure design which enables to prepare adjustable membrane permeability through stimuli-responsive segments and selective recognition by integrating functional groups before or after the polymersome formation. In this part, two conventional routes used for cargo encapsulation are described as below.

Cargo Loading During Polymersomes Formation (in-Situ Loading)

As the name suggests, in-situ loading means both BCPs and cargos are mixed in the same solvent, following the self-assembly process was performed through above-mentioned preparation methods. For organic solvent-assisted method, the cargo should be soluble and stable in the corresponding organic solvent, which limits the applications of specific cargos. For example, the bioactive molecules like protein and enzyme cannot be employed in this method. However, the direct dissolution method is the mostly common method to encapsulate the bioactive molecules in polymersomes by in-situ loading, owing to the friendly environment without any organic solvent. For this method, the BCPs are mostly stimuli-responsive, especially pH-responsive. Apart from that, polymerization-induced self-assembly in aqueous solution is another approach to in-situ load cargos.

Cargo Loading After Polymersomes Formation (Post Loading)

Inspired by the endocytic behavior in the nature, cargo can be encapsulated or uptaken after polymersomes formation. The cargo can conjugate with the functional groups of polymersome surface or pass across the membrane pores of polymersomes assisted with specific stimulating

factors or channel proteins. Finally, after closing the membrane the cargos could be located in the lumen or on the membrane of polymersomes.

1.2 Clustering Methods of Synthetic Vesicle

In cell, it is well known that compartmentalization is an essential prerequisite for carrying out its cell functions, but the distance between these bio-compartments is equally critical for a successful communication, signalling or transferring biomolecules.⁸⁶⁻⁸⁸ Significant efforts have been made to mimic nature's designs and develop nano-compartments where specific enzymatic reactions take place providing spatiotemporal control on demand.^{89, 90} A promising biomimetic approach that embraces compartmentalization and narrows the distances between synthetic nano-compartments is the self-organization by achieving network/cluster with a controlled spatial topology and activity. Therefore, self-assembly of artificial synthetic vesicles to clusters or aggregates through interconnection as bionic way is a potential route to establish artificial intelligent biological systems for emergent properties.^{89, 91, 92} Compared with simple blending of nanoreactors with different functions, assembly into clusters or aggregates could not only make the visualization easier, but also potentially mimic the cellular biological processes such as coagulation process and intercellular signaling due to the orthogonal spatial structure. A variety of bridging methods including host-guest interaction, DNA double-strand hybridization and click chemistry, have been used to assemble synthetic vesicles into large-scale aggregates and controlled clusters as below.⁹¹⁻⁹⁴

1.2.1 Host-Guest Interaction

Among the various supramolecular non-covalent interactions, host-guest interaction describes complexes that are composed of two molecules or materials that are held together in unique shape using complementary relationships by forces other than those of full covalent bonds.⁹⁵ Host-guest chemistry encompasses the idea of molecular recognition and interactions through non-covalent bonding and exhibits outstanding properties arising from the introduction of macrocyclic hosts. Therefore, host-guest interactions attracted the attention of many researchers and have been widely used for designing self-healable materials and drug delivery systems.

In terms of hosts, the well-defined shape is most often achieved by introducing one or more cyclic constraints (e.g. cyclodextrin, crown ethers, pillarenes and calixarenes) into the molecule, so that the surface of host moleculars can be created to act as “artificial receptors” and at least

partially encompass small guest molecules such as drugs and cations.⁹⁶⁻¹⁰⁰ The binding affinities of host-guest complexes can be modulated by external stimuli including pH, temperature, light, redox and the number of binding sites, etc.¹⁰¹⁻¹⁰⁵

Among numerous host molecules, particularly, cyclodextrins has excellent performance in the many research fields due to their chemical stability, water solubility, biocompatibility and biodegradability.¹⁰⁶ Cyclodextrins are categorized into 3 types: α -, β -, and γ -cyclodextrins. Depending on the shape and size of the guest molecule, different types of cyclodextrins are selected. Cyclodextrins exhibit hollow cylindrical structures with a hydrophobic interior cavity and a hydrophilic exterior. They have a strong host-guest affinity with a variety of lipophilic compounds driven by hydrophobic and Van der Waals interactions, forming inclusion complexes in aqueous solution.^{107, 108} Compared to other host molecules, cyclodextrins can be simply obtained since they are already produced in the industry on a large scale.

Hence, the first example of clustered polymersomes based on host-guest interactions is derived from the host-guest binding between β -cyclodextrin and azobenzene, which exhibits light-responsive reversible clustering and disassembly behavior.⁹²

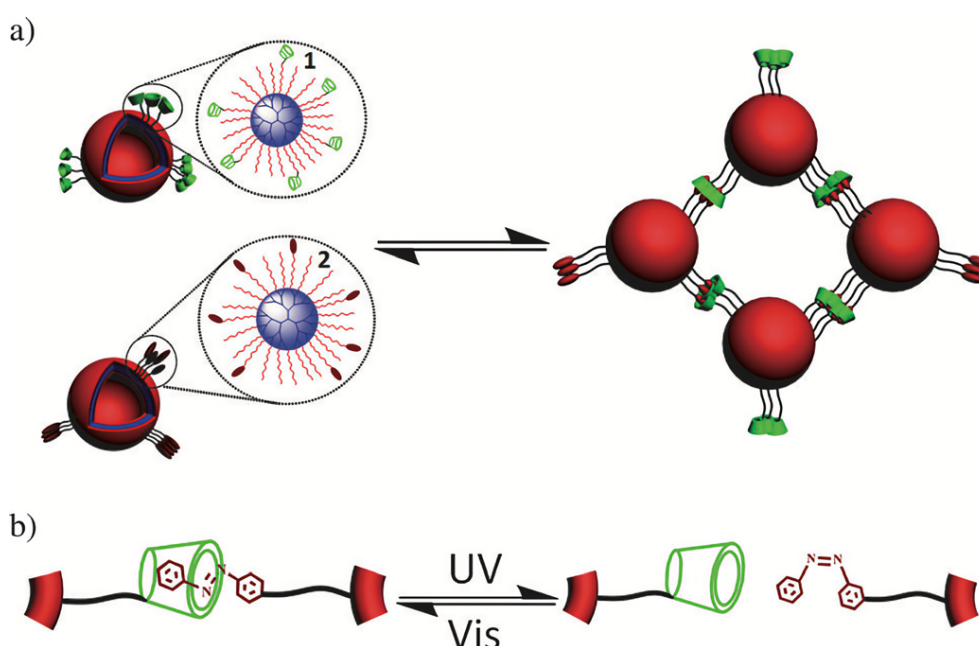


Figure 1.4 (a) Reversible aggregation of polymeric vesicles self-assembly by amphiphilic hyperbranched multiarm copolymers. (b) Light-responsive host-guest recognition between β -cyclodextrin and azobenzene that triggers the aggregation.⁹² (Reproduced with permission from ref. 92. Copyright (2011) John Wiley and Sons)

As shown in Figure 1.4, Zhou et al. used polymeric vesicles as the building blocks (one functionalized with β -cyclodextrin and the other with azobenzene) to coassemble large-scale macroscopic aggregates to stimulate cell aggregation behavior. Azobenzene under trans-state can be specifically encompassed by β -cyclodextrin with strong binding affinity, however, folded azobenzene under cis-state will detach from the β -cyclodextrin cavity as the occupied space becomes larger.

Due to the photoisomerization of azobenzene moiety, the polymeric vesicles achieved photo-responsive aggregation under visible light irradiation and disassembly behavior under UV light irradiation. Moreover, the vesicle aggregates are stable for at least half a year, which also proves the strong binding affinity and stability of β -cyclodextrin-azobenzene interactions. Besides, Zhou et al. also successfully achieved vesicle aggregation through β -cyclodextrin-adamantane interactions although vesicle fusion frequently happened.⁹³ Non-covalent interactions lead to fast and uncontrollable aggregation, however, controlled aggregation is an ideal way to mimic organelles to perform intracellular behaviors.

1.2.2 DNA Hybridization

DNA as a double-stranded molecule which has two strands bind to one another in a complementary fashion by a process called hybridization. Hybridization is a basic property of nucleotide sequences and takes advantage of numerous molecular biology techniques. Among all molecular moieties used for self-organization of nano-objects, DNA is considered as one of the most powerful tools that favors highly regulated and complex structures including superlattices, colloidal molecules, asymmetric nanoclusters and chiral nanostructures.¹⁰⁹⁻¹¹⁶ The advantages of DNA arise from its remarkable inherent molecular recognition, feasible structural design by software, and forming rigid structure when hybridization takes place.¹¹⁷⁻¹¹⁹

Palivan et al. employed DNA double strands to self-organize polymersomes separately modified with single stranded DNA (ssDNA) and complementary ssDNA for mimicking the connection of natural organelles (Figure 1.5).⁹¹ The spatial distance between tethered polymersomes can be fine-tuned through manipulating the length of single stranded DNA on the polymersomes and exploiting the rigid nature of double-stranded DNA. Moreover, no fusion and aggregation happened in the DNA hybridization process.

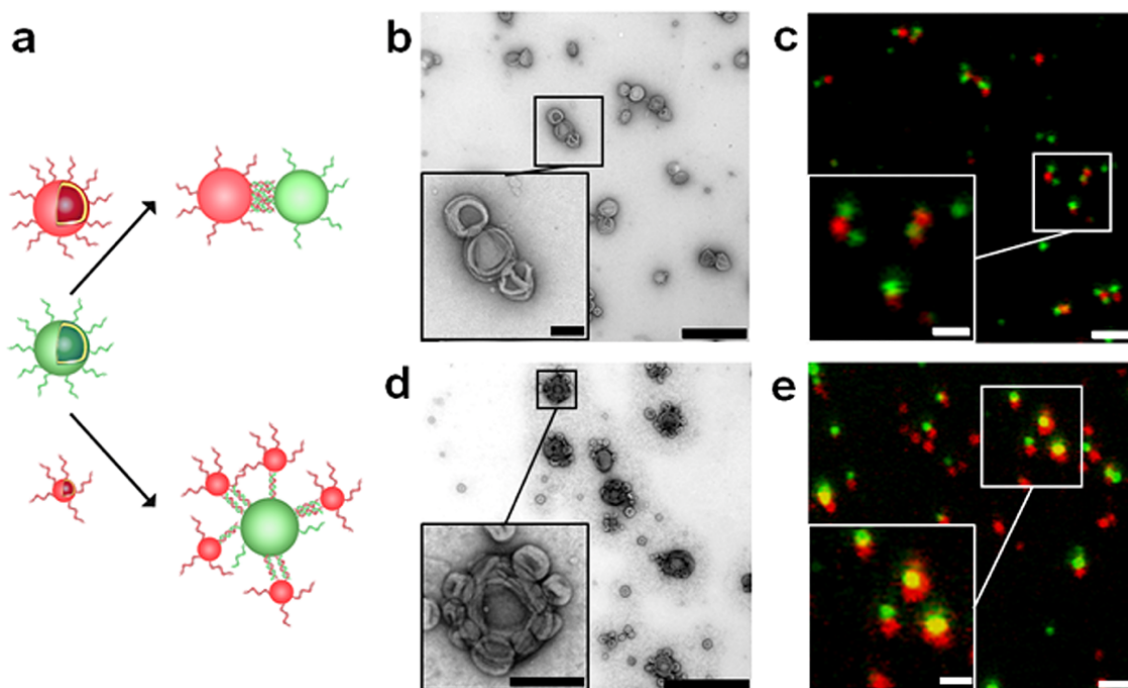


Figure 1.5 Self-organization of complementary ssDNA-polymersomes. (a) Schematic representation of distinct spatial topology resulting from mixing differently sized complementary ssDNA-polymersomes. TEM and CLSM micrographs of chain-like (b, c) and satellite-like polymersome clusters (d, e). The scale bar for TEM micrographs is 1000 and 200 nm in the inset; in CLSM micrographs it is 2000 and 1000 nm in the inset.⁹¹ (Reproduced with permission from ref. 91. Copyright (2016) American Chemical Society).

To further translate DNA hybridization on the self-organization of artificial organelles, Palivan et al. constructed individual catalytic nanocompartments by conjugating complementary DNA strands to the polymersomes' surface (Figure 1.6).⁸⁹ By encapsulating glucose oxidase (GOx) and lactoperoxidase (LPO) within different polymersomes and/or attaching amyloglucosidase (AMG) to their surface, man-made cascade reaction was designed and applied. Furthermore, residual DNA single strands that were not engaged in clustering process but acted as ligands to interact with cell surface receptors and were used to decorate the cell surface with clusters endowed the cells with a nonnative enzymatic cascade. Owing to the close proximity and structure stability of catalytic nanocompartments, the cascade reaction between spatially segregated enzymes was significantly more efficient than when the catalytic nanocompartments were not interconnected by DNA duplexes.

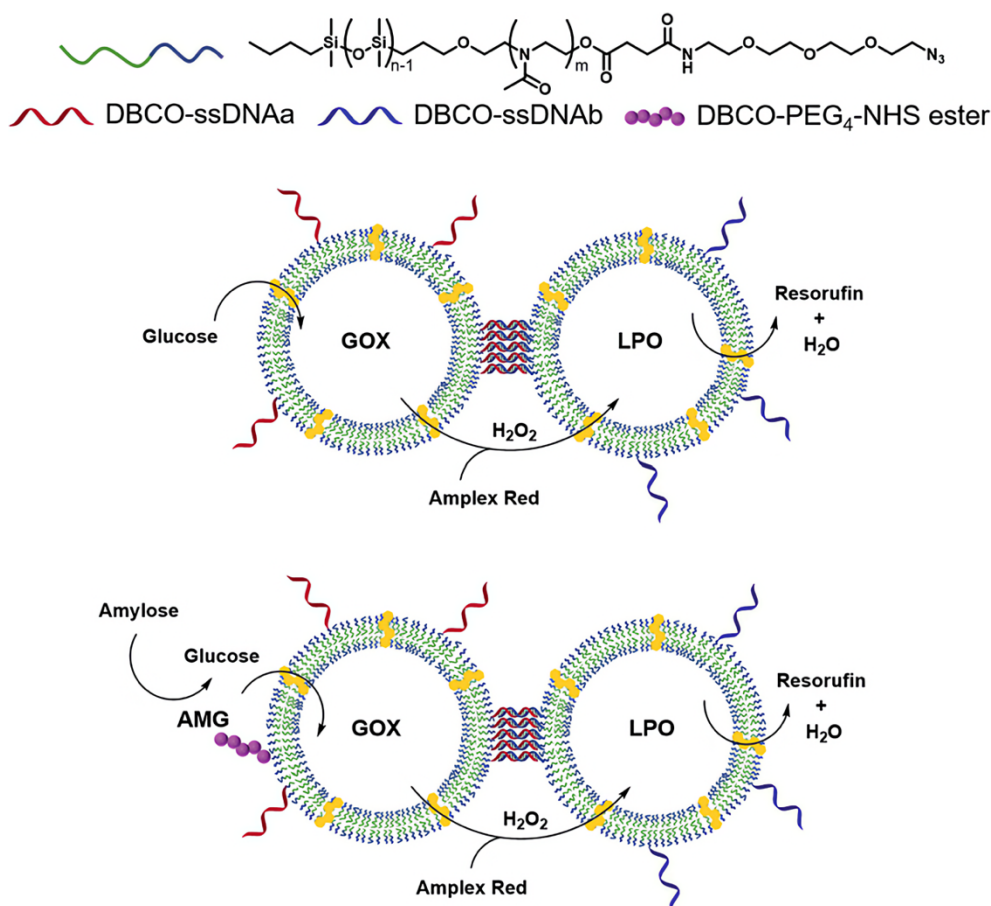


Figure 1.6 Concepts of a GOx-LPO cascade between two clustered catalytic nanocompartments, tethered via complementary single stranded DNA, in order to facilitate the diffusion of H₂O₂ and thus improve the overall reaction efficiency. Similarly, an AMG-GOx-LPO cascade achieves an improved diffusion of the glucose derived from amylose, and the enzyme on the surface allows the access to bulky substrates that would otherwise be out of reach for encapsulated enzymes.⁸⁹ (Reproduced with permission from ref. 89. Copyright (2021) Royal Society of Chemistry).

1.2.3 Copper-Free Click Chemistry

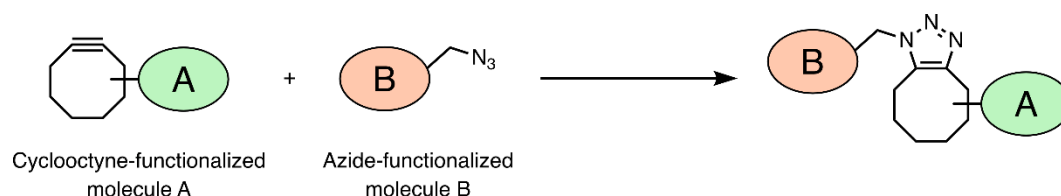


Figure 1.7 Schematic overview of SPAAC reaction.¹²⁰ (Reproduced with permission from ref. 120. Copyright (2004) American Chemical Society).

The term "click chemistry" was coined in 1998 and fully described in 2001 by K. Barry Sharpless, which describe reactions that are high yielding, wide in scope, create only byproducts that can be removed without chromatography, are stereospecific, simple to perform, and can be conducted in easily removable or benign solvents.¹²¹

Click reactions are generally classified into four major categories: (i) Copper(I)-catalyzed azide-alkyne cycloaddition (CuAAC); (ii) Strain-promoted azide-alkyne cycloaddition (SPAAC); (iii) Strain-promoted alkyne-nitrone cycloaddition (SPANAC); and (iv) Other reactions of strained alkenes. CuAAC as most classic click reaction has an inherent shortcoming that is toxicity of copper ions in the biological applications. Thus, the copper-free click reactions were further developed to overcome the cytotoxicity of the CuAAC reaction. Instead of using Cu(I) to activate the alkyne, the alkyne is instead introduced in a strained-cyclooctynes. The cyclooctynes and azides could react with each other rapidly and efficiently without the presence of Cu(I) catalysts, forming a stable triazole (Figure 1.7).¹²⁰ Meanwhile, they could also remain inert to naturally occur functional groups such as amines. Therefore, SPAAC is becoming a promising alternative in the biological research fields. Regarding the convenience and safety of assembly process, copper-free click chemistry is a desirable way that applied to living systems due to the elimination of cytotoxic copper catalysts and the absence of by-products.

Mann et al. crosslinked proteinosomes assembly of BSA-PNIPAM conjugate separately modified with azide and strained alkyne through SPAAC, and then used w/o/w Pickering emulsion method to control the size and shape and finally obtained a relatively uniform spheroidal crosslinked proteinosomes (Figure 1.8).⁹⁴ The thermo-responsive properties of the interlinked proteinosomes are used collectively to generate prototissue spheroids capable of reversible contractions that can be enzymatically modulated and exploited for mechanochemical transduction. That means the interfacial SPAAC reaction affords convenient assembly, good biocompatibility and structural stability on crosslinked proteinosomes.

In general, the above-mentioned cases provide the idea of controllable clustering, whether it is DNA hybridization or click reaction. Compared with copper-free click reaction for clustering catalytic compartments, DNA hybridization is an expensive and vulnerable route. In the process of cluster optimization, it is a complicated and inefficient route to modify complementary single stranded DNA or azide-cyclooctyne separately for different catalytic compartments. Inspired

by this, crosslinker with double cyclooctyne groups could be used to one-step connect polymersomes with surface azido groups to fabricate clustered catalytic nanocompartments.

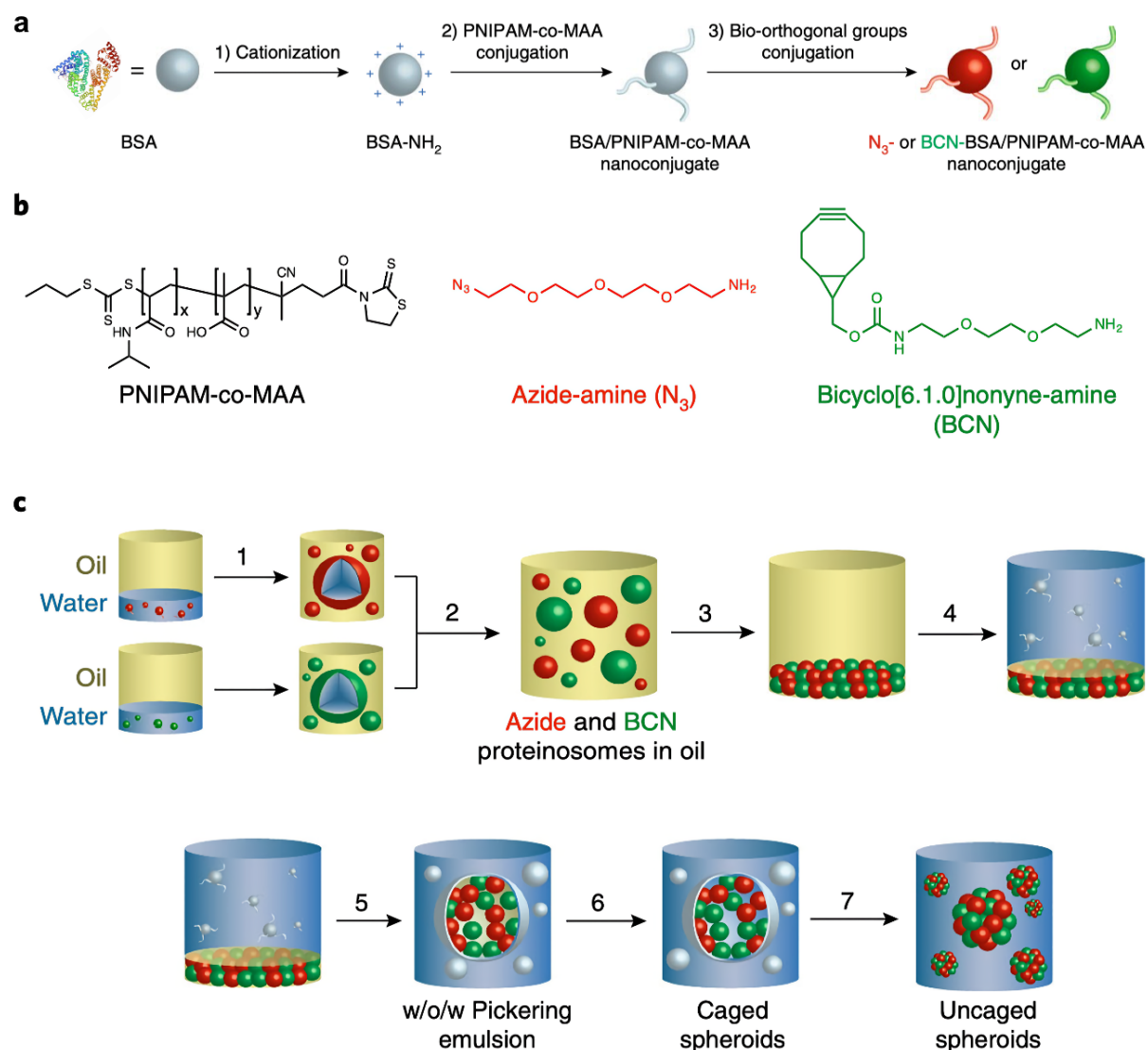


Figure 1.8 Programmed assembly of proteinosomes into synthetic prototissue spheroids. (a) Synthesis pathway for the preparation of amphiphilic thermoresponsive protein-polymer nanoconjugates with bio-orthogonal functionalities. (b) Molecular structures of the activated copolymer poly(*N*-isopropylacrylamide-co-methacrylic acid) (PNIPAM-co-MAA) and bio-orthogonal prosthetic groups (azide-amine and bicyclo[6.1.0]nonyne-amine). (c) Scheme showing experimental procedure for the preparation of proteinosome-based prototissue spheroids.⁹⁴ (Reproduced with permission from ref. 94. Copyright (2018) Springer Nature).

1.3 Stimuli-Responsive Polymersomes with Controllable Membrane Permeability

Stimuli-responsive polymersomes have emerged as novel programmable delivery systems in which the tunable membrane permeability is often achieved by inserting the stimuli-sensitive segments, make the membrane responsive to internal or external stimuli, like light, pH, redox, magnetic field, and temperature. Particular stimuli can be applied for loading drugs and various particles to be favored in different areas of biomedical applications.¹³ In the scope of this thesis, some of these stimuli including pH and light responsiveness are discussed in the following.

1.3.1 pH-Responsive Polymersomes

The pH-responsive polymersomes are of great interest because of the physiological pH gradients within the body, which endows pH-responsive polymersomes a promising future in the on-demand delivery of gene, drug, proteins, diagnostic probes and various other chemical compounds.^{23, 39, 122-125}

A number of acid-degradable polymeric systems through attaching cyclic benzylidene acetals to either the backbone or the pendant chains of synthetic materials were developed.¹²⁶⁻¹²⁸ By the copolymerization of pH-responsive acetal-based monomers, Liu et al. fabricated pH-sensitive polymersomes by self-assembly of amphiphilic diblock copolymers poly(ethylene oxide)-b-poly(2-(((5-methyl-2-(2,4,6-trimethoxyphenyl)-1,3-dioxan-5-yl)methoxy)carbonyl)amino)ethyl methacrylate) (PEO-b-PTTAMA) (Figure 1.9).²³

Because of the incorporation of pH-responsive cyclic benzylidene acetal groups, the polymersomes were distinguished by unique pH-responsive characteristic. Albeit relatively stable under neutral pH, the polymersomes were subjected to pH-triggered hydrolysis with the release of 2,4,6-trimethoxybenzaldehyde in acidic organelles, resulting in the disruption of vesicular nanocarriers and concomitant release of encapsulated drugs.

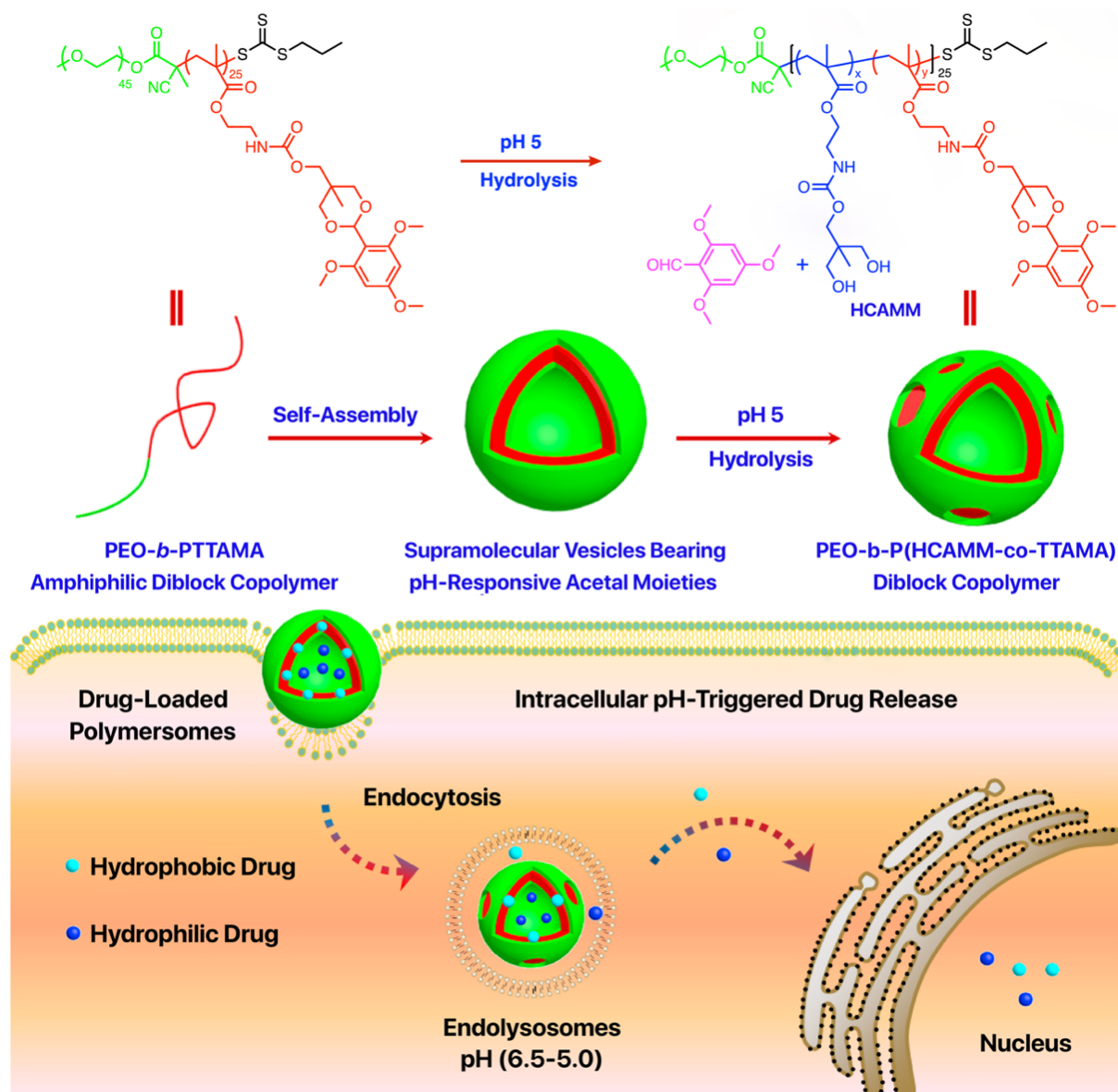


Figure 1.9 Schematic representation of pH-responsive polymersomes self-assembled from PEO-*b*-PTTAMA amphiphilic diblock copolymers containing acid-cleavable cyclic acetal side linkages in the hydrophobic block.²³ (Reproduced with permission from ref. 23. Copyright (2015) American Chemical Society).

However, pH-dependent vesicles can easily disassemble or change the original shape permanently in response to alternate pH values. One efficient approach is to crosslink the polymer chains in the vesicle membrane. The crosslinking can either happen physically or chemically using a photochemical reaction.^{78, 129-132}

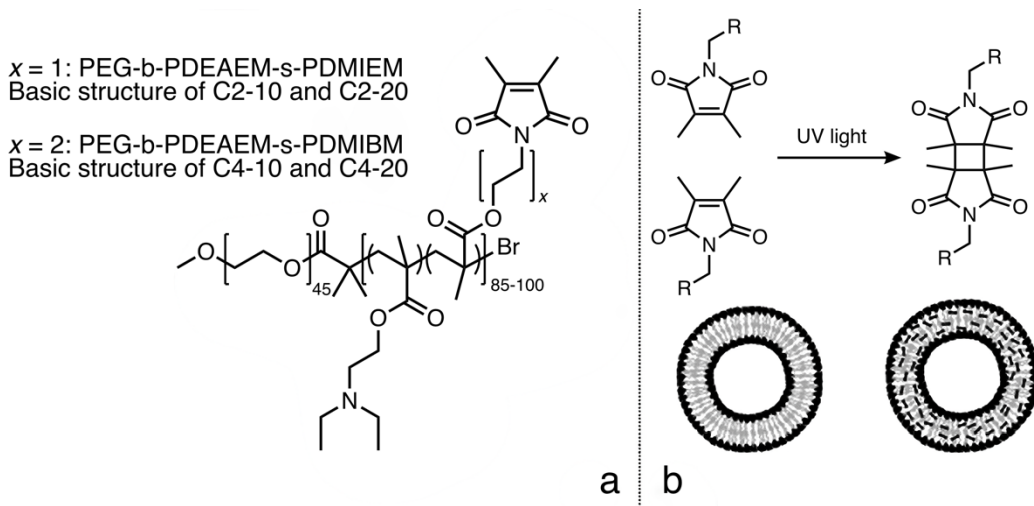


Figure 1.10 (a) Chemical structure of amphiphilic block copolymers with an ethyl (C2) and butyl (C4) spacer in the cross-linking units DMIEMA and DMIBMA, which are used in 10 or 20 mol%, respectively (resulting in C2-10, C2-20, C4-10, and C4-20 nomenclature) and (b) the crosslinking reaction occurring within the membrane.²⁰ (Reproduced with permission from ref. 20. Copyright (2012) John Wiley and Sons)

To enhance mechanical strength and achieve reversibly swelling/shrinking of pH-responsive polymersomes, Voit et al. developed photo-crosslinked polymersomes with pH-sensitive monomer 2-(diethylamino)ethyl methacrylate (DEAEMA) (Figure 1.10).²⁰ Moreover, the BCPs with different lengths of photo-crosslinker 3,4-dimethyl maleic imidobutyl methacrylate (DMIBMA) and 3,4-dimethyl maleic imidoethyl methacrylate (DMIEMA) as well the block ratio in the hydrophobic section were successfully synthesized to compare the influence by shear-rate-induced release. In short, the pore size and transmembrane trafficking of the reagents can be controlled in the case of enzymatic reactions inside polymersomes by pH-induced swelling and shrinking of the pH-stable polymersomes. Along with the tunable membrane permeability, this way of crosslinking also offers a clean process which is advantageous for using these polymersomes in biomedical science. In addition, poly(2-(diisopropylamino)ethyl methacrylate) and poly(2-(dimethylamino)ethyl methacrylate) have been extensively investigated as polymersome systems by the groups of Armes and Voit.^{80, 84, 133, 134}

1.3.2 Light-Responsive Polymersomes

Among those conventionally stimuli to regulate polymersome permeability, light stimulus possesses distinctive advantages such as facile operation, spatiotemporal and wavelength-selective precision, no external additives, and feasibility of remote control within closed

systems.¹³⁵⁻¹⁴⁰ Molecular photoswitches have opened up a myriad of opportunities in applications ranging from responsive materials and control of biological function to molecular logics.¹⁴¹⁻¹⁴⁸ The well-established chromophores including azobenzene, spiropyran, donor-acceptor Stenhouse adducts, and coumarin derivatives have been successfully incorporated into the amphiphilic BCPs to reversibly modulate the membrane permeability via light stimuli without affecting its structural integrity and stability.^{14, 15, 19, 149} Upon light irradiation with specific wavelength, the structural change of the hydrophobic segment results in the disorder of membrane, leading the change of membrane permeability.

Donor-Acceptor Stenhouse Adducts-Functionalized Polymersomes

Donor-acceptor Stenhouse adducts (DASAs) as a novel type of photo switchable molecules have great potential for various applications, such as smart materials, sensors and drug delivery.¹⁵⁰⁻¹⁵² They are particularly attractive due to their modular nature and rapid synthesis and undergo a large structural change upon photoswitching with visible light.¹³⁵ Compared with traditional UV switchable molecules, the photo switchable behavior of DASAs does not rely on high-energy UV light which does not cause damage to biological tissues. Therefore, they also have good application prospects in the field of biomedicine.¹⁵³

The DASAs as highly colored moiety can be discolored upon photoexcitation with visible light, constituting an original class of negative molecular photoswitches.¹⁵⁴ When kept in the dark, the colored form can be restored by isomerization, the cyclized form being converted into a linear nonpolar form (Figure 1.11).¹⁵⁵

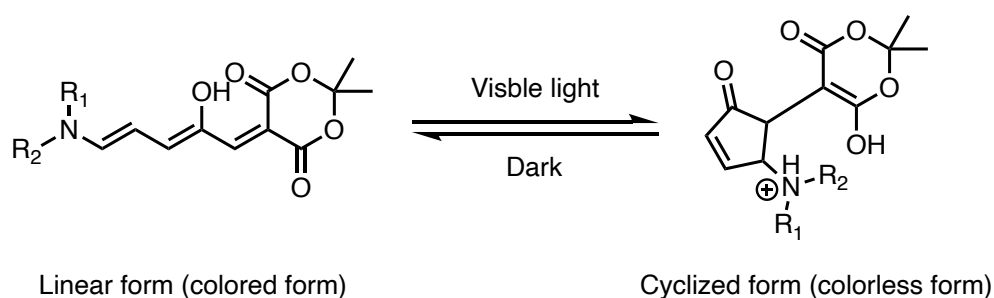


Figure 1.11 General structures of the open/closed forms of the donor-acceptor Stenhouse adducts (DASAs) based on Meldrum's acid.¹⁵⁵ (Reproduced with permission from ref. 155. Copyright (2020) MDPI)

Transient activation of biochemical reactions by visible light and subsequent return to the inactive state in the absence of light is an essential feature of the biochemical processes in photoreceptor cells.¹⁵⁶ To mimic such light-responsiveness with artificial nanoreactors, Bruns et al. separately incorporated the two different DASA variants into the BCPs to self-assemble light-responsive polymersomes through the solvent exchange method (Figure 1.12).¹⁴

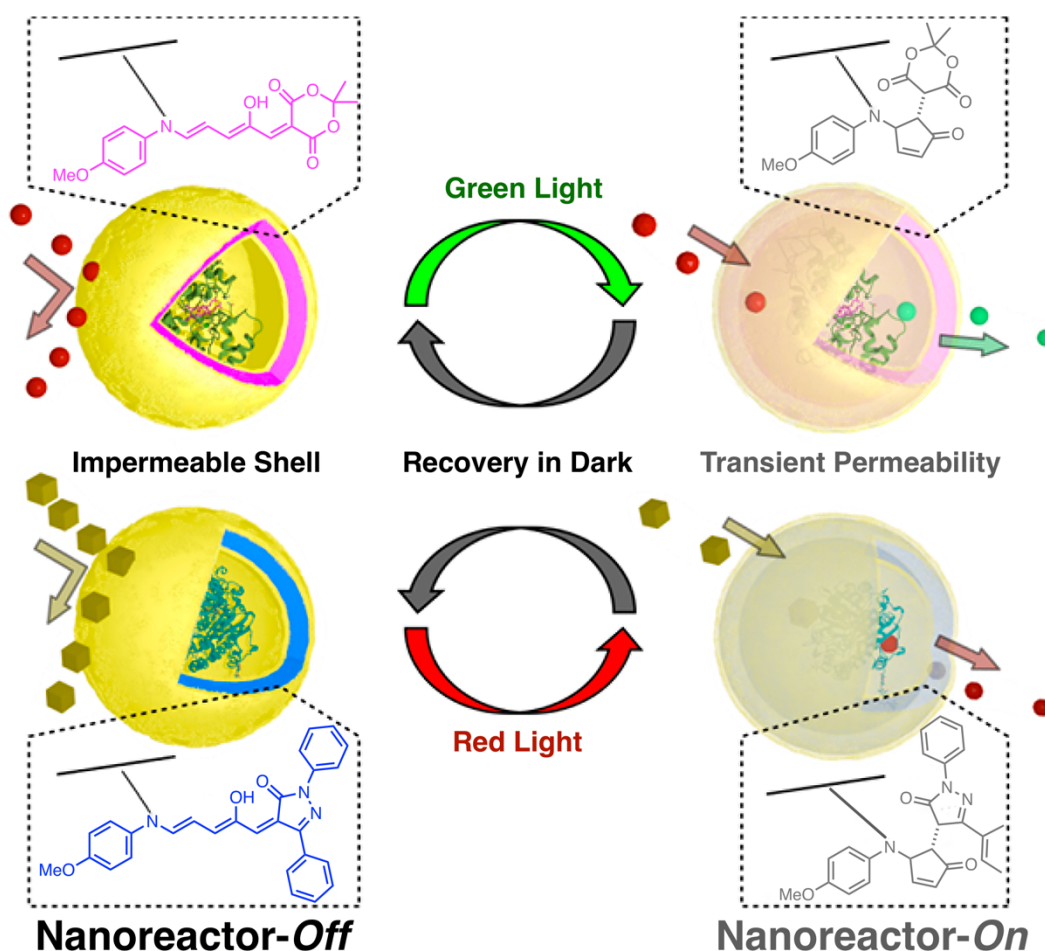


Figure 1.12 DASA-functionalized visible light-responsive nanoreactors. Two sets of enzyme-loaded polymersomes with different DASAs respond to irradiation with lower wavelength (green) or higher wavelength (red) light. The light stimuli switch the DASAs in the hydrophobic leaflet of the polymersome membrane, resulting in an increased permeability of the polymersome membrane and the activation of the enzyme nanoreactor. The polymersomes self-revert to their impermeable state in the dark at room temperature.¹⁴ (Reproduced with permission from ref. 14. Copyright (2018) American Chemical Society).

The DASAs, with their ability to isomerize upon irradiation with visible light, were utilized to change the permeability of polymersome membranes by switching polarity from a nonpolar

triene-enol form to a cyclopentenone with increased polarity.¹⁵⁷ The polymersomes based on Meldrum's acid response to green light ($\lambda = 525$ nm) and the other based on pyrazolone response to red light ($\lambda = 630$ nm). Substrates diffusion and enzyme reaction can be initiated by light irradiation at specific wavelength. Once the stimuli are withdrawn, the polymersome membrane instantaneously returns to impermeable state and the enzyme reaction terminates. Therefore, the DASA-based light-responsive polymersomes demonstrate the potential of DASAs to switch permeability of membranes.

Spiropyran-Functionalized Polymersomes

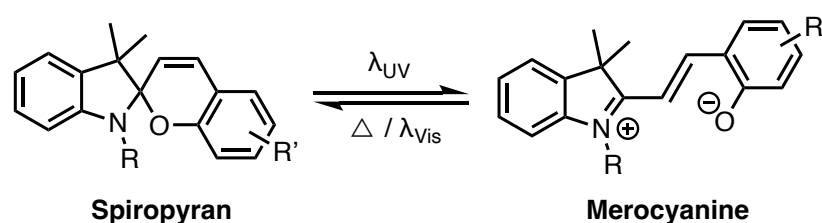


Figure 1.13 Schematic illustration of photoswitch between spiropyran and merocyanine.¹⁵⁸ (Reproduced with permission from ref. 158. Copyright (2020) Elsevier).

Photochromic spiropyrans undergo drastic structural changes between closed spiropyran and open merocyanine isoforms, which are inter-switchable with UV and visible light (Figure 1.13).¹⁵⁸ Upon UV irradiation, the spiropyran transforms into its colour emitting merocyanin-form by breaking the C-O binding. Once the irradiation has stopped, the merocyanine starts to discolour and to revert to its original form, the spiropyran. Owing to their photo-switching properties, spiropyran as a well-known photochromic molecule has been widely employed in photoresponsive dynamic materials for optical/electrical switches, drug nanocarriers, self-erasing (reusable) paper, and super-resolution imaging.¹⁵⁹⁻¹⁶⁵

Inspired by the light-tunable feature, Liu et al. incorporated the monomer based on spiropyran into BCPs to self-assemble light-responsive polymersomes (Figure 1.14).¹⁹ The photochromic polymersomes exhibited photoswitchable and reversible membrane permeability from poly(ethylene oxide)-b-PSPA diblock copolymers, where SPA is spiropyran-based monomer containing a unique carbamate linkage. Upon self-assembling into polymersomes, spiropyran moieties within vesicle bilayers undergo reversible phototriggered isomerization between hydrophobic spiropyran ($\lambda > 450$ nm) and zwitterionic merocyanine ($\lambda < 420$ nm) states. It is worthy to note that only the merocyanine-based polymersomes displayed selective membrane

permeability for small molecules release. Interestingly, UV-induced merocyanine polymersomes have two kinds of release mechanism: (i) continuous release upon short UV irradiation period through taking advantage of the unexpectedly slow spontaneous merocyanine-to-spiropyran transition kinetics ($t_{1/2} > 20$ h) under dark conditions; (ii) on-demand and switchable release under alternated UV-Vis light irradiation. Thus, the spiropyran-based light-responsive polymersomes confirm the capacity of spiropyran to control permeability of membranes.

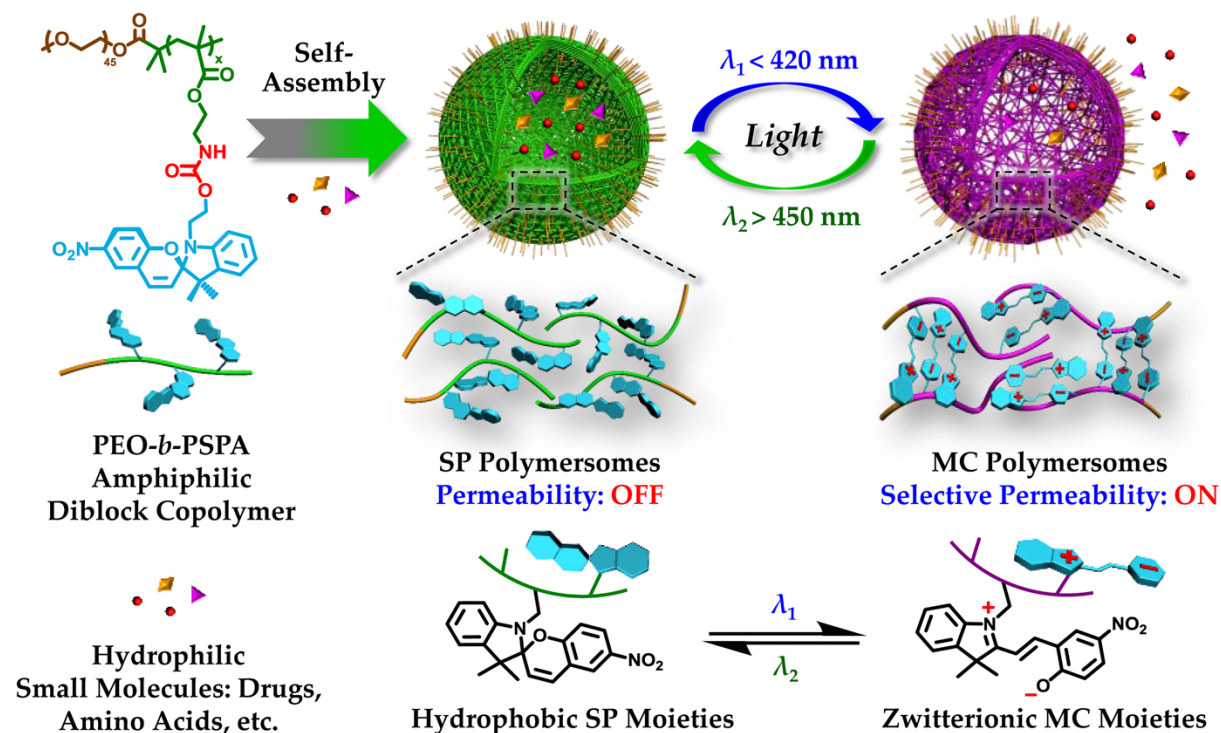


Figure 1.14 Photochromic polymersomes exhibiting photoswitchable and reversible bilayer permeability. Spiropyran-based polymersomes (SP Polymersomes) and merocyanine-based polymersomes (MC Polymersomes).¹⁹ (Reproduced with permission from ref. 19. Copyright (2015) American Chemical Society).

Azobenzene-Functionalized Polymersomes

Azobenzene is a photoswitchable chemical compound composed of two phenyl rings linked by a N=N double bond. As a photoswitching molecule, the trans form can be isomerized to the cis form by UV irradiation (λ : 300-400 nm). In opposite, the visible light ($\lambda > 400$ nm) can convert the molecule back to the trans form. Alternately, the molecule will thermally relax to the stable trans form (Figure 1.15).

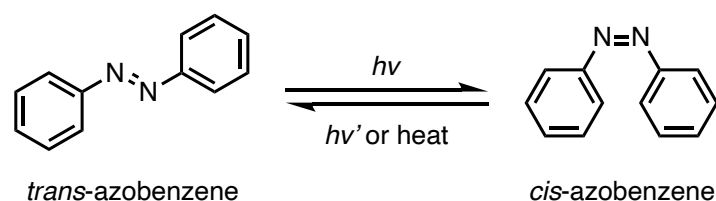


Figure 1.15 The photo-isomerization of azobenzene.

There's no doubt that azobenzene and its derivatives are the most frequently used photoswitches because their inherent physicochemical property of small, stability, reliability, and simplification of synthesis and derivative. Until now, azobenzene-based homopolymers have been exploited for photoinduced changes in the volume and shape of soft materials, as well as their dichroism and birefringence.^{166, 167}

However, Thayumanavan et al. relied on a different mechanism—the sensitivity of non-equilibrium glassy films to interfacial mobility—to achieve unique photo-induced mechanical effects with extremely low loadings of azobenzene (only one unit per polymer chain) and in the self-assembled solution state.¹⁵ Owing to the well-equilibrated glasses induced by high interfacial mobility, the interface structure has a profound impact on the bulk material.¹⁶⁸⁻¹⁷⁰

The polymersomes were self-assembled from a hydrophilic-azobenzene-hydrophobic diblock copolymer (PEG-azobenzene-poly-DL-lactide) and can achieve light-induced dye release based on the trans-cis photo-isomerization of the azobenzene group, whether it is a water-insoluble dye 1,1'-dioctadecyl-3,3',3',3'-tetramethylindocarbocyanine perchlorate (DiI) or a water-soluble dye rhodamin 6G as shown in Figure 1.16. The donor-acceptor-substituted azobenzene as the thin interfacial layer of polymersomes extended the response wavelength range from 365 nm (UV light) to 450 nm (blue light). Moreover, in the absence of light irradiation, the azobenzene groups are tightly packed and create an interface of low mobility which means the polymersomes lose the membrane permeability for dye motion.

The principles developed here have implications in applications such as on-demand release of encapsulated cargos. For this reason, the azobenzene-based light-responsive polymersomes could be used for the diffusion of enzyme substrates under light irradiation.

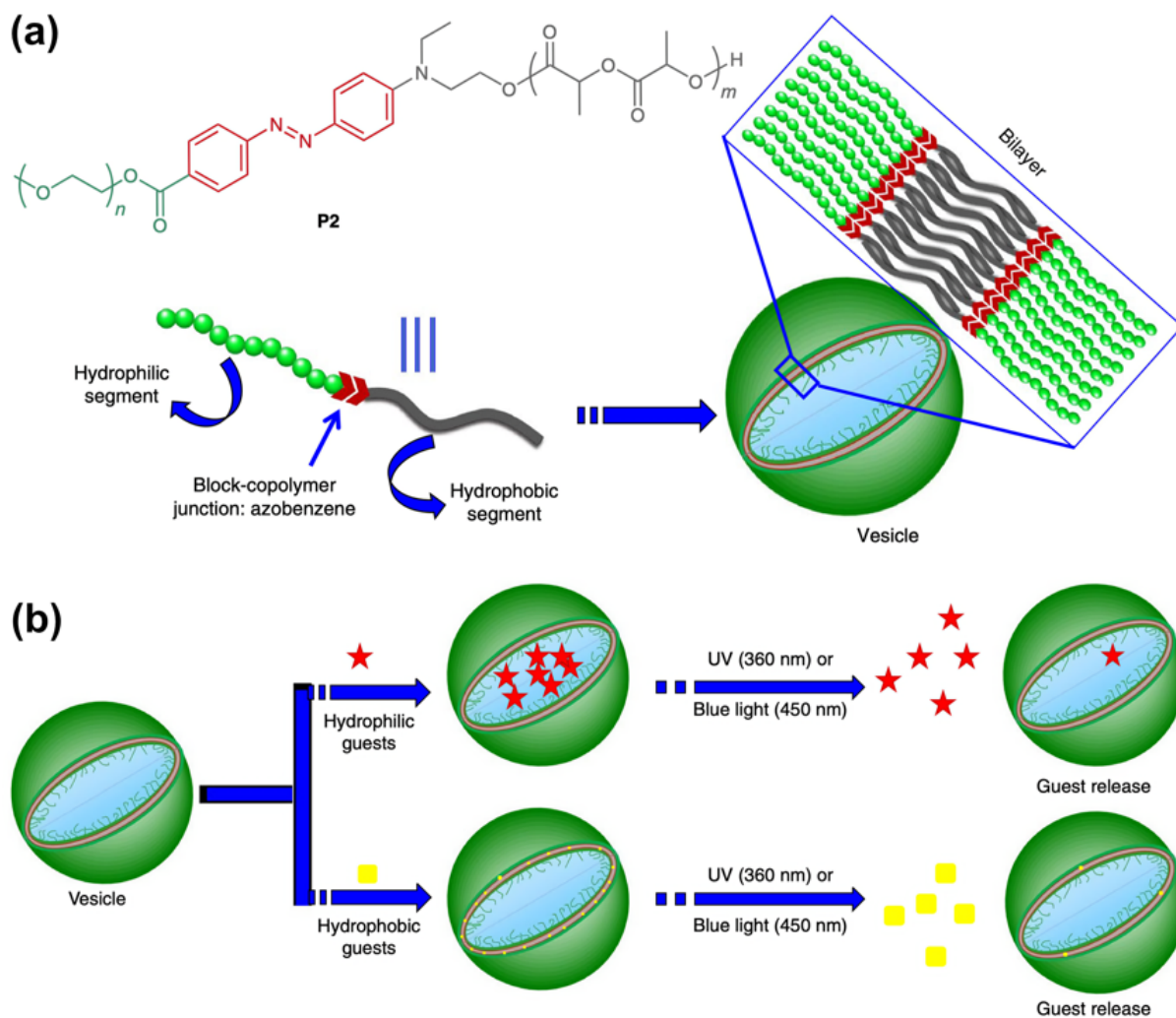


Figure 1.16 (a) Chemical structure and self-assembly of block copolymer. The cartoon representation of the vesicle with magnified region representing bilayer assembly. (b) Schematic representation of hydrophilic and hydrophobic guest encapsulation and release from the polymersomes upon the UV ($\lambda = 365$ nm) or blue light ($\lambda = 450$ nm) irradiation. Stars indicate hydrophilic guests and squares hydrophobic guests.¹⁵ (Reproduced with permission from ref. 15. Copyright (2018) Springer Nature)

2 Motivation and Aim

As outlined in the theoretical background, polymersomes as synthetic vesicles fabricated by self-assembly of amphiphilic block copolymers to mimic cellular process, have gained considerable research interest due to their high stability, flexible functionalization, and tunable membrane permeability.^{1, 4, 6} Moreover, polymersomes can be used to encapsulate or uptake not only small molecules like drug or dye but also biomacromolecules like proteins and enzymes.^{8, 15, 85, 171} Besides, the membrane permeability tends to be achieved by inserting stimuli-sensitive moieties into the polymersome membrane.^{9, 13, 34, 172} The responsiveness is necessary for the cargos to be released in a controlled way when polymersomes are used as nanocontainers or nanoreactors. Among the external stimulus, pH and light triggers are one of the cleanest and feasible ways for designing smart polymersomes. The biological and physiological systems are naturally prone to pH variation, like having more acidic environment for inflamed tissue or cancerous cells.^{173, 174} It is worthy to note that bioactive molecules can only be in-situ loaded in the pH-responsive polymersomes through direct dissolution method without any organic solvent. Besides, light is very convenient for biomedical applications since it does not require any additional chemicals to trigger membrane permeability.

Until now, existing reports of stimuli-responsive polymersomes for enzymatic cascade reaction are mostly based on simple mix of two kinds of polymersomes loaded with different enzymes, whereas the real cellular organelle is an intricate system and exhibits sophisticated biological functions. In nature, compartmentalization is a prerequisite for the spatiotemporal control of signalling pathways and for intra- and intercellular communication. Self-organization or clustering is a process by which several components become ordered in space and/or time according to interaction rules, and generally characterized by emergent properties that differ from those of the single components.¹⁷⁵ Mimicking these complex living ensembles through the design and construction of artificial organelles-like systems based on the controlled assembly and functional integration of synthetic cell-like entities is a major challenge that has important technological implications in bottom-up synthetic biology.¹⁷⁶ In addition, considering the abovementioned uncontrollable aggregation by host-guest interaction and the expensive DNA hybridization, copper-free click reaction is the most simple, efficient and safe method to connect synthetic vesicles into enzyme assemblies.

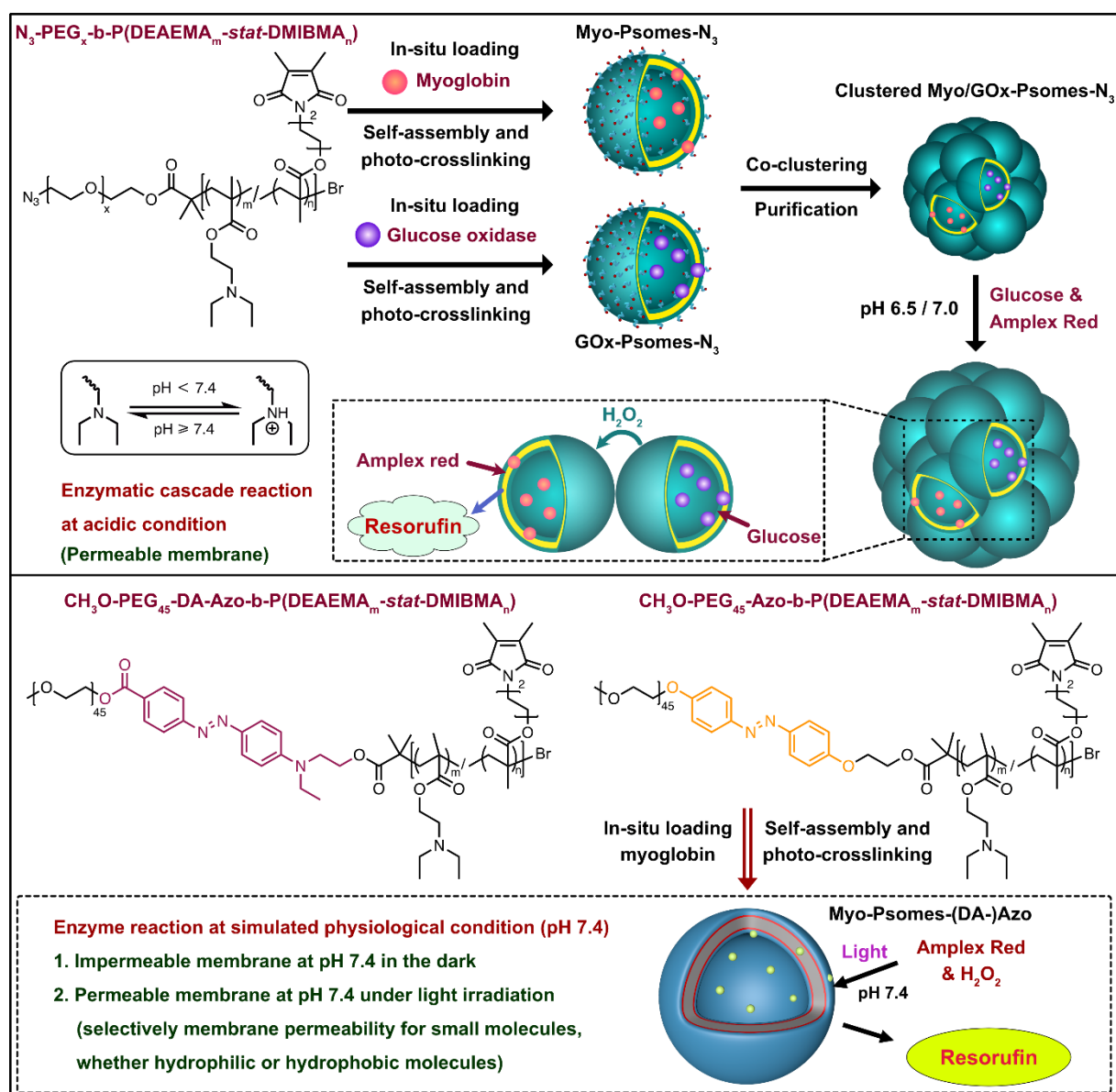


Figure 2.1 The aims of this work: i) Fabrication of photo-crosslinked pH-responsive and clustered polymersomes through copper-free click chemistry; Study of enzyme activity of co-clustered enzyme-loaded polymersomes at different pH values to enhance the enzymatic cascade reaction; ii) Construction of two novel light-responsive polymersomes with one donor-acceptor substituted azobenzene unit or one ether substituted azobenzene unit as junction between hydrophilic and hydrophobic segments of BCP; Investigation of enzyme reaction of enzyme-loaded polymersomes at physiological conditions (pH 7.4).

Although pH-responsive polymersomes present a good membrane permeability in response to alternate pH values and good stability in swelling/shrinking behavior due to the photo-crosslinked membrane, they are still inadequate for mimicking more sophisticated cellular

behavior. The inherent pH values for molecules diffusion are always at acidic condition, whereas most of cellular behavior occurred at physiological conditions. Thus, this polymersome system presents its inherent drawbacks: i) sophisticated biological functions cannot be realized in the simple polymersomes-enzyme system; ii) the enzyme reaction cannot be carried out efficiently under simulated physiological condition (pH 7.4) due to the closed membrane.

With regard to this, the overall aim of this work (Figure 2.1) is to fabricate clustered pH-responsive polymersomes based on SPAAC click reaction for enzymatic cascade reaction and construct novel light-responsive polymersomes based on original photo-crosslinked pH-responsive polymersomes for enzyme reaction under physiological conditions. The aims will be accomplished by fulfilling the following objectives:

a) Optimization of clustering conditions of photo-crosslinked pH-responsive polymersomes, include (i) temperature (ii) the ratio of BCP-N₃ (iii) the reaction time (iv) the feed ratio of surface azido group of the polymersomes and bis(bicyclo[6.1.0]non-4-yn-9-ylmethyl)-PEG (bisBCN-PEG) crosslinker (v) the length of bisBCN-PEG crosslinker and (vi) the concentration of Psomes-N₃; Screening of purification methods through different visualization approaches. Purification methods involve centrifugation times and redispersion methods (mechanical stirring, vortex as well as acidification process) and visualization approaches include TEM, cryo-TEM, in-situ AFM, CLSM and Morphologi G3-ID; Study of enzyme activity of mixed or co-clustered enzyme-loaded polymersomes at different pH values through enzymatic cascade reaction.

b) Construction of two novel light-responsive polymersomes with one donor-acceptor substituted azobenzene unit or one ether substituted azobenzene unit as junction between hydrophilic and hydrophobic segments of BCP; Exploration of photo-crosslinking time, morphology, photo-isomerization property of both light-responsive polymersomes; Study of dye release behaviors from two different light-responsive polymersomes upon different light sources, include UV light (365 nm) and blue light (400-500 nm); Investigation of enzyme reaction of enzyme-loaded polymersomes at simulated physiological condition (pH 7.4) under different light stimuli.

Part II Experiments

3 Materials and Methods

3.1 Materials

All chemicals and solvents were used as received without further purification unless stated. All anhydrous solvents were stored over molecular sieves, and dialysis membrane were rinsed with distilled water prior to use. The pH value of the aqueous dialysis medium was adjusted by HCl or NaOH solutions via the test of pH meter unless otherwise indicated.

Table 3.1 List of chemicals.

Chemical	Purity	Supplier
Aluminum oxide (neutral, activated)	-	Sigma-Aldrich
4-Aminobenzoic acid	99%	Sigma-Aldrich
4-Amino-1-butanol	98%	Sigma-Aldrich
Ammonium chloride (NH ₄ Cl)	99.5%	Sigma-Aldrich
Amplex Red	-	Thermo Fischer Scientific
Aniline	99.5%	Sigma-Aldrich
(α -Azide, ω -hydroxy)-terminated poly(ethylene glycol) (N ₃ -PEG ₆₀ -OH, M _n ~2700; Đ: 1.18)	90%	Polymer Source
2-[2-(2-Azidoethoxy)ethoxy]ethanol (N ₃ -PEG ₃ -OH, 0.5 M in tert-butyl methyl ether)	95%	Sigma-Aldrich
Bicyclo[6.1.0]non-4-yn-9-ylmethyl N-succinimidyl carbonate (exo-BCN-NHS carbonate)	95%	SiChem
2,2'-Bipyridine	99%	Sigma-Aldrich
Bis-amino poly(ethylene glycol) (NH ₂ -PEG _{2k} -NH ₂ , M _w 2000)	-	Iris Biotech
Bovine serum albumin (BSA, heat shock fraction, protease free, fatty acid free, essentially globulin free)	98%	Sigma-Aldrich
2-Bromoethanol	95%	Sigma-Aldrich

α -Bromoisobutyryl bromide	98%	Sigma-Aldrich
2-Butanone	99%	Sigma-Aldrich
Celite®545	-	Sigma-Aldrich
Copper(I) bromide (CuBr)	98%	Sigma-Aldrich
Cyanin 5 NHS-Ester (Cy5-NHS)	90%	Lumiprobe
D-(+)-glucose (glucose)	96%	Sigma-Aldrich
Dichloromethane (DCM, anhydrous)	99.9%	Sigma-Aldrich
2-(Diethylamino)ethyl methacrylate (DEAEMA)	99%	Sigma-Aldrich
Diethyl ether	99%	Sigma-Aldrich
2,3-Dimethylmaleic anhydride	98%	Sigma-Aldrich
Dimethyl sulfoxide (DMSO, anhydrous)	99.9%	Sigma-Aldrich
Disodium phosphate	99%	Sigma-Aldrich
Ethanol, absolute	99.5%	Acros Organics
Ethyl acetate (EA)	99.5%	Acros Organics
2,2'-(Ethylenedioxy)bis(ethylamine) (NH ₂ -PEG _{0.1k} -NH ₂)	98%	Sigma-Aldrich
Glucose oxidase from <i>Aspergillus niger</i> (GOx, essentially salt-free, lyophilized powder)	65%	Sigma-Aldrich
Hydrochloric acid (HCl)	37%	Honeywell Fluka
Hydrogen peroxide (H ₂ O ₂)	30%	VWR Chemicals
α -Hydroxy- ω -azido poly(ethylene glycol) (M _w 3000, N ₃ -PEG _{77.5} -OH)	-	Rapp Polymere
Magnesium sulfate (MgSO ₄ , anhydrous)	97%	Honeywell Fluka
Methacryloyl chloride	97%	Sigma-Aldrich
Methanol, anhydrous	99.8%	Sigma-Aldrich
Methanol, technical grade	99%	Acros Organics

Monosodium phosphate	99%	Sigma-Aldrich
Myoglobin from equine skeletal muscle (Myo, essentially salt-free, lyophilized powder)	95%	Sigma-Aldrich
<i>n</i> -Hexane	99%	Acros Organics
4-Nitrophenol	99%	Sigma-Aldrich
<i>N,N</i> -Dimethylformamide (DMF, anhydrous)	99.8%	Sigma-Aldrich
O,O'-Bis(2-aminoethyl)hexacosathylene glycol (NH ₂ -PEG _{1k} -NH ₂ , M _w 1249.5)	-	Polypure AS
Palladium on activated carbon (10% Pd/C)	-	Thermo Fischer Scientific
Phenol	99%	Sigma-Aldrich
Phosphate buffered saline (PBS, tablet, biotech grade)	-	Sigma-Aldrich
Phosphotungstic acid (PTA)	-	Sigma-Aldrich
Poly(ethylene glycol) methyl ether (CH ₃ O-PEG ₄₅ -OH, M _n ~ 2000; Đ: 1.05)	-	Sigma-Aldrich
Potassium carbonate (K ₂ CO ₃)	99%	Honeywell Fluka
Potassium iodide (KI)	99%	Sigma-Aldrich
<i>p</i> -Toluenesulfonyl chloride	98%	Sigma-Aldrich
Raney®-Nickel (slurry, in H ₂ O)	-	Sigma-Aldrich
Rhodamine B isothiocyanate (RhB-ITC)	-	Sigma-Aldrich
Silica gel	-	Sigma-Aldrich
Sodium azide (NaN ₃)	99.5%	Sigma-Aldrich
Sodium bicarbonate (NaHCO ₃)	99.7%	Sigma-Aldrich
Sodium borohydride (NaBH ₄)	99%	Sigma-Aldrich
Sodium carbonate (Na ₂ CO ₃)	99.5%	Sigma-Aldrich
Sodium chloride (NaCl)	99%	Sigma-Aldrich

Sodium hydroxide (NaOH, pellets, anhydrous)	98%	Sigma-Aldrich
Sodium nitrite (NaNO ₂)	97%	Sigma-Aldrich
Sodium sulfate (Na ₂ SO ₄ , anhydrous, powder)	99%	Sigma-Aldrich
Sulfuric acid (H ₂ SO ₄)	95-98%	Honeywell Fluka
Tetrahydrofuran (THF, anhydrous)	99.5%	Sigma-Aldrich
Toluene, anhydrous	99.8%	Acros Organics
Triethylamine (TEA)	99.5%	Sigma-Aldrich

Table 3.2 List of materials.

Materials	Supplier
Dialysis membranes made from cellulose ester (MWCO 100-500 Da)	Carl Roth
Dialysis membranes made from regenerated cellulose (MWCO 5 kDa)	Carl Roth
Hollow fiber filtration membrane, polyethersulfone (MWCO 500 kDa)	Spectrum Labs
Syringe filters with pore size 0.8 μm (membrane: cellulose mixed ester)	Carl Roth
Syringe filters with pore size 0.2 μm (membrane: nylon)	Carl Roth

3.2 Analytical Methods

NMR Spectroscopy. Bruker Advance III 500 spectrometer (Bruker Biospin, Germany) was used to record ¹H NMR (500 MHz) and ¹³C NMR (126 MHz) spectra using CDCl₃ or DMSO-*d*₆ as solvents at room temperature (RT). The chemical shifts were referenced to the corresponding solvent signals (CDCl₃: δ = 7.26 ppm; DMSO-*d*₆: δ = 2.49 ppm) and are expressed in ppm.

Gel Permeation Chromatography (GPC). The molar mass distributions (\mathcal{D}), weight average molar mass (M_w), and number average molar mass (M_n) of block copolymers (BCP-OCH₃ and BCP-N₃) were measured using size exclusion chromatography (SEC) equipped with an Agilent 1260 Infinity variable wavelength detector (VWD) (Agilent Technologies, Germany), a multi-angle laser light scattering (MALLS) detector (DAWN HELEOS II, Wyatt Technology Europe,

Germany), a viscometer (Viscostar III, Wyatt Technology Europe, Germany) and a refractive index (RI) detector (Optilab T-rEX, Wyatt Technology Europe, Germany). The column (HPLC Column Plgel, Mixed-C, 300 × 7.5 mm, average bead size: 5 μm) and the pump (Isocratic pump, Agilent 1200 series) were from Agilent Technologies (Germany). THF stabilized with 0.025 % butylated hydroxytoluene (BHT) was used as an eluent with a flow rate of 1 mL/min; The \bar{M}_w and \bar{M}_n of block copolymers (BCP-DA-Azo and BCP-Azo) were measured using SEC equipped with an RI detector (K-2301, KNAUER, Germany) and a MALLS detector (miniDAWN Treos II, Wyatt Technology Europe, Germany). The column (PolarGel-M-Column, 300 × 7.5 mm, average bead size: 8 μm) and the pump (HPLC pump, Agilent 1200 series) were from Agilent Technologies (Germany). *N*-dimethylacetamide (DMAc) containing 3 mg/mL LiCl was used as an eluent with a flow rate of 1 mL/min.

Hollow Fiber Filtration (HFF). HFF was carried out using KrosFlo Research Iii System equipped with a separation module made of polyether sulfone membrane (MWCO: 500 kDa, Spectrum Labs, USA). The transmembrane pressure was 130 mbar with a flow rate of 15 mL/min.

Dynamic Light Scattering (DLS). DLS measurements of aqueous polymersome solutions (≤ 1 mg/mL) were carried out using a Zetasizer Nano-series instrument (Malvern Instruments, UK) equipped with Dispersion Technology Software (Version 5.00). The measurements were carried out over a range of pH values at 25 °C. The data were collected using the NIBS (Non-Invasive BackScatter) method with a 633 nm He-Ne laser (4 mW) at a fixed angle of 173° (measurement duration: automatic; 3 measurements). The data were analyzed using Malvern Software 7.12.

Fluorescence Spectroscopy. Fluorescence spectra were mainly measured on an Infinite® 200 PRO microplate reader (Tecan Trading AG, Switzerland) equipped with Tecan i-control™ software (Version: 2.0.10.0). The main measurements conditions: Greiner 96 Flat Bottom Transparent Polystyrene; for influence of centrifugation times, BSA-Cy5-Psomes-N₃ (0.5 mg/mL Psomes and 0.1 mg/mL BSA-Cy5) before (in 10 mM PBS buffer, pH 7.4) and after centrifugation (in 1 mM PBS buffer, pH 8.0) for several times (100 μL per well), $\lambda_{ex} = 622$ nm, $\lambda_{em} = 668$ nm; for loading efficiency of GOx, GOx-Cy5-Psomes-N₃ (1 mg/mL Psomes and 0.2 mg/mL GOx-Cy5) before (in 10 mM NaCl, pH 8.0) and after HFF purification (in 1 mM PBS buffer, pH 7.4) (100 μL per well), $\lambda_{ex} = 622$ nm, $\lambda_{em} = 668$ nm; for loading efficiency of Myo, Myo-RhB-Psomes-N₃ (1 mg/mL Psomes and 0.2 mg/mL Myo-RhB) before (in 10 mM NaCl,

pH 8.0) and after HFF purification (in 1 mM PBS buffer, pH 7.4) (100 μ L per well), $\lambda_{\text{ex}} = 519$ nm, $\lambda_{\text{em}} = 578$ nm; for enzymatic cascade reaction: 0.15 mg/mL GOx-Psomes- N_3 and/or Myo-Psomes- N_3 (100 μ L per well), $\lambda_{\text{ex}} = 534$ nm, $\lambda_{\text{em}} = 585$ nm; for enzyme reaction: 0.5 mg/mL Myo-Psomes-(DA-)Azo (in 1 mM PBS buffer, pH 7.4, 200 μ L per well), $\lambda_{\text{ex}} = 534$ nm, $\lambda_{\text{em}} = 590$ nm. In addition, fluorescence spectra from dye release experiments were collected using a FS5 spectrofluorometer (Edinburgh Instruments Ltd., UK) equipped with a 150 W xenon lamp. The main measurements conditions: for dye photobleaching: 1 μ g/mL Nile red in DMF (1 mL in quartz cuvette), $\lambda_{\text{ex}} = 515$ nm, $\lambda_{\text{em}} = 626$ nm, bandwidth = 2 nm; for dye release: 0.5 mg/mL in 1 mM PBS buffer at pH 7.4 (1 mL in quartz cuvette), $\lambda_{\text{ex}} = 515$ nm, $\lambda_{\text{em}} = 600$ nm, bandwidth = 3 nm.

Atomic Force Microscopy (AFM). In-situ AFM measurements of the clustered Psomes- N_3 were performed in 10 mM PBS buffer with different pH values (pH 8.0, 7.0, 6.5, 6.0) using a Dimension Icon AFM with NanoScope V Controller (Bruker-Nano, Santa Barbara, CA). The image analyses were carried out by NanoScope Analysis 2.0 Software by determining height and diameter values of several well-isolated particles from the corresponding images.

UV-Vis Spectroscopy. The UV-vis absorption spectra were recorded on a SPECORD 210 Plus (Analytic Jena, Germany). All investigations were performed in 1.5 mL semi-micro cuvettes of PMMA (Brand, Germany) or semi-micro quartz cuvettes (Hellma Analytics, Germany).

UV Lamp for Crosslinking Polymersomes and Photo-isomerization of Azobenzene Unit. OmniCure S2000 Spot UV Curing System (Lumen Dynamics Group Inc., Canada) equipped with a high-pressure mercury lamp (High Pressure 200-Watt Mercury Vapor Short Arc) as the UV source (wavelength: 250-650 nm) was used to crosslink the polymersomes (Psomes- OCH_3 , Psomes- N_3 and enzyme loaded Psomes- N_3). The dedicated bandpass filters with 365 nm and 400-500 nm were equipped with the UV lamp through external filter adapter kit to cut off light in other wavelength ranges and used for photo-isomerization of macroinitiator, block copolymers (BCPs) and polymersomes with azobenzene unit as well as corresponding dye release and enzyme assays. Additionally, the bandpass filter with 320-390 nm was used to crosslink polymersomes with azobenzene unit ((myoglobin loaded) Psomes-DA-Azo and Psomes-Azo). The irradiation intensity of UV light with and without external filter was measured through OmniCure R2000 UV Radiometer (Lumen Dynamics Group Inc., Canada). The UV exposure level was set to 100 and the light output (power and irradiance) was measured and described as below: (a) original (without filter): 3.88 W, 19.7 W/cm²; (b) after 365 nm

filtration: 0.968 W, 4.93 W/cm²; (c) after 400-500 nm filtration: 1.52 W, 7.74 W/cm²; (d) after 320-390 nm filtration: 1.34 W, 6.8 W/cm².

Cryogenic Transmission Electron Microscopy (Cryo-TEM). Cryo-TEM images were acquired on a Libra 120 microscope (Carl Zeiss Microscopy GmbH, Oberkochen, Germany) at an acceleration voltage of 120 kV. The samples were prepared by dropping 2 μ L of (clustered) polymersome solution (1 mg BCP/mL Psomes-X%N₃ or Psomes-(DA)-Azo in 10 mM NaCl at pH 8.0; 1 mg BCP/mL Enzyme-Psomes-N₃ or NR-Psomes-(DA)-Azo or Myo-Psomes-(DA)-Azo in 1 mM PBS buffer at pH 7.4; 0.5 mg BCP/mL clustered (Enzyme)-Psomes-N₃ in 10 mM PBS buffer at pH 7.4 (without purification) or in 1 mM PBS buffer at pH 8.0 (after purification)) on copper grids coated with holey carbon foil (so-called Lacey type). A piece of filter paper was used to remove excess water; the sample was then rapidly frozen in liquid ethane at -178 °C. The blotting with the filter paper and plunging into liquid ethane was done in a Leica GP device (Leica Microsystems GmbH, Wetzlar, Germany). All images were recorded in bright field at -172 °C. The diameter and membrane thickness of the (clustered) polymersomes were determined from cryo-TEM images by using image processing software Fiji. The average diameter and membrane thickness of (enzyme or dye loaded) polymersomes were calculated by analyzing no less than 58 particles and 13 particles, respectively. The average size of clusters before and after purification was calculated by analyzing no less than 18 particles.

Transmission Electron Microscopy (TEM). TEM images were acquired on a Libra 120 microscope (Carl Zeiss Microscopy GmbH, Oberkochen, Germany) at an acceleration voltage of 120 kV. For the conventional preparation, 5 μ L of clustered Psomes-N₃ solution (0.5 mg BCP/ml, in 1 mM PBS buffer at pH 8.0, purified by Protocol 1) was deposited onto the copper grid and the aqueous suspension was air-dried before measurement. For negative staining, 5 μ L of clustered Psomes-N₃ solution (0.5 mg BCP/ml, in 1 mM PBS buffer at pH 8.0, before purification and purified by Protocol 2) was deposited onto the grids for 5 min and then the grid was blotted with filter paper and immersed in the PTA (2% w/w) water solution staining solution for 5 s. Following the grid was blotted again and dried on the air for 5 min. For the freeze-dry process, 2 μ L of clustered Psomes-N₃ or co-clustered Myo/GOx-Psomes-N₃ solution (0.5 mg BCP/ml, in 1 mM PBS buffer at pH 8.0, purified by Protocol 3) was frozen first in liquid nitrogen and then loading the sample inside the TEM (same with Cryo-TEM protocol). Following the temperature was slowly increased from -172 °C to -80 °C, the ice was sublimated and the clustered Psomes-N₃ kept the original hollow structure for each polymersome unit. The

size of the clustered Psomes-N₃ were determined from TEM images by using image processing software Fiji. The average size of clustered Psomes-N₃ and co-clustered Myo/GOx-Psomes-N₃ was calculated by analyzing no less than 24 particles.

Confocal Laser Scanning Microscopy (CLSM). Protein/enzyme labeled fluorescent probe in-situ loaded Psomes-N₃ after clustering were imaged with a Leica TCS SP2 AOBS confocal microscope equipped with an argon laser ($\lambda = 488 \text{ nm}$) using a 63x oil immersion objective.

Microscopic Imaging and Raman Analysis. The particle size and shape of clustered Psomes-N₃ and co-clustered Myo/GOx-Psomes-N₃ was automatically measured by Morphologi G3-ID (Malvern Panalytical GmbH, Germany) equipped with Sysmex FPIA-2100. The Morphologi G3-ID is an integrated system with a microscope and a Raman Spectroscope which extends the capabilities of image analysis by applying the technique of morphologically directed Raman spectroscopy to enable the chemical identification of multi-component agglomerates that cannot be reliably classified based on size and shape alone. The clustered Psomes-N₃ (0.5 mg BCP/ml, before and after centrifugal purification and redispersion by mechanical stirring or vortex, in 10 mM PBS buffer at pH 8.0 or 6.5) or co-clustered Myo/GOx-Psomes-N₃ (0.5 mg BCP/ml, purified by Protocol 3, in 10 mM PBS buffer at pH 8.0, 7.0 or 6.5) were put on the thin-path wet cell and measured through lens (50x, 0.5-40 μm) and differential Z stacking (50x, +/- 3.1 μm). An input of approximate 50000 particles was selected for automatic imaging by the microscope. A few particles were highlighted for Raman spectra performed using the integrated Raman spectrophotometer available in the Morphologi G3-ID instrument. The diagram is smoothed over 11 points. Small particles below 0.5 μm cannot be measured and the size values are also based on an ideal sphere.

Asymmetrical Flow Field Flow Fractionation (AF4). AF4 measurements were performed with an Eclipse DUALTEC system (Wyatt Technology Europe, Germany) with a 1 mM PBS buffer (at pH 7.4) as carrier liquid and 0.02 % (w/v) NaN₃ to prevent the growth of bacteria and algae. The channel spacer made of poly(tetrafluoroethylene) had a thickness of 490 μm and the channel dimensions were 26.5 cm in length and 0.6-2.1 cm in width. Regenerated cellulose membranes with a molecular weight cut-off (MWCO) of 10 kDa were used as accumulation wall (Superon GmbH, Germany). Flow rates were controlled with an Agilent Technologies 1260er series isocratic pump equipped with a vacuum degasser. The detection system consisted of a MALLS detector (DAWN HELEOS II, Wyatt Technology Europe, Germany) operating at a wavelength of 660 nm, a diode array detector (DAD, SPD-M20A, Shimadzu Europe), and a

refractive index (RI) detector (Optilab T-rEX, Wyatt Technology Europe GmbH, Germany) operating at a wavelength of 660 nm. All injections were performed with an autosampler (1260 series, Agilent Technologies Deutschland GmbH). The data collection and calculation of molar masses and radii were performed by Astra 6.1.2.84 software (Wyatt Technologies, USA). For the calculation of R_g Berry fit was applied. For the optimized separation method, the channel flow rate (F_c) was maintained at 0.5 mL/min for all AF4 measurements. Unless mentioned otherwise, the focus flow (F_f) was set at 2 mL/min for 6 min. The injection volume for molar mass determination was set to 150 μ L. For the separation of samples, the separation starts with an isocratic step with a cross flow rate (F_x) of 2 mL/min for 10 min followed by an exponential F_x gradient from 2 to 0 mL/min within 15 min. The last step proceeds with F_x of 0 mL/min for 5 min. The scaling exponent (ν) was calculated using $R_g \propto M^\nu$, in which the scaling exponent ν is defined by the increase of the radius of gyration dependent on molar mass. Theoretical values of ν are 0.33 for a spherical shape and 0.5 for a statistical coil in a theta solvent. The apparent density (ρ_{app}) was calculated as $\rho_{app} = M_w / (V_{app}(R_g) \cdot N_A)$, where $V_{app}(R_g)$ is the apparent volume calculated by R_g and N_A is the Avogadro constant.

Statistical Analysis. One-way ANOVA statistical analysis was performed to evaluate the significance of the experimental data. Differences between groups were measured for statistical significance using Student's paired t-test. A value of 0.05 was selected as significance level, and the data were indicated with (*) for $p < 0.05$, (**) for $p < 0.01$, (***) for $p < 0.001$, respectively.

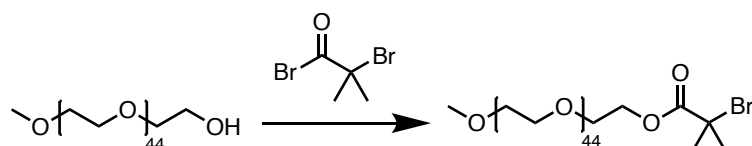
4 Clustered pH-Responsive Polymersomes for Enzymatic Cascade Reaction

4.1 Synthetic Methods and Characterization of Block Copolymer (BCP) for Self-Assembly of Polymersomes

4.1.1 Synthesis of Poly(Ethylene Glycol) (PEG) Macroinitiator

The PEG macroinitiators with α -bromoisobutyryl end group (PEG-Br macroinitiators) were synthesized according to previous published approach with slight modifications.¹⁷

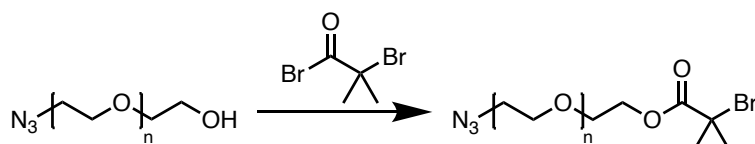
PEG-Br Macroinitiator with Methoxy Terminal Group



Here, CH₃O-PEG₄₅-OH (5 g, 2.5 mmol, 1 eq.) was directly dissolved in anhydrous DCM (30 mL) under ice bath with continuous stirring and then filled with argon. Following TEA (558 μ L, 4 mmol, 1.6 eq.) and α -bromoisobutyryl bromide (371 μ L, 3 mmol, 1.2 eq.) were in sequence slowly added to the solution. The gloomy mixture was stirred for 2 days at RT in the dark. The final macroinitiator was precipitated in the cold diethyl ether for three times and then recrystallized in ethanol until a white solid was obtained. Yield: 63 % (3.38 g).

CH₃O-PEG₄₅-Br Macroinitiator: ¹H NMR (500 MHz, DMSO-*d*₆) (Figure A1): δ = 4.23 (t, 2H), 3.50 (s, 178H), 3.23 (s, 3H), 1.88 (s, 6H).

PEG-Br Macroinitiator with Azido Terminal Group



Here, N₃-PEG₆₀-OH (600 mg, 0.222 mmol, 1 eq.) or N₃-PEG_{77.5}-OH (755 mg, 0.222 mmol, 1 eq.) was directly dissolved in anhydrous DCM (30 mL) under ice bath with continuous stirring and then filled with argon. Following TEA (49.5 μ L, 0.355 mmol, 1.6 eq.) and α -bromoisobutyryl bromide (32.9 μ L, 0.266 mmol, 1.2 eq.) were in sequence slowly added to the

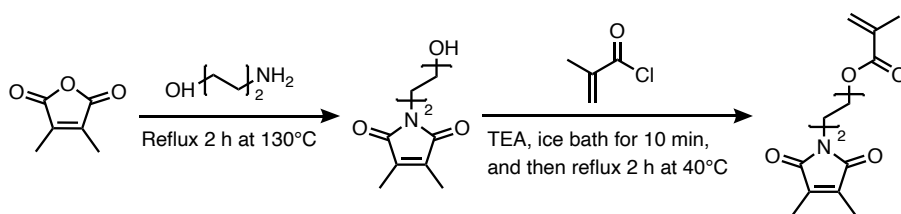
solution. The gloomy mixture was stirred for 2 days at RT in the dark. The final macroinitiator was precipitated in cold diethyl ether for three times and then recrystallized in ethanol until a white solid was obtained. Yield: 74 % for N₃-PEG₆₀-Br macroinitiator (469 mg) and 65% for N₃-PEG_{77.5}-Br macroinitiator (512 mg).

N₃-PEG₆₀-Br Macroinitiator: ¹H NMR (500 MHz, DMSO-*d*₆) (Figure A2): δ = 4.25 (t, 2H), 3.52 (s, 238H), 1.90 (s, 6H).

N₃-PEG_{77.5}-Br Macroinitiator: ¹H NMR (500 MHz, DMSO-*d*₆) (Figure A3): δ = 4.23 (t, 2H), 3.50 (s, 310H), 1.87 (s, 6H).

4.1.2 Synthesis of Photo-Crosslinker

Photo-crosslinker 3,4-dimethyl maleic imidobutyl methacrylate (DMIBMA) was synthesized by two steps according to previous work.²⁰



Step 1: 2,3-Dimethylmaleic anhydride (5 g, 39.6 mmol, 1 eq.) was mixed with 4-amino-1-butanol (3.53 g, 39.6 mmol, 1 eq.) in 120 mL anhydrous toluene. The mixture was reflux at 130 °C in oil bath for 2 h. Following the mixture was dried by anhydrous Na₂SO₄ and then rotary evaporated to remove the solvent. The crude product was further purified by column chromatography with *n*-hexane/EA (1: 1, vol/vol) mixture to obtain the compound 3,4-dimethyl maleic imidobutanol. Yield: 98% (7.66 g).

¹H NMR (500 MHz, DMSO-*d*₆) (Figure A4): δ = 4.35 (t, 1H), 3.36 (dt, 4H), 1.88 (s, 6H), 1.50 (m, 2H), 1.33 (m, 2H).

¹³C NMR (126 MHz, DMSO-*d*₆) (Figure A5): δ = 171.76 (C=O), 136.54 (C), 60.11 (CH₂), 37.17 (CH₂), 29.65 (CH₂), 24.81 (CH₂), 8.36 (CH₃).

Step 2: The synthesized 3,4-dimethyl maleic imidobutanol (7 g, 35.5 mmol, 1 eq.) was dissolved in 50 mL anhydrous DCM and then put it under ice bath and filled with argon. Following methacryloyl chloride (5.15 mL, 53.2 mmol, 1 eq.) was dissolved in 10 ml dry DCM and then added to the above solution. After dry TEA (9.89 mL, 71 mmol, 2 eq.) are added, the

mixture becomes gloomy and the ice was removed. Next, the reaction was reflux at 40 °C for 2 h and aborted by pouring the reaction into water. The water is extracted three times with DCM. The organic phase was dried over MgSO₄ and the solvent was removed at reduced pressure. The crude product is purified using column chromatography with a *n*-hexane/EA (4: 1, vol/vol) mixture to give a colorless oil. Yield: 64 % (6.03 g).

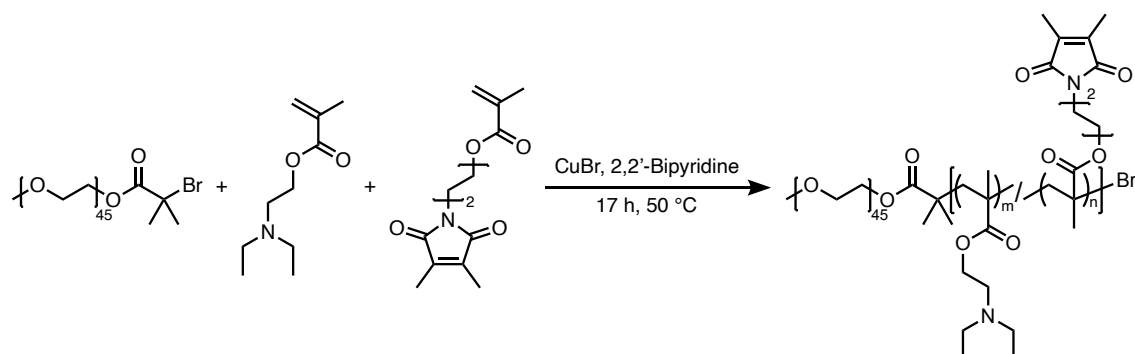
¹H NMR (500 MHz, DMSO-*d*₆) (Figure A6): δ = 5.99 (m, 1H), 5.65 (m, 1H), 4.07 (m, 2H), 3.40 (m, 2H), 1.88 (s, 6H), 1.86 (s, 2H), 1.55 (dt, 4H).

¹³C NMR (126 MHz, DMSO-*d*₆) (Figure A7): δ = 171.75 (C=O), 166.46 (C=O), 136.59 (C), 135.88 (C), 125.51 (CH₂), 63.65 (CH₂), 36.81 (CH₂), 25.37 (CH₂), 24.61 (CH₂), 17.91 (CH₃), 8.36 (CH₃).

4.1.3 Synthesis of BCP with Different Terminal Groups

The ATRP polymerization of BCP was carried out as described by Gumz et al. with slight modifications.⁸⁰

BCP with Methoxy Terminal Group (BCP-OCH₃)

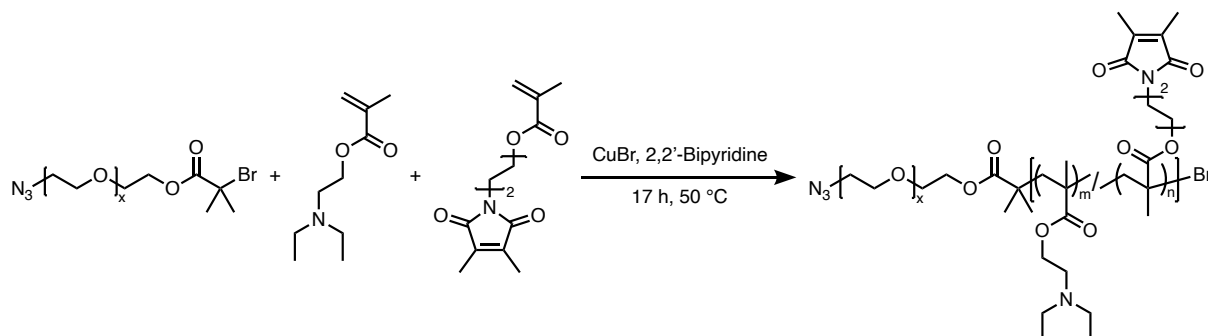


BCP-OCH₃: CH₃O-PEG₄₅-Br macroinitiator (100 mg, 0.046 mmol, 1 eq.), 2,2'-bipyridine (14.4 mg, 0.092 mmol, 2 eq.), DEAEMA (616.6 mg, 3.328 mmol, 72 eq.) and DMIBMA (220.7 mg, 0.832 mmol, 18 eq.) were added to a Schlenk tube equipped with a stirring bar. The mixed compounds were dissolved in 1.5 ml of 2-butanone and completely frozen in liquid nitrogen. The mixture was degassed using two freeze-pump-thaw-cycles and backfilled with argon. Following CuBr (6.6 mg, 0.046 mmol, 1 eq.) was added and the mixture was degassed using three freeze-pump-thaw-cycles again, backfilled with argon and stirred 17 h at 50 °C. To end the polymerization, the tube was opened, and the reaction mixture was diluted with THF and filtrated over neutral aluminum oxide to remove all copper species. The mixture was transferred

to a dialysis membrane (regenerated cellulose, MWCO 5 kDa) and was dialysed against methanol (technical grade) for three days exchanging the solvent twice a day. Afterwards the solvent was removed under reduced pressure and the final product was dried in vacuo. Yield: 78% (731 mg).

^1H NMR (500 MHz, CDCl_3) (Figure A8): $\delta = 4.12\text{-}3.84$ (m, 204H), 3.64 (s, 180H), 3.58-3.45 (m, 42H), 2.70 (t, $J = 6.3$ Hz, 164H), 2.56 (tt, $J = 9.2, 6.2, 5.3$ Hz, 329H), 1.97 (s, 114H), 1.90 (s, 31H), 1.80 (s, 55H), 1.06-1.00 (m, 548H), 0.92-0.84 (m, 176H).

BCP with Azido Terminal Group (BCP- N_3)



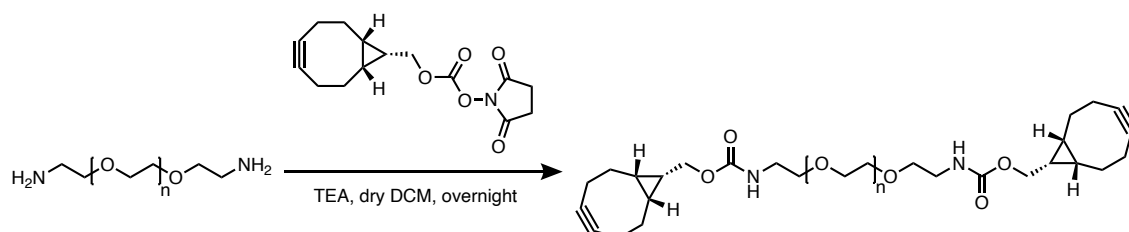
BCP- N_3 -1: N_3 -PEG₆₀-Br macroinitiator (100 mg, 34.7 μmol , 1 eq.), 2,2'-bipyridine (10.8 mg, 69.5 μmol , 2 eq.), DEAEMA (617.7 mg, 3.334 mmol, 96 eq.) and DMIBMA (221.1 mg, 0.834 mmol, 24 eq.) were added to a Schlenk tube equipped with a stirring bar. The mixed compounds were dissolved in 1.5 ml of 2-butanone and completely frozen in liquid nitrogen. The mixture was degassed using two freeze-pump-thaw-cycles and backfilled with argon. Following CuBr (5.0 mg, 34.7 μmol , 1 eq.) was added and the mixture was degassed using three freeze-pump-thaw-cycles again, backfilled with argon and stirred 17 h at 50 °C. To end the polymerization, the tube was opened, and the reaction mixture was diluted with THF and filtrated over neutral aluminum oxide to remove all copper species. The mixture was transferred to a dialysis membrane (regenerated cellulose, MWCO 5 kDa) and was dialysed against methanol (technical grade) for three days exchanging the solvent twice a day. Afterwards the solvent was removed under reduced pressure and the final product was dried in vacuo. Yield: 63% (591 mg).

^1H NMR (500 MHz, CDCl_3) (Figure A9): $\delta = 4.12\text{-}3.83$ (m, 205H), 3.64 (s, 240H), 3.51 (d, $J = 9.1$ Hz, 40H), 2.70 (t, $J = 6.1$ Hz, 171H), 2.56 (tt, $J = 8.8, 5.8, 5.2$ Hz, 339H), 1.97 (s, 119H), 1.90 (s, 31H), 1.80 (s, 57H), 1.08-1.00 (m, 581H), 0.92-0.82 (m, 187H).

BCP-N₃-2: N₃-PEG_{77.5}-Br macroinitiator (150 mg, 41.6 μmol, 1 eq.), 2,2'-bipyridine (13 mg, 83.2 μmol, 2 eq.), DEAEMA (955.6 mg, 5.158 mmol, 124 eq.) and DMIBMA (342.1 mg, 1.289 mmol, 31 eq.) were added to a Schlenk tube equipped with a stirring bar. The mixed compounds were dissolved in 1.5 ml of 2-butanone and completely frozen in liquid nitrogen. The mixture was degassed using two freeze-pump-thaw-cycles and backfilled with argon. Following CuBr (6.0 mg, 41.6 μmol, 1 eq.) was added and the mixture was degassed using three freeze-pump-thaw-cycles again, backfilled with argon and stirred 17 h at 50 °C. To end the polymerization, the tube was opened, and the reaction mixture was diluted with THF and filtrated over neutral aluminum oxide to remove all copper species. The mixture was transferred to a dialysis membrane (regenerated cellulose, MWCO 5 kDa) and was dialysed against methanol (technical grade) for three days exchanging the solvent twice a day. Afterwards the solvent was removed under reduced pressure and the final product was dried in vacuo. Yield: 61% (883 mg).

¹H NMR (500 MHz, CDCl₃) (Figure A10): δ = 3.95 (d, *J* = 35.8 Hz, 324H), 3.64 (s, 310H), 3.51 (s, 64H), 2.69 (d, *J* = 6.7 Hz, 261H), 2.56 (q, *J* = 7.6 Hz, 517H), 1.97 (s, 181H), 1.90 (s, 51H), 1.82-1.78 (m, 108H), 1.03 (t, *J* = 7.1 Hz, 860H), 0.92-0.82 (m, 266H).

4.1.4 Synthesis of Bis-BCN Poly(ethylene glycol) Crosslinker (BisBCN-PEG)



Synthesis of BisBCN-PEG_{2k} Crosslinker. Anhydrous TEA (10.5 μL, 0.075 mmol, 3 eq.) and then exo-BCN-NHS carbonate solution (18.2 mg dissolved in 4 mL anhydrous DCM, 0.0625 mmol, 2.5 eq.) were slowly added into a solution of NH₂-PEG_{2k}-NH₂ (50 mg, 0.025 mmol, 1.0 eq.) in anhydrous DCM (10 mL) under ice bath. The reaction mixture was stirred 1 h at 0 °C and then removing the ice bath. Then the mixture was continued to stir overnight at RT. After that, the mixture was rotary evaporated to remove the solvent and re-dissolved in water. Then the suspension was filtrated by syringe filter with 0.2 μm pore size to remove insoluble BCN compound. Following the solution was transferred to a dialysis membrane (cellulose ester, MWCO 100-500 Da) and was dialysed against distilled water for three days to remove any impurities. Afterwards the bisBCN-PEG_{2k} solution was freeze-dried (white powder) and re-

dissolved in Milli-Q water to prepare 1 mg/mL solution. The bisBCN-PEG_{2k} solution should be stored in refrigerator at -20 °C to avoid self-crosslinking. Yield: 79% (46.5 mg).

¹H NMR (500 MHz, DMSO-*d*₆) (Figure A11): δ = 7.03 (s, 2H), 4.13-3.95 (m, 4H), 3.64 (s, 2H), 3.42-3.34 (m, 224H), 3.10 (q, *J* = 5.9 Hz, 4H), 2.32-2.02 (m, 11H), 1.51 (d, *J* = 11.7 Hz, 4H), 1.29-1.19 (m, 2H), 0.85 (t, *J* = 9.9 Hz, 4H).

¹³C NMR (126 MHz, DMSO-*d*₆) (Figure A12): δ = 171.75 (C=O), 166.46 (C=O), 136.59 (C), 135.88 (C), 125.51 (CH₂), 63.65 (CH₂), 36.81 (CH₂), 25.37 (CH₂), 24.61 (CH₂), 17.91 (CH₃), 8.36 (CH₃).

Synthesis of BisBCN-PEG_{1k} Crosslinker. Anhydrous TEA (16.7 μL, 0.12 mmol, 3 eq.) and then *exo*-BCN-NHS carbonate solution (29.1 mg dissolved in 5 mL anhydrous DCM, 0.10 mmol, 2.5 eq.) were slowly added into a solution of NH₂-PEG_{1k}-NH₂ (50 mg, 0.04 mmol, 1.0 eq.) in anhydrous DCM (10 mL) under ice bath. The reaction mixture was stirred 1 h at 0 °C and then removing the ice bath. Then the mixture was continued to stir overnight at RT. After that, the mixture was rotary evaporated to remove the solvent and re-dissolved in water. Then the suspension was filtrated by syringe filter with 0.2 μm pore size to remove insoluble BCN compound. Following the solution was transferred to a dialysis membrane (cellulose ester, MWCO 100-500 Da) dialysed against distilled water for three days to remove any impurities. Afterwards the bisBCN-PEG_{1k} solution was freeze-dried (yellowish oil) and re-dissolved in Milli-Q water to prepare 1 mg/mL solution. The bisBCN-PEG_{1k} solution should be stored in refrigerator at -20 °C to avoid self-crosslinking. Yield: 58% (37.2 mg).

¹H NMR (500 MHz, DMSO-*d*₆) (Figure A13): δ = 7.20-6.87 (m, 2H), 4.02 (d, *J* = 8.0 Hz, 4H), 3.38 (d, *J* = 6.1 Hz, 112H), 3.10 (q, *J* = 6.0 Hz, 4H), 2.30-1.68 (m, 11H), 1.65-1.40 (m, 4H), 1.26 (dt, *J* = 15.6, 7.6 Hz, 2H), 1.03 (s, 2H), 0.90-0.81 (m, 2H).

Synthesis of BisBCN-PEG_{0.1k} Crosslinker. Anhydrous TEA (56.4 μL, 0.405 mmol, 3 eq.) and then *exo*-BCN-NHS carbonate solution (98.3 mg dissolved in 10 mL anhydrous DCM, 0.337 mmol, 2.5 eq.) were slowly added into a solution of NH₂-PEG_{0.1k}-NH₂ (20 mg, 0.135 mmol, 1.0 eq.) in anhydrous DCM (10 mL) under ice bath. The reaction mixture was stirred 1 h at 0 °C and then removing the ice bath. Then the mixture was continued to stir overnight at RT. After that, the mixture was quenched with saturated aqueous NH₄Cl (20 mL). The product was extracted with DCM (3 x 20 mL), washed with saturated aqueous NaHCO₃ (20 mL) and brine (20 mL), dried by MgSO₄ and concentrated in vacuo. The bisBCN-PEG_{0.1k} was obtained after

column chromatography with *n*-hexane/EA (1: 1, vol/vol) mixture as a yellow oil. Yield: 74% (50 mg).

¹H NMR (500 MHz, CDCl₃) (Figure A14): δ = 5.28 (s, 2H), 4.32-4.00 (m, 4H), 3.66-3.49 (m, 8H), 3.44-3.27 (m, 4H), 2.59-1.80 (m, 11H), 1.62-1.50 (m, 4H), 1.26 (dd, J = 18.3, 9.5 Hz, 2H), 1.06-0.77 (m, 4H).

4.2 Formation of Empty and Loaded Psomes-N₃

4.2.1 Formation and Photo-Crosslinking of Empty-Psomes-N₃

10 mg BCP-N₃ or BCP-OCH₃ or mixed BCPs (w/w) was dissolved in 10 mL 0.01 M aqueous HCl solution (1 mg/mL) and then filtrated by syringe filter with 0.2 μ m pore size to remove any impurities. To initiate the self-assembly process, the pH value was adjusted slowly to pH 9 through dropwise addition of 1 M NaOH and then 0.1 M NaOH solution. Thus, Psomes-N₃ were formed after 3 days of stirring under dark conditions. Next, Psomes-N₃ were passed through 0.8 μ m nylon filter to remove any aggregates and crosslinked 180 s under UV irradiation for each 2 mL sample. (BCP-N₃-1 was used for optimization of clustering process, BCP-N₃-2 was used for characterization of purification steps and further enzymatic reactions).

4.2.2 Preparation of Cy5 Labeled BSA (BSA-Cy5)

6 mg BSA (90 nmol, 1 eq.) was dissolved in 6 mL 10 mM PBS buffer solution (pH 7.4) and then filtrated by syringe filter with 0.2 μ m pore size to remove any impurities. 120 μ L Cy5-NHS (1 mg/mL in DMSO, 180 nmol, 2 eq.) was slowly added into BSA solution. After overnight stirring at RT, the BSA-Cy5 was transferred to dialysis membrane (regenerated cellulose, MWCO 5 kDa), and dialysis against 0.1 mM PBS buffer (pH 7.4) was carried out for three days to remove DMSO, non-labeled Cy5 dye and NHS salt. Afterwards the BSA-Cy5 solution was freeze-dried and re-dissolved in 1 mM PBS buffer (pH 7.4) to prepare 2 mg/mL solution.

4.2.3 Preparation of RhB Labeled Myo (Myo-RhB)

10 mg Myo (0.6 μ mol, 1 eq.) was dissolved in 10 mL 10 mM PBS buffer solution (pH 7.4) and then filtrated by syringe filter with 0.2 μ m pore size to remove any impurities. 642 μ L RhB-ITC (1 mg/mL in DMSO, 1.2 μ mol, 2 eq.) was slowly added into Myo solution. After overnight stirring at RT, the Myo-RhB was transferred to dialysis membrane (regenerated cellulose,

MWCO 5 kDa) and dialysis against 0.1 mM PBS buffer (pH 7.4) was carried out for three days to remove DMSO and non-labeled RhB dye. Afterwards the Myo-RhB solution was freeze-dried and re-dissolved in 1 mM PBS buffer (pH 7.4) to prepare 2 mg/mL solution.

4.2.4 Preparation of Cy5 Labeled GOx (GOx-Cy5)

20 mg GOx (125 nmol, 1 eq.) was dissolved in 20 mL 10 mM PBS buffer solution (pH 7.4) and then filtrated by syringe filter with 0.2 μm pore size to remove any impurities. 167 μL Cy5-NHS (1 mg/mL in DMSO, 250 nmol, 2 eq.) was slowly added into GOx solution. After overnight stirring at RT, the GOx-Cy5 was transferred to dialysis membrane (regenerated cellulose, MWCO 5 kDa) and dialysed against 0.1 mM PBS buffer (pH 7.4) was carried out for three days to remove DMSO, non-labeled Cy5 dye and NHS salt. Afterwards the GOx-Cy5 solution was freeze-dried and re-dissolved in 1 mM PBS buffer (pH 7.4) to prepare 2 mg/mL solution.

4.2.5 Formation and Photo-Crosslinking of Loaded Psomes-N₃

11 mg BCP-N₃ was dissolved in 10 mL 0.01 M aqueous HCl solution and then filtrated by syringe filter with 0.2 μm pore size to remove any impurities. Then taking 9 mL BCP-N₃ solution into the 20 mL flask and the pH value was slowly adjusted to pH 5.0 through the dropwise addition of 1 M NaOH. Then the filtrated (dye labeled) enzyme/dye labeled protein aqueous solution (1 mL, 2 mg/mL) was added to the BCP-N₃ solution, and the pH value was slowly increased to pH 9.0 to initiate the self-assembly process of BCP-N₃ ($C[\text{BCP-N}_3] = 1 \text{ mg/mL}$; $C[\text{Enzyme/Protein}] = 0.2 \text{ mg/mL}$). Thus, GOx loaded Psomes-N₃ (GOx-Psomes-N₃), GOx-Cy5 loaded Psomes-N₃ (GOx-Cy5-Psomes-N₃), Myo loaded Psomes-N₃ (Myo-Psomes-N₃), Myo-RhB loaded Psomes-N₃ (Myo-RhB-Psomes-N₃), or BSA-Cy5 loaded Psomes-N₃ (BSA-Cy5-Psomes-N₃) were formed after 3 days of stirring under dark conditions. Next, loaded Psomes-N₃ were passed through 0.8 μm nylon filter to remove any aggregates and crosslinked 180 s under UV irradiation for each 2 mL sample. The HFF purification was used to remove non-encapsulated (Cy5 labeled) GOx or (RhB labeled) Myo or BSA-Cy5. 9 mL of the unpurified above solution (1 mg/mL) was transferred into a 50 mL cone tube attached to the hollow-fiber filtration system. The sample was diluted with a 10 mM PBS solution (pH 7.4) to 18 mL and constantly refilled until the extraction volume was reached. The transmembrane pressure was kept at 130 mbar during the whole process until extracting a total volume of 100 mL.

4.3 Preparation and Purification of Clustered Empty-Psomes-N₃

4.3.1 Preparation of Clustered Empty-Psomes-N₃ at Different Conditions

Clustering Polymersomes at Different Temperatures

BisBCN-PEG_{1k} (252 μ L, 1 mg/mL in water, 161.5 nmol, 5 eq. molar ratio to outside azido groups of polymersomes) was added to polymersomes solution, prepared by the self-assembly of 30% BCP-N₃-1 (10 mL, 0.5 mg/mL in 10 mM PBS buffer, pH 7.4, 32.3 nmol azido group on the outer surface of polymersomes). After 2 days of stirring at 40 °C, 50 °C, or 60 °C, the sizes of clusters were directly measured by DLS without termination step.

Clustering Polymersomes with Different Ratios of BCP-N₃

Clustering Polymersomes with 10% BCP-N₃. BisBCN-PEG_{1k} (17 μ L, 1 mg/mL in water, 10.8 nmol, 1 eq. molar ratio to outside azido groups of polymersomes) or bisBCN-PEG_{2k} (25 μ L, 1 mg/mL in water, 10.8 nmol, 1 eq. molar ratio to outside azido groups of polymersomes) was added to polymersomes solution, prepared by the self-assembly of 10% BCP-N₃-1 (10 mL, 0.5 mg/mL in 10 mM PBS buffer, pH 7.4, 10.8 nmol azido group on the outer surface of polymersomes). After 2 days of stirring at 40 °C, the sizes of clusters were directly measured by DLS without termination step.

Clustering Polymersomes with 30% BCP-N₃. BisBCN-PEG_{1k} (50 μ L, 1 mg/mL in water, 32.3 nmol, 1 eq. molar ratio to outside azido groups of polymersomes) or bisBCN-PEG_{2k} (76 μ L, 1 mg/mL in water, 32.3 nmol, 1 eq. molar ratio to outside azido groups of polymersomes) was added to polymersomes solution, prepared by the self-assembly of 30% BCP-N₃-1 (10 mL, 0.5 mg/mL in 10 mM PBS buffer, pH 7.4, 32.3 nmol azido group on the outer surface of polymersomes). After 2 days of stirring at 40 °C the sizes of clusters were directly measured by DLS without termination step.

Clustering Polymersomes with 40% BCP-N₃. BisBCN-PEG_{1k} (67 μ L, 1 mg/mL in water, 43.1 nmol, 1 eq. molar ratio to outside azido groups of polymersomes) or bisBCN-PEG_{2k} (101 μ L, 1 mg/mL in water, 43.1 nmol, 1 eq. molar ratio to outside azido groups of polymersomes) was added to polymersomes solution, prepared by the self-assembly of 40% BCP-N₃-1 (10 mL, 0.5 mg/mL in 10 mM PBS buffer, pH 7.4, 43.1 nmol azido group on the outer surface of

polymersomes). After 2 days of stirring at 40 °C, the sizes of clusters were directly measured by DLS without termination step.

Clustering Polymersomes with 60% BCP-N₃. BisBCN-PEG_{1k} (101 μL, 1 mg/mL in water, 64.6 nmol, 1 eq. molar ratio to outside azido groups of polymersomes) or bisBCN-PEG_{2k} (152 μL, 1 mg/mL in water, 64.6 nmol, 1 eq. molar ratio to outside azido groups of polymersomes) was added to polymersomes solution, prepared by the self-assembly of 60% BCP-N₃-1 (10 mL, 0.5 mg/mL in 10 mM PBS buffer, pH 7.4, 64.6 nmol azido group on the outer surface of polymersomes). After 2 days of stirring at 40 °C, the sizes of clusters were directly measured by DLS without termination step.

Clustering Polymersomes with 80% BCP-N₃. BisBCN-PEG_{1k} (134 μL, 1 mg/mL in water, 86.1 nmol, 1 eq. molar ratio to outside azido groups of polymersomes) or bisBCN-PEG_{2k} (202 μL, 1 mg/mL in water, 86.1 nmol, 1 eq. molar ratio to outside azido groups of polymersomes) was added to polymersomes solution, prepared by the self-assembly of 80% BCP-N₃-1 (10 mL, 0.5 mg/mL in 10 mM PBS buffer, pH 7.4, 86.1 nmol azido group on the outer surface of polymersomes). After 2 days of stirring at 40 °C, the sizes of clusters were directly measured by DLS without termination step.

Clustering Polymersomes with 100% BCP-N₃. BisBCN-PEG_{1k} (168 μL, 1 mg/mL in water, 107.7 nmol, 1 eq. molar ratio to outside azido groups of polymersomes) or bisBCN-PEG_{2k} (253 μL, 1 mg/mL in water, 107.7 nmol, 1 eq. molar ratio to outside azido groups of polymersomes) was added to polymersomes solution, prepared by the self-assembly of 100% BCP-N₃-1 (10 mL, 0.5 mg/mL in 10 mM PBS buffer, pH 7.4, 107.7 nmol azido group on the outer surface of polymersomes). After 2 days of stirring at 40 °C, the sizes of clusters were directly measured by DLS without termination step.

Clustering Polymersomes for Different Reaction Time

Clustering Polymersomes with 10% BCP-N₃. BisBCN-PEG_{1k} (17 μL, 1 mg/mL in water, 10.8 nmol, 1 eq. molar ratio to outside azido groups of polymersomes) or bisBCN-PEG_{2k} (25 μL, 1 mg/mL in water, 10.8 nmol, 1 eq. molar ratio to outside azido groups of polymersomes) was added to polymersomes solution, prepared by the self-assembly of 10% BCP-N₃-1 (10 mL, 0.5 mg/mL in 10 mM PBS buffer, pH 7.4, 10.8 nmol azido group on the outer surface of polymersomes). After 2, 9, 30 days of stirring at 40 °C, the sizes of clusters were directly measured by DLS without termination step.

Clustering Polymersomes with 30% BCP-N₃. BisBCN-PEG_{1k} (50 μL, 1 mg/mL in water, 32.3 nmol, 1 eq. molar ratio to outside azido groups of polymersomes) or bisBCN-PEG_{2k} (76 μL, 1 mg/mL in water, 32.3 nmol, 1 eq. molar ratio to outside azido groups of polymersomes) was added to polymersomes solution, prepared by the self-assembly of 30% BCP-N₃-1 (10 mL, 0.5 mg/mL in 10 mM PBS buffer, pH 7.4, 32.3 nmol azido group on the outer surface of polymersomes). After 1, 2, 4 days of stirring at 40 °C the sizes of clusters were directly measured by DLS without termination step.

Clustering Polymersomes with Different Ratios of Crosslinker

Different equivalents molar ratio (1 eq.: 10 μL, 6.5 nmol; 5 eq.: 50 μL, 32.3 nmol; 10 eq.: 100 μL, 64.6 nmol; 20 eq.: 200 μL, 129.2 nmol; 50 eq.: 500 μL, 323 nmol; 100 eq.: 1 mL, 646 nmol) of bisBCN-PEG_{1k} (1 mg/mL in water) to outside azido groups of polymersomes were respectively added to polymersomes solution, prepared by the self-assembly of 30% BCP-N₃-1 (2 mL, 0.5 mg/mL in 10 mM PBS buffer, pH 7.4, 6.5 nmol azido group on the outer surface of polymersomes). After 2 days of stirring at 40 °C the sizes of clusters were directly measured by DLS without termination step.

Clustering Polymersomes with Different Lengths of Crosslinker

Clustering Polymersomes with 30% BCP-N₃. BisBCN-PEG_{0.1k} (16 μL, 1 mg/mL in DMSO, 32.3 nmol, 1 eq. molar ratio to outside azido groups of polymersomes) or bisBCN-PEG_{1k} (50 μL, 1 mg/mL in water, 32.3 nmol, 1 eq. molar ratio to outside azido groups of polymersomes) or bisBCN-PEG_{2k} (76 μL, 1 mg/mL in water, 32.3 nmol, 1 eq. molar ratio to outside azido groups of polymersomes) was added to polymersomes solution, prepared by the self-assembly of 30% BCP-N₃-1 (10 mL, 0.5 mg/mL in 10 mM PBS buffer, pH 7.4, 32.3 nmol azido group on the outer surface of polymersomes). After 4 days of stirring at 40 °C the sizes of clusters were directly measured by DLS without termination step.

Clustering Polymersomes with 40% BCP-N₃. BisBCN-PEG_{0.1k} (22 μL, 1 mg/mL in DMSO, 43.1 nmol, 1 eq. molar ratio to outside azido groups of polymersomes) or bisBCN-PEG_{1k} (67 μL, 1 mg/mL in water, 43.1 nmol, 1 eq. molar ratio to outside azido groups of polymersomes) or bisBCN-PEG_{2k} (101 μL, 1 mg/mL in water, 43.1 nmol, 1 eq. molar ratio to outside azido groups of polymersomes) was added to polymersomes solution, prepared by the self-assembly of 40% BCP-N₃-1 (10 mL, 0.5 mg/mL in 10 mM PBS buffer, pH 7.4, 43.1 nmol azido group

on the outer surface of polymersomes). After 2 days of stirring at 40 °C, the sizes of clusters were directly measured by DLS without termination step.

Clustering Polymersomes with 100% BCP-N₃. BisBCN-PEG_{0.1k} (54 μL, 1 mg/mL in DMSO, 107.7 nmol, 1 eq. molar ratio to outside azido groups of polymersomes) or bisBCN-PEG_{1k} (168 μL, 1 mg/mL in water, 107.7 nmol, 1 eq. molar ratio to outside azido groups of polymersomes) or bisBCN-PEG_{2k} (253 μL, 1 mg/mL in water, 107.7 nmol, 1 eq. molar ratio to outside azido groups of polymersomes) was added to polymersomes solution, prepared by the self-assembly of 100% BCP-N₃-1 (10 mL, 0.5 mg/mL in 10 mM PBS buffer, pH 7.4, 107.7 nmol azido group on the outer surface of polymersomes). After 2 days of stirring at 40 °C, the sizes of clusters were directly measured by DLS without termination step.

Clustering Polymersomes at Different Concentrations

BisBCN-PEG_{1k} (1 mg/mL in water, 1 eq. molar ratio to outside azido groups of polymersomes: 33.6 μL (21.5 nmol) for 0.1 mg/mL polymersomes, 168 μL (107.7 nmol) for 0.5 mg/mL polymersomes, or 336 μL (215.4 nmol) for 1 mg/mL polymersomes) was added to polymersomes solution, prepared by the self-assembly of 100% BCP-N₃-1 (10 mL 0.1 mg/mL or 0.5 mg/mL in 10 mM PBS buffer at pH 7.4 or 10 mL 1 mg/mL in 10 mM NaCl solution at pH 7.4). After 1 day of stirring at 40 °C, the sizes of clusters were directly measured by DLS without termination step.

4.3.2 Optimized Preparation of Clustered Empty-Psomes-N₃

BisBCN-PEG_{1k} (216 μL, 1 mg/mL in water, 138 nmol, 1 eq. molar ratio to outside azido groups of polymersomes) was added to polymersomes solution, prepared by the self-assembly of 100% BCP-N₃-2 (20 mL, 0.5 mg/mL in 10 mM PBS buffer, pH 7.4, 138 nmol azido group on the outer surface of polymersomes). After 2 days of stirring at 40 °C, the N₃-PEG₃-OH (2.8 μL, 0.5 M in tert-butyl methyl ether, 1.38 μmol, 10 eq. molar ratio to bisBCN-PEG_{1k}) was added to the suspension to terminate the reaction for 6 h at 40 °C. The resulting suspension was purified by three different protocols to remove isolated polymersomes and smaller clustered polymersomes.

4.3.3 Purification Method of Clustered Empty-Psomes-N₃

Protocol 1: The resulting suspension (5 mL) was purified by 4 times centrifugation at 6000 rpm for 5 min. After each centrifugation step the precipitates were redispersed in the same

volume of PBS buffer (5 mL, 1 mM, pH 8.0) by mechanical stirring treatment for several seconds. After that, the suspension was performed acidification step to redisperse the aggregates triggered by centrifugation. The acidification process includes three steps: (i) adjusting the pH value of the suspension from pH 8.0 to pH 6.0; (ii) followed up continuous 5 min mechanical stirring at pH 6.0; (iii) finally the pH value of the suspension was adjusted back to pH 8.0.

Protocol 2: The resulting suspension (5 mL) was purified by once centrifugation at 6000 rpm for 5 min and then the precipitates were redispersed in PBS buffer (5 mL, 1 mM, pH 8.0) by mechanical stirring treatment for several seconds. Then the acidification process was performed to redisperse the aggregates triggered by centrifugation. Following the suspension was purified again by 3 times centrifugation at 6000 rpm for 5 min. After each centrifugation step the precipitates were redispersed in the same volume of PBS buffer (5 mL, 1 mM, pH 8.0) by mechanical stirring treatment for several seconds. The final suspension was repeated with acidification process to redisperse the undesired aggregates.

Protocol 3: The resulting suspension (5 mL) was purified by 4 times centrifugation at 6000 rpm for 5 min. After each centrifugation step the precipitate was redispersed in the same volume of PBS buffer (5 mL, 1 mM, pH 8.0) by vortex treatment for several seconds. The suspension was used for various investigations without any acidification step.

4.3.4 DLS Measurement of the Empty-Psomes-N₃ in the Supernatant

After terminating the clustering process and once centrifugation at 6000 rpm for 5 min, the size of supernatant was measured by DLS. To know the composition in the supernatant, 5 cycles of pH switch of the supernatant were performed through adjusting pH value between 8.0 and 6.0.

4.3.5 Quantification of Removed Psomes-N₃ after Centrifugal Purification

To completely remove isolated polymersomes from clustered polymersomes, the fluorescence spectra of clustered BSA-Cy5-Psomes-N₃ (0.5 mg/mL in 1 mM PBS buffer, pH 8.0) after repetitive centrifugation steps were recorded at an excitation wavelength of 622 nm by fluorescence spectroscopy. Clustered BSA-Cy5-Psomes-N₃ without centrifugation (0.5 mg/mL in 10 mM PBS buffer, pH 7.4) as control was also investigated.

4.4 Preparation and Purification of Clustered Enzyme-Psomes-N₃: Enzymatic Cascade Reaction

4.4.1 Preparation of Clustered GOx or Myo Loaded Psomes-N₃ (GOx-Psomes-N₃ or Myo-Psomes-N₃)

BisBCN-PEG_{1k} (108 μ L, 1 mg/mL in water, 69 nmol, 1 eq. molar ratio to outside azido groups of polymersomes) was added to GOx-Psomes-N₃ or Myo-Psomes-N₃ solution (10 mL, 0.5 mg Psomes-N₃/mL in 10 mM PBS buffer, pH 7.4). After stirring 2 days at 40 °C, N₃-PEG₃-OH (1.4 μ L, 0.5 M in tert-butyl methyl ether, 0.69 μ mol, 10 eq. molar ratio to bisBCN-PEG_{1k}) was added to the suspension to terminate the reaction for 6 h at 40 °C. The resulting suspension was purified to remove bisBCN-PEG_{1k} crosslinker, N₃-PEG₃-OH, isolated Psomes-N₃ and smaller clustered Psomes-N₃. After purification, clustered GOx-Psomes-N₃ or Myo-Psomes-N₃ lost 40% Enzyme-Psomes and then the concentration of Psomes-N₃ is identified as 0.3 mg/mL. As control, GOx-Psomes-N₃, Myo-Psomes-N₃ and heated Myo/GOx-Psomes-N₃ without crosslinker (40 °C for 2 d) were also used to check the enzyme activity.

4.4.2 Enzyme Activity of Myo Samples

To check the influence of Myo activity, the pH values of Myo-Psomes-N₃ (2.2 mL, 0.3 mg/mL in 10 mM PBS buffer, pH 8.0), heated Myo-Psomes-N₃ (2.2 mL, 0.3 mg/mL in 10 mM PBS buffer, pH 8.0) or clustered Myo-Psomes-N₃ (2.2 mL, 0.3 mg/mL in 10 mM PBS buffer) were adjusted from pH 8.0 to pH 6.5. The resulting solutions were divided into 2 samples (one for 200 μ L, another for 2 mL), respectively: (i) For the samples with 200 μ L, the same volume of PBS buffer (0.1 M, pH 7.5) was directly added to the sample to immediately increase the pH value to 7.5. Then 3.2 μ L Amplex Red solution (0.02 mg/mL) and 3.2 μ L H₂O₂ solution (0.02 M) were added to the solution to initiate the enzyme assay. After 30 min stirring, fluorescence spectra were recorded at an excitation wavelength of 534 nm; and (ii) for the samples with 2 mL, 32 μ L Amplex Red (0.02 mg/mL) and 32 μ L H₂O₂ aqueous solution (0.02 M) were added to the solution to initiate the enzyme assay. After different time points (10, 20, 30 and 60 min), taking 200 μ l from each assay solution into a vial and the same volume of PBS buffer (0.1 M, pH 7.5) was directly added to the vial solution to increase the pH value to 7.5 immediately. After 30 min stirring under dark conditions, fluorescence spectra were recorded at an excitation wavelength of 534 nm by microplate reader ($\lambda_{em} = 585$ nm).

4.4.3 Enzyme Activity of GOx Samples

To check the influence of GOx activity, the pH values of GOx-Psomes-N₃ (2.2 mL, 0.3 mg Psomes-N₃/mL in 10 mM PBS buffer, pH 8.0), heated GOx-Psomes-N₃ (2.2 mL, 0.3 mg Psomes-N₃/mL in 10 mM PBS buffer, pH 8.0) or clustered GOx-Psomes-N₃ (2.2 mL, 0.3 mg Psomes-N₃/mL in 10 mM PBS buffer) were adjusted from pH 8.0 to pH 6.5. The resulting solutions were divided into 2 samples (one for 200 μ L, another for 2 mL), respectively: (i) For the samples with 200 μ L, the same volume of PBS buffer (0.1 M, pH 7.5) was directly added to the sample to increase the pH value to 7.5 immediately. Then 2.24 μ L glucose (0.02 mg/mL) was added to the solution to initiate the enzyme assay in total for 9 min. Then 3.2 μ L Amplex Red (0.02 mg/mL) and 4.2 μ L Myo (0.2 mg/mL, fresh prepared in ultrapure water) were added to the solution. After 30 min stirring, fluorescence spectra were recorded at an excitation wavelength of 534 nm; and (ii) for the samples with 2 mL, 22.4 μ L glucose (0.02 mg/mL) was added to the solution to initiate the enzyme assay in total for 9 min. Then 32 μ L Amplex Red (0.02 mg/mL) and 42 μ L Myo solution (0.02 M) were added to the solution. After different time points (10, 20, 30 and 60 min), taking 200 μ L from each assay solution into a vial and the same volume of PBS buffer (0.1 M, pH 7.5) was directly added to the solution to immediately increase the pH value to 7.5. After 30 min stirring, fluorescence spectra were recorded at an excitation wavelength of 534 nm by microplate reader ($\lambda_{em} = 585$ nm).

4.5 Preparation and Purification of Co-Clustered Enzyme-Psomes-N₃: Enzymatic Cascade Reaction

4.5.1 Preparation of Co-Clustered Myo/GOx-Psomes-N₃

BisBCN-PEG_{1k} (108 μ L, 1 mg/mL in water, 69 nmol, 1 eq. molar ratio to outside azido groups of Psomes) was added to mixed HFF-purified GOx-Psomes-N₃ and Myo-Psomes-N₃ solution (10 mL, V[GOx-Psomes-N₃]: V[Myo-Psomes-N₃] = 1: 1, 0.5 mg Psomes-N₃/mL in 10 mM PBS buffer, pH 8.0). After 2 days stirring at 40 °C, N₃-PEG₃-OH (1.4 μ L, 0.5 M in tert-butyl methyl ether, 0.69 μ mol, 10 eq. molar ratio to bisBCN-PEG_{1k}) was added to the suspension to terminate the reaction for 6 h at 40 °C. The resulting suspension was purified by the same protocol as described before. As control, mixed Myo/GOx-Psomes-N₃ and heated Myo/GOx-Psomes-N₃ without crosslinker (40 °C for 2 days) were also used to check the enzyme activity.

4.5.2 Enzyme Activity of Co-Clustered Myo/GOx-Psomes-N₃ Samples

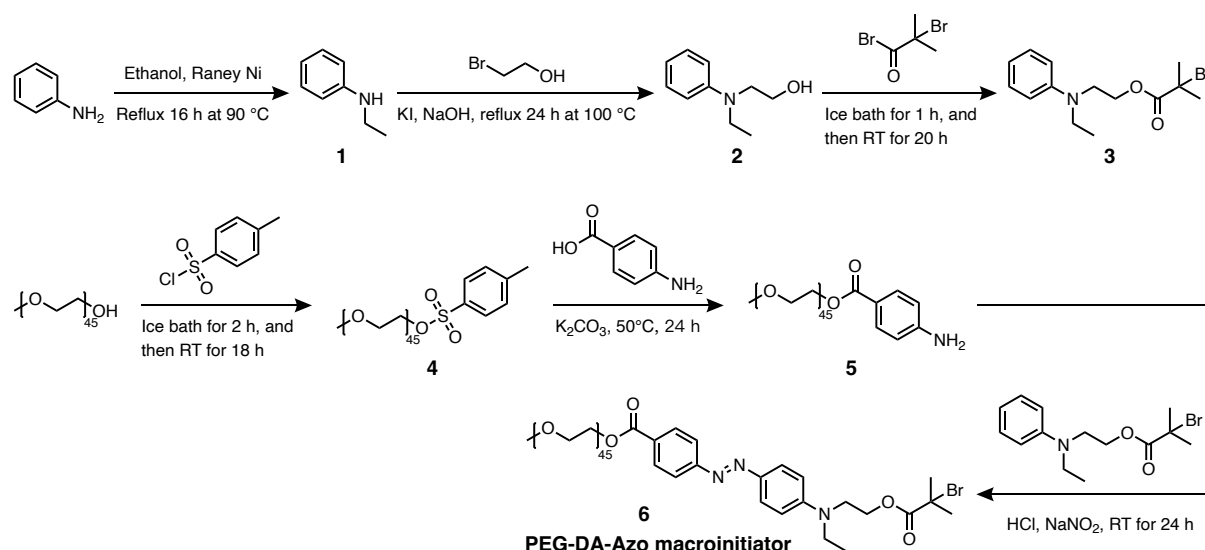
To measure the efficiency of enzymatic cascade reaction, the pH values of mixed Myo/GOx-Psomes-N₃ (2.2 mL, 0.3 mg Psomes-N₃/mL in 10 mM PBS buffer, pH 8.0), heated Myo/GOx-Psomes-N₃ (2.2 mL, 0.3 mg Psomes-N₃/mL in 10 mM PBS buffer, pH 8.0) and co-clustered Myo/GOx-Psomes-N₃ (2.2 mL, 0.3 mg Psomes-N₃/mL in 10 mM PBS buffer, pH 8.0) were adjusted from pH 8.0 to pH 6.5 to protonate the membrane completely and to pH 7.0 to semi-protonate the membrane, respectively. In addition, pH 8.0 and pH 7.5 (membrane totally deprotonated) as control. The resulting solutions were divided into 2 samples (one for 200 μ L, another for 2 mL), respectively: (i) For the samples with 200 μ L, the pH value was adjusted to 7.5 by the dropwise addition of 0.1 M and 0.01 M NaOH solution. Then 5.6 μ L glucose (0.02 mg/mL) and 8 μ L Amplex Red (0.02 mg/mL) were added to the solution to initiate the enzyme assay. After 30 min stirring, fluorescence spectra were recorded at an excitation wavelength of 534 nm; and (ii) for the samples with 2 mL, 56 μ L glucose (0.02 mg/mL) and 80 μ L Amplex Red (0.02 mg/mL) were added to the solution to initiate the enzyme assay. After different time points (10, 20, 30 and 60 min), taking 200 μ l from each assay solution into a vial and then the pH value was increased to 7.5 by 0.1 M and 0.01 M NaOH solution. After 30 min stirring, fluorescence spectra were recorded at an excitation wavelength of 534 nm by microplate reader ($\lambda_{em} = 585$ nm).

5 Light-Driven Enzyme Reaction Based on pH-Responsive Polymersomes

5.1 Synthetic Methods and Characterization of Block Copolymers with Single Azobenzene Unit

5.1.1 Synthesis of Block Copolymer with Donor-Acceptor-Substituted Azobenzene Linkage between Hydrophilic and Hydrophobic Segments (BCP-DA-Azo)

Synthesis of PEG Macroinitiator with Donor-Acceptor-Substituted Azobenzene (PEG-DA-Azo Macroinitiator)



Synthesis of Compound 1: Raney®-Nickel (25 g) after washing by ethanol and aniline (20 g, 214.8 mmol) dissolved in 100 mL ethanol were added into a 250 mL round-bottom flask. Then the mixture was refluxed 90 °C for 16 h. Following the reaction was cooled down to RT and was filtrated under reduced pressure with filter aid Celite®545 to remove catalyst Raney®-Nickel. Finally, the product was obtained as yellow oil after evaporating the solvent ethanol and water. Yield: 71% (18.5 g).

^1H NMR (500 MHz, $\text{DMSO-}d_6$) (Figure A15): δ = 7.13-6.98 (m, 2H), 6.55-6.50 (m, 2H), 6.50-6.43 (m, 1H), 5.41 (t, J = 5.3 Hz, 1H), 3.00 (qd, J = 7.1, 5.4 Hz, 2H), 1.14 (t, J = 7.1 Hz, 3H).

^{13}C NMR (126 MHz, $\text{DMSO-}d_6$) (Figure A16): δ = 149.45, 129.29, 115.87, 112.39, 37.74, 14.88.

Synthesis of Compound 2: **Compound 1** (10 g, 82.5 mmol, 1 eq.), 2-bromoethanol (20.62 g, 165 mmol, 2 eq.), NaOH (6.60 g, 165 mmol, 2 eq.) and KI (2.74 g, 16.5 mmol, 0.2 eq.) were mixed in a 100 mL round-bottom flask and then placed it in a pre-heated oil bath at 100 °C. After reflux for 24 h, the yellow liquid and white powder changed to a red brown liquid. Following the reaction was cooled to RT and was extracted by EA. Then washing 3 times with brine and drying by anhydrous MgSO₄. Finally, the product was obtained as red brown oil by column chromatography with *n*-hexane/EA (2: 1, vol/vol) mixture. Yield: 56% (7.64 g).

¹H NMR (500 MHz, DMSO-*d*₆) (Figure A17): δ = 7.14-7.07 (m, 2H), 6.67-6.61 (m, 2H), 6.52 (t, *J* = 7.2 Hz, 1H), 4.64 (t, *J* = 5.3 Hz, 1H), 3.51 (q, *J* = 6.2 Hz, 2H), 3.38-3.30 (m, 4H), 1.05 (t, *J* = 7.0 Hz, 3H).

¹³C NMR (126 MHz, DMSO-*d*₆) (Figure A18): δ = 148.18, 129.52, 115.36, 111.80, 58.83, 52.56, 44.98, 12.41.

Synthesis of Compound 3: **Compound 2** (1.4 g, 8.47 mmol, 1 eq.) dissolved in 20 mL anhydrous DCM was mixed with dry TEA (2.36 mL, 16.95 mmol, 2 eq.). Then α-bromoisobutyryl bromide (1.57 mL, 12.71 mmol, 1.5 eq.) was dropwise added into the mixture under ice bath. After stirring at 0 °C for 1 h, the reaction was continued to stir at RT for 20 h. Following the mixture was washed 3 times by brine and then was dried by anhydrous MgSO₄. Finally, the product was obtained as red brown oil by column chromatography with EA: *n*-Hexane (1: 4, vol/vol) mixture. Yield: 88% (2.34 g).

¹H NMR (500 MHz, DMSO-*d*₆) (Figure A19): δ = 7.17-7.10 (m, 2H), 6.71 (d, *J* = 8.2 Hz, 2H), 6.58 (t, *J* = 7.2 Hz, 1H), 4.26 (t, *J* = 5.8 Hz, 2H), 3.57 (t, *J* = 5.8 Hz, 2H), 3.39 (q, *J* = 7.0 Hz, 2H), 1.85 (s, 6H), 1.08 (t, *J* = 6.9 Hz, 3H).

¹³C NMR (126 MHz, DMSO-*d*₆) (Figure A20): δ = 171.40, 147.84, 129.60, 116.11, 112.30, 64.08, 57.65, 48.23, 44.78, 30.69, 12.39.

Synthesis of Compound 4: CH₃O-PEG₄₅-OH (5 g, 2.5 mmol, 1 eq.) and TEA (1.05 mL, 7.5 mmol, 3 eq.) were added into a 100 mL round-bottom flask and were dissolved in 50 mL dry DCM. Then the reaction mixture was cooled down to 0 °C. Then *p*-toluenesulfonyl chloride (1.192 g, 6.25 mmol, 2.5 eq.) was added to the reaction mixture and it was allowed to go on for 2 h under ice bath followed by 18 h at RT. After this, the product was precipitated from cold diethyl ether and was recrystallized from ethanol. Yield: 92% (4.95 g).

¹H NMR (500 MHz, CDCl₃) (Figure A21): δ = 7.88-7.73 (m, 2H), 7.34 (d, *J* = 7.9 Hz, 2H), 4.15 (t, *J* = 4.9 Hz, 2H), 3.64 (s, 181H), 3.37 (s, 3H), 2.44 (s, 3H).

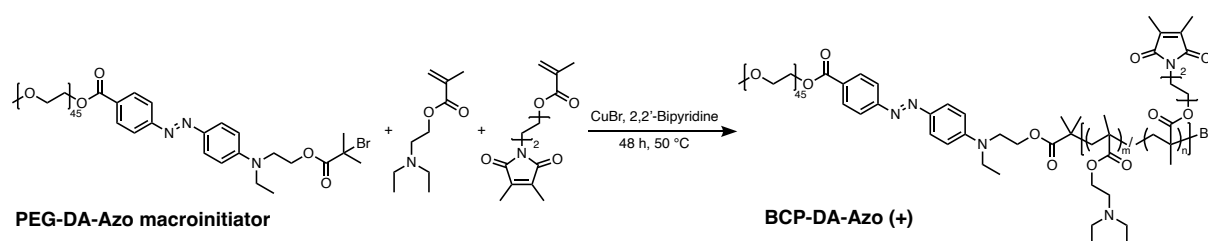
Synthesis of Compound 5: **Compound 4** (4 g, 1.85 mmol, 1 eq.) and 4-aminobenzoic acid (505.9 mg, 3.69 mmol, 2 eq.) were taken up in a round-bottom flask and were dissolved in 50 mL dry DMF along with K₂CO₃ powder (509.8 mg, 3.69 mmol, 2 eq.). The reaction mixture was placed in a preheated oil bath at 50 °C and was stirred for 24 h. Then the reaction was stopped and was poured into an excess of cold diethyl ether to precipitate the product. It was recrystallized in ethanol to get pure product. Yield: 85% (3.35 g).

¹H NMR (500 MHz, CDCl₃) (Figure A22): δ = 7.95-7.71 (m, 2H), 6.72-6.54 (m, 2H), 4.49-4.35 (m, 2H), 4.20 (s, 2H), 3.64 (s, 185H), 3.38 (s, 3H).

Synthesis of Compound 6 (PEG-DA-Azo Macroinitiator): Aqueous solution (30 mL) of **Compound 5** (3 g, 1.41 mmol, 1 eq.) was cooled down to 0 °C and 375 μL of concentrated HCl solution (4.51 mmol, 3.2 eq.) was added along with aqueous NaNO₂ solution (310.5 mg in 2 mL water, 4.51 mmol, 3.2 eq.). Then cold DMF solution of **Compound 3** (883.7 mg, 2.81 mmol, 2 eq.) was added dropwise to the reaction mixture and was allowed to stir at RT for 24 h under inert atmosphere. The reaction mixture was firstly neutralized by saturated Na₂CO₃ solution and then was evaporated to remove water and DMF. Following the mixture was recrystallized in 400 mL ethanol at -20 °C. The recrystallization process was repeated 5 times until the filtrate becomes colorless. Yield: 77% (2.66 g).

¹H NMR (500 MHz, CDCl₃) (Figure A23): δ = 8.17-8.08 (m, 2H), 7.94-7.77 (m, 4H), 6.89-6.69 (m, 2H), 4.51-4.45 (m, 2H), 4.38 (t, *J* = 6.1 Hz, 2H), 3.62 (d, *J* = 3.3 Hz, 201H), 3.36 (s, 3H), 1.90 (s, 6H), 1.25 (t, *J* = 7.0 Hz, 3H).

Synthesis of Block Copolymer with Donor-Acceptor-Substituted Azobenzene Linkage and Copolymerization of Photo-Crosslinker (BCP-DA-Azo (+))

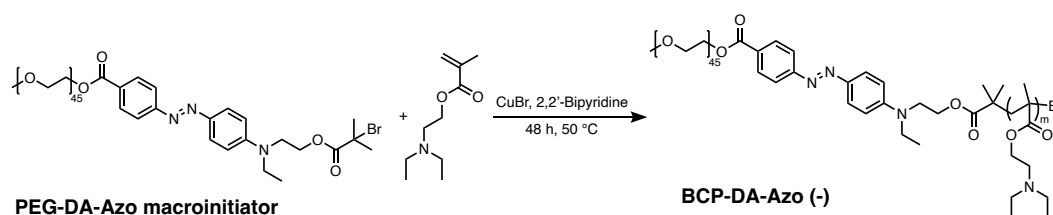


Polymerization of BCP-DA-Azo (+): PEG-DA-Azo macroinitiator (**Compound 6**, 100 mg, 0.0407 mmol, 1 eq.), 2,2'-bipyridine (12.7 mg, 0.0813 mmol, 2 eq.), DEAEEMA (542.5 mg,

2.928 mmol, 72 eq.) and DMIBMA (194.2 mg, 0.732 mmol, 18 eq.) were added to a Schlenk tube equipped with a stirring bar. The compounds were dissolved in 1.5 ml of 2-butanone and were completely frozen in liquid nitrogen. The mixture was degassed using two freeze-pump-thaw-cycles and then backfilled with argon. Now CuBr (5.8 mg, 0.0407mmol, 1 eq.) was added onto the frozen solution. Following the mixture was degassed using three freeze-pump-thaw-cycles and then backfilled with argon and stirred 48 h at 50°C. To end the polymerization, the tube was opened, and the reaction mixture was diluted with 3 mL THF and was filtrated over aluminium oxide to remove all copper species. The concentrated mixture after evaporating part of solvent was precipitated in the cold *n*-hexane. Then the supernatant was poured out and then the solid was transferred to a dialysis membrane (regenerated cellulose, MWCO 5 kDa) and dialysed against methanol (technical grade) for two days exchanging the solvent twice a day. Afterwards the solvent is removed under reduced pressure and the final product is dried in vacuo. Yield: 66% (522 mg).

¹H NMR (500 MHz, CDCl₃) (Figure A24): δ = 8.14 (d, *J* = 8.3 Hz, 2H), 7.86 (dd, *J* = 17.4, 8.2 Hz, 4H), 6.80 (d, *J* = 8.8 Hz, 2H), 4.49 (t, *J* = 4.9 Hz, 2H), 4.31-3.80 (m, 215H), 3.64 (s, 198H), 3.52 (d, *J* = 9.0 Hz, 26H), 3.37 (s, 3H), 2.90-2.36 (m, 513H), 1.03 (t, *J* = 7.0 Hz, 608H), 0.86 (d, *J* = 20.1 Hz, 214H).

Synthesis of Block Copolymer with Donor-Acceptor-Substituted Azobenzene Linkage but without Copolymerization of Photo-Crosslinker (BCP-DA-Azo (-))



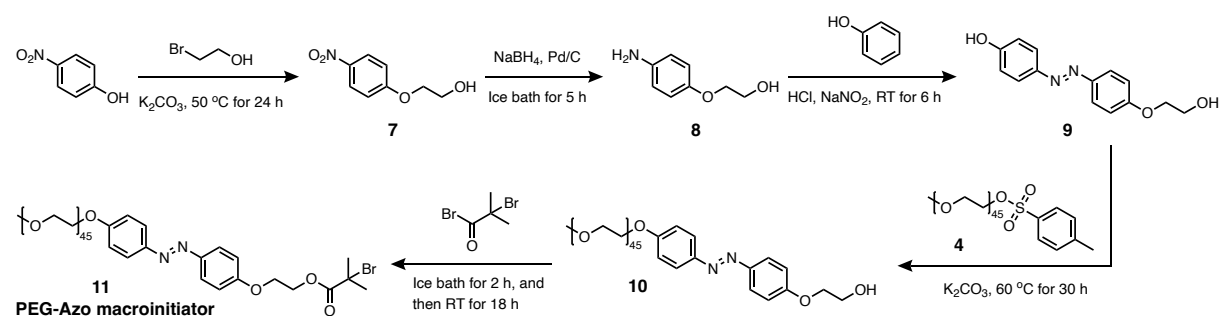
Polymerization of BCP-DA-Azo (-): PEG-DA-Azo macroinitiator (**Compound 6**, 100 mg, 0.0407 mmol, 1 eq.), 2,2'-bipyridine (12.7 mg, 0.0813 mmol, 2 eq.) and DEAEEMA (678.1 mg, 3.66 mmol, 90 eq.) were added to a Schlenk tube equipped with a stirring bar. The compounds were dissolved in 1.5 ml of 2-butanone and completely frozen in liquid nitrogen. The mixture was degassed using two freeze-pump-thaw-cycles and then backfilled with argon. Now CuBr (5.8 mg, 0.0407mmol, 1 eq.) was added onto the frozen solution. Following the mixture was degassed using three freeze-pump-thaw-cycles and then backfilled with argon and stirred 48 h at 50 °C. To end the polymerization, the tube was opened, and the reaction mixture was diluted

with 3 mL THF and was filtrated over aluminium oxide to remove all copper species. The concentrated mixture after evaporating a part of the solvent was precipitated in the cold *n*-hexane. Then pouring out the supernatant and then the solid was transferred to a dialysis membrane (regenerated cellulose, MWCO 5 kDa) and was dialysed against methanol (technical grade) for two days exchanging the solvent twice a day. Afterwards the solvent was removed under reduced pressure and the final product was dried in vacuo. Yield: 69% (537 mg).

^1H NMR (500 MHz, CDCl_3) (Figure A25): δ = 8.15 (d, J = 8.3 Hz, 2H), 7.86 (dd, J = 17.0, 8.5 Hz, 4H), 6.80 (d, J = 8.8 Hz, 2H), 4.49 (t, J = 4.8 Hz, 2H), 4.14-3.89 (m, 255H), 3.64 (s, 180H), 3.38 (s, 3H), 2.86-2.38 (m, 789H), 1.04 (q, J = 7.2, 6.6 Hz, 900H), 0.89 (t, J = 8.7 Hz, 255H).

5.1.2 Synthesis of Block Copolymer with Ether Substituted Azobenzene Linkage between Hydrophilic and Hydrophobic Segments (BCP-Azo)

Synthesis of PEG Macroinitiator with Ether Substituted Azobenzene (PEG-Azo Macroinitiator)



Synthesis of Compound 7: 4-Nitrophenol (5.0 g, 35.9 mmol, 1 eq.) and 2-bromoethanol (6.7 g, 53.9 mmol, 1.5 eq.) were dissolved in 100 mL anhydrous DMF, and then the mixture was placed in pre-heated oil bath at 50°C . K_2CO_3 powder (9.9 g, 71.9 mmol, 2 eq.) was added to the mixture. After stirring 24 h at 50°C , the reaction mixture was poured into 3 L water, and the crude product was precipitated out. Following the precipitate was extracted by EA and was washed by saturated Na_2CO_3 solution for 3 times as well as dried by anhydrous MgSO_4 . Finally, the product was obtained as white powder after evaporating the EA. Yield: 85% (5.6 g).

^1H NMR (500 MHz, $\text{DMSO}-d_6$) (Figure A26): δ = 8.19 (d, J = 8.9 Hz, 2H), 7.14 (d, J = 8.9 Hz, 2H), 4.93 (t, J = 5.4 Hz, 1H), 4.13 (t, J = 4.8 Hz, 2H), 3.74 (q, J = 4.9 Hz, 2H).

^{13}C NMR (126 MHz, $\text{DMSO}-d_6$) (Figure A27): δ = 164.60, 141.22, 126.33, 115.52, 71.10, 59.78.

Synthesis of Compound 8: **Compound 7** (2.4 g, 13.1 mmol, 1 eq.) was dissolved in 30 mL methanol and was mixed with 10% Pd/C (400 mg) under ice bath. Following the NaBH₄ powder (1.5 g, 39.3 mmol, 3 eq.) was very slowly added to the mixture at 0 °C within 30 min. After stirring 5 h under ice bath, the reaction was filtered under reduced pressure with filter aid Celite®545 to remove Pd/C catalyst. Then the mixture was evaporated to remove methanol, and the crude product was extracted by DCM and was washed 3 times by brine as well as dried by anhydrous MgSO₄. Finally, the product was obtained as red brown crystal after removing the solvent DCM. Yield: 85% (1.71 g).

¹H NMR (500 MHz, DMSO-*d*₆) (Figure A28): δ = 6.63 (d, *J* = 8.3 Hz, 2H), 6.49 (d, *J* = 8.4 Hz, 2H), 4.72 (t, *J* = 5.6 Hz, 1H), 4.54 (s, 2H), 3.81 (t, *J* = 5.2 Hz, 2H), 3.63 (q, *J* = 5.3 Hz, 2H).

¹³C NMR (126 MHz, DMSO-*d*₆) (Figure A29): δ = 150.47, 142.81, 115.85, 115.42, 70.50, 60.27.

Synthesis of Compound 9: **Compound 8** (1.5 g, 9.8 mmol, 1 eq.) was dissolved in 10 mL DMF. Then concentrated HCl solution (979 μL, 11.8 mmol, 1.2 eq.) and NaNO₂ aqueous solution (810.8 mg dissolved in 5 mL distilled water, 11.8 mmol, 1.2 eq.) were dropwise added to the solution under ice bath. After stirring 30 min under 0 °C, phenol (921.6 mg, 9.8 mmol, 1 eq.) dissolved in 3 mL DMF was dropwise added to the mixture. Following continuous stirring 30 min under ice bath and then 6 h at RT, the mixture was evaporated to remove DMF and water. Then the mixture was extracted by EA and was washed by brine for 3 times. Finally, the product was recrystallized from ethanol at -20 °C for overnight as red brown crystal. Yield: 55% (1.39 g).

¹H NMR (500 MHz, DMSO-*d*₆) (Figure A30): δ = 10.15 (s, 1H), 7.78 (d, *J* = 8.5 Hz, 2H), 7.73 (d, *J* = 8.3 Hz, 2H), 7.09 (d, *J* = 8.4 Hz, 2H), 6.91 (d, *J* = 8.4 Hz, 2H), 4.88 (s, 1H), 4.07 (t, *J* = 4.9 Hz, 2H), 3.74 (t, *J* = 4.9 Hz, 2H).

¹³C NMR (126 MHz, DMSO-*d*₆) (Figure A31): δ = 161.17, 160.79, 146.68, 145.71, 124.81, 124.37, 116.32, 115.45, 70.43, 59.98.

Synthesis of Compound 10: **Compound 4** (2 g, 0.92 mmol, 1 eq.) and **Compound 9** (285.8 mg, 1.11 mmol, 1.2 eq.) were taken up in a round-bottom flask and dissolved in 50 mL dry DMF along with K₂CO₃ (254.9 mg, 1.85 mmol, 2 eq.). The reaction mixture was placed in a preheated oil bath at 60 °C and stirred for 30 h. Then the reaction was stopped and poured into

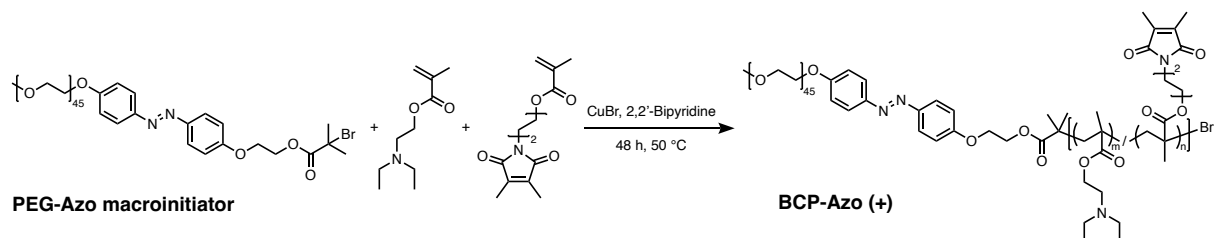
an excess of cold diethyl ether to precipitate the product. It was recrystallized in ethanol to get pure product. Yield: 92% (1.91 g).

^1H NMR (500 MHz, CDCl_3) (Figure A32): δ = 8.06-7.67 (m, 3H), 7.10-6.93 (m, 3H), 6.87 (ddd, J = 8.7, 5.7, 2.5 Hz, 1H), 6.80 (ddt, J = 6.7, 4.5, 2.6 Hz, 1H), 4.21 (t, J = 4.9 Hz, 2H), 4.17 (t, J = 4.5 Hz, 2H), 4.03-3.97 (m, 2H), 3.89 (t, J = 4.8 Hz, 2H), 3.64 (d, J = 2.5 Hz, 180H), 3.37 (s, 3H).

Synthesis of Compound 11 (PEG-Azo Macroinitiator): Compound 10 (1.5 g, 0.67 mmol, 1 eq.) and TEA (278 μL , 2.0 mmol, 3 eq.) were added into a 100 mL round bottomed flask and dissolved in 30 mL dry DCM, and then the reaction mixture was cooled down to 0 $^\circ\text{C}$. Then α -bromoisobutyryl bromide (205.6 μL , 1.66 mmol, 2.5 eq.) was added to the reaction mixture and it was allowed to go on for 2 h under ice bath followed by 18 h at RT. After this, the product was precipitated from cold diethyl ether and recrystallized from ethanol. Yield: 87% (1.39 g).

^1H NMR (500 MHz, CDCl_3) (Figure A33): δ = 8.08-7.62 (m, 4H), 7.04-6.98 (m, 4H), 4.59-4.52 (m, 2H), 4.33-4.27 (m, 2H), 4.23-4.17 (m, 2H), 3.92-3.86 (m, 2H), 3.63 (d, J = 2.1 Hz, 181H), 3.81-3.45 (m, 191H), 3.37 (s, 3H), 1.94 (s, 6H).

Synthesis of Block Copolymer with Ether Substituted Azobenzene Linkage and Copolymerization of Photo-Crosslinker (BCP-Azo (+))

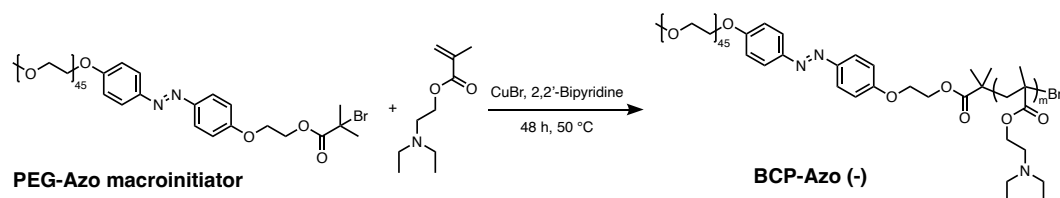


Polymerization of BCP-Azo (+): PEG-Azo macroinitiator (Compound 11, 100 mg, 0.0416 mmol, 1 eq.), 2,2'-bipyridine (13.0 mg, 0.0832 mmol, 2 eq.), DEAEEMA (554.9 mg, 2.995 mmol, 72 eq.) and DMIBMA (198.7 mg, 0.749 mmol, 18 eq.) were added to a Schlenk tube equipped with a stirring bar. The compounds were dissolved in 1.5 ml of 2-butanone and completely frozen in liquid nitrogen. The mixture was degassed using two freeze-pump-thaw-cycles and then backfilled with argon. Now CuBr (6.0 mg, 0.0416mmol, 1 eq.) was added onto the frozen solution. Following the mixture was degassed using three freeze-pump-thaw-cycles and then backfilled with argon and stirred 48 h at 50 $^\circ\text{C}$. To end the polymerization, the tube was opened, and the reaction mixture was diluted with 3 mL THF and filtrated over aluminium

oxide to remove all copper species. The concentrated mixture after evaporating a part of the solvent was precipitated in cold *n*-hexane. Then pouring out the supernatant and the solid was transferred to a dialysis membrane (regenerated cellulose, MWCO 5 kDa) and dialysed against methanol (technical grade) for two days exchanging the solvent twice a day. Afterwards the solvent was removed under reduced pressure and the final product is dried in vacuo. Yield: 66% (563 mg).

¹H NMR (500 MHz, CDCl₃) (Figure A34): δ = 7.86 (dd, J = 8.8, 3.8 Hz, 3H), 7.00 (dd, J = 9.0, 3.7 Hz, 3H), 6.88 (dd, J = 9.0, 3.6 Hz, 1H), 6.82-6.72 (m, 1H), 4.12-3.84 (m, 177H), 3.64 (s, 180H), 3.57-3.44 (m, 37H), 3.37 (s, 3H), 2.78-2.44 (m, 431H), 1.03 (t, J = 7.1 Hz, 515H), 0.89 (d, J = 13.0 Hz, 168H).

Synthesis of Block Copolymer with Ether Substituted Azobenzene Linkage but without Copolymerization of Photo-Crosslinker (BCP-Azo (-))



Polymerization of BCP-Azo (-): PEG-Azo macroinitiator (**Compound 11**, 100 mg, 0.0416 mmol, 1 eq.), 2,2'-bipyridine (13.0 mg, 0.0832 mmol, 2 eq.) and DEAEMA (693.7 mg, 3.744 mmol, 90 eq.) were added to a Schlenk tube equipped with a stirring bar. The compounds were dissolved in 1.5 ml of 2-butanone and completely frozen in liquid nitrogen. The mixture was degassed using two freeze-pump-thaw-cycles and then backfilled with argon. Now CuBr (6.0 mg, 0.0416mmol, 1 eq.) was added onto the frozen solution. Following the mixture was degassed using three freeze-pump-thaw-cycles and then backfilled with argon and stirred 48 h at 50°C. To end the polymerization, the tube was opened, and the reaction mixture was diluted with 3 mL THF and filtrated over aluminium oxide to remove all copper species. The concentrated mixture after evaporating a part of the solvent was precipitated in cold *n*-hexane. And then pouring out the supernatant and the solid was transferred to a dialysis membrane (regenerated cellulose, MWCO 5 kDa) and dialysed against methanol (technical grade) for two days exchanging the solvent twice a day. Afterwards the solvent was removed under reduced pressure and the final product is dried in vacuo. Yield: 57% (452 mg).

¹H NMR (500 MHz, CDCl₃) (Figure A35): δ = 7.86 (dd, J = 8.7, 4.0 Hz, 3H), 7.00 (dt, J = 7.3, 3.6 Hz, 3H), 6.88 (dd, J = 8.8, 3.6 Hz, 1H), 6.78 (dd, J = 8.9, 3.7 Hz, 1H), 3.99 (q, J = 12.2, 6.9 Hz, 202H), 3.64 (s, 180H), 3.37 (s, 3H), 2.62 (dt, J = 67.6, 5.5 Hz, 627H), 1.03 (t, J = 6.7 Hz, 720H), 0.96-0.71 (m, 206H).

5.2 Photo-Isomerization of Macroinitiator and Block Copolymer with Azobenzene Linkage

5.2.1 Photo-Isomerization of PEG-DA-Azo Macroinitiator Based on Blue Light Irradiation or UV Irradiation

PEG-DA-Azo macroinitiator (Compound 6) was dissolved in water to prepare 0.1 mg/mL solution. Before and after UV irradiation (with 365 nm filter) or blue light irradiation (with 400-500 nm filter) different time for 1 mL solution, the UV-Vis spectra with 250-650 nm wavelength range were recorded to check the photo-isomerization degree and efficiency.

5.2.2 Photo-Isomerization of PEG-Azo Macroinitiator Based on Blue Light Irradiation or UV Irradiation

PEG-Azo macroinitiator (Compound 11) was dissolved in water to prepare 0.1 mg/mL solution. Before and after UV irradiation (with 365 nm filter) different time for 1 mL solution, the UV-Vis spectra with 250-650 nm wavelength range were recorded to check the photo-isomerization degree and efficiency. Besides, after photo-isomerization from trans-state to cis-state under UV irradiation, blue light (with 400-500 nm filter) was used to initiate the opposite photo-isomerization from cis-state to trans-state.

5.2.3 Photo-Isomerization of BCP-DA-Azo (-) Based on Blue Light Irradiation or UV Irradiation

BCP-DA-Azo (-) was dissolved in 0.01 M HCl solution to prepare 1 mg/mL solution. After fully dissolution, the pH value was adjusted to pH 6.0 through 1 M and 0.1 M NaOH solution. Before and after UV irradiation (365 nm) or blue light irradiation (400-500 nm) different time for 1 mL solution, the UV-Vis spectra with 250-650 nm wavelength range were recorded to check the photo-isomerization degree and efficiency. It is worthy to note that the use of BCP without photo-crosslinker was to avoid photo-crosslinking between BCPs.

5.2.4 Photo-Isomerization of BCP-Azo (-) Based on Blue Light Irradiation or UV Irradiation

BCP-Azo (-) was dissolved in 0.01 M HCl solution to prepare 1 mg/mL solution. After fully dissolution, the pH value was adjusted to pH 6.0 through 1 M and 0.1 M NaOH solution. Before and after UV irradiation (365 nm) different time for 1 mL solution, the UV-Vis spectra with 250-650 nm wavelength range were recorded to check the photo-isomerization degree and efficiency. Besides, after photo-isomerization from trans-state to cis-state under UV irradiation, blue light (400-500 nm) was used to initiate the opposite photo-isomerization from cis-state to trans-state.

5.3 Formation and Characterization of Polymersomes with Azobenzene

5.3.1 Self-Assembly of Polymersomes with Azobenzene

10 mg BCP with azobenzene linkage was dissolved in 10 mL 0.01 M aqueous HCl solution (1 mg/mL) and then filtrated by syringe filter with 0.2 μm pore size to remove any impurities. To initiate the self-assembly process, the pH value was adjusted slowly to pH 8.5 ($\text{pH} \leq 9$) through dropwise addition of 1 M NaOH and then 0.1 M NaOH solution. Thus, polymersomes were formed after 1 day of stirring under dark conditions. Next, polymersomes were passed through 0.8 μm nylon filter to remove any aggregates.

5.3.2 Photo-Isomerization of Psomes-DA-Azo (-) Based on Blue Light Irradiation or UV Irradiation

BCP-DA-Azo (-) was used to assemble Psomes-DA-Azo (-) without photo-crosslinker DMIBMA according above-described method. Then the Psomes-DA-Azo (-) solution (1 mL, 1 mg/mL, pH 8) was moved to quartz cuvette to carry out the photo-isomerization experiment. Before and after UV irradiation (365 nm) or blue light irradiation (400-500 nm) different time for 1 mL solution, the UV-Vis spectra with 250-650 nm wavelength range were recorded to check the photo-isomerization degree and efficiency. It is worthy to note that the use of BCP without photo-crosslinker was to avoid photo-crosslinking between BCPs during the photo-isomerization process.

5.3.3 Photo-Isomerization of Psomes-Azo (-) Based on Blue Light Irradiation or UV Irradiation

BCP-Azo (-) was used to assemble Psomes-Azo (-) without photo-crosslinker DMIBMA according above-described method. Then the Psomes-Azo (-) solution (1 mL, 1 mg/mL, pH 8) was moved to quartz cuvette to carry out the photo-isomerization experiment. Before and after UV irradiation (365 nm) different time for 1 mL solution, the UV-Vis spectra with 250-650 nm wavelength range were recorded to check the photo-isomerization degree and efficiency. Besides, after photo-isomerization from trans-state to cis-state under UV irradiation, blue light (400-500 nm) was used to initiate the opposite photo-isomerization from cis-state to trans-state.

5.3.4 Photo-Crosslinking of Polymersomes with Azobenzene

The polymersomes self-assembled by BCP-DA-Azo (+) or BCP-Azo (+) were photo-crosslinked with different time (from 60 s to 300 s) under UV irradiation (320-390 nm) for each 2 mL sample. Then the Psomes-DA-Azo (+) and Psomes-Azo (+) were diluted to 0.5 mg/mL in 1 mM PBS buffer and then pH value was adjusted to pH 5.0 and again pH 8.0 for 1-3 cycles. DLS was used to track the crosslinking degree of membrane.

5.3.5 DLS Measurement of Photo-Crosslinked Polymersomes with Azobenzene through pH Titration

After 180 s photo-crosslinking upon UV irradiation (320-390 nm), Psomes-DA-Azo (+) and Psomes-Azo (+) were diluted to 0.5 mg/mL in 1 mM PBS buffer. Then pH titration from pH 9 to pH 5 was carried out by 1M HCl and NaOH solution. The hydrodynamic diameter was checked by DLS for each around 0.2 pH slit.

5.3.6 Photo-Stability of Polymersomes with Azobenzene

Polymersomes self-assembled by BCP-DA-Azo (-) or BCP-Azo (-) were put into the quartz cuvette for 1 mL. Then hydrodynamic size was measured before and after different time (up to 30 min) UV irradiation (365 nm) or blue light irradiation (400-500 nm) for Psomes-DA-Azo (-) or 10 s UV irradiation (365 nm) for Psomes-Azo (-).

5.3.7 In-Situ Loaded Nile Red in Non-Photo-Crosslinked Polymersomes with Azobenzene (NR-Psomes-DA-Azo (+) or NR-Psomes-Azo (+))

10.2 mg BCP with azobenzene linkage (BCP-DA-Azo (+) and BCP-Azo (+)) was dissolved in 10 mL * 0.01 M HCl (stir 2 h to make it completely dissolve in the HCl solution). After filtration by 0.2 μ m membrane, taking 9.6 mL in the bottle and then adjusting the pH from 2 to 5 through 0.1 M and 0.01 M NaOH solution, then adding 100 μ L Nile red solution (dissolved in DMF, 0.1 mg/mL) into the above solution and then adjusting the pH to 8.5 ($\text{pH} \leq 9.0$). Finally, loaded polymersomes were passed through 0.8 μ m nylon filter to remove any aggregates and then dialyzed against 1 mM PBS buffer (pH 7.4) for 1 day. To avoid the light-induced dye release, the photo-crosslinking was not carried out here.

5.3.8 In-Situ Loaded Myo in Photo-Crosslinked Polymersomes with Azobenzene (Myo-Psomes-DA-Azo (+) or Myo-Psomes-Azo (+))

11 mg BCP with azobenzene linkage (BCP-DA-Azo (+) and BCP-Azo (+)) was dissolved in 10 mL * 0.01 M HCl (stir 2 h to make it completely dissolve in the HCl solution). After filtration by 0.2 μ m membrane, taking 9 mL in the bottle and then adjusting the pH from 2 to 5 through 0.1 M and 0.01 M NaOH solution, then adding 1 mL Myo solution (2 mg/mL) into the above solution and then adjusting the pH to 8.5 ($\text{pH} \leq 9.0$). Finally, loaded polymersomes were passed through 0.8 μ m nylon filter to remove any aggregates and crosslinked with 180 s under UV irradiation (320-390 nm) per 2 mL sample. The HFF purification was used to remove non-encapsulated Myo. 9 mL of the unpurified solution (1 mg/mL) was transferred into a 50 mL cone tube attached to the hollow-fiber filtration system. The sample was diluted with a 1 mM PBS solution (pH 7.4) to 18 mL and constantly refilled until the extraction volume was reached. The transmembrane pressure was kept at 130 mbar during the whole process until extracting a total of 100 mL.

5.4 Light-Induced Dye Release from Polymersomes with Azobenzene

5.4.1 Fluorescence Photobleaching of Nile Red under Blue Light or UV Irradiation

To check the influence of fluorescence quenching under different light stimuli, 1 mL Nile red solution (dissolved in DMF, 1 μ g/mL) was added to the quartz cuvette. Before and after 12 min

blue light (400-500 nm) or UV irradiation (365 nm), fluorescence spectra were recorded at an excitation wavelength of 515 nm and an emission wavelength of 626 nm (bandwidth = 2 nm).

5.4.2 Nile Red Release under Blue Light or UV Irradiation

To study the dye release behavior of polymersomes with azobenzene linkage under light stimuli, NR-Psomes-DA-Azo (+) and NR-Psomes-Azo (+) (without photo-crosslinking) were diluted to 0.5 mg/mL in 1 mM PBS buffer (pH 7.4) and moved to quartz cuvette for each 1 mL. For interval irradiation experiments, fluorescence spectra were recorded before and after each 1 min irradiation (each cycle for 3 min) and then standing under dark for each 1 min (each cycle for 4 min) for 4 cycles at an excitation wavelength of 515 nm and an emission wavelength of 600 nm (bandwidth = 3 nm); For interval irradiation experiments, fluorescence spectra were recorded before and after each 1 min irradiation (each cycle for 3 min) and then standing under dark for each 1 min (each cycle for 4 min) for 4 cycles at an excitation wavelength of 515 nm and an emission wavelength of 600 nm (bandwidth = 3 nm); for continuous irradiation, fluorescence spectra were recorded before and after each 1 min irradiation (total 12 min) at an excitation wavelength of 515 nm and an emission wavelength of 600 nm (bandwidth = 3 nm); as control, fluorescence spectra were recorded before and after standing under dark for each 3 min (total 12 min) at an excitation wavelength of 515 nm and an emission wavelength of 600 nm (bandwidth = 3 nm). Besides, the hydrodynamic size of NR-Psomes-DA-Azo (+) and NR-Psomes-Azo (+) (without photo-crosslinking) was also measured before and after different irradiation time of blue light or UV light (total 12 min) to prove the dye release behavior.

5.5 Light-Driven Enzyme Reaction Based on Polymersomes with Azobenzene

To check the Myo activity in simulated physiological environment (pH 7.4), 3.2 μ L Amplex Red solution (0.02 mg/mL) and 3.2 μ L H₂O₂ solution (0.02 M) were directly added to the purified 200 μ L Myo-Psomes-DA-Azo (+) or Myo-Psomes-Azo (+) solution (0.5 mg/mL in 1 mM PBS buffer, pH = 7.4) under continuous stirring (stir for 2 min). To initiate the enzyme assay, the sample was put under blue light irradiation (400-500 nm) or UV irradiation (365 nm). After different time light stimuli (up to 10 min) and standing under dark for a while for each portion (total 30 min incubation time), fluorescence spectra were recorded at an excitation wavelength of 534 nm and an emission wavelength of 590 nm.

Part III Results and Discussions

6 Clustered pH-Responsive Polymersomes for Enzymatic Cascade Reaction

6.1 Aim and Strategy

The aim of this study was to prepare clustered polymersomes with pH-responsiveness and photo-crosslinked structure for enzymatic cascade reaction. So far, polymersomes as synthetic vesicles fabricated by the self-assembly of amphiphilic BCPs to mimic cellular process, have gained considerable research interest due to their high stability, flexible functionalization and tunable membrane permeability.^{1, 4, 6} The tunable membrane permeability is often achieved by designing membrane composition to make it selectively open and close, make the membrane responsive to internal or external stimuli, like light, pH, redox, magnetic field, and temperature.¹³⁻³³ The controllable membrane permeability and the loading capacity of the polymersome's cavity have enabled polymersomes as artificial organelles to simulate biological behaviors such as drug release, gene expression, and enzyme reaction.^{34, 36, 78} However, polymersomes as nanoreactors can only achieve simple and single function, the real cellular organelle is an intricate system that exhibits sophisticated biological functions.

For this reason, self-assembly of artificial synthetic vesicles to clusters or to aggregates through interconnection as bionic way is a potential route to establish artificial intelligent biological systems for emergent distinct and common properties. Various bridging methods, include non-covalent bonding, DNA hybridization and click chemistry, have been used to assemble polymersomes into (large-scale) aggregates and controlled clusters.⁹¹⁻⁹⁴ Considering the convenience and safety of assembly process, copper-free click chemistry is a desirable way that can be applied to living systems due to the elimination of cytotoxic copper catalysts and the absence of by-products.¹⁷⁷⁻¹⁸⁰

In this case, we aimed at fabricating clustered polymersomes in-situ loaded enzyme GOx (GOx-Psomes-N₃) and Myo (Myo-Psomes-N₃) through above-mentioned copper-free click reaction for enzymatic cascade reaction (Figure 6.1). Herein, hydrophilic PEG chain with cyclooctyne at both ends (bisBCN-PEG_{1k}) defined as crosslinker was used to assemble polymersomes via SPAAC click chemistry to achieve efficient one-step assembly process (Figure 6.1). In this chapter, various influencing factors in the clustering process and subsequent purification

methods were studied to obtain optimal clustered polymersomes. The size and shape of clustered polymersomes were further characterized by different visualization methods. Finally, the efficiency of enzyme cascade reaction for clustered Enzyme-Psomes-N₃ with spatially separated enzymes, GOx and Myo, were also studied.

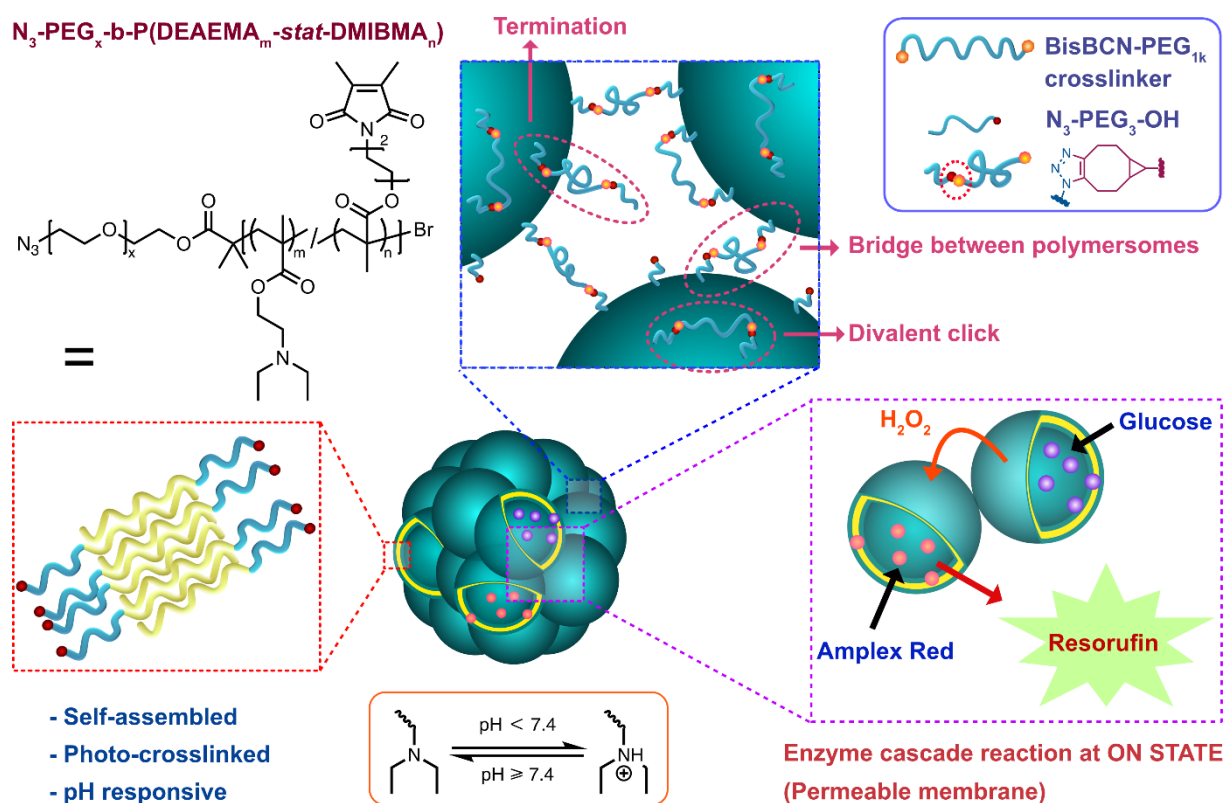


Figure 6.1 Schematic illustration shows the assembly mechanism and the application in enzymatic cascade reaction of pH-responsive clustered Enzyme-Psomes-N₃. The top inset displays the clustering mechanism based on divalent click and bridging reaction and the termination reaction mechanism based on non-reactive short PEG end-capping. The right bottom inset shows the mechanism of enzymatic cascade reaction at the swollen state based on co-clustered Myo/GOx-Psomes-N₃.

6.2 Photo-Crosslinked and pH-Responsive Polymersomes

In previous work, pH-responsive, photo-crosslinked, and functional polymersomes were established, self-assembled by amphiphilic BCP which consist of PEG as the hydrophilic section and pH-responsive monomer DEAEMA as well as photo-crosslinker DMIBMA as the hydrophobic section.^{17, 80, 85} These polymersomes have been widely used as nanoreactor for drug delivery and enzyme reaction.^{78, 129}

6.2.1 Synthesis and Characterization of Block Copolymers (BCPs)

Atom transfer radical polymerization (ATRP) was selected as the polymerization method to synthesize such BCPs. According to previous work, PEG-Br macroinitiator with methoxy or azido end group, pH-responsive monomer DEAEMA and photo-crosslinker DMIBMA were statistically copolymerized to achieve the desired BCP with different functional groups (Figure 6.2).¹⁷

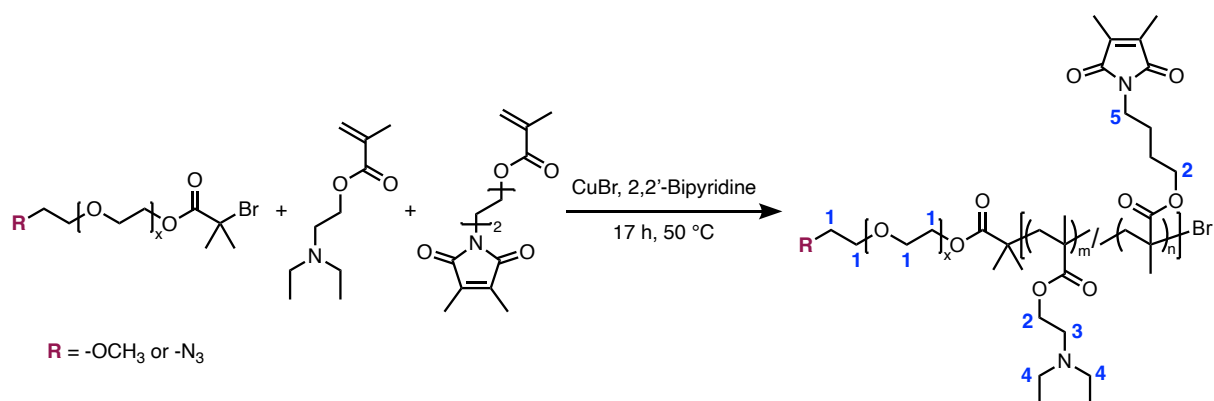


Figure 6.2 ATRP polymerization to synthesize BCPs with methoxy or azido end groups.

The successful synthesis of macroinitiator, photo-crosslinker and BCP was proven by NMR spectra (Figure A1-10 and Figure 6.3). Besides, the block composition of BCP-OCH₃ (CH₃O-PEG-b-p(DEAEMA-s-DMIBMA)) and BCP-N₃ (N₃-PEG-b-p(DEAEMA-s-DMIBMA)) was calculated by ¹H NMR spectra (Figure A8-10) and shown in Table 6.1.

Here, the methylene groups in BCP (labeled as 1, 2, 3, 4, 5 in Figure 6.3) were used to calculate each block length. The intensity of signal “1” from the PEG part is taken as a reference, because of the PEG is a commercial product and has a certain amount of ethylene oxide units (45 units for PEG-OCH₃, 60 units for PEG-N₃-1 and 77.5 units for PEG-N₃-2). Besides, each ethylene oxide has 4 H atoms. Signal “2” represents the polymerization degree. Thus, the integration around 4.0 ppm peak shift was used to calculate total amounts of PEG. In addition, signal “3” and “4” indicates the methylene groups around the tertiary amine of DEAEMA monomer and the signal “4” is 2 times forwards the signal “3” because of 2 methylene groups on assigned to signal “4”. The integration of these peaks can be used to calculate the amounts of DEAEMA monomer. However, signal “5” shows the methylene group around the tertiary amine of photo-crosslinker DMIBMA and the relative integration was used to calculate the amounts of it. Finally, the crosslinker ratio in the hydrophobic part is around 20%, which is an essential ratio to crosslink polymersomes under UV irradiation.

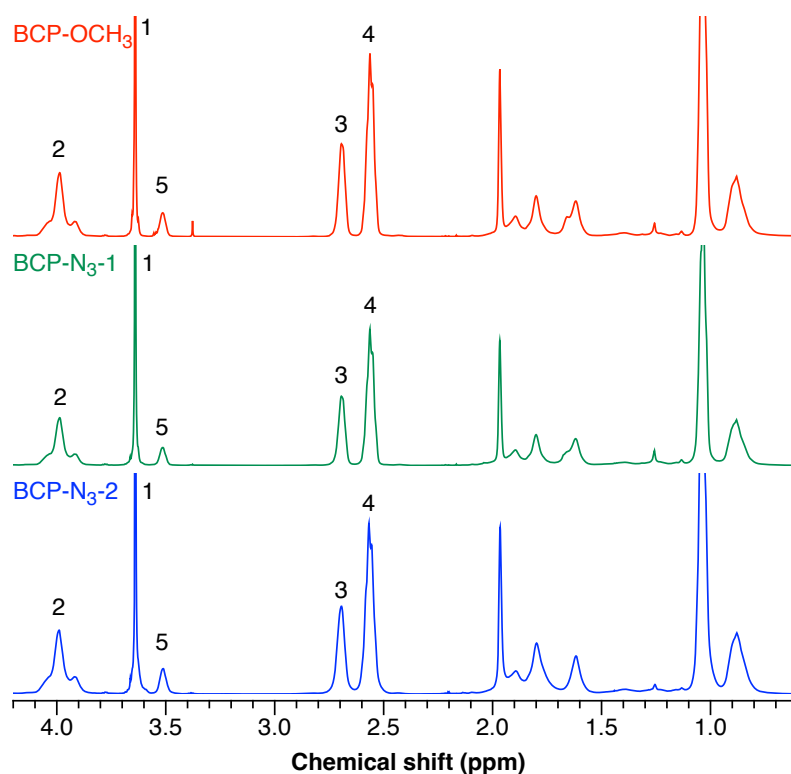


Figure 6.3 ^1H NMR spectra of BCP-OCH₃, BCP-N₃-1, and BCP-N₃-2.

In order to maintain the length of the hydrophobic section of BCP-OCH₃ and BCP-N₃-1 for protruding the azido groups on the surface of polymersomes, the length of the hydrophobic sections of BCP-OCH₃ and BCP-N₃-1 was maintained (103 units for BCP-OCH₃ and 105 units for BCP-N₃-1), but a longer PEG-N₃ (60 repeating ethylene oxide units) for BCP-N₃-1 as well as shorter PEG-OCH₃ (45 repeating ethylene glycol units) for BCP-OCH₃ was selected. Moreover, in order to be able to assemble the polymersomes by BCP-N₃-2, the hydrophobic block is maintained twice the hydrophilic block (the block ratio is 1: 2.09).

Table 6.1 Block composition of BCPs with methoxy and azido end groups.

Polymer	Repeating units in PEG ^a	DEAEMA units ^a	DMIBMA units ^a	Block ratio ^a	DMIBMA ratio ^b
BCP-OCH ₃	45	82	21	1: 2.29	20.4%
BCP-N ₃ -1	60	85	20	1: 1.75	19.0%
BCP-N ₃ -2	77.5	130	32	1: 2.09	19.8%

^a Number of repeating units in PEG (hydrophilic section): number of copolymerized pH-responsive monomer DEAEMA and photo-crosslinker DMIBMA (hydrophobic section), obtained by ^1H NMR analysis; ^b Percentage of photo-crosslinker DMIBMA in hydrophobic section, calculated by the ratio of polymerization degree by ^a.

Table 6.2 Molar mass characteristics of BCPs with methoxy and azido end groups.

Polymer	M_n^a (g/mol)	M_n^b (g/mol)	M_w^b (g/mol)	\mathcal{D}^b (M_w/M_n)
BCP-OCH ₃	22935	40300	53200	1.31
BCP-N ₃ -1	23217	56600	77300	1.36
BCP-N ₃ -2	36063	35500	43600	1.23

^a Calculated by ¹H NMR; ^b Measured by GPC.

Furthermore, molecular weights of BCPs were calculated by ¹H NMR spectra and measured by GPC. The GPC results show that BCPs has a narrow molar mass distribution (\mathcal{D}) from 1.23 to 1.36, suggesting a controllable polymerization process (Table 6.2). Besides, the calculated molecular weights of BCP-OCH₃ and BCP-N₃-1 by NMR spectra were smaller than the weight-average molecular weights determined by GPC, which could be explained that the interaction of polymers with GPC material in column.

6.2.2 Formation and Characterization of Polymersomes

Polymersomes were self-assembled by gradually increasing pH, at which no organic solvent was used. In this way, BCP was dissolved in 0.01 M HCl solution to make protonation of the tertiary amine in the pDEAEMA segments of hydrophobic block. Then, to initiate the self-assembly process, deprotonation process was carried out through increasing the pH value to a basic condition (pH 9.0). After 3 days of stirring under dark conditions, the final polymersomes were formed with a bilayer membrane and aqueous lumen. The bilayer membrane is composed by central hydrophobic part based on copolymerized DEAEMA and DMIBMA units, with the hydrophilic inner and outer corona is equipped with PEG chains. After the formation of polymersomes, the pDMIBMA moieties were used to crosslink the polymersome membrane under UV irradiation. This makes the polymersomes robust and mechanically stable at various pH values, as previously published by Gaitzsch et al.²⁰

In previous research, the mixture of BCP-N₃ (reactive azido end group) and BCP-OCH₃ (non-reactive methoxy end group) can increase the accessibility of the reactive azido groups on the Psomes' surface due to the longer PEG chain in BCP-N₃ (60 ethylene oxide repeating units compared with 45 repeating units of PEG-OCH₃ in BCP-OCH₃).¹⁷ In addition, polymersomes with different weight ratio of BCP-N₃ (Psomes-X%N₃, X = 30, 40 or 100; Psomes-100%N₃ = Psomes-N₃) were self-assembled to regulate the clustering process. It is worth noting that in

order to maintain protruding functional azido groups, similar length of the hydrophobic section and different PEG lengths of BCPs were selected for the optimization process (BCP-OCH₃: CH₃O-PEG₄₅-b-p(DEAEMA₈₂-stat-DMIBMA₂₁; BCP-N₃: N₃-PEG₆₀-b-p(DEAEMA₈₅-stat-DMIBMA₂₀)).

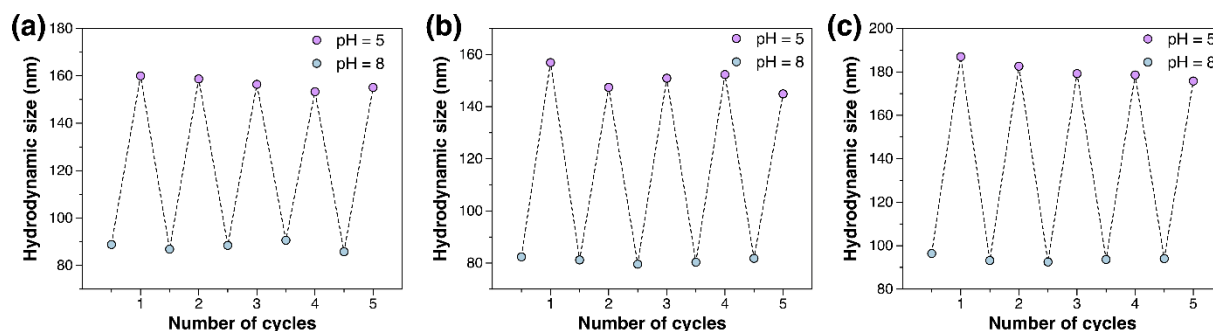


Figure 6.4 Hydrodynamic size of Psomes-N₃ assembled with 30% (a), 40% (b) and 100% (c) BCP-N₃ with cyclic pH switches between pH 8 and pH 5. Conditions: 0.25 mg/mL Psomes in 10 mM PBS buffer; measured by DLS.

To characterize the pH-responsive behavior of the crosslinked polymersomes with different ratio of BCP-N₃, its stability was investigated by DLS test upon reversible pH switch for 5 cycles. The average hydrodynamic diameters measured by DLS at each cycle indicate that polymersomes with mixed BCPs can swell and shrink reversibly at acidic and basic conditions due to the protonation/deprotonation of the pDEAEMA segments in the membrane (Figure 6.4). In more detail, the hydrodynamic diameters of polymersomes with 30%, 40% and 100% BCP-N₃ increase from 89, 82 and 96 nm to 160, 157, and 187 nm at pH 5.0, respectively, and then finally return to the original sizes at pH 8.0 (88, 81 and 94 nm). In other words, it is obvious that the photo-crosslinking time and the block ratio between hydrophobic and hydrophilic are enough to get stable crosslinked polymersomes. This also indicates that enough photo-crosslinkers are integrated in the hydrophobic segment of each BCP. Therefore, this stable swelling-shrinking capability against pH changes endows the opportunity of polymersomes with mixed BCPs to assemble into larger clusters usable as an enzymatic nanoreactors.

To further investigate the morphology, size, and membrane thickness of the different Psomes-X%N₃, Cryo-TEM was used to visualize their shape and to prove their hollow structure (Figure 6.5). The histograms show that the average sizes of Psomes-N₃ with 30%, 40% and 100% of BCP-N₃ are 75 nm, 76 nm and 67 nm, while the corresponding membrane thicknesses are 17 nm, 19 nm and 16 nm, respectively. The results are the same as found in previous studies using

“standard” polymersomes.^{79, 123} The spherical vesicle structure with a certain membrane thickness and narrow size range proves the successful assembly of relatively uniform Psomes-X%N₃. Moreover, Psomes-X%N₃ exhibit enhanced mechanical stability and potentially endless switching on and off membrane permeability by pH cycles (Figure 6.4). This is one requirement for the assembly of polymersomes into pH-stable and pH-responsive clusters at which an excellent membrane permeability would be beneficial for feeding and switching on and off enzymatic reactions.

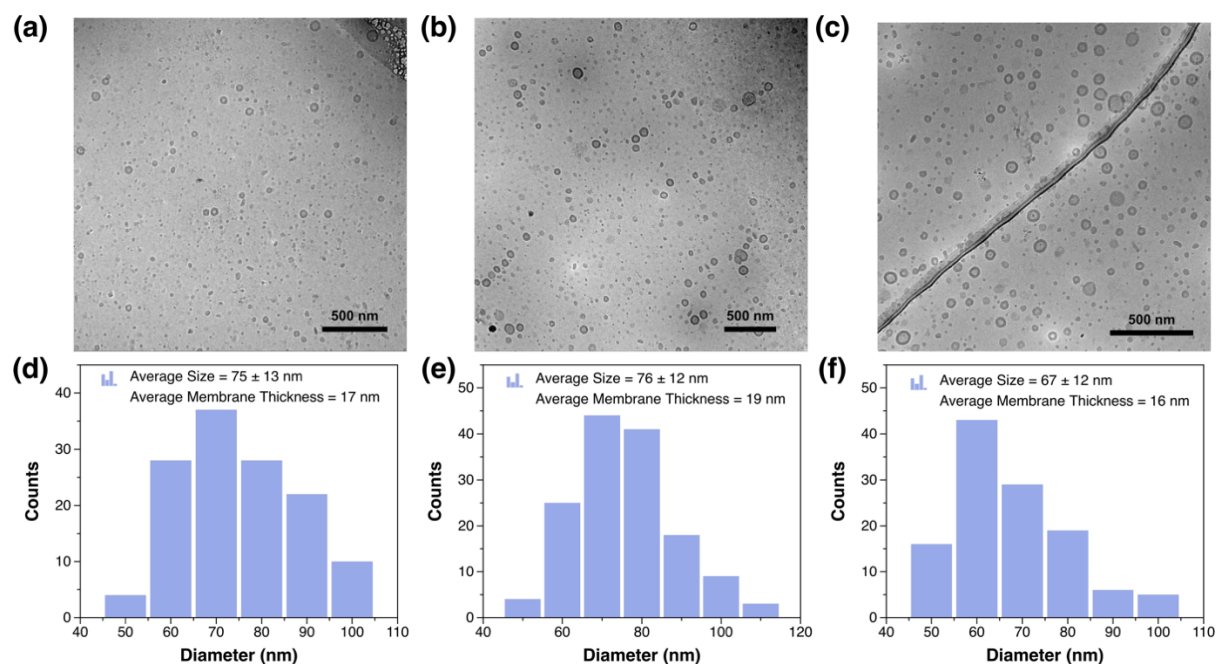


Figure 6.5 Cryo-TEM images of Psomes-N₃ assembled with 30% (a), 40% (b) and 100% (c) BCP-N₃ at pH 8 and diameter distribution histograms of Psomes-N₃ assembled with 30% (d), 40% (e) and 100% (f) BCP-N₃. The average diameter and membrane thickness of polymersomes were calculated by analyzing no less than 118 particles and 13 particles, respectively.

6.3 Preparation and Purification of Clustered Empty-Psomes-N₃

6.3.1 Key Parameters of Clustering Process

As above-mentioned for clustered polymersomes, bisBCN-PEG crosslinker was synthesized and well characterized (Figure A11-14). Following, the crosslinker was added into Psomes-X%N₃ solution under different reaction conditions to carry out clustering process (Figure 6.6). Here, several key parameters were studied and then the corresponding hypothetical mechanisms

were also assumed. Besides, various purification protocols have also been performed to obtain micron-level clustered Psomes-N₃. DLS measurement was used to track the clustering degree of Psomes-N₃ in a first series of experiments through the investigation of key parameters, followed by deeper characterization steps later. According to the size distribution by volume, peak size and corresponding peak area are used to track the clustering process of the polymersomes. The peak around 100 nm represents individual polymersomes, while the aggregates (formed by covalent bonding and non-covalent bonding) show the peak size between 4 to 10 μm.

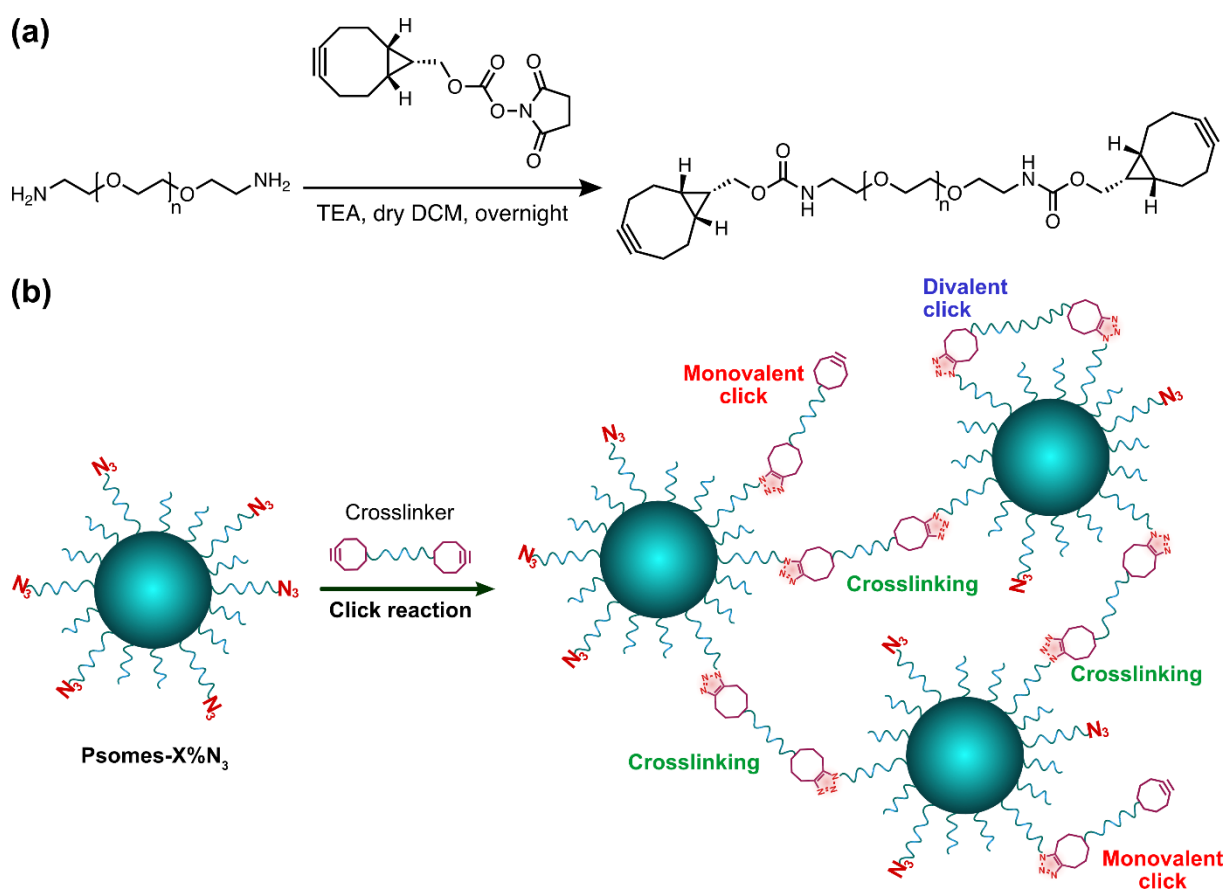


Figure 6.6 (a) Synthetic route of bisPEG-BCN crosslinker. (b) Click reaction in the clustering process of Psomes-X%N₃, including monovalent click, divalent click and crosslinking reaction.

Key Parameter I: Temperature. The temperature is a general parameter that can affect the rate of a reaction, Psomes-30%N₃ were used to study the effect of temperature on the clustering process. Clustering process does not proceed at RT for even 5 days, in opposite, different temperatures higher than RT were selected to accelerate the clustering process. After 2 days stirring, size distribution shows that just a few clusters are formed by increasing the temperature (from 40 °C to 60 °C) (Figure 6.7a). Finally, single Psomes-30%N₃ are preferred in the reaction

solution and more clusters formed at 40 °C (40.1% clusters) than them at higher temperature (5.5% clusters at 50 °C and only 2.5% aggregates at 60 °C) (Table 6.3). A higher temperature might cause a fast attachment of the crosslinker in a bivalent manner (self-sacrificing event) on the same Psomes-30%N₃ surface (Figure 6.7b). Self-sacrificing event is caused by the crosslinkers to consume a large proportion of reactive azido groups, and then few residual azido groups slow the clustering process. Moreover, the dense PEG shell and/or lack of free reactive azido group can hamper the clustering between Psomes-30%N₃. After all, clusters are only available after 2 days incubation at 40°C. Therefore, all further clustering experiments for the formation of clustered Psomes-X%N₃ were performed at 40 °C.

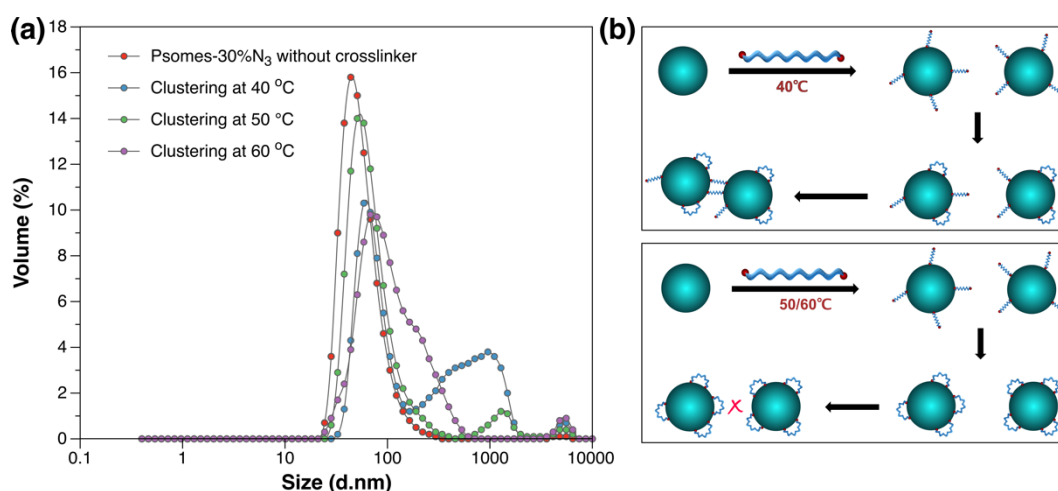


Figure 6.7 (a) Size distribution of the Psomes-30%N₃ mixed without and with 5 eq. bisBCN-PEG_{1k} crosslinker stirred 2 days at different temperatures; initial addition of excess crosslinker aims to speed up the clustering process. (b) The possible mechanism triggered by temperature changes for clustered Psomes-N₃ formation shows that the higher temperature (50 or 60 °C) could hinder the click reaction between Psomes-N₃ due to self-sacrificing event.

Table 6.3 Hydrodynamic size of the Psomes-30%N₃ mixed with 5 eq. bisBCN-PEG_{1k} crosslinker stir 2 days at different temperatures investigated by DLS study.

Temperature (°C)	Peak size (d. nm*)			Percent of peak area (%)		
	1	2	3	1	2	3
40	81	725	5171	58	40.1	1.9
50	73	1261	4725	93.1	5.5	1.4
60	125	0	5234	97.5	0	2.5

* d. nm means diameter values in nanometers.

Key Parameter II: Ratio of BCP-N₃. Different Psomes-X%N₃ (X = from 10 to 100) were self-assembled and then used to assemble into clustered polymersomes through crosslinking. Figure 6.8a-b and Table 6.4 show that as the ratio of BCP-N₃ increases, a higher percentage of Psomes-X%N₃ are assembled into clusters within the same reaction time (2 days). Moreover, the majority of Psomes-X%N₃ are clusters after 2 days when X ≥ 80 is independent of used crosslinker. In case between Psomes-10%N₃ and Psomes-60%N₃, it is unavoidable to obtain monovalent conjugation and self-sacrificing issues, while the increasing increment of reactive azido groups promotes the desired clustering (Figure 6.8c). It is worthy to note that 100% peak area with 0.3-1.5 μm peak size does not represent real situation that all polymersomes form clusters. Here, the detection limit based on DLS measurement determines such size distribution results which can be used as a database for tracking the clustering degree.

Table 6.4 Hydrodynamic size of different Psomes-X%N₃ mixed with 1 eq. crosslinker both bisBCN-PEG_{1k} and bisBCN-PEG_{2k} at 40 °C for 2 days investigated by DLS study.

Proportion of BCP-N ₃	Crosslinker	Peak size (d. nm)			Percent of peak area (%)		
		1	2	3	1	2	3
10%	BisBCN-PEG _{1k}	89	1455	4936	92.1	5.4	2.5
30%		61	512	0	67.7	32.3	0
40%		82	462	4929	56.9	34.3	8.8
60%		75	1294	4729	25.1	63	11.9
80%		94	1494	0	12.1	87.9	0
100%		0	1204	0	0	100	0
10%	BisBCN-PEG _{2k}	91	1321	4425	89.6	7.5	2.9
30%		75	650	5467	70	27.1	3
40%		103	805	5203	48.4	49.5	2.0
60%		91	1020	5389	23.6	75	1.4
80%		68.4	1448	0	13.1	86.9	0
100%		0	1285	0	100	100	0

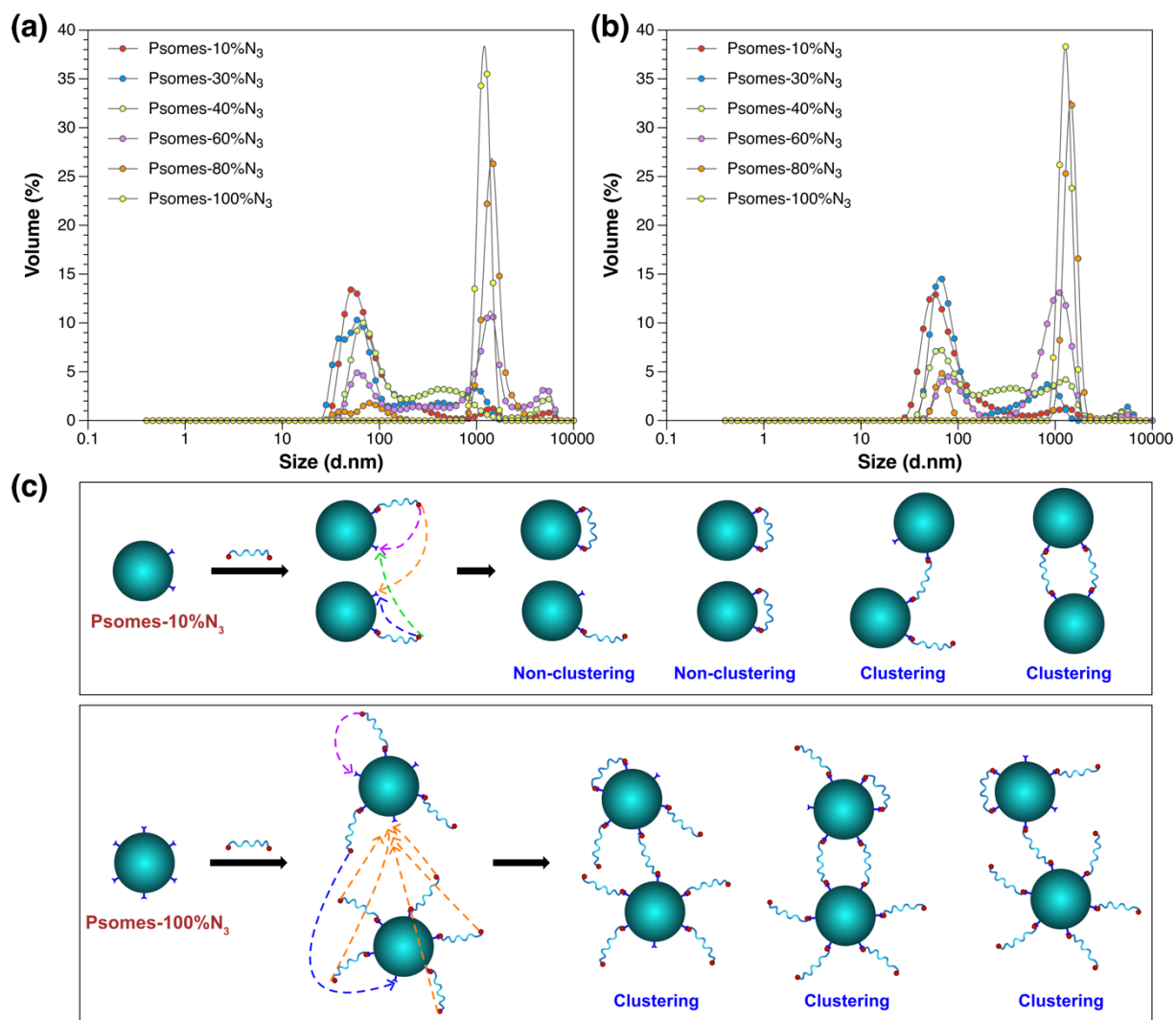


Figure 6.8 Size distribution of the Psomes-X%N₃ mixed with 1 eq. bisBCN-PEG_{1k} (a) and bisBCN-PEG_{2k} (b) crosslinker at 40 °C for 2 days. (c) The possible mechanism caused by the proportion of BCP-N₃ in Psomes-N₃ for clustered Psomes-N₃ formation indicates that increasing the proportion of BCP-N₃ in the final Psomes-N₃ with 100 % BCP-N₃ can drastically boost the clustering process.

Key Parameter III: Reaction Time. It was previously observed that the clustering process is not completed after 2 days of reaction, therefore longer reaction times were studied. Two different Psomes-X%N₃ (X = 10 or 30, Figure 6.9) were used to validate the influence of different reaction times and kind of crosslinker (bisBCN-PEG_{1k} and bisBCN-PEG_{2k}) on the clustering process.

More Psomes-X%N₃ assembled into clusters can be observed with time (Figure 6.9 and Table 6.5). Psomes-10%N₃ are not fully clustered via bisBCN-PEG_{1k} crosslinker even after

continuous stirring for 30 days. Compared to bisBCN-PEG_{1k}, bisBCN-PEG_{2k} crosslinker is much less suitable for the clustering due to more unclustered Psomes-10%N₃ existed. However, Psomes-30%N₃ were fully clustered after 4 days via both crosslinkers, while more clusters formed after 2 days clustering via bisBCN-PEG_{1k} crosslinker than via bisBCN-PEG_{2k} (32.3% vs 27.1%). A complete clustering can be achieved by increasing the reaction time, triggered by (i) the proportion of azido groups in this process, but (ii) also the use of shorter crosslinker, bisBCN-PEG_{1k}.

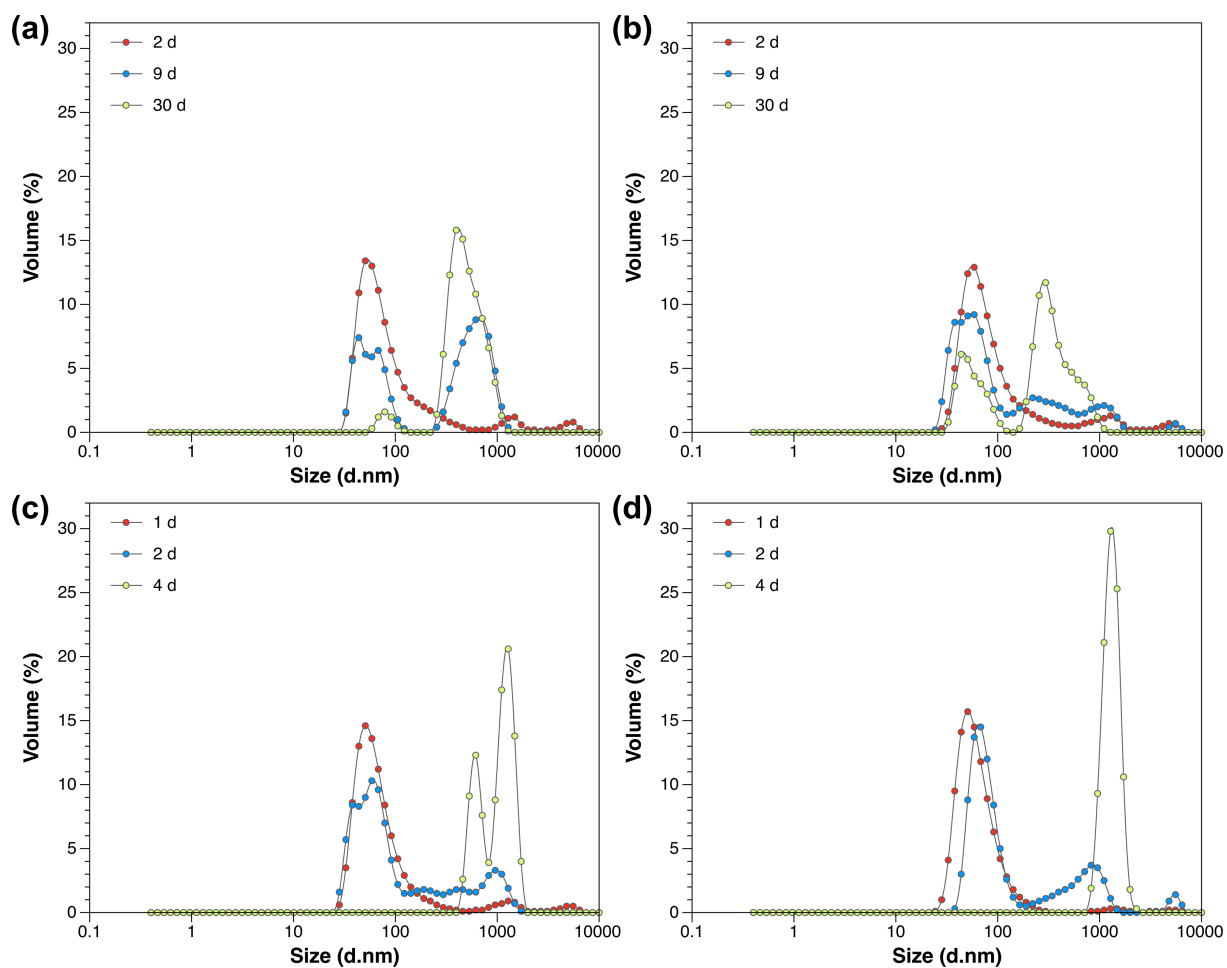


Figure 6.9 Size distribution of the Psomes-10%N₃ mixed with 1 eq. crosslinker bisBCN-PEG_{1k} (a) and bisBCN-PEG_{2k} (b) after different reaction times. Size distribution of the Psomes-30%N₃ mixed with 1 eq. crosslinker bisBCN-PEG_{1k} (c) and bisBCN-PEG_{2k} (d) at 40 °C after different reaction times.

Table 6.5 Hydrodynamic size of the Psomes-10%N₃ and Psomes-30%N₃ mixed with 1 eq. crosslinker both bisBCN-PEG_{1k} and bisBCN-PEG_{2k} at 40 °C for different reaction time investigated by DLS study.

Time (d)	% of BCP-N ₃	Crosslinker	Peak size (d. nm)			Percent of peak area (%)		
			1	2	3	1	2	3
2	10%		89	1455	4936	92.1	5.4	2.5
9	10%	BisBCN-PEG _{1k}	63	595	0	41.7	58.3	0
30	10%		81	537	0	5	95	0
2	10%		91	1321	4425	89.6	7.5	2.9
9	10%	BisBCN-PEG _{2k}	59	487	5504	64.7	33.8	1.6
30	10%		60	418	0	30	70	0
1	30%		72	1186	4680	93.4	4.5	2.1
2	30%	BisBCN-PEG _{1k}	61	512	0	67.7	32.3	0
4	30%		0	1070	0	0	100	0
1	30%		66	1401	4784	97.6	1.5	0.9
2	30%	BisBCN-PEG _{2k}	75	650	5467	70	27.1	3
4	30%		0	1319	0	0	100	0

Key Parameter IV: Feed Ratio of Surface Azido Group of Polymersomes and Crosslinker.

Depending on the concentration of crosslinker and its ratio to present azido groups at Psomes-X%N₃ surface, the clustering process can be accelerated. However, an excess of crosslinker may also prevent the clustering process. For achieving the formation of desired clustered polymersomes with larger dimension (along the micron-level), different feed ratios between outside azido groups of Psomes-30%N₃ and bisBCN-PEG_{1k} crosslinker (from 1: 1 to 1: 100) were applied at 40 °C for 2 days (Figure 6.10a). When the feed ratio is between 1: 1 and 1: 20, more than 32% clusters are formed successfully (Table 6.6). However, only 4.1% aggregates are formed when the feed ratio is 100. The non-clustering effect is most likely due to the excess crosslinker occupying most of surface azido groups through monovalent click and self-sacrificing event, which results in a dense PEG shell to shield residual azido groups for undergoing intermolecular clustering process (Figure 6.10b-c).

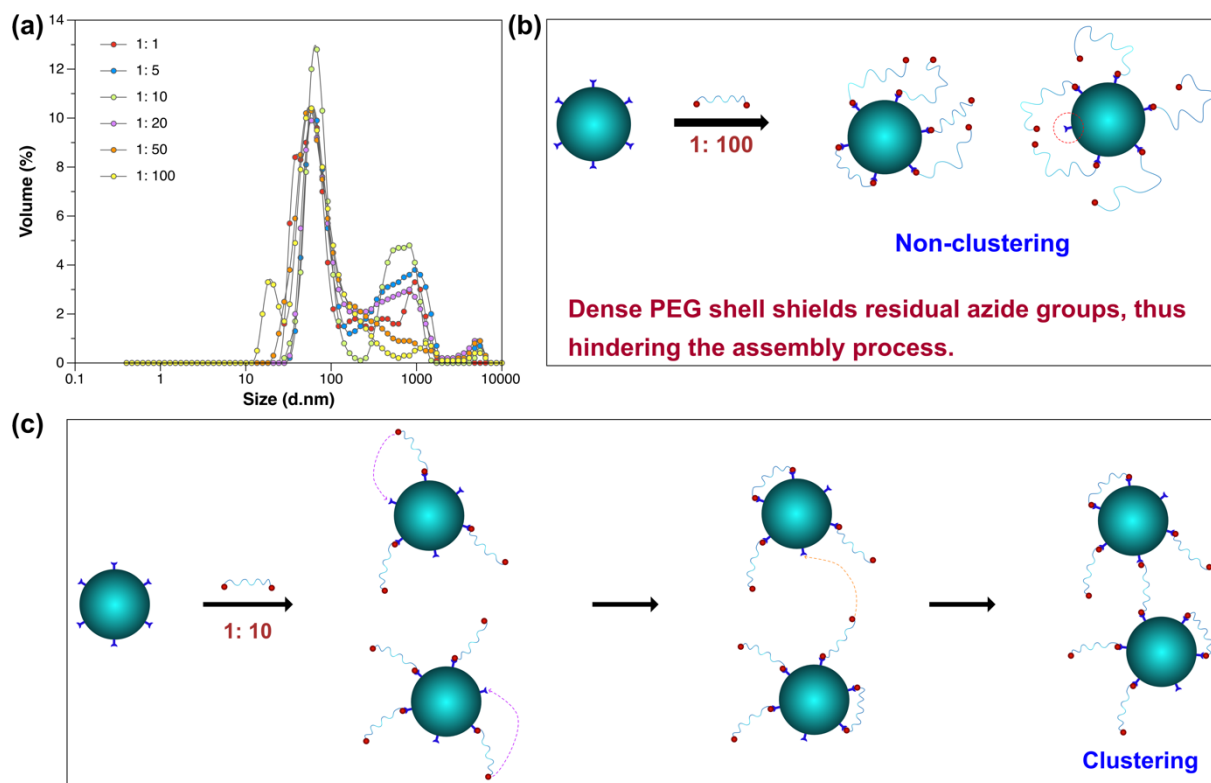


Figure 6.10 Size distribution of the Psomes-30%N₃ mixed with different ratios of crosslinker bisBCN-PEG_{1k} (a) at 40 °C for 2 days as well as possible mechanisms based on excess crosslinker (b) and defined Psomes: crosslinker ratio (c) for clustered Psomes-N₃ formation.

Table 6.6 Hydrodynamic diameter of the Psomes-30%N₃ mixed with different ratio of crosslinker bisBCN-PEG_{1k} at 40 °C for 2 days investigated by DLS study.

Surface Azido Group: Crosslinker	Peak size (d. nm)			Percent of peak area (%)		
	1	2	3	1	2	3
1: 1	61	512	0	67.7	32.3	0
1: 5	81	725	5171	58	40.1	1.9
1: 10	71	660	5590	62.6	36.5	0.9
1: 20	77	599	4527	53.5	42.7	3.7
1: 50	80	827	4887	82.2	14.8	3.1
1: 100	84	1255	4897	94.5	4.1	1.4

Key Parameter V: Length of BisBCN-PEG Crosslinker. The crosslinker length might affect the clustering process and swelling-shrinkage ratio of the final clusters in response to pH changes. Firstly, different Psomes-X%N₃ (X = 30, 40 or 100) and crosslinkers with three

different lengths (PEG_{0.1k}, PEG_{1k} and PEG_{2k}) were chosen to study its effect on the clustering process. By DLS no influence is observed under given clustering conditions (feed ratio 1:1 at 40 °C for 4 days; Figure 6.11 and Table 6.7). Besides, the peak size of clusters was all between 1-1.8 μm, which also reflects the size distribution range of the clusters. In addition, due to the stacked structure of clustered polymersomes and the quite short Flory radius (2.8 nm for PEG_{2k}) compared with the size of polymersomes, it was difficult to observe any differences in crosslinkers of different lengths even through cryo-TEM or in-situ AFM.¹⁸¹ It is believed that PEG_{15k} (Flory radius = 9.3 nm) or even longer PEG chain as crosslinker may affect the swelling-shrinkage capability of clustered polymersomes.¹⁸¹

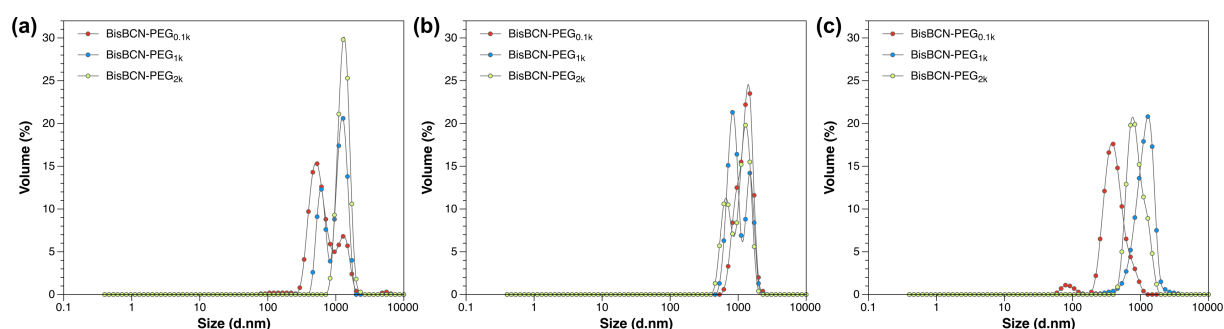


Figure 6.11 Size distribution of the Pomes-X%N₃ with 30% (a), 40% (b) and 100% (c) BCP-N₃ mixed with 1 eq. bisBCN-PEG crosslinker with different chain lengths at 40 °C for 4 days.

Table 6.7 Hydrodynamic diameter of the Pomes-N₃ with different proportion of BCP-N₃ mixed with 1 eq. bisBCN-PEG crosslinker with different length at 40 °C for 4 days.

PEG length of crosslinker	Ratio of BCP-N ₃	Peak size (d. nm)			Percent of peak area (%)		
		1	2	3	1	2	3
0.1k	30%	153	754	5459	1.6	97.7	0.7
1k		0	1036	0	0	100	0
2k		0	1319	0	0	100	0
0.1k	40%	0	1270	0	0	100	0
1k		0	1057	0	0	100	0
2k		0	1070	0	0	100	0
0.1k	100%	88	443	0	4	96	0
1k		0	1188	0	0	100	0
2k		0	892	0	0	100	0

Key Parameter VI: Psomes-N₃ Concentration. Psomes-N₃ (= Psomes-100%N₃) were clustered at different concentrations (from 0.1 to 1 mg/mL) and following up observations were made after 1 day of clustering. It can be seen from Figure 6.12 and Table 6.8 that after 1 day of continuous stirring, higher concentration leads to faster clustering rate (from 71.3% to 80.8%). Besides, the size of right-shift clusters' peak was also increased from 367 nm to 1003 nm with increasing concentration of Psomes-N₃. Considering that high concentration (1 mg/mL) is likely to cause irreversible aggregation in the enzymatic cascade reaction and considering high reaction efficiency along with increasing concentration of Psomes-N₃, the optimal concentration (0.5 mg/mL Psomes-N₃) was selected for the cluster's formation and purification as well as the following experiments about enzyme reaction.

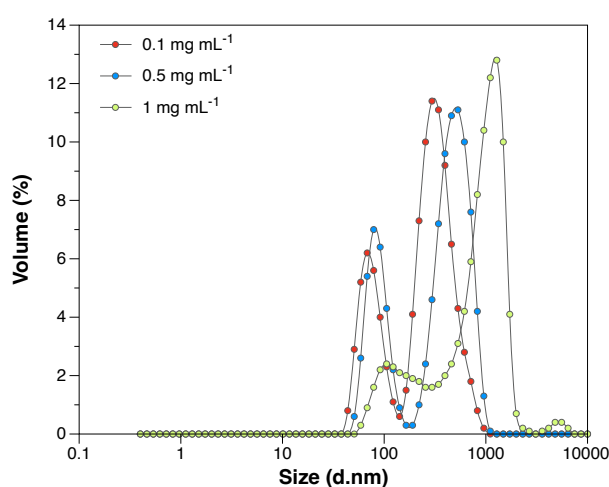


Figure 6.12 Size distribution of the Psomes-N₃ at different concentrations (from 0.1 to 1 mg/mL) mixed with 1 eq. bisBCN-PEG_{1k} crosslinker at 40 °C for 1 day. (Solvent of 1 mg/mL Psomes-N₃ is 10 mM NaCl solution, pH = 7.4; solvent of both 0.1 and 0.5 mg/mL Psomes-N₃ is PBS buffer without NaCl, 10 mM, pH = 7.4).

Table 6.8 Hydrodynamic size of the Psomes-N₃ at different concentrations (from 0.1 to 1 mg/mL) mixed with 1 eq. crosslinker bisBCN-PEG_{1k} at 40 °C for 1 day.

Concentration of Psomes-N ₃ (mg/mL)	Peak size (d. nm)			Percent of peak area (%)		
	1	2	3	1	2	3
0.1	76	367	0	28.7	71.3	0
0.5	87	509	0	29.9	70.1	0
1.0	140	1003	5085	17.9	80.8	1.2

To sum up the key parameters, different reaction conditions in the clustering process were explored and corresponding ratios of clusters counted by volume distribution are listed in Table 6.9. The effect of different conditions on the clustering reaction is more intuitively shown in Figure 6.13. After summarizing various conditions, 0.5 mg/ml of Psomes-N₃ were used in the clustering process using bisBCN-PEG_{1k} crosslinker at 1: 1 molar ratio and at 40 ° C for 2 days (Figure 6.13). It is worth mentioning that all the following experiments used a new batch of BCP-N₃ (N₃-PEG_{77.5}-b-p(DEAEMA₁₃₀-stat-DMIBMA₃₂ in Table 6.1) to cluster polymersomes (enzyme loaded polymersomes) due to its lower dispersity index ($\bar{D} = 1.23$) and higher ratio between hydrophobic segment and hydrophilic segment (2.09: 1) for preferred polymersomes formation, which means less micelles formation as side-product for assembled Psomes-N₃ compared with previously used BCP-N₃ (1.75: 1).

Table 6.9 Summary of optimal reaction conditions based on the percentage of Psomes-X%N₃ clusters in the clustering reaction.

Parameter	Temperature (°C)	Ratio of BCP-N ₃	Reaction time (d)	Surface N ₃ : Crosslinker	Length of crosslinker	Concentration of Psomes-N ₃ (mg/mL)	Clusters (%)
I	40	30%	2	1: 5	PEG _{1k}	0.5	40.1
	50	30%	2	1: 5	PEG _{1k}	0.5	5.5
	60	30%	2	1: 5	PEG _{1k}	0.5	0
II	40	10%	2	1: 1	PEG _{1k}	0.5	5.4
	40	30%	2	1: 1	PEG _{1k}	0.5	32.3
	40	40%	2	1: 1	PEG _{1k}	0.5	34.3
	40	60%	2	1: 1	PEG _{1k}	0.5	63
	40	80%	2	1: 1	PEG _{1k}	0.5	87.9
	40	100%	2	1: 1	PEG _{1k}	0.5	100
	40	10%	2	1: 1	PEG _{2k}	0.5	7.5
	40	30%	2	1: 1	PEG _{2k}	0.5	27.1
	40	40%	2	1: 1	PEG _{2k}	0.5	49.5
	40	60%	2	1: 1	PEG _{2k}	0.5	75
	40	80%	2	1: 1	PEG _{2k}	0.5	86.9
	40	100%	2	1: 1	PEG _{2k}	0.5	100

III	40	10%	2	1: 1	PEG _{1k}	0.5	5.4
	40	10%	9	1: 1	PEG _{1k}	0.5	58.3
	40	10%	30	1: 1	PEG _{1k}	0.5	95
	40	10%	2	1: 1	PEG _{2k}	0.5	7.5
	40	10%	9	1: 1	PEG _{2k}	0.5	33.8
	40	10%	30	1: 1	PEG _{2k}	0.5	70
	40	30%	1	1: 1	PEG _{1k}	0.5	4.5
	40	30%	2	1: 1	PEG _{1k}	0.5	32.3
	40	30%	4	1: 1	PEG _{1k}	0.5	100
	40	30%	1	1: 1	PEG _{2k}	0.5	1.5
	40	30%	2	1: 1	PEG _{2k}	0.5	27.1
	40	30%	4	1: 1	PEG _{2k}	0.5	100
IV	40	30%	2	1: 1	PEG _{1k}	0.5	32.3
	40	30%	2	1: 5	PEG _{1k}	0.5	40.1
	40	30%	2	1: 10	PEG _{1k}	0.5	36.5
	40	30%	2	1: 20	PEG _{1k}	0.5	42.7
	40	30%	2	1: 50	PEG _{1k}	0.5	14.8
	40	30%	2	1: 100	PEG _{1k}	0.5	4.1
V	40	30%	4	1: 1	PEG_{0.1k}	0.5	97.7
	40	30%	4	1: 1	PEG_{1k}	0.5	100
	40	30%	4	1: 1	PEG_{2k}	0.5	100
	40	40%	4	1: 1	PEG_{0.1k}	0.5	100
	40	40%	4	1: 1	PEG_{1k}	0.5	100
	40	40%	4	1: 1	PEG_{2k}	0.5	100
	40	100%	4	1: 1	PEG_{0.1k}	0.5	96
	40	100%	4	1: 1	PEG_{1k}	0.5	100
	40	100%	4	1: 1	PEG_{2k}	0.5	100
VI	40	100%	1	1: 1	PEG _{1k}	0.1	71.3
	40	100%	1	1: 1	PEG _{1k}	0.5	70.1
	40	100%	1	1: 1	PEG _{1k}	1.0	80.8

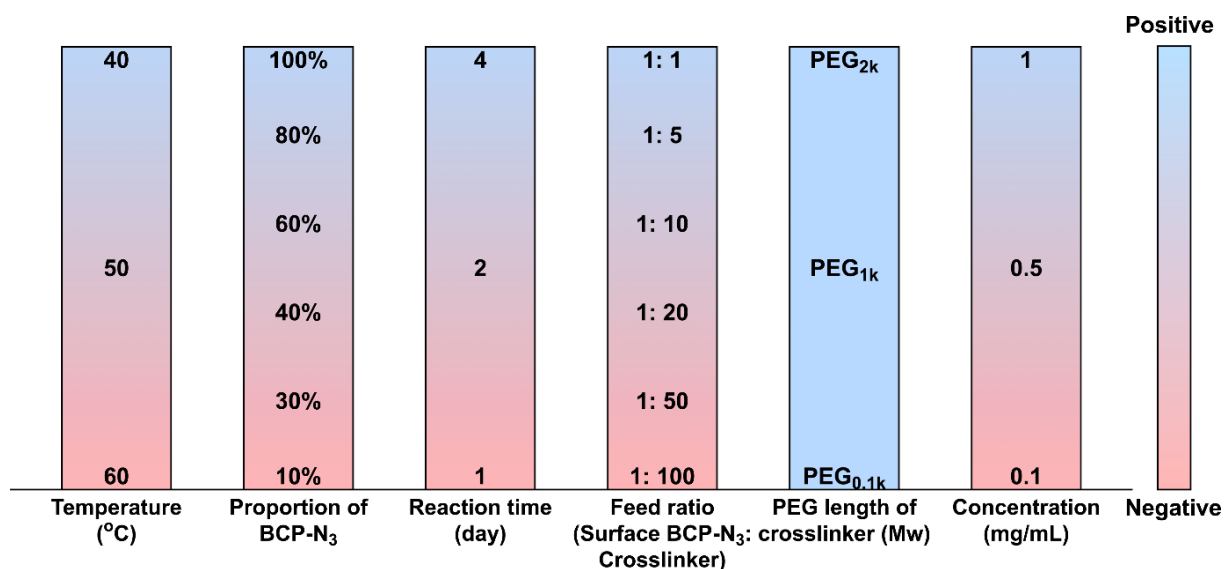


Figure 6.13 The influence of different parameters on the clustering reaction. Blue indicates a positive effect and red indicates a negative effect on the clustering reaction.

6.3.2 Purification Methods of Clustered Empty-Psomes-N₃

Next, centrifugal purification was used to remove unclustered Psomes-N₃ and small clusters. Before that, N₃-PEG₃-OH was utilized to terminate the clustering reaction to avoid any uncontrollable aggregates processes of clustered Psomes-N₃ (Figure 6.14). Considering the possible aggregation caused by centrifugation and the possible embedded isolated Psomes-N₃, different purification protocols have been studied to get optimal clustered Psomes-N₃.

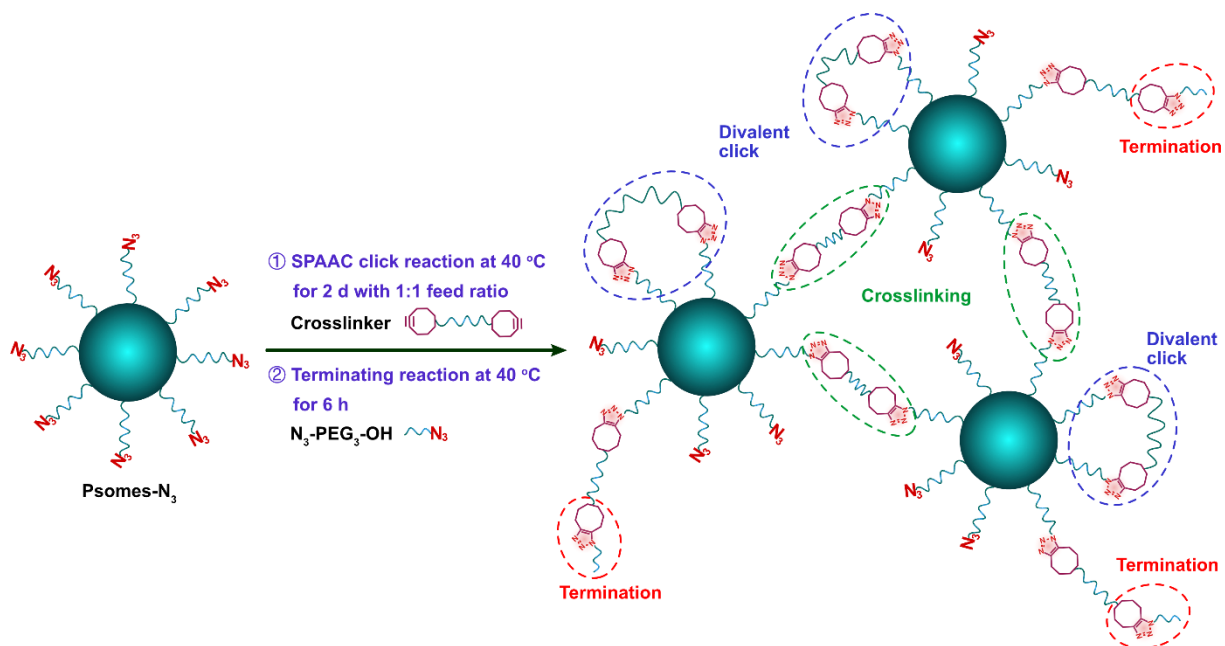


Figure 6.14 Schematic illustration shows the optimal process for the formation of pH-responsive clustered Psomes-N₃.

As shown in Figure 6.15, Protocol 1 was used to remove isolated polymersomes and small clusters through 4 times centrifugation and redispersion by mechanical stirring. After that, some large clusters still cannot be completely redispersed. Therefore, acidification process (pH switch between 6.0 and 8.0) was used to disaggregate the non-covalent bonding induced by centrifugation.

Considering the possible embedded polymersomes between clusters after centrifugation, acidification process was performed after one centrifugation to dissociate the aggregates to release isolated polymersomes (Protocol 2). After 4 times centrifugation, acidification process was carried out again to redisperse the clusters. Besides, vortex was also used to redisperse the clustered polymersomes after centrifugal steps (Protocol 3). After purifying the clusters with 4 cycles centrifugation and vortex redispersion, no aggregates were observed, for that reason the acidification step in the Protocol 3 was eliminated.

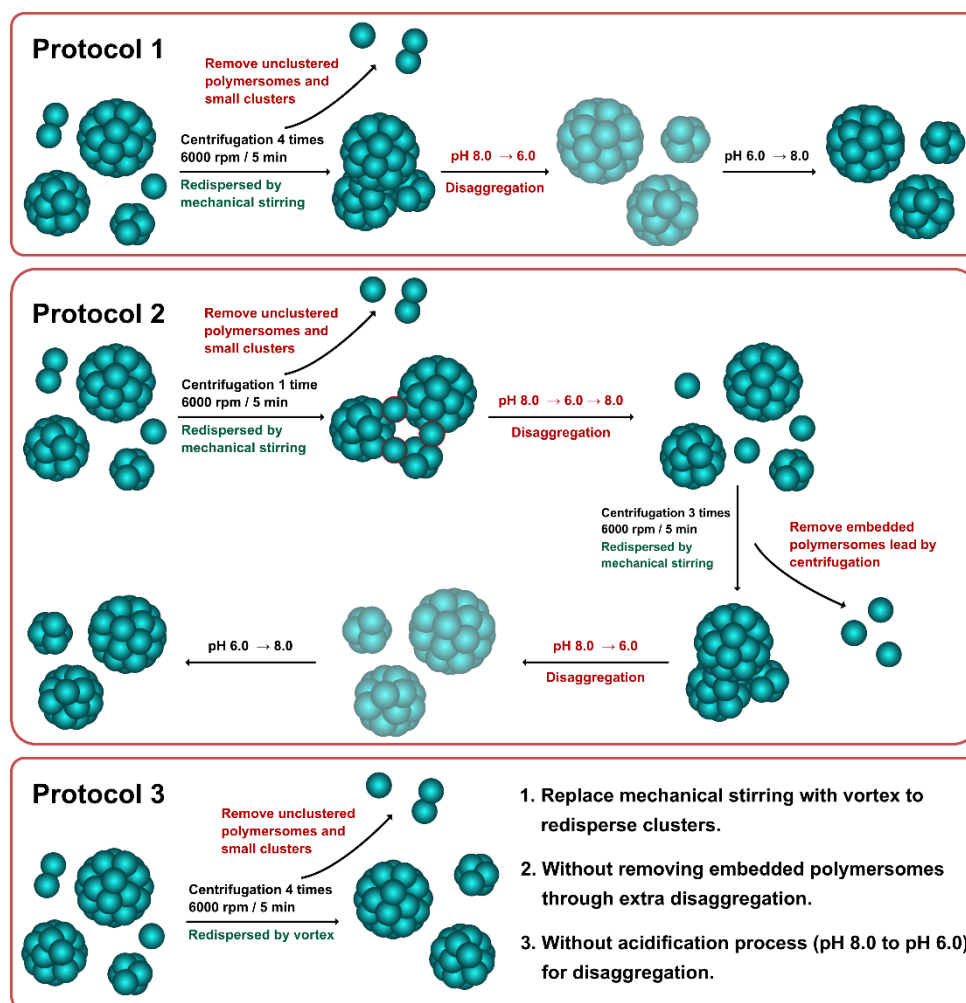


Figure 6.15 Schematic illustration shows the three different protocols for purification of clustered Psomes- N_3 .

To further understand the composition in the supernatant during the purification process, cyclic pH switches were carried out (Protocol 3). As shown in Figure 6.16a, unclustered Psomes-N₃ present stable swelling/shrinking ability even after 5 cycles of pH switch. After monovalent clicking with crosslinker (bisBCN-PEG_{1k}) and divalent clicking onto the surface of polymersomes through copper-free click reaction, the size of unclustered polymersomes (Posomes-N₃-BCN-PEG_{1k}-BCN) increased from 98 nm to 117 nm at collapsed state and increased from 178 nm to 230 nm at swollen state due to prolonged hydrophilic section on the polymersomes surface (Figure 6.16b). The low polydispersity index (0.133) also indicates that the polymersomes in the supernatant has uniform size and do not form small cluster with 2 or 3 polymersome units.

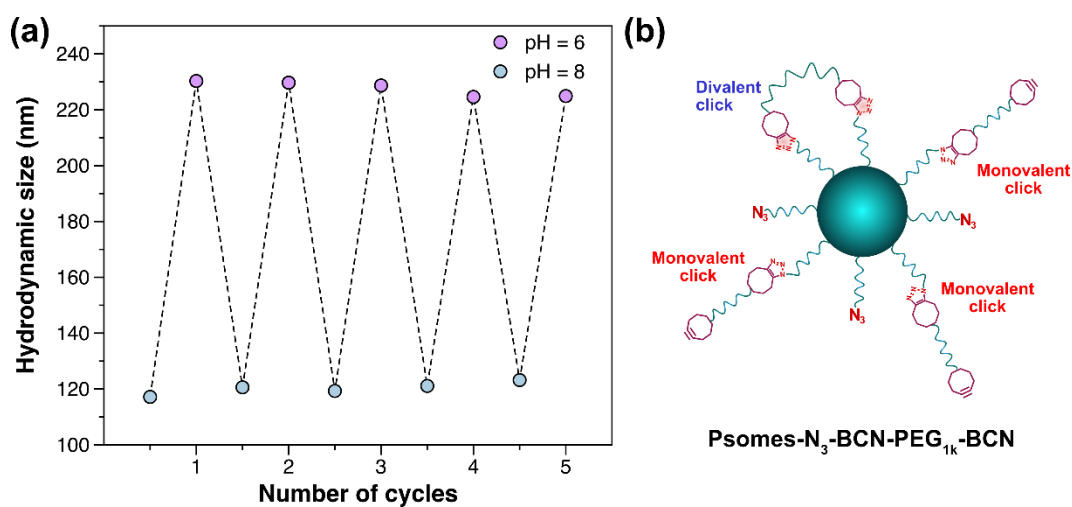


Figure 6.16 (a) Hydrodynamic size of Psomes-N₃ with cyclic pH switches between pH 8 and pH 5, obtained from the supernatant (clustered Psomes-N₃ after one centrifugation at protocol 3; Figure 6.15). Conditions: 10 mM PBS buffer. (b) Hypothetical structure of unclustered polymersomes monovalent or divalent click with crosslinker (Posomes-N₃-BCN-PEG_{1k}-BCN).

Additionally, to validate the loss of unclustered Psomes-N₃ during the centrifugation process, BSA-Cy5 in-situ loaded Psomes-N₃ (BSA-Cy5-Posomes-N₃) were fabricated and purified by HFF. After that, BSA-Cy5-Posomes-N₃ were assembled to clusters and purified by aforementioned protocols and checked by fluorescence spectroscopy. After 4 times centrifugation, the remaining clustered BSA-Cy5-Posomes-N₃ has 58.1% (Protocol 1), 59.0% (Protocol 2) and 60.8% (Protocol 3) fluorescence intensity compared with previous fluorescence intensity (clustered BSA-Cy5-Posomes-N₃ without centrifugation, Figure 6.17). It indicates that about 40% unclustered polymersomes are removed after four times centrifugation. In addition, it is obvious that most of single polymersomes were removed after first centrifugation step.

However, no significant differences between different purification protocols were observed, that means further characterization is necessary to prove their differences.

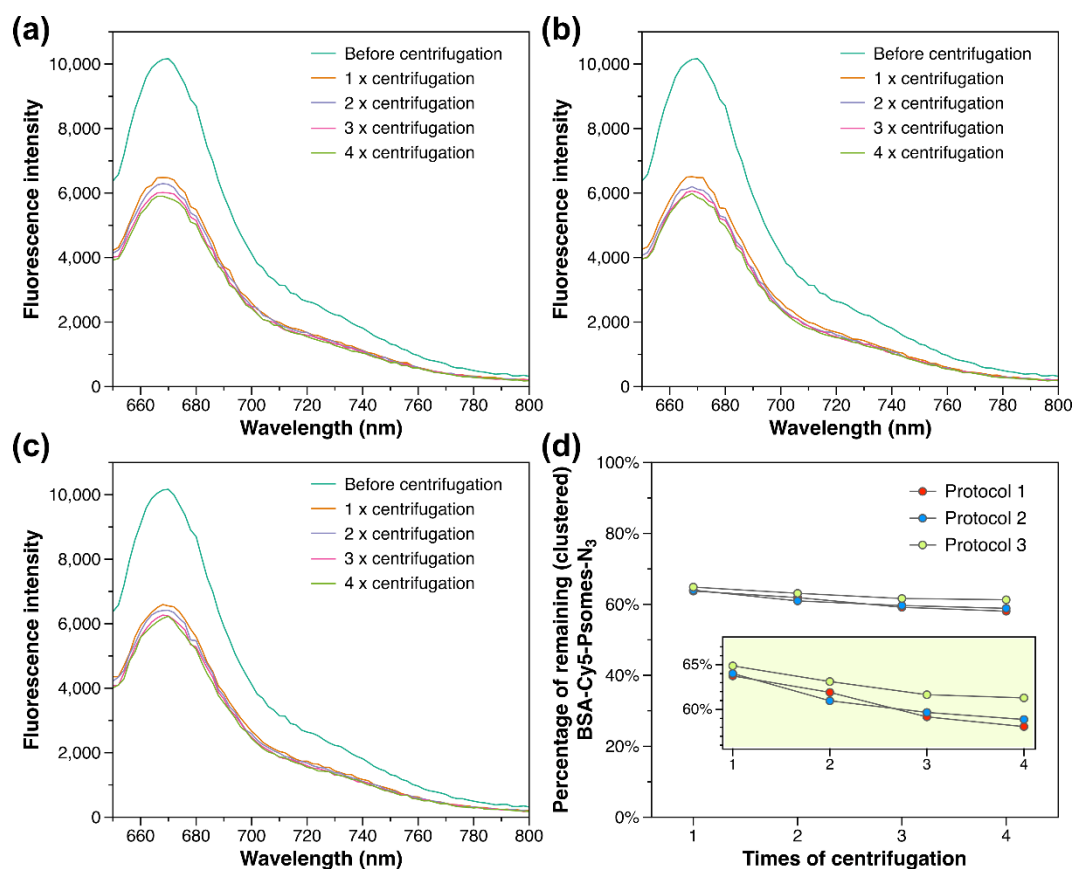


Figure 6.17 Fluorescence intensity of clustered BSA-Cy5-Psomes-N₃ solution before and after purification by Protocol 1 (a), Protocol 2 (b) and Protocol 3 (c). Percentage of remaining (clustered) BSA-Cy5-Psomes-N₃ in the residue solution (d) after different times centrifugation, compared with the original solution before centrifugation and calculated by fluorescence intensity. The inset is an enlarged view of the plots. Conditions: 0.5 mg/mL BSA-Cy5-Psomes-N₃ for clustering process in 1 mM PBS buffer (pH 8.0).

6.4 Preparation and Purification of Clustered Empty-Psomes-N₃ and Enzyme-Psomes-N₃

6.4.1 Formation and Characterization of Enzyme in-Situ Loaded Psomes-N₃ (Enzyme-Psomes-N₃)

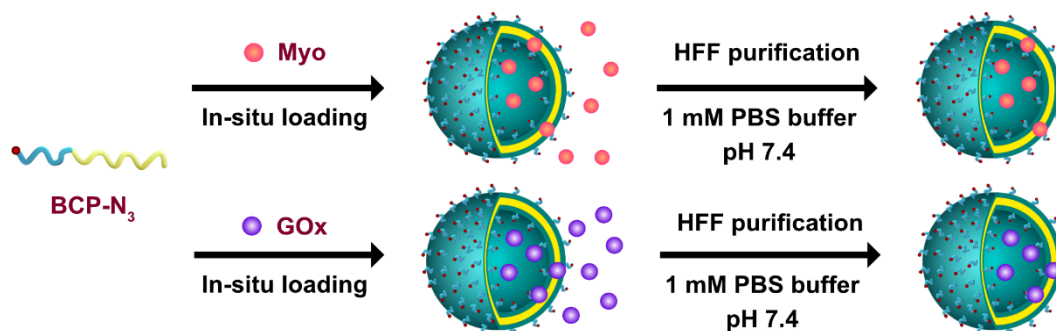


Figure 6.18 Schematic illustration shows the process for the formation and purification of Psomes-N₃ with in-situ encapsulated enzymes, Myo and GOx (Myo-Psomes-N₃ and GOx-Psomes-N₃).

GOx and Myo were in-situ loaded during Psomes-N₃ formation using a previously published protocol, and enzyme-loaded Psomes-N₃ were purified by hollow fiber filtration (HFF) (Figure 6.18).⁸⁵ The loading efficiencies were determined as 4.5% for GOx and 9.3% for Myo through fluorescent labeling of the enzyme and tracking their fluorescence intensity before and after HFF purification (Figure 6.19).

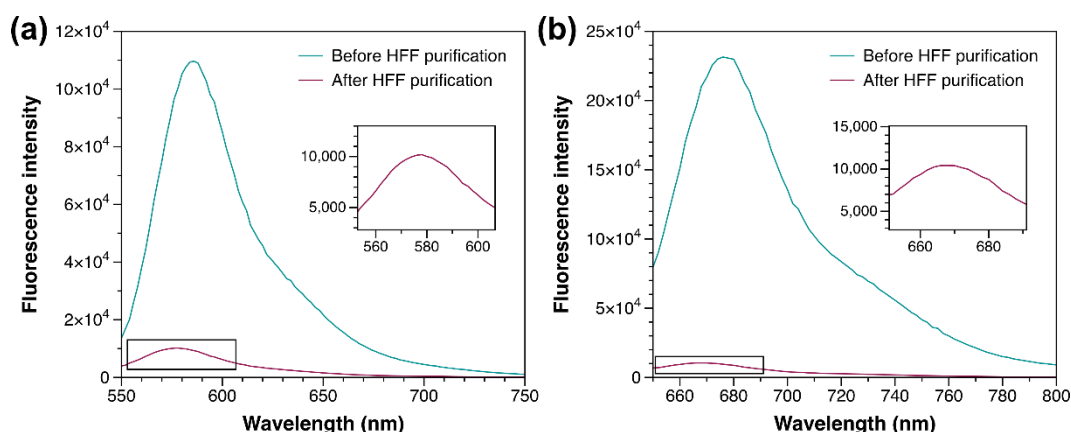


Figure 6.19 Fluorescence intensity of Myo-Psomes-N₃ (a) and GOx-Psomes-N₃ (b) before and after HFF purification. The insets are enlarged views of the fluorescence spectra after HFF purification.

To prove the pH-responsive stability of Psomes-N₃, Myo-Posomes-N₃ and GOx-Posomes-N₃, pH switches were also carried out through pH switch from 8.0 to 5.0 (Figure 6.20a-c). All polymersomes show stable swelling/shrinking ability even after 5 cycles of pH-switch. The average sizes of Empty-Posomes-N₃, Myo-Posomes-N₃ and GOx-Posomes-N₃ under shrinking state and swelling state are 92-174 nm, 90-173 nm, and 76-154 nm, respectively.

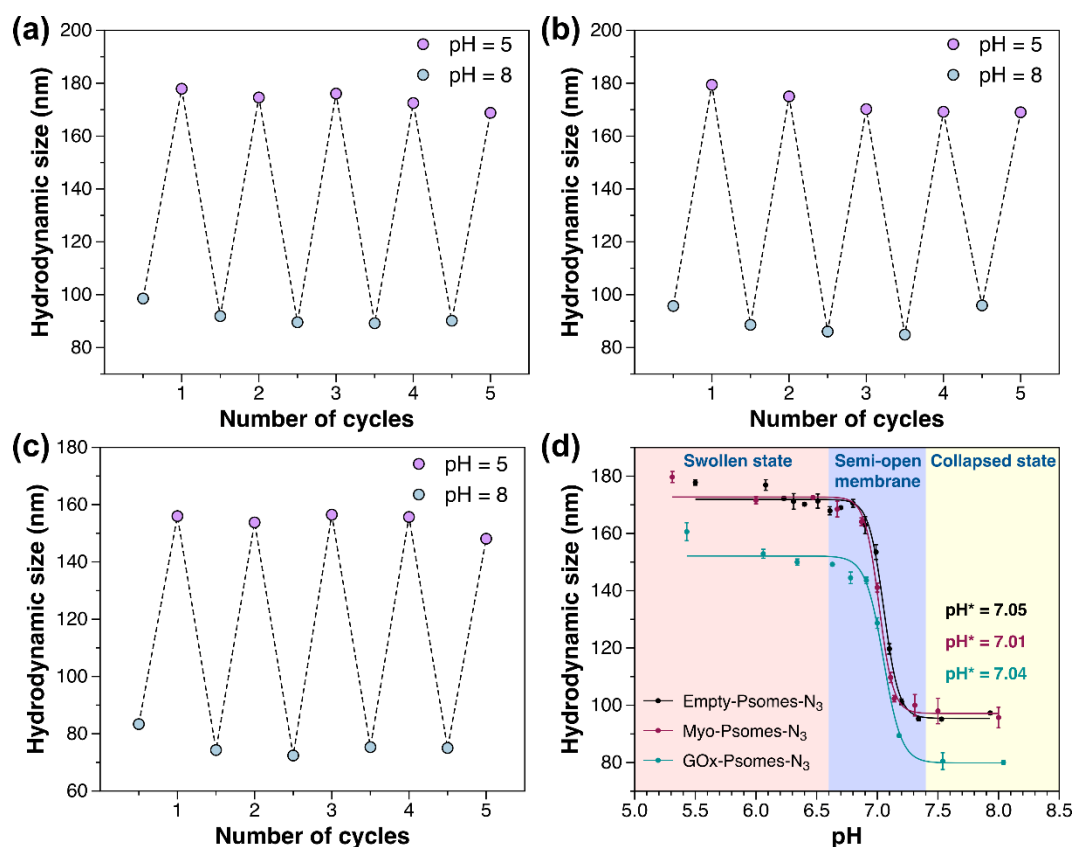


Figure 6.20 Hydrodynamic size of Empty-Posomes-N₃ (a), Myo-Posomes-N₃ (b) and GOx-Posomes-N₃ (c) after HFF purification followed by cyclic pH switches between pH 8 and pH 5. (d) Hydrodynamic size of Empty-Posomes-N₃, Myo-Posomes-N₃ and GOx-Posomes-N₃ through pH titration from pH 8 to pH 5. Condition: 0.25 mg/mL Psomes-N₃ in 10 mM PBS buffer.

Besides, to realize controllable switch-on/-off of polymersomes membrane of co-clustered Myo/GOx-Posomes-N₃ for enzymatic cascade reaction, the swelling/shrinking characteristics of their membrane with changing pH values were further explored (Figure 6.20d). Herein, pH titrations of Empty-Posomes-N₃, Myo-Posomes-N₃ and GOx-Posomes-N₃ were performed at 10 mM PBS. The pH* (pH value for semi-open membrane) are 7.05, 7.01 and 7.04, respectively. This also indicates that at \geq pH 7.5 Psomes-N₃ membrane is in a collapsed state. Thus, smaller molecule diffusion into the lumen of enzyme loaded polymersomes is almost hampered.

To prove the hollow structure and shape, cryo-TEM study of Empty-Psomes-N₃, Myo-Psomes-N₃ and GOx-Psomes-N₃ was performed at pH 8.0 (Figure 6.21a-c). The size histograms (Figure 6.21d-f) show the average sizes of 112.7 nm for Psomes-N₃, 117.0 nm for Myo-Psomes-N₃, and 117.2 nm for GOx-Psomes-N₃, respectively. Besides, the membrane histograms (Figure 6.21g-i) show that the average membrane thicknesses of Psomes-N₃, Myo-Psomes-N₃ and GOx-Psomes-N₃ are 25.9 nm, 27.6 nm, and 25.7 nm, respectively. The thicker membrane proves longer BCP-N₃-2 composition compared with previously used BCP-N₃-1 in the optimization process of Psomes-X%N₃.

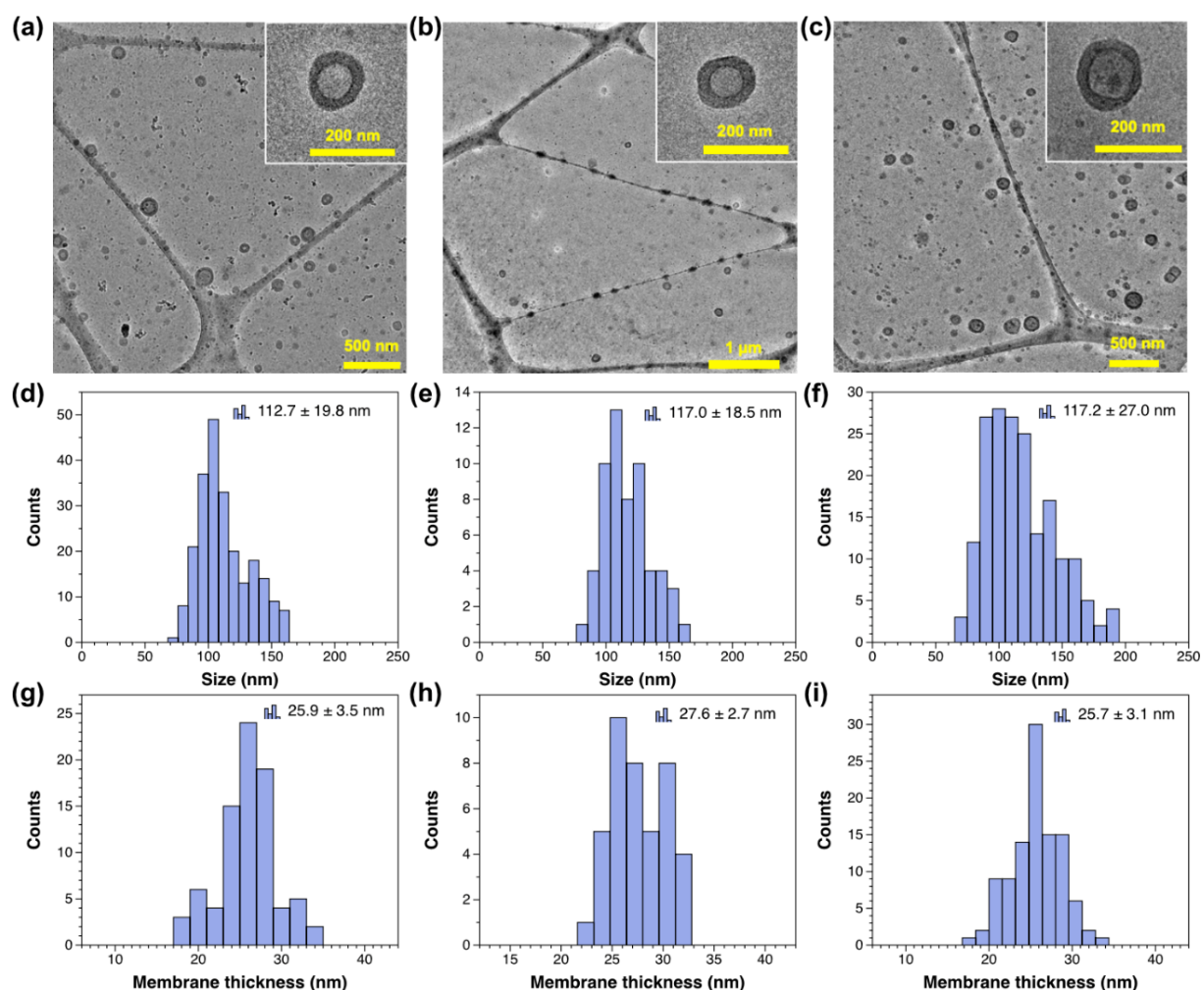


Figure 6.21 Cryo-TEM (a-c), size histograms (d-f) and membrane thickness histograms (g-i) of Empty-Psomes-N₃ (left), Myo-Psomes-N₃ (center) and GOx-Psomes-N₃ (right) after HFF purification. Condition: 1 mg/mL Psomes-N₃ in 1 mM PBS buffer (pH 7.4) for cryo-TEM.

6.4.2 Enzyme Location in Polymersomes

To prove the main locations of enzyme in the Enzyme-Psomes-N₃ and also to study the structural parameters, asymmetrical flow-field flow fractionation (AF4) coupled to light scattering was performed to evaluate the conformation and morphology of the particles and locations of the enzyme within the hybrid structure.⁸⁵ The potential locations, include polymersomes' lumen, inner and outer surface of the membrane, as well as the interior of the membrane.¹⁸² The dependence of the radius of gyration, R_g , on the molar mass, M was plotted (Figure 6.22a): $R_g \propto M^{\nu}$, (where ν is the scaling exponent) for the GOx-Psomes-N₃ and Myo-Psomes-N₃, which Empty-Psomes-N₃ was used as a reference after HFF purification. For GOx-Psomes-N₃, a slightly larger R_g can be observed when the enzymes are integrated within polymersomes' membrane. For hard sphere, $\nu = 0.33$ is expected corresponding to the three-dimensional (3D) fractal object. Though, this value is additionally strongly depending on the nature of particles surface. The conformation plots of Empty-Psomes-N₃ and Myo-Psomes-N₃ after HFF purification determined at pH 7.4 in 1 mM PBS buffer ($\nu = 0.30-0.31$), indicate uniform particle conformation close to ideal sphere. However, in case of GOx-Psomes-N₃ after HFF purification is increased ($\nu = 0.41$), indicating a more heterogenous surface. Indeed, the study of the polymersomes membrane conformation after enzyme loading shows clear differences depending on the type of enzyme.^{85, 123} The differences in the scaling parameters of both Enzyme-Psomes-N₃ can be directly attributed to the size of the enzyme used. GOx (160 kDa, Ø 10 nm) is much larger than Myo (17 kDa, Ø 5 nm). It follows that the incorporation of Myo within the membrane or its attachment onto polymersomes surface does not significantly affect the surface morphology of the polymersomes.⁸⁵ In this context, larger diameters of Myo-Psomes-N₃ and GOx-Psomes-N₃ in respect to Empty-Psomes-N₃ is given by cryo-TEM study (Figure 6.21) which support the possible (partial) membrane-integration of both enzymes during Psomes-N₃ formation. Analyzed membrane thickness of Enzyme-Psomes-N₃ is in the range of Empty-Psomes-N₃ (Figure 6.21). Finally, this indicates that possible membrane-integration of both enzymes does not result in an increase of membrane thickness, but both enzymes influence the self-assembly process of BCP-N₃-2 into Psomes-N₃, leading to larger diameters. A similar tendency is observed for apparent density, the decrease is stronger in the case of GOx-Psomes-N₃. This may be due to a higher integration of GOx into the membrane, which generates more substantial changes than in the case of Myo-Psomes-N₃ (Figure 6.22b).

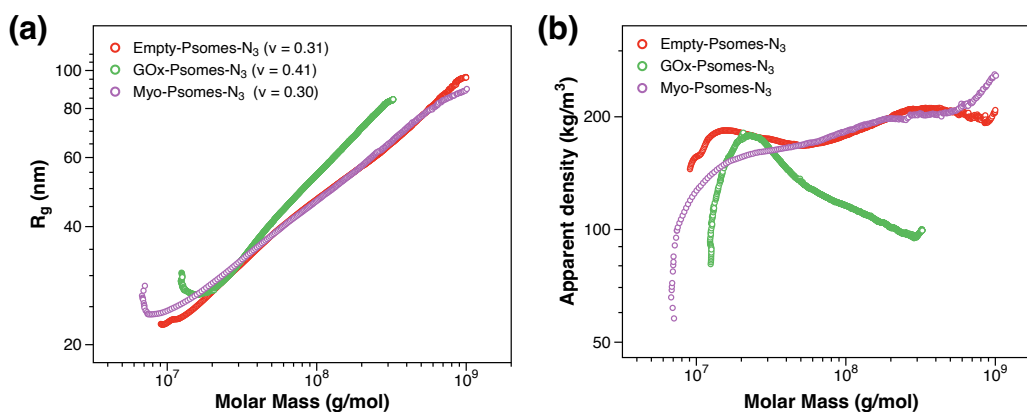


Figure 6.22 Conformation properties of polymersomes studied by AF4-LS analysis at pH 7.4. Conditions: 0.5 mg/mL polymersomes (+ 0.1 mg/mL enzyme) for preparing Empty-Psomes- N_3 and Enzyme-Psomes- N_3 . Dependence of the radius of gyration (R_g) (a) and apparent density (b) on the molar mass calculated for polymersomes: Empty-Psomes- N_3 , Myo-Psomes- N_3 , GOx-Psomes- N_3 after HFF purification.

As shown in Figure 6.23, the fractograms (detector signals versus time) before and after HFF purification demonstrate the completely remove of the free enzyme, include GOx and Myo, in early elution area. The factor ρ (R_g/R_h) is an important parameter to understand the conformation of the nanoparticles in solution.

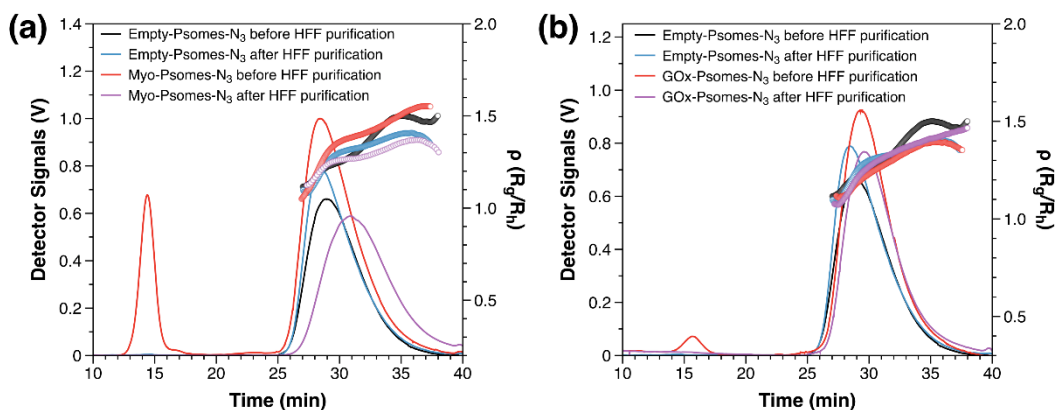


Figure 6.23 AF4 fractograms with light scattering detector signals (lines) and ρ parameter (R_g/R_h , circles) for Empty-Psomes- N_3 (a&b), Myo-Psomes- N_3 (a), and GOx-Psomes- N_3 (b) before and after HFF purification. Conditions: 1 mg/mL Psomes- N_3 in 1 mM PBS buffer (pH 7.4).

Considering the ρ parameter (R_g/R_h), it can be observed that GOx-Psomes- N_3 and Empty-Psomes- N_3 present a similar value 1.1 in the main fraction, close to 1, typical for hollow spheres. At later elution time or larger polymersome dimensions, the parameter increases,

which can be attributed to an increasing heterogeneity of the morphology caused, for example, by aggregation of individual polymersomes. Thus, some GOx molecules are integrated into the membrane and, but also few in the lumen. However, ρ is 1.0 in the case of Myo after HFF purification, which confirms that Myo is more present in the lumen than into the membrane in comparison with GOx (Figure 6.23). Conclusion on the membrane integration of GOx and Myo in Psomes-N₃ will be finalized in the pH-dependent enzyme assays.

6.4.3 Deeper Characterization of Clustered Empty-Psomes-N₃ and Clustered Enzyme-Psomes-N₃

To visualize the clustered polymersomes, different imaging methods were used to prove the successful clustering process and also provide ideas for the optimization of clustered polymersomes.

Cryo-TEM and TEM Measurement. The morphology and size of the clustered Empty-Psomes-N₃ before and after purification were firstly investigated by cryo-TEM and TEM (Figure 6.24).

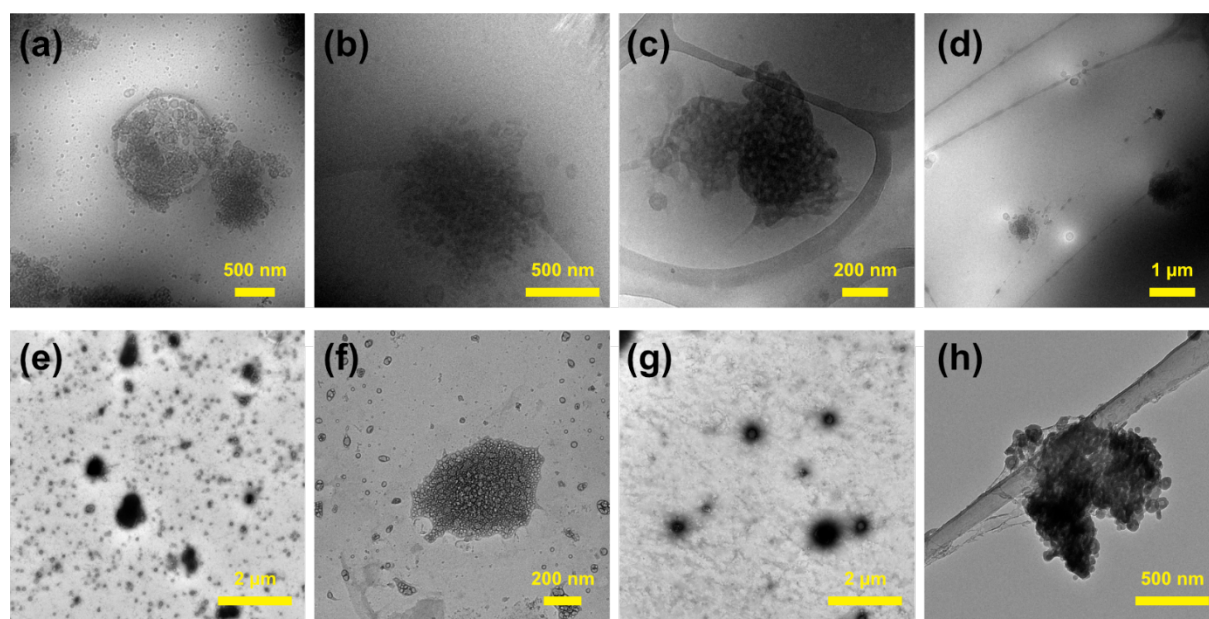


Figure 6.24 Cryo-TEM images (a-d) and TEM images (e-h) of clustered Empty-Psomes-N₃ at pH 8.0 before and after purification by different protocols. (a&e): Without purification. (b&f): Purified by Protocol 1. (c&g): Purified by Protocol 2. (d&h): Purified by Protocol 3. (e&g): Stained by PTA (2% w/w) water solution. (h): Prepared by freeze-drying method.

In the cryo-TEM images of unpurified clusters, we can observe some dark regions. This indicates that the clustered polymersomes are too large and excessively overlapped which leads to thick ice layer and then dark and blurry image (ice thickness depends on the size of the clusters). Thus, it is difficult to see the boundaries and membranes of each polymersome (Figure 6.24a-d). However, unclustered polymersomes can be clearly observed as nanoscaled polymersomes. Comparing the cryo-TEM images before and after centrifugation, most of the isolated polymersomes and small clusters are removed, although few isolated polymersomes still exist. In most cases, all clusters show irregular shapes. Thus, the clustering reaction is still uncontrolled.

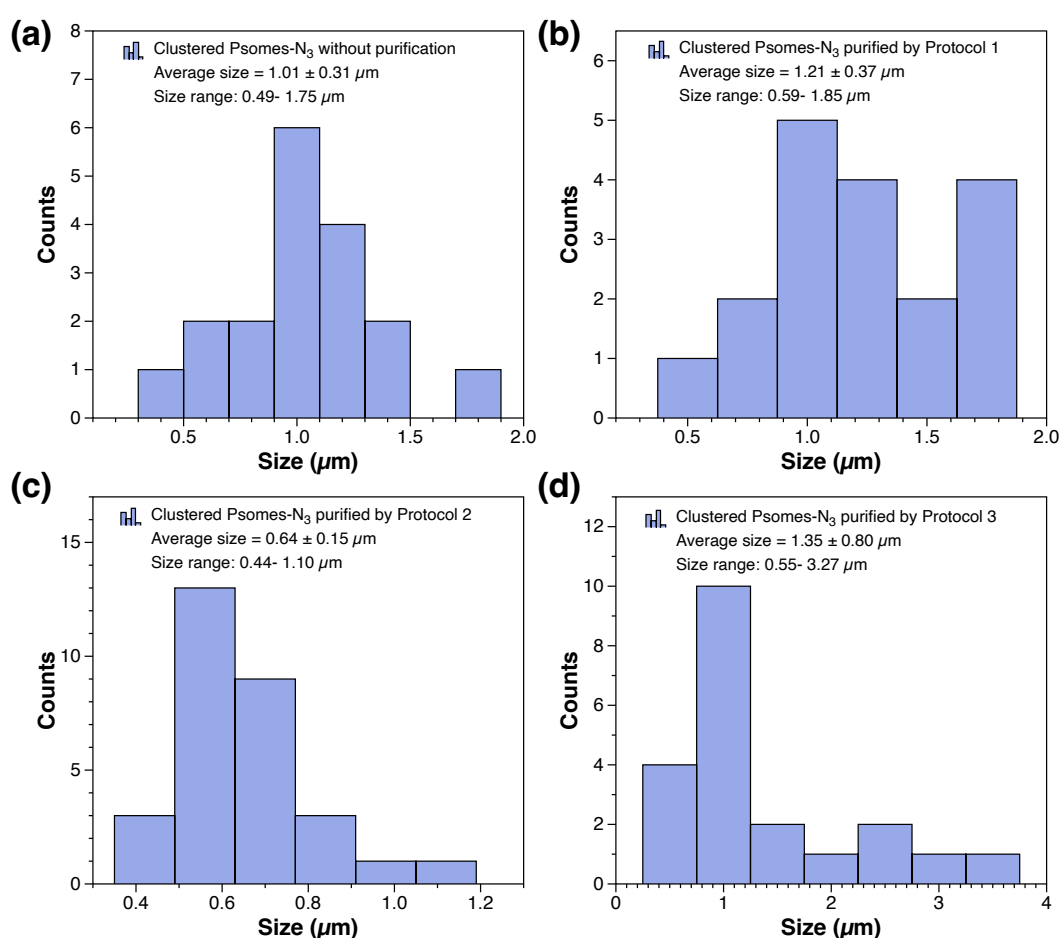


Figure 6.25 Cryo-TEM histograms of clustered Empty-Psomes-N₃ before (a) and after purification by Protocol 1 (b), Protocol 2 (c) and Protocol 3 (d).

Furthermore, the cryo-TEM histograms show that the average sizes of clustered Psomes-N₃ before and after purification are 1.01 μm (before purification), 1.21 μm (Protocol 1), 0.64 μm (Protocol 2), 1.35 μm (Protocol 3), respectively (Figure 6.25 and Table 6.10). The decreased size of clusters purified by Protocol 2 (0.64 μm) could be due to fewer number of samples (\geq

18 clusters were measured for each sample) rather than the use of acidification step (pH 8.0 to 6.0 for 5 min and then back to pH 8.0). The size of clusters purified by Protocol 1 shows increasing tendency compared with the clusters without purification (smaller clusters were removed after centrifugation, so the average size increased slightly).

Since it is difficult to observe the structure of the clusters clearly through cryo-TEM, TEM imaging were taken for the clustered Psomes-N₃ purified by Protocol 1 (Figure 6.24f). It is easy to see the clustered Psomes-N₃ and isolated Psomes-N₃. However, since dry Psomes-N₃ collapsed, the membrane of Psomes-N₃ cannot be observed. Besides, the clusters after centrifugation still contain some isolated Psomes-N₃. It may be that acidification process induces the dissociation process of the freely embedded Psomes-N₃ from the clustered Psomes-N₃. It is worth noting that the acidification process achieves complete protonation of the polymersome membrane and then the isolated Psomes-N₃ bound by non-covalent bonding can be separated from clusters due to the repulsive force of the positive charge between the Psomes-N₃.

Table 6.10 Size of clustered Psomes-N₃ at pH 8.0 before and after purification by different protocols, characterized by TEM and cryo-TEM.

Purification Methods	Average size from TEM (μm)	Average size from cryo-TEM (μm)
Without purification	1.10 ± 0.66 ^a	1.01 ± 0.31
Purified by Protocol 1	0.48 ± 0.17 ^b	1.21 ± 0.37
Purified by Protocol 2	0.80 ± 0.33 ^a	0.64 ± 0.15
Purified by Protocol 3	1.03 ± 0.34 ^c	1.35 ± 0.80

^a Normal TEM images; ^b Negative staining by PTA solution; ^c In-situ freeze dry under -80 °C.

Next, Protocol 2 was used to remove embedded Psomes-N₃ through two-step acidification process. In the TEM images of clustered Psomes-N₃ before and after centrifugation, in order to highlight the hollow capsule structure of Psomes-N₃, the clustered Psomes-N₃ were stained with 2% PTA (w/w) solution (Figure 6.24e&g).

The larger cluster showed black sphere shape due to overlapped stained Psomes-N₃, while the unclustered Psomes-N₃ showed hollow structure. By observing the magnified images of the cluster, it is easy to see that the hollow spherical Psomes-N₃ showed clear outline on the edge

of clusters, which proves that the black sphere is composed of the clustered Psomes-N₃. Comparing the clustered Psomes-N₃ before and after centrifugation, most of the isolated Psomes-N₃ were removed after centrifugation, although some free Psomes-N₃ still exist.

This may be due to the fact that most of embedded Psomes-N₃ were separated from the clusters after acidification process and some isolated Psomes-N₃ re-absorbed onto the surface of clusters again after centrifugation. In the final acidification process, the packed Psomes-N₃ redispersed in the solution because of the repulsive force of the positive charge between the Psomes-N₃.

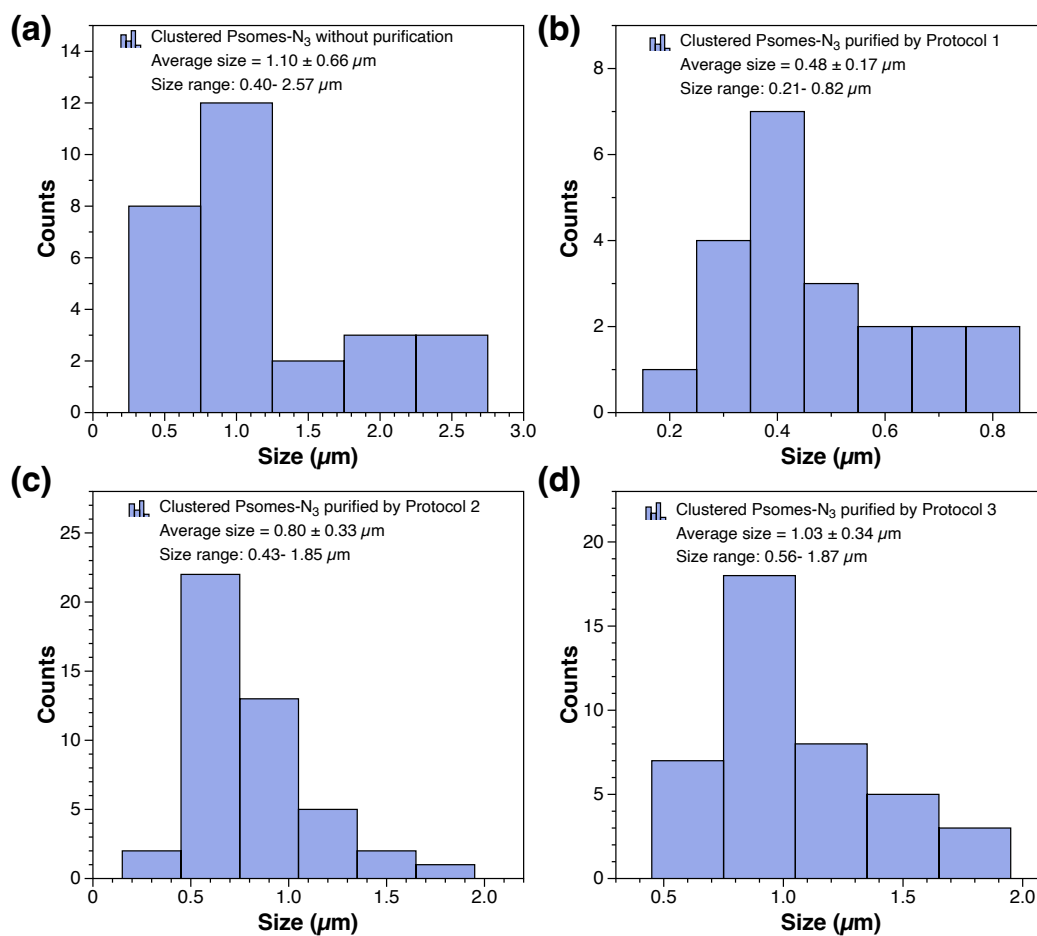


Figure 6.26 TEM Histograms of clustered Empty-Psomes-N₃ before (a) and after purification by Protocol 1 (b), Protocol 2 (c) and Protocol 3 (d).

The TEM histograms show that the average sizes of clustered Psomes-N₃ after purification by protocol 1 and 2 are 0.48 and 0.80 μm, respectively (Figure 6.26 and Table 6.10). Compared with their original size, the decline in size of clustered Psomes-N₃ is ascribed to the dry state after evaporating the solvent. Besides, the traditional TEM study cannot achieve clear and compelling images.

To observe the structure of clusters more clearly, freeze-drying method was used to clustered Psomes-N₃ (Figure 6.27). For the freeze dry process, the sample was frozen first in liquid nitrogen and then loading the sample inside the TEM. Following, the temperature was slowly increased from -172 °C to -80 °C, the ice was sublimated and the clustered Psomes-N₃ kept the original hollow structure for each polymersome unit. The table shows the size of clustered Psomes-N₃ and co-clustered Myo/GOx-Psomes-N₃ at pH 8.0 before and after purification, characterized by TEM and cryo-TEM (Table 6.10).

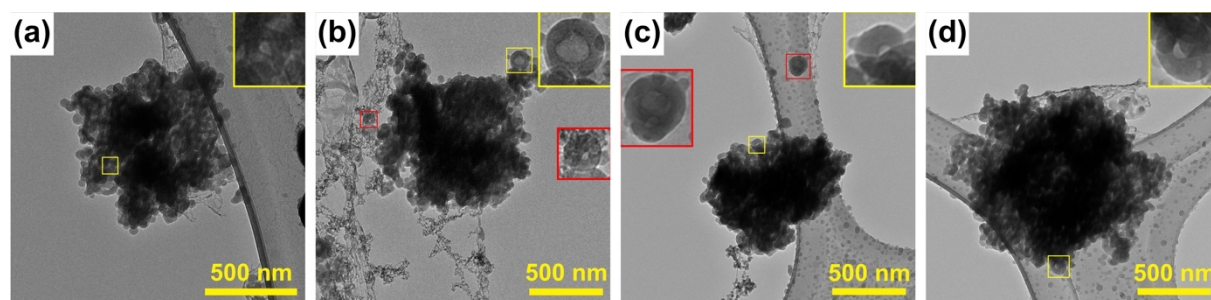


Figure 6.27 TEM images of in-situ freeze-dried clustered Psomes-N₃ at pH 8.0 (a) without and (b) with acidification process after purification. Co-clustered Myo/GOx-Psomes-N₃ at pH 8.0 (c) without and (d) with acidification process after purification by Protocol 3. The inset shows the magnified polymersome in the cluster (yellow box) and isolated polymersome (red box).

Compared with the collapsed Psomes-N₃ prepared through air-dried method, the freeze-drying can maintain the spatial structure of the clustered Psomes-N₃. This allows a better observation of the structure of clustered Psomes-N₃. After purification by Protocol 3, it can be observed from the boundary polymersomes of clusters that the cluster is composed of many Psomes-N₃, as well as the hollow structure and membrane of single Psomes-N₃ (Figure 6.24h and Figure 6.27a-b). The same results occur for co-clustered Enzyme-Psomes-N₃ (Figure 6.27c-d). Overall, the TEM results consequently support the formation of desired clusters with different compositions. In addition, very few isolated Psomes-N₃ still can be seen from the images.

As a control, the clustered Psomes-N₃ and co-clustered Enzyme-Psomes-N₃ were treated with a weak acidification process (pH 8.0 to pH 6.5 for 5 min and back to pH 8.0) to check their pH stability. As seen from these images, there is no obvious disaggregation process (Figure 6.27b&d). This shows that weak acidification will not affect the structural stability of the clusters and that multiple centrifugations alone cannot remove all isolated Psomes-N₃. Furthermore, the TEM histograms show that the average sizes of clustered polymersomes before and after purification are 1.10 μm and 1.03 μm , respectively. The purified clusters show

slightly decreased size (1.03 μm) compared with the size from cryo-TEM (1.35 μm), which is due to the shrinking triggered by the vaporization of ice. Furthermore, the TEM histogram of co-clustered Enzyme-Psomes- N_3 purified by Protocol 3 shows that the average size is 0.81 μm , which also confirm the successful formation of clusters (Figure 6.28).

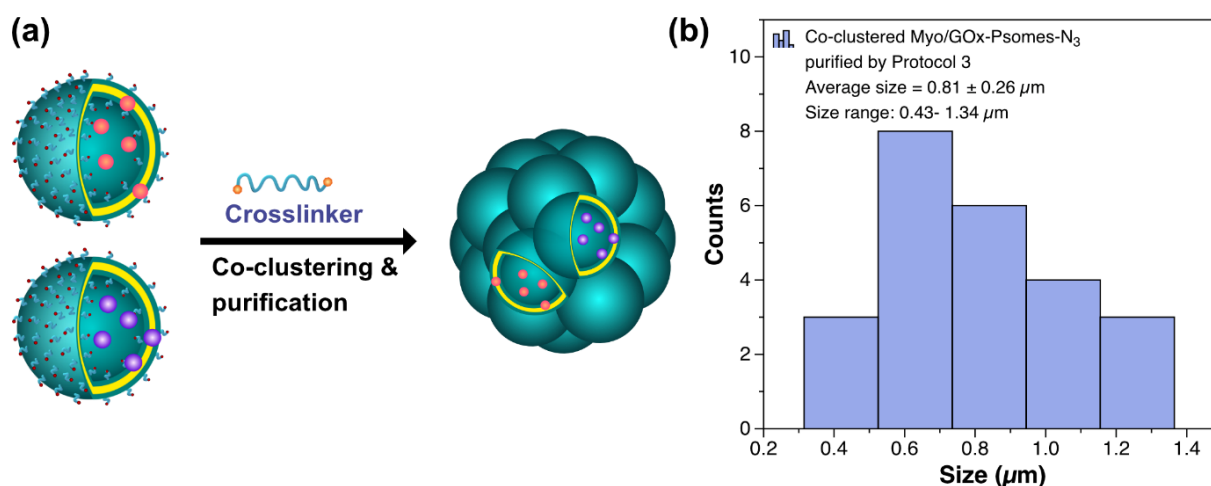


Figure 6.28 Schematic illustration (a) and TEM Histograms (b) of co-clustered Myo/GOx-Psomes- N_3 at pH 8.0 after purification by Protocol 3 in Figure 6.15.

In general, TEM and cryo-TEM images proved the formation of clustered Psomes- N_3 and Enzyme-Psomes- N_3 and can be used to roughly counted their size. In opposite, TEM and cryo-TEM images cannot be used to accurately express the influence of the acidification process and the redispersion method on the size development.

In-Situ AFM Measurement. Under acidic conditions, clustered Psomes- N_3 are difficult to observe the swelling and shrinking properties under TEM/cryo-TEM. For it, in-situ AFM was performed for the size definition of clustered Psomes- N_3 under basic and acidic conditions. Here, plasma-cleaned Si wafer was used as substrate for clustered Psomes- N_3 . The plasma cleaning removes any residual organic matter from the surface and imparts a slightly negative charge onto it. The clusters solution was added onto the surface of cleaned Si wafer and then deposited for 1 min. Then the most of solution was absorbed by filter paper to obtain a thin layer clusters solution onto the surface for in-situ AFM measurement.

It can be seen from Figure 6.29 and Figure 6.30 that clusters and isolated Psomes- N_3 at pH 8.0 from the in-situ AFM images after purification by different protocols. This proves again that the isolated Psomes- N_3 cannot be completely removed by centrifugation, which agrees with the observation at cryo-TEM and TEM images. Besides, these AFM images show some clusters

with irregular shape at pH 8.0, and most of their sizes are significantly larger than the sizes obtained from TEM and cryo-TEM study. As measured from in-situ AFM images, the maximum sizes of adsorbed clustered Psomes-N₃ purified by protocol 1-3 are 1.37 μm (Figure A36), 5.50 μm (Figure A37) and 5.56 μm (Figure A38), and the maximum size of co-clustered Myo/GOx-Psomes-N₃ even reached 11.66 μm (Figure A39). Because the number of samples is not enough, the average size cannot be determined. In addition, the isolated polymersomes and/or small clustered polymersomes in the clustering process maintain their shape of hollow sphere with a height between 30-70 nm under basic conditions (Figure A40 and Figure A41).

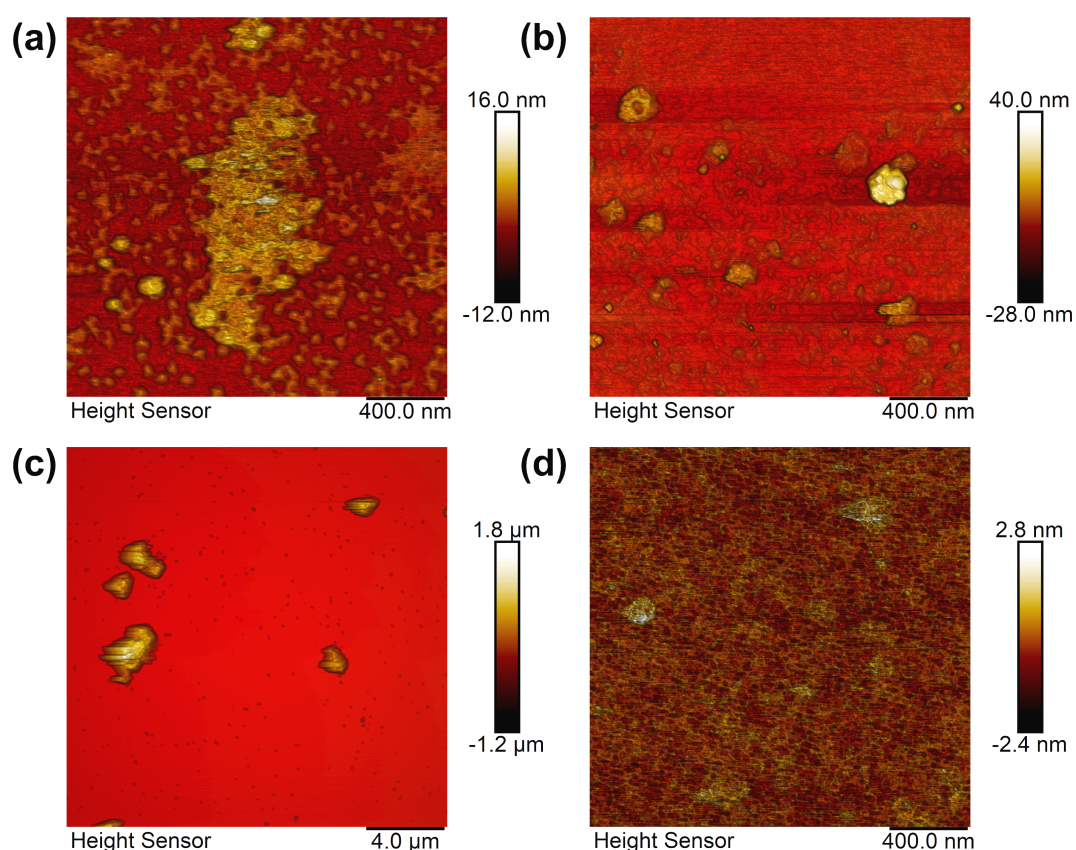


Figure 6.29 In-situ AFM images of clustered Psomes-N₃ purified by Protocol 1 (a-b) and Protocol 2 (c-d) at pH 8.0 (a&c) and pH 6.0 (b&d).

With decreasing pH values from 8.0 to 6.5, the membrane of Psomes-N₃ was in a low protonated state at pH 7.0 and in a high protonated state at pH 6.5. At the same time, the clustered Psomes-N₃ with positive charge became more flattened and compacted under acidic conditions due to electrostatic attraction (the color bar range in Figure 6.30 shows the height change of clusters from micrometer to nanometer withing decreasing pH values). This makes it hard to see the boundary of clustered Psomes-N₃.

In addition, attractive electrostatic interactions are enhanced between anionic substrate and cationic swollen clusters at pH 6.5. As a consequence, completely covered Si wafer with adsorbed clusters is given at which only swollen cluster surface is scanned (Figure 6.30c&f) leading to the visualization of individual Empty-Psomes-N₃ and co-clustered Myo/GOx-Psomes-N₃ (purified by Protocol 3) within adsorbed clusters with approximate size of 100 nm (Figure A42) and 50 nm (Figure A43). Therefore, the size range of individual polymersomes is undoubtedly given at acidic pH value. Moreover, it can be assumed that polymersomes are not destroyed in the crosslinked state. That means the size of individual Psomes-N₃ is almost kept; no change and no fusion was observed.

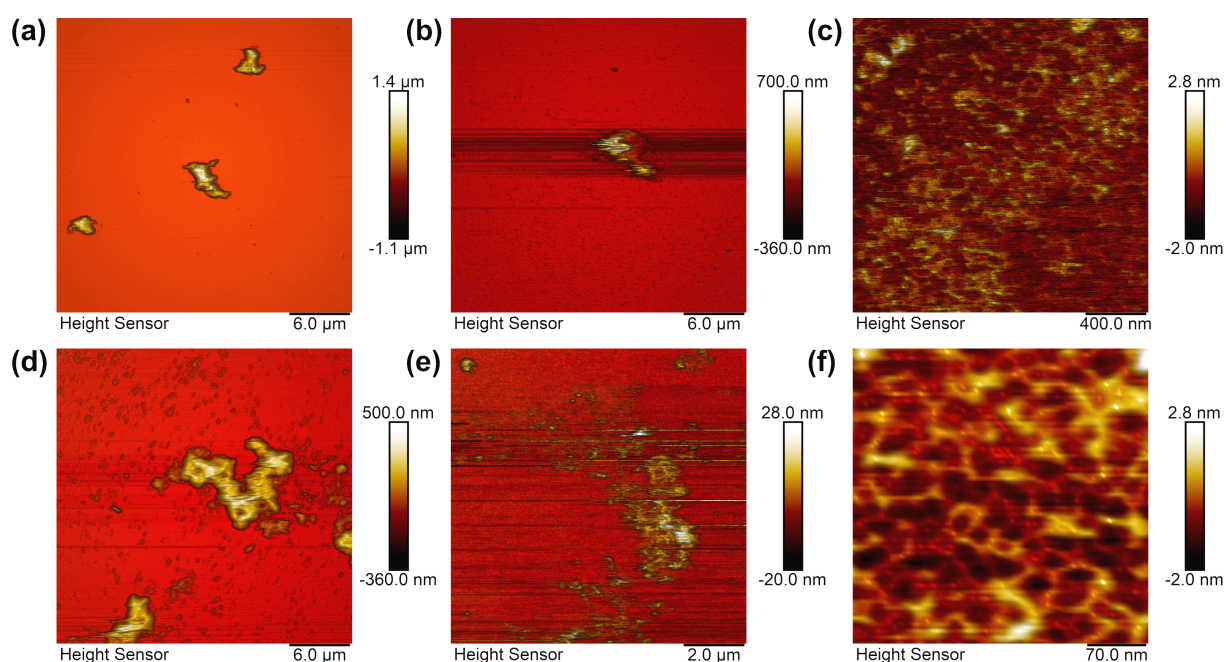


Figure 6.30 In-situ AFM images of clustered Empty-Psomes-N₃ (a-c) and co-clustered Myo/GOx-Psomes-N₃ (d-f) purified by Protocol 3 at pH 8.0 (a&d), pH 7.0 (b&e) and pH 6.5 (c&f).

Finally, the depth histograms demonstrate the average height (= surface homogeneity) of formed Psomes-N₃ in cluster layer adsorbed at pH 6.0 and 6.5 to be 2.69 nm (clustered Psomes-N₃ purified by Protocol 1, Figure 6.31a), 3.54 nm (clustered Psomes-N₃ purified by Protocol 2, Figure 6.31b), 2.60 nm (clustered Psomes-N₃ purified by Protocol 3, Figure 6.31c), and 3.46 nm (co-clustered Myo/GOx-Psomes-N₃ purified by Protocol 3, Figure 6.31d) at swollen state, respectively. The results indicate the swollen state of adsorbed clusters, independent on the used purification protocols, generally leads to mainly smooth cluster surfaces.

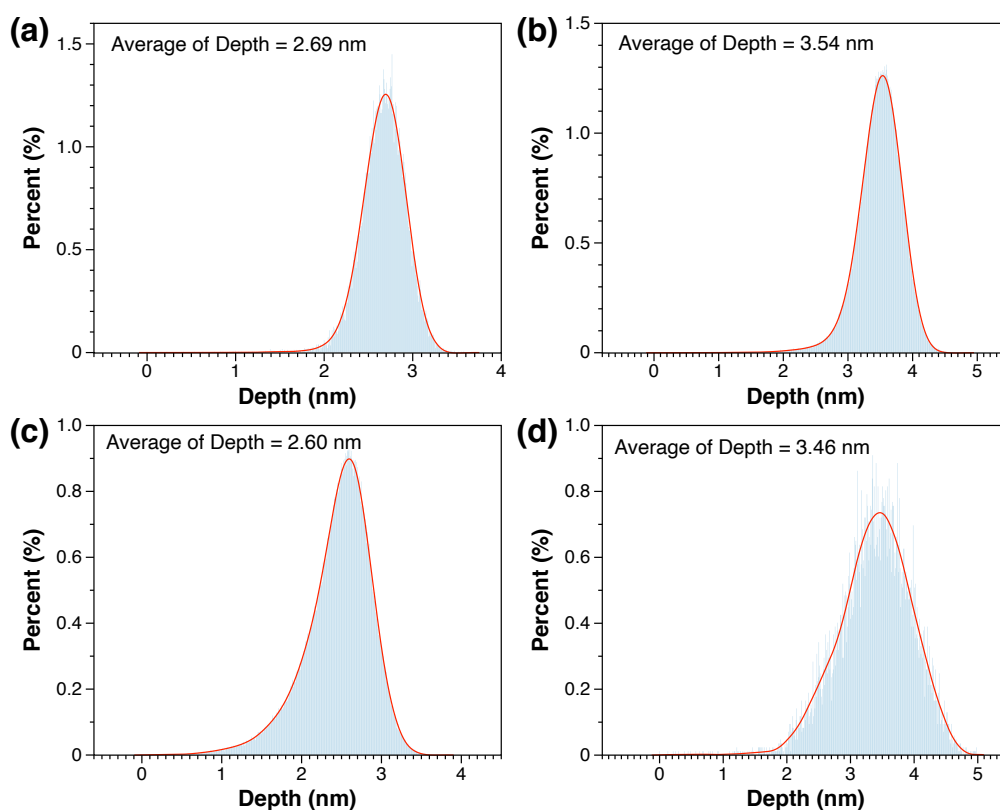


Figure 6.31 Depth histograms of Psomes- N_3 layer from in-situ AFM images: (a-c) Clustered Psomes- N_3 purified by (a) Protocol 1 at pH 6.0 (Figure 6.29b), (b) Protocol 2 at pH 6.0 (Figure 6.29d) and (c) Protocol 3 at pH 6.5 (Figure 6.30c); (d) co-clustered Myo/GOx-Psomes- N_3 purified by Protocol 3 at pH 6.5 (Figure 6.30f).

CLSM Measurement. To further realize the visualization of the clustered Psomes- N_3 , different dye-labeled enzymes (Myo-RhB and GOx-Cy5) were respectively in-situ loaded into Psomes- N_3 , followed by clustering the mixed Enzyme-Psomes- N_3 (1: 1) were carried out for the CLSM study after the purification steps. Next, the co-clustered Myo-RhB/GOx-Cy5-Psomes- N_3 purified by Protocol 3 under different pH values were observed by CLSM (Figure 6.32).

It shows that each cluster contains mixture of both Enzyme-Psomes- N_3 by matching the positional relationship. However, the difference between swelling and shrinking state of co-clustered Enzyme-Psomes- N_3 cannot be validated. The co-clustered Enzyme-Psomes- N_3 have a relatively narrow size range (0.6-2.9 μm). The histograms show the average sizes at pH 8.0, 7.0 and 6.5 to be 1.15, 1.04 and 1.15 μm , respectively (Figure 6.32). The size is consistent with the size of clusters from abovementioned cryo-TEM and TEM results (about 1 μm). CLSM images also outline those larger sizes are originated by undesired aggregation processes of clusters in solution and/or adsorption processes on substrate leading to even more irregular structures.

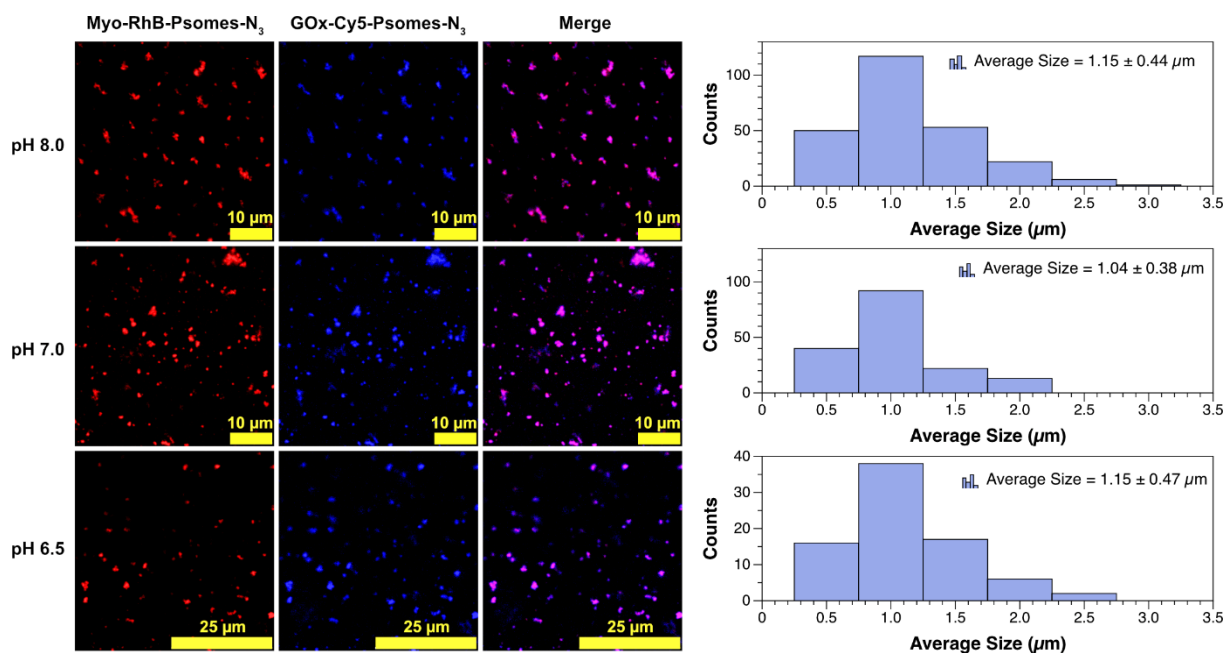


Figure 6.32 CLSM images and size histograms of co-clustered Myo-RhB/GOx-Cy5-Psomes-N₃ after purification by Protocol 3 at different pH values.

Particle Size and Shape Measurement. In order to accurately measure the size and visualize the shape of the clustered Psomes-N₃, clustered Psomes-N₃ before and after 4 times centrifugation and redispersion by mechanical stirring or vortex have been measured through Morphologi G3-ID equipped with Raman spectrometer and microscope. The integrated facility takes images of target particles and retrieves their size and shape parameters through Raman spectrum and microscopy. For this analysis, the size range of interest was between 0.5 and 10 μm and Raman spectra were acquired from only particles in this size range. Besides, these images were automatically categorized by different size ranges of particles.

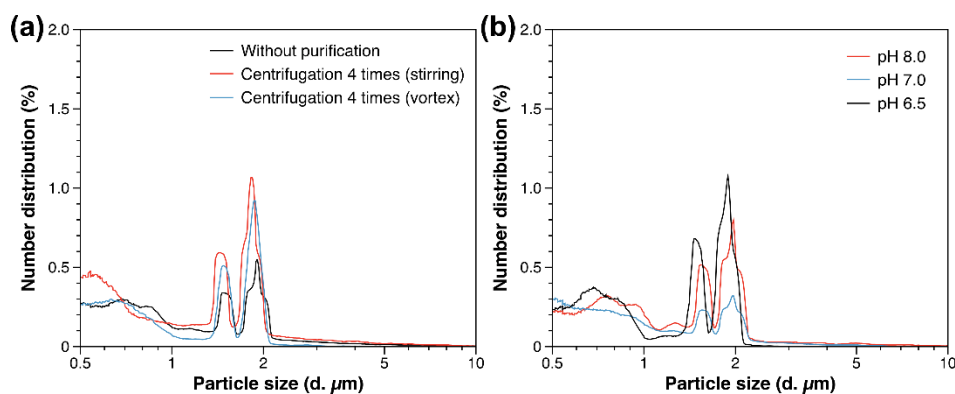


Figure 6.33 (a) Number distribution of clustered Psomes-N₃ before and after 4 times centrifugation as well as redispersed by stirring and vortex, respectively. (b) Number distribution of co-clustered Myo/GOx-Psomes-N₃ purified by Protocol 3 at different pH values. (Particle size is based on an ideal sphere.)

It can be seen from Figure 6.33 that the results of number distribution show more than 90% clustered Psomes-N₃, possessing diameters of less than 2 μm. Thus, the most clusters' size belonged to the range 0.5-5 μm. Finally, the average size of particles was measured based on two classifications of images (0.5-1 μm for unignorable small clusters and 1-5 μm for major clusters). In addition, the two-dimensional morphological images display the shape of most clusters as quasi-circular (Figure A44-46). Besides, more and more circular and uniformly sized clusters are formed after weak protonation at pH 7.0 and pH 6.5, which indicates the dissociation of aggregates based on non-covalently linked clusters. After measuring the size of clusters from these images, the size distribution and average size of clustered Psomes-N₃ before and after centrifugation as well as redispersion by mechanical stirring and vortex are shown in Figure 6.34 and Table 6.11. After centrifugation for same times, the size of clustered Psomes-N₃ redispersed by vortex is slightly smaller than the clusters redispersed by mechanical stirring (1.81 μm vs 1.52 μm and 1.41 μm vs 1.31 μm) in the size range 1-5 μm. In addition, redispersion by vortex displays narrower size distribution compared with mechanical stirring. For this reason, the Protocol 3 was selected as optimal purification method for clustered Psomes-N₃ and for control of the next enzyme reaction experiments.

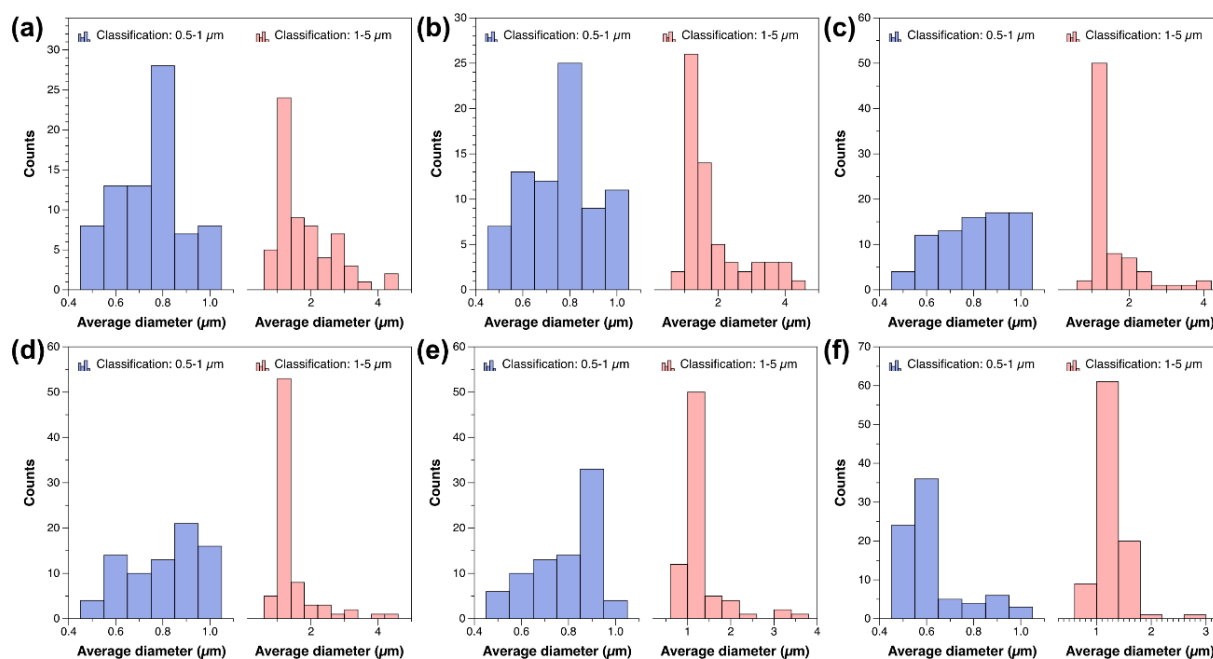


Figure 6.34 Histogram of clustered Psomes-N₃ at pH 7.4 before (a) and at pH 8.0 after one centrifugation redispersed by stirring (b) or vortex (c) as well as after 4 times centrifugation redispersed by stirring (d) or vortex (e), and at pH 6.5 after 4 times centrifugation redispersed by vortex (f).

Moreover, compared with original size (1.81 μm) (Table 6.11), the decreased size of clusters after four times centrifugation (1.31 μm by vortex and 1.41 μm by stirring) demonstrates that the redispersion destroys part of aggregates connected by non-covalent bonds. However, the size of clustered Psomes- N_3 in the size range 0.5-1 μm is similar whether redispersion by mechanical stirring or vortex as well as the centrifugation times. That means different redispersion methods do not differentiate the size of small clusters. Furthermore, the size of clustered Psomes- N_3 purified by Protocol 3 after weak protonation (pH 8.0 to pH 6.5) decreased from 1.31 μm to 1.18 μm in the 1-5 μm classification and 0.79 μm to 0.63 μm in the 0.5-1 μm classification, which can be attributed to the shedding of isolated polymersomes caused by the charge repulsion of protonated membrane.

Table 6.11 Size measurement of clustered Psomes- N_3 before and after different times centrifugation and redispersion by different purification steps.

Centrifugation times	Redispersion methods	pH value	Average size of (μm) ^a	
			Classification: 0.5-1 μm	Classification: 1-5 μm
0		8.0	0.75 \pm 0.14	1.81 \pm 0.84
1	Stirring	8.0	0.76 \pm 0.15	1.81 \pm 0.91
1	Vortex	8.0	0.80 \pm 0.15	1.52 \pm 0.65
4	Stirring	8.0	0.81 \pm 0.15	1.41 \pm 0.64
4	Vortex	8.0	0.79 \pm 0.13	1.31 \pm 0.50
4	Vortex	6.5	0.63 \pm 0.13	1.18 \pm 0.28

^a Calculation based on the morphological images and corresponding size histograms, attached to Figure A44&45 and Figure 6.34.

The size histograms and average size of co-clustered Myo/GOx-Psomes- N_3 after purification by Protocol 3 have also been checked, as shown in Table 6.12 and Figure 6.35. Its size in 1-5 μm range is alike to the clustered Psomes- N_3 after purification by Protocol 3 (pH 8.0: 1.39 μm vs 1.31 μm ; pH 6.5: 1.18 μm vs 1.18 μm), except that the size in 0.5-1 μm at pH 6.5 (0.80 μm) is slightly larger than the size of clustered Psomes- N_3 at pH 6.5 (0.63 μm). Consistent with above results, weak protonation process can indeed remove some of non-covalently attached polymersomes or small clusters on the big clusters. Beyond that, the automatically measured sizes of co-clustered Myo/GOx-Psomes- N_3 are consistent to above TEM and cryo-TEM results (average size belong to the size range 0.8-1.4 μm).

Table 6.12 Size measurement of co-clustered Myo/GOx-Psomes-N₃ at different pH values based on purification by Protocol 3.

pH value	Average diameter (μm) ^a	
	Classification: 0.5-1 μm	Classification: 1-5 μm
8.0	0.78 ± 0.17	1.39 ± 0.53
7.0	0.79 ± 0.15	1.18 ± 0.18
6.5	0.80 ± 0.12	1.18 ± 0.17

^a Calculation based on the morphological images and corresponding size histograms, attached to Figure A46 and Figure 6.35.

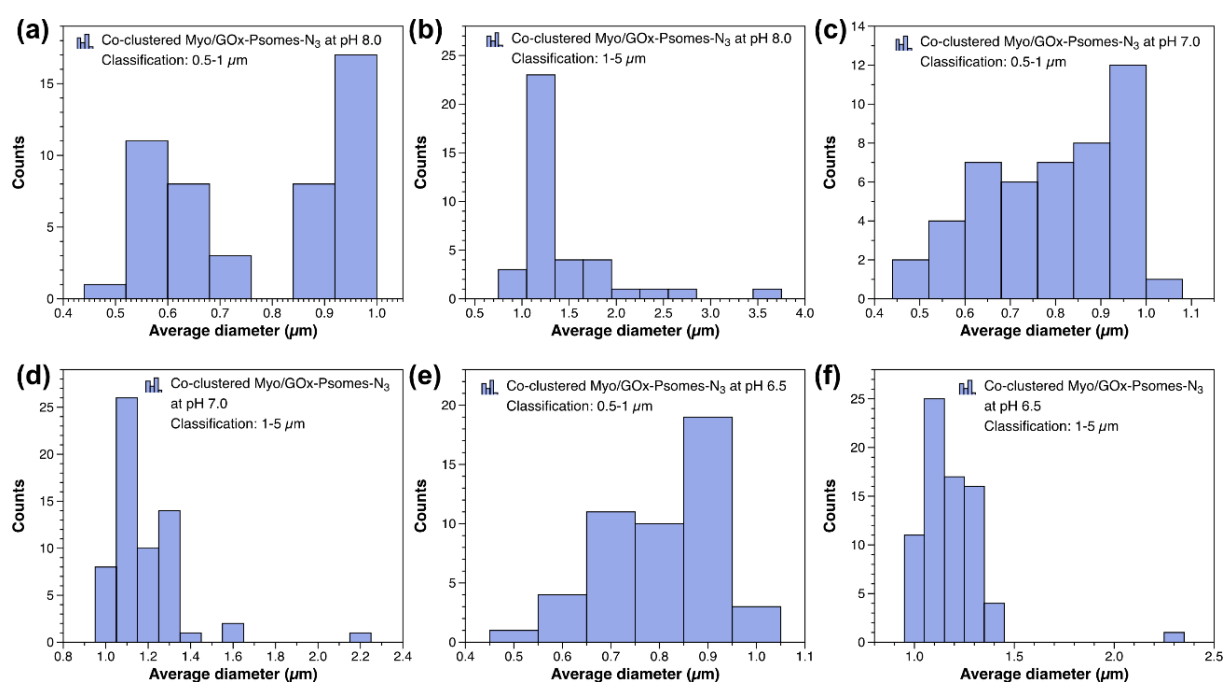


Figure 6.35 Histogram of co-clustered Myo/GOx-Psomes-N₃ at pH 8.0 (a&b), pH 7.0 (c&d) and pH 6.5 (e&f) purified by Protocol 3. Classification: 0.5-1 μm (a, c, e); 1-5 μm (b, d, f).

6.5 Clustered Enzyme-Psomes-N₃ for Enzymatic Cascade Reaction

6.5.1 Influence of Enzyme Activity on Clustering Condition

To prove that clustering of polymersomes is a feasible strategy for the successful proceeding of enzymatic cascade reaction, a preliminary protocol for the enzyme activity influence under the clustering conditions was designed as shown in Figure 6.36a&b. Specifically, Amplex Red

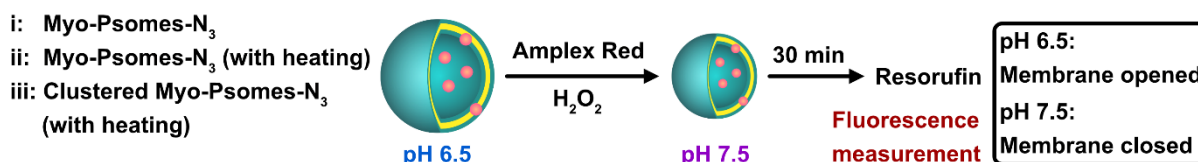
and glucose as Myo's substrates were added into Myo-Psomes-N₃ (without adding crosslinker and store at RT for 2 days), Myo-Psomes-N₃ (without adding crosslinker and heating 2 days at 40 °C as control), and clustered Myo-Psomes-N₃ (mixing with crosslinker and heating 2 days at 40 °C for clustering) at pH 6.5 that the polymersomes' membrane is fully open, allowing the substrates and product of Myo to pass across the membrane. After different incubation time from 10 to 60 min at RT, 0.1 M PBS buffer was added to adjust pH value to pH 7.5 that the polymersomes' membrane is closed. After continuous 30 min stirring at pH 7.5, the fluorescence spectrum of resorufin as the final product of enzyme reaction was recorded ($\lambda_{\text{ex}} = 534 \text{ nm}$, $\lambda_{\text{em}} = 585 \text{ nm}$). It is worth noting that the concentration of free Myo-Psomes-N₃ (0.3 mg/mL Psomes-N₃) was set to 60% of original concentration of clustered Myo-Psomes-N₃ (0.5 mg/mL Psomes-N₃ was used to carry out clustering process and the purified clusters was identified as 0.3 mg/mL) due to losses from the purification process (40% polymersomes lost in the purification process, as shown in Figure 6.17).

Besides, a control experiment about the influence of reaction conditions (heating 2 days at 40 °C) on GOx activity was also studied. The different substrates include glucose, Amplex Red and Myo were sequentially added to GOx-Psomes-N₃ (without adding crosslinker and store at RT for 2 days), GOx-Psomes-N₃ (without adding crosslinker and heating 2 days at 40 °C as control), and clustered GOx-Psomes-N₃ (mixing with crosslinker and heating 2 days at 40 °C for clustering) at pH 6.5. After incubation for different time at RT, the pH was changed to pH 7.5 by 0.1 M PBS buffer. In the end, the fluorescence spectrum of resorufin as the final product of enzyme reaction was recorded ($\lambda_{\text{ex}} = 534 \text{ nm}$, $\lambda_{\text{em}} = 585 \text{ nm}$). In the same way, the concentration of free GOx-Psomes-N₃ (0.3 mg/mL Psomes-N₃) was also set to 60% of original concentration of clustered GOx-Psomes-N₃ (0.5 mg/mL Psomes-N₃ was used to carry out clustering process and the purified clusters was identified as 0.3 mg/mL) due to the lost polymersomes in the purification process.

Firstly, the influence of clustering conditions, heating at 40 °C for 2 days, on the enzyme activity of Enzyme-Psomes-N₃ was observed. It is obvious that the enzyme activity of HFF-purified Myo-Psomes-N₃ in both cases (with and without heating at 40 °C for 2 days) does not change (Figure 6.36c&d). In opposite, the enzyme activity of purified clustered Myo-Psomes-N₃ is ~ 20% lower than that of heated Myo-Psomes-N₃ after incubation of 60 min due to slow diffusion of substrates (Figure 6.36c). Decreased enzyme activity (5.5%) of purified clustered GOx-Psomes-N₃ after incubation 60 min could be also due to the difficulty of substrates

diffusion in the clustered GOx-Psomes-N₃ (Figure 6.36d). For comparison, the data of clustered Myo-Psomes-N₃ was normalized with 100%. Therefore, (clustered) GOx-Psomes-N₃ groups show lower enzyme activity compared with (clustered) Myo-Psomes-N₃ groups, which could be attributed to low GOx loading efficiency (4.5%) and high Myo loading efficiency (9.3%).

(a) Enzyme reaction of Myo



(b) Enzyme reaction of GOx

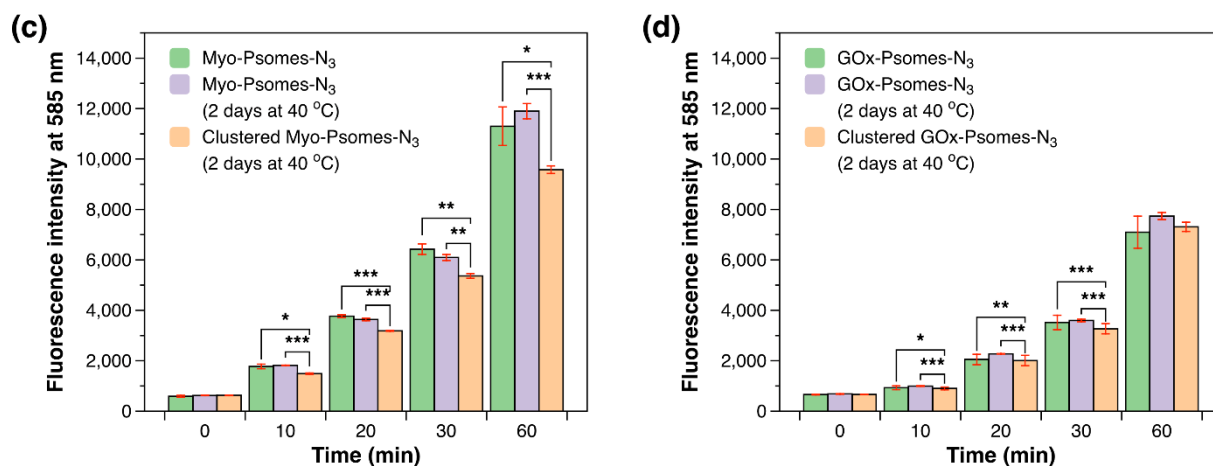
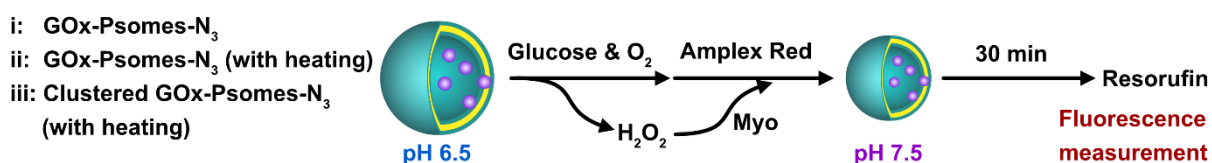


Figure 6.36 Schematic illustration of enzyme reaction of (a) Myo-Psomes-N₃ and (b) GOx-Psomes-N₃. (c) Fluorescence intensity at 585 nm of Myo-Psomes-N₃, Myo-Psomes-N₃ after heating 2 days at 40 °C and clustered Myo-Psomes-N₃ after adding Amplex Red and H₂O₂ at pH 6.5 with different times, and then adjusting the pH value back to pH 7.5 through 0.1 M PBS buffer. (d) Fluorescence intensity at 585 nm of GOx-Psomes-N₃, GOx-Psomes-N₃ after heating 2 days at 40 °C and clustered GOx-Psomes-N₃ after adding Amplex Red, glucose and Myo at pH 5.5 with different times, and then adjusting the pH value back to pH 7.5 through 0.1 M PBS buffer.

6.5.2 Mixed Enzyme-Psomes-N₃ for Enzymatic Cascade Reaction

To further study the influence of pH values on the enzymatic cascade reaction in the Enzyme-Psomes-N₃ system, different pH values from 6.5 to pH 8.0 at the incubation process were used

to carry out the enzymatic cascade reaction as shown in Figure 6.37. In detail, glucose as GOx's substrates and Amplex Red as Myo's substrates were added into mixed Myo/GOx-Psomes-N₃ (store at RT for 2 days) and mixed Myo/GOx-Psomes-N₃ (heating 2 days at 40 °C) at pH 6.5, 7.0, 7.5 and 8.0, respectively. After different incubation time from 10 to 60 min at RT, 0.1 M PBS buffer was added to adjust pH value to pH 7.5 that the polymersomes' membrane is closed. After continuous 30 min stirring at pH 7.5, the fluorescence spectrum of resorufin as the final product of enzyme reaction was recorded ($\lambda_{\text{ex}} = 534 \text{ nm}$, $\lambda_{\text{em}} = 585 \text{ nm}$).

The mechanism of enzymatic cascade reaction is shown in Figure 6.37. Different pH values making Enzyme-Psomes-N₃ fully open (pH 6.5), semi-open (pH 7.0) and closed (pH 7.5 and pH 8.0) (as shown in Figure 6.20d) were selected to study the enzyme reaction by fluorescence spectroscopy.

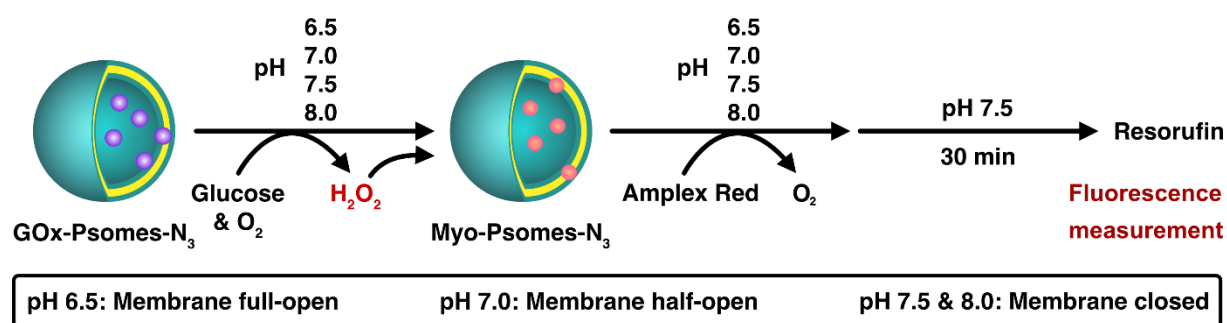


Figure 6.37 Schematic illustration of enzymatic cascade reaction in mixed or co-clustered Myo/GOx-Psomes-N₃.

Following, the enzyme activities of mixed Myo/GOx-Psomes-N₃ at pH 6.5 (swollen state) to pH 7.0 (semi-swollen) without and with heating for 2 days at 40 °C were checked (Figure 6.38a-b). Both show increasing fluorescence intensity over time, while mixed Myo/GOx-Psomes-N₃ at pH 6.5 reveal higher enzyme activities than mixed Myo/GOx-Psomes-N₃ at pH 7.0. This is ascribed to the degree of membrane protonation, which leads to a relative fast substrates diffusion as passing across the membrane of polymersomes. Besides, the mixed Myo/GOx-Psomes-N₃ without and with heating process display negligible difference, which confirm previous results that enzymes GOx and Myo do not lose any activity after heating process.

Additionally, incubation at pH 7.5 and 8.0 were selected to reduce or to stop the enzymatic cascade reaction (Figure 6.38c&d). As shown in Figure 6.20d, the membrane of Enzyme-Psomes-N₃ is under collapsed state, so the substrates cannot pass across the membrane to carry out enzyme reaction from the theoretical point of view. However, both show increasing

fluorescence intensity over time while their fluorescence intensities are very low compared with the mixed Myo/GOx-Psomes-N₃ at pH 6.5 or pH 7.0. This is ascribed to membrane integrated GOx and Myo, and the enzymes at outer surface of membrane were exposed to substrates lead to an inevitable and slow enzyme reaction. These results show that enzymes could not be eliminated from the outer membrane surface during HFF purification. In other words, the substrate can access the outer membrane-exposed enzyme even in the collapsed state of the polymersome membrane at pH 7.5 or pH 8.0. Furthermore, since neither Myo nor GOx lost the enzyme activity under heating conditions, the enzyme cascade reaction shows almost the same enzyme reaction efficiency (Figure 6.38c&d).

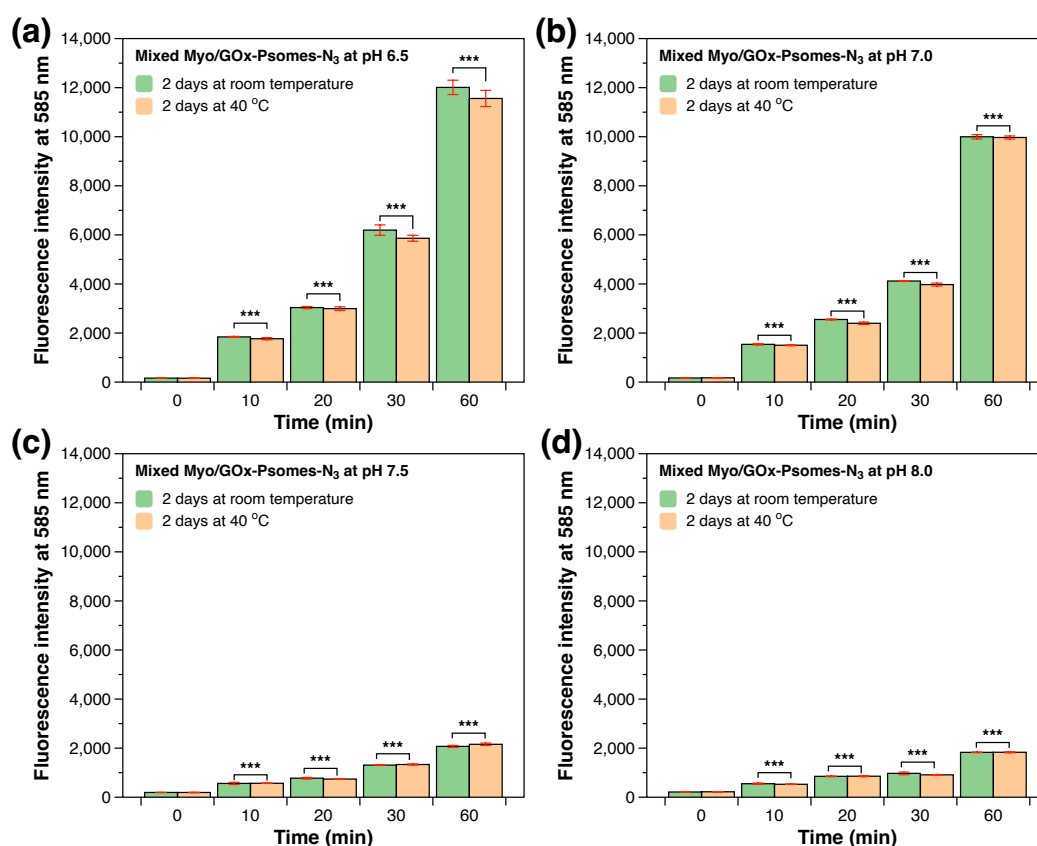


Figure 6.38 Fluorescence intensity at 585 nm of mixed Myo/GOx-Psomes-N₃ at RT and 40 °C for 2 days after adding Amplex Red and glucose at different pH 6.5 (a), pH 7.0 (b), pH 7.5 (c) and pH 8.0 (d) with different reaction times, and then adjusting the pH value back to pH 7.5. Condition: 0.15 mg/mL Myo-Psomes-N₃ and 0.15 mg/mL GOx-Psomes-N₃.

6.5.3 Co-Clustered Enzyme-Psomes-N₃ for Enzymatic Cascade Reaction

To further study the influence of compact spatial structure of co-clustered Myo/GOx-Psomes-N₃ on the enzymatic cascade reaction compared with free distribution of mixed Myo/GOx-

Psomes-N₃, the enzymatic cascade reaction based on them was performed as shown in Figure 6.37. The protocol of enzymatic cascade reaction is the same to above protocol of mixed Myo/GOx-Psomes-N₃ without crosslinker in Figure 6.38. Besides, different pH values (pH 6.5, 7.0, 7.5 and 8.0) in the incubation process were also explored to check the influence between co-clustered Myo/GOx-Psomes-N₃ and mixed Myo/GOx-Psomes-N₃ (Figure 6.39). Significantly, the concentration of mixed Myo/GOx-Psomes-N₃ (0.3 mg/mL Psomes-N₃) was set to 60% of original concentration of clustered Myo/GOx-Psomes-N₃ (0.5 mg/mL Psomes-N₃) to calibrate the concentration difference between both groups through purification process (40% loss of Enzyme-Psomes-N₃).

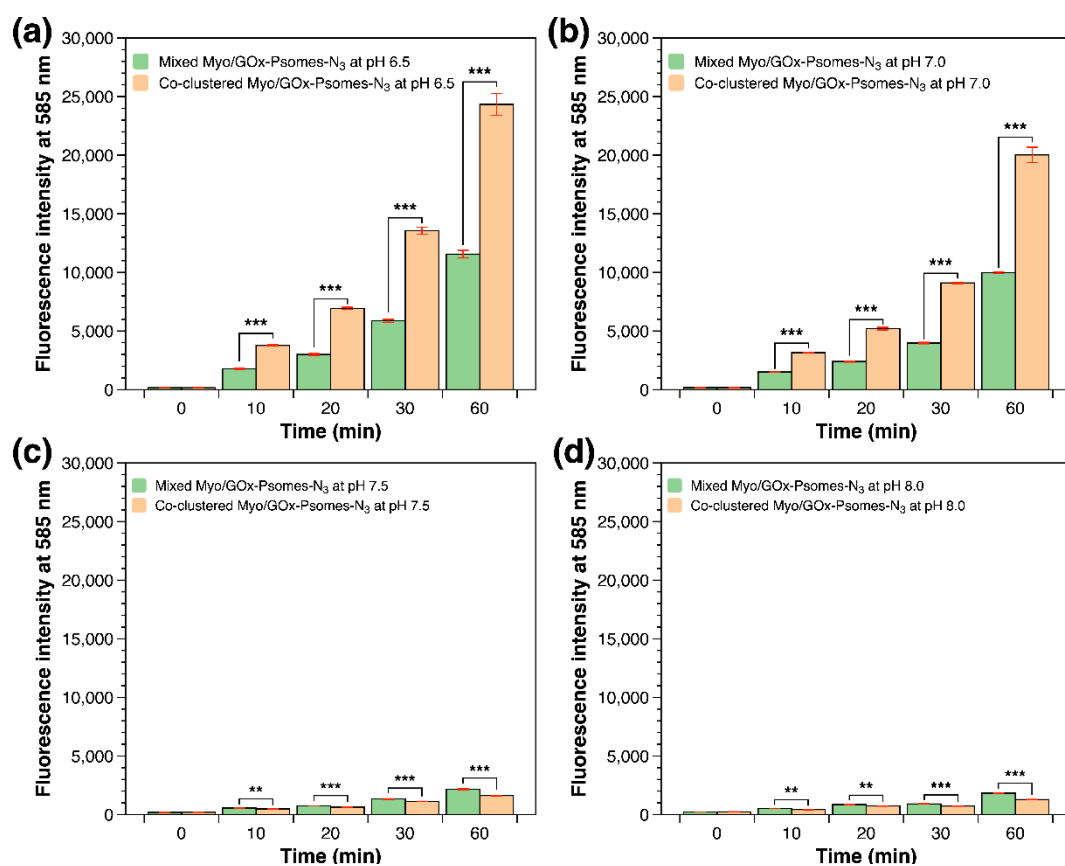


Figure 6.39 Fluorescence intensity at 585 nm of mixed Myo/GOx-Psomes-N₃ after heating 2 days at 40 °C and co-clustered Myo/GOx-Psomes-N₃ after adding Amplex Red and glucose at different pH 6.5 (c), pH 7.0 (d), pH 7.5 (e) and pH 8.0 (f) with different times, and then adjusting the pH value back to pH 7.5.

In contrast to mixed Enzyme-Psomes-N₃, the clusters assembled by mixed Myo/GOx-Psomes-N₃ showed a significantly improved efficiency (210.5% at pH 6.5 and 200.8% at pH 7.0) of the enzyme cascade reaction (Figure 6.39a-b). This is eventually caused by the closer distance between polymersomes in the clusters. Slightly higher efficiency at pH 6.5 compared with that

at pH 7.0 could be owing to the Myo's optimal pH value. After the membrane is protonated, substrates (glucose and Amplex Red) and intermediate products (H_2O_2) can rapidly diffuse between GOx-Psomes- N_3 and Myo-Psomes- N_3 to achieve a higher efficiency of the enzymatic cascade reaction (Figure 6.40). Even so, the high enzymatic efficiency at neutral pH (7.0) indicates its potential advantages in mimicking artificial organelles. As control, incubation at pH 7.5 and 8.0 were selected to carry out the enzymatic cascade reaction (Figure 6.39c-d). Both show increasing fluorescence intensity over time due to the membrane-integrated enzymes exposed to substrates ($\leq 10\%$). Besides, co-clustered Myo/GOx-Psomes- N_3 shows lower enzymatic efficiency (24.7% at pH 7.5 and 30.0% at pH 8.0) compared with mixed Myo/GOx-Psomes- N_3 after incubation 60 min, which could be due to the same reason: relatively lower diffusion ability of clusters under collapsed state.

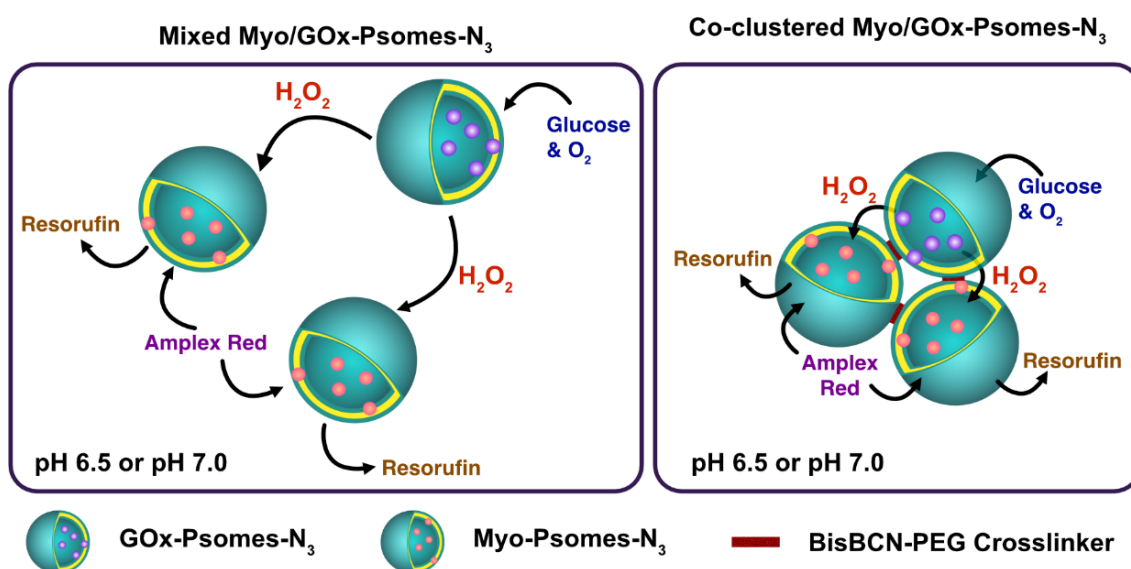


Figure 6.40 Schematic illustration of intermediates diffusion mechanism of mixed Myo/GOx-Psomes- N_3 and co-clustered Myo/GOx-Psomes- N_3 .

To conclude this part, the optimal co-clustered Myo/GOx-Psomes- N_3 present significantly increased efficiency of enzymatic cascade reaction compared with mixed Myo/GOx-Psomes- N_3 at weakly acidic conditions (more than 200% at pH 6.5 and pH 7.0) due to the compact spatial structure compared with freely dispersed Enzyme-Psomes- N_3 .

6.6 Summary

Within this chapter, pH-responsive BCPs with methoxy and azido end groups were synthesized and well characterized. Next, the swelling-shrinking ability, size, and membrane thickness of

polymersomes self-assembled by different BCPs were characterized and the Psomes-N₃ were used to assemble pH-responsive clusters.

To obtain desired clusters, multiple influencing factors in the clustering process, including temperature, proportion of BCP-N₃, reaction time, feed ratio, crosslinker length, and concentration, were further explored. Following, the optimal clustering conditions was chosen to construct clustered Psomes-N₃ and then different visualization methods, such as TEM, cryo-TEM, in-situ AFM, CLSM and particle size measurement, were utilized to characterize their structure, shape, and size at different pH values. Besides, different purification pathways were utilized to optimize the structure of clusters and the optimal purification approach was proven by above visualization approaches. Multiple centrifugations and redispersion by vortex are essential to get micrometer-sized clusters with relative narrow size distribution. Moreover, a weak acidification process cannot affect its structural stability because it cannot split crosslinked polymersomes in the clusters and can only facilitate disaggregation of aggregated clusters, induced by centrifugal force or removing non-covalently packed polymersomes in the clusters.

Furthermore, Myo-Psomes-N₃ and GOx-Psomes-N₃ were prepared by in-situ loading and followed by HFF purification. Subsequently, the optimal clustering conditions and purification steps were chosen to construct micrometer-sized co-clustered pH-responsive Myo/GOx-Psomes-N₃ through copper-free click reaction.

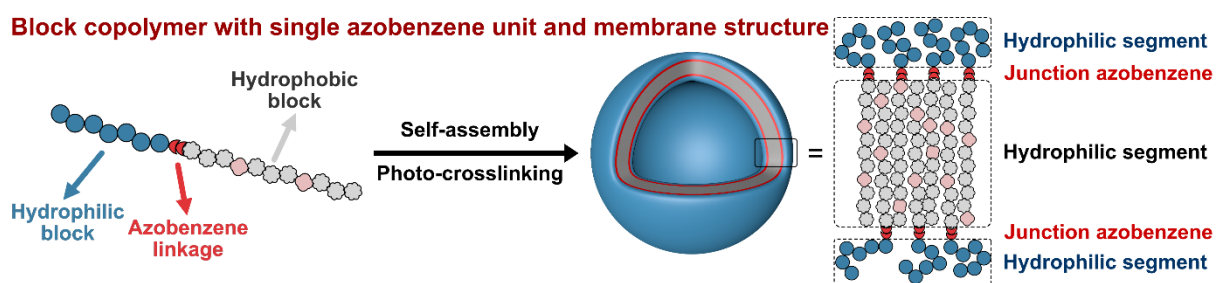
To better compare the differences of enzyme reaction activity between mixed Myo/GOx-Psomes-N₃ and co-clustered Myo/GOx-Psomes-N₃, the influence of enzyme activity on clustering condition was studied. The results suggested that heating does not change the activity of the enzyme Myo and GOx, however, the clustered Enzyme-Psomes-N₃ with closer spatial structure lost 20% enzyme activity (Myo) and 5.5% enzyme activity (GOx), respectively, due to the effect of steric hindrance.

Finally, compared with the conventional enzyme cascade reaction through simple mixing Myo/GOx-Psomes-N₃, the co-clustered Myo/GOx-Psomes-N₃ show high efficiency (210.5% at incubation pH 6.5) of enzymatic cascade reaction at lower polymersomes concentration (0.15 mg Psomes-N₃/mL). This strategy provides a straightforward concept for the exploitation of co-clustered Psomes-N₃ with different cargo in the cascade reaction to mimic sophisticated functions of organelles.

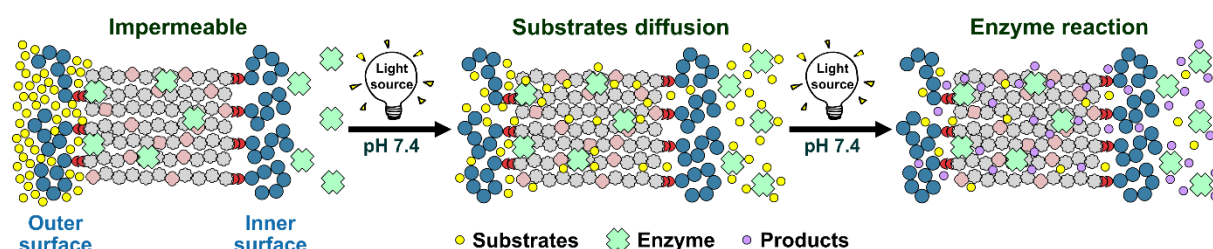
7 Light-Driven Enzyme Reaction Based on pH-Responsive Polymersomes

7.1 Aim and Strategy

The aim of this study was to prepare polymersomes with different azobenzene linkages responsive to different light sources for enzyme reaction under physiological pH value (pH 7.4). At this condition, the “standard” pH-responsive and photo-crosslinked polymersomes are in collapsed state with an impermeable membrane. Even a small molecule cannot pass through the membrane in this environment, which limits the applications under specific conditions.



Mechanism of light-triggered permeable membrane for enzyme reaction



Properties of collapsed membrane at physiological pH value

1. Impermeable membrane in the collapsed state (pH 7.4)
2. Size-dependent membrane permeability under light stimuli
 - a) No observable structural change of membrane
 - b) Retention of macromolecules (enzyme)
 - c) Cross-membrane transport of small molecules (substrates)

Selection of light source (wavelength)

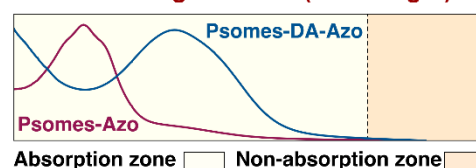


Figure 7.1 Schematic illustration shows the bilayer structure of polymersomes with azobenzene linkage between hydrophilic and hydrophobic segments as well as light-initiated membrane permeability for enzyme reaction at physiological pH value (pH 7.4). Light source that induces membrane perturbation depends on absorption wavelength, rather than the light from non-absorption zone or thermal-induced relaxation.

In the process of mimicking artificial organelles, polymersomes loaded with enzymes or other biomolecules as nanoreactors have attracted a great attention. This has been demonstrated with

traditional pH-responsive and photo-crosslinked polymersomes. However, their enzyme activity is limited to acidic environment and the enzyme retention efficiency depends on the enzyme and the loading process used.^{123, 182} But real organelles serve as containers that cannot only carry, but also retain biological macromolecules, even while performing biological actions. However, traditional pH-responsive and photo-crosslinked polymersomes have limited enzymatic activity under preferential acidic conditions (\leq pH 7), while most enzymes smoothly work under physiological conditions. Additional enzyme-loaded polymersomes may lose their loaded enzyme during the enzymatic reaction due to the opening of membrane. This point is not really validated and should be considered as well when studying enzymatic reaction under acidic conditions. Therefore, precision control and versatility of membrane permeability become particularly important for metabolite exchange and retaining enzymes in polymersomes lumen at defined pH ranges.

For this reason, it is an ideal approach to introduce new stimuli into existing systems to achieve controllable membrane permeability while maintaining the original structure and properties. One azobenzene unit as the junction molecule between hydrophilic and hydrophobic segments made up light-responsive polymersomes with high potential (Figure 7.1). Light-induced actuation of junction azobenzene by photochemical trans-cis isomerization can propagate the increased mobility of azobenzene to the whole membrane of polymersomes and then result in perturbation of membrane which facilitates cross-membrane transport of water-solvated and membrane-bound molecules. The fluidic enhancement of small molecule in the membrane makes selective membrane permeability which allows efficient substrates diffusion across the deprotonated membrane to initiate enzyme reaction in catalytic nanoreactors at physiological pH value (pH 7.4) (Figure 7.1).

Furthermore, the activation of membrane fluidity only depends on the absorption wavelength of the junction azobenzene and is not affected by other factors that lead to azobenzene isomerization, such as thermal relaxation and light at wavelengths outside the absorption range.¹⁵ The typical azobenzene suffers from trans-to-cis isomerization under UV illumination (< 400 nm) and cis-to-trans isomerization under visible light irradiation, especially for blue light (400-500 nm). However, derivatization of azobenzene can significantly change its light response wavelength range. For example, adding a push-pull (donor-acceptor) group to azobenzene unit can reduce its thermal relaxation time and lead to a markedly red-shift of the $\pi\pi^*$ absorption band from UV to visible spectral region.^{183, 184} Due to the shift of the

characteristic absorption peak caused by the derivatized azobenzene as junction molecule, the wavelengths of the light sources, also leading to membrane perturbation, can vary for initiating enzymatic reactions in nanoreactors. Besides, the membrane structure of polymersomes does not change despite photo-isomerization of azobenzene.¹⁵ This is due to the fact that the isomerization of trace amounts of azobenzene cannot cause observable effects on the overall membrane structural integrity. In general, considering the enhancement of membrane mobility under light irradiation and the unchanged structural integrity, it is very likely that external small molecules diffuse into the lumen of polymersomes while leaving macromolecules inside.

In this case, we aimed at constructing light-responsive polymersomes with junction azobenzene and in-situ loaded enzyme Myo for light-triggered enzyme reaction under simulated physiological conditions (pH 7.4) (Figure 7.1). Given by the different wavelengths of the maximum absorption peaks, two different types of azobenzene junction can result in distinct membrane fluidity with light stimuli, thereby reaching different diffusion rates of substrates and then different efficiency of enzyme reaction. Herein, the novel PEG-Br macroinitiators with donor-acceptor-substituted and ether substituted azobenzene were used to synthesize BCPs by ATRP and then were self-assembled into polymersomes that respond to different light sources (UV with 365 nm wavelength and blue light with 400-500 nm wavelength range). In this chapter, the photo-isomerization behavior of PEG-Br macroinitiators, BCPs and polymersomes with different types of azobenzene were studied. Following light-driven dye release from polymersomes was carried out at physiological pH value (pH 7.4). Finally, the enzyme reaction triggered by the light-induced substrates diffusion was performed at same conditions.

7.2 Preparation and Characterization of Light-Responsive Polymersomes

In previous work, pH-responsive and photo-crosslinked polymersomes were self-assembled by amphiphilic BCP which consist of PEG as the hydrophilic block and pH-responsive monomer DEAEMA and photo-crosslinker DMIBMA as the hydrophobic block.^{20, 79, 123} In view of the existing advantages, herein, two novel PEG macroinitiators were synthesized (see experimental part 5.1.1 and 5.1.2) and used to prepare the BCPs with different azobenzene linkages obtaining potential light-responsive polymersomes.

7.2.1 Synthesis and Characterization of BCP with Different Types of Azobenzene Unit

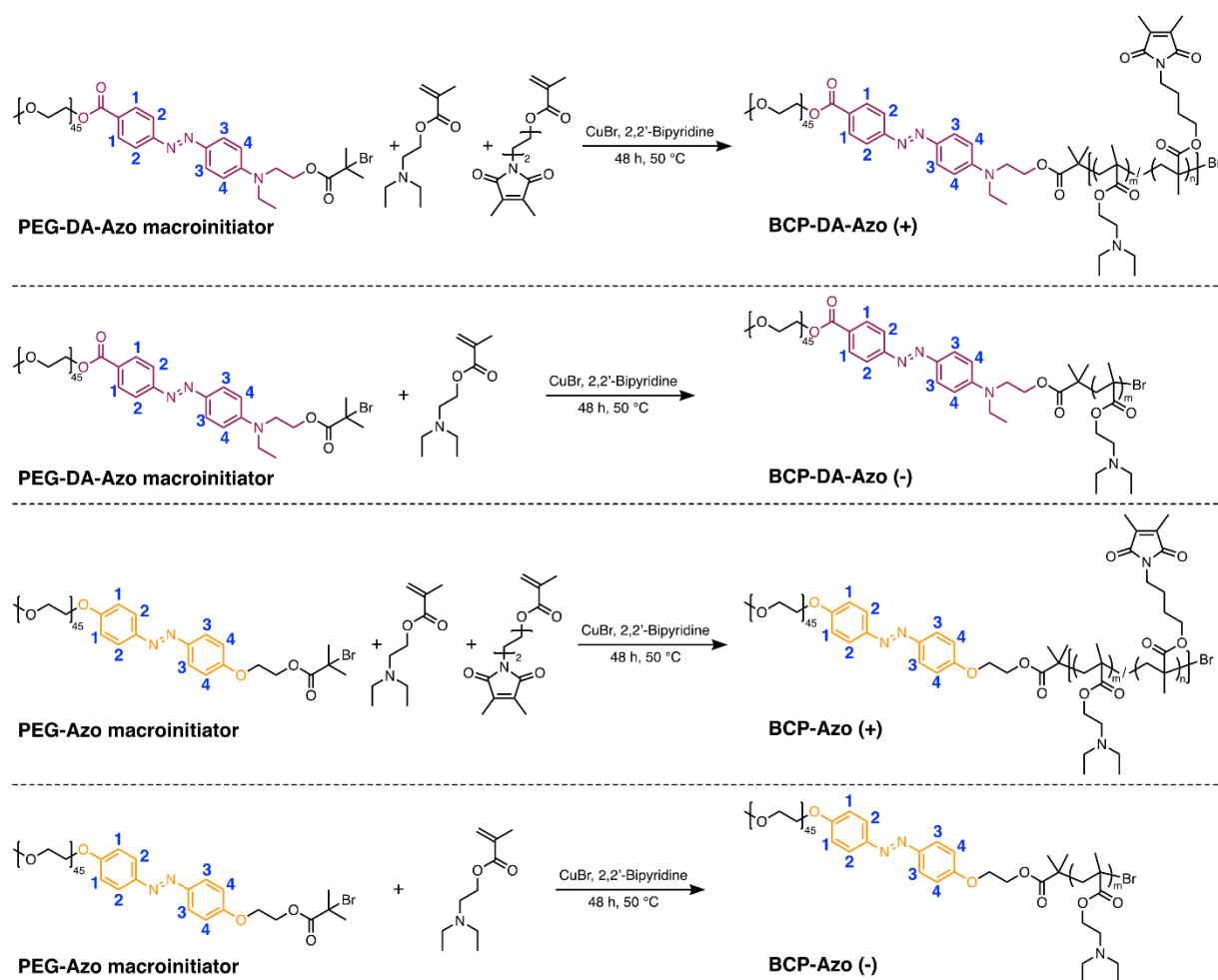


Figure 7.2 ATRP polymerization of monomers for synthesizing BCPs with donor-acceptor-substituted azobenzene linkage and ether substituted azobenzene linkage. (+) indicates copolymerization of pH-responsive monomer DEAEMA and photo-crosslinker DMIBMA, and (-) indicates only polymerization of pH-responsive monomer DEAEMA.

Donor-acceptor-substituted and ether substituted BCPs (BCP-DA-Azo (+) and BCP-Azo (+)) with pH-responsive monomer DEAEMA and photo-crosslinker DMIBMA were synthesized by 48 h ATRP polymerization (Figure Figure 7.2). For the study of photo-isomerization of BCPs, the BCP-DA-Azo (-) and BCP-Azo (-) without photo-crosslinker DMIBMA were also prepared to avoid the effect of photo-crosslinking (Figure 7.2).

The successful synthesis of novel macroinitiators and BCPs were proven by NMR spectra (Figure A15-35). Besides, the block compositions of BCP-DA-Azo and BCP-Azo with or without photo-crosslinker DMIBMA (BCP-DA-Azo (+): PEG-DA-Azo-b-p(DEAEMA-s-DMIBMA); BCP-DA-Azo (-): PEG-DA-Azo-b-p(DEAEMA); BCP-Azo (+): PEG-Azo-b-

p(DEAEMA-*s*-DMIBMA); BCP-Azo (-): PEG-Azo-*b*-p(DEAEMA)) were calculated by ¹H NMR spectra and listed in the Table 7.1 and Table 7.2.

Table 7.1 Block composition of BCPs with different azobenzene linkages.

Polymer	Repeating units in PEG^a	DEAEMA units^a	DMIBMA units^a	Block ratio^a	DMIBMA ratio^b
BCP-DA-Azo (+)	45	86	23	1: 2.42	21.1%
BCP-DA-Azo (-)	45	132	0	1: 2.93	0%
BCP-Azo (+)	45	72	19	1: 2.02	20.9%
BCP-Azo (-)	45	105	0	1: 2.33	0%

(+) With or (-) without copolymerization of photo-crosslinker DMIBMA; ^a Number of repeating units in PEG (hydrophilic section): number of copolymerized pH-responsive monomer DEAEMA and photo-crosslinker DMIBMA (hydrophobic section), determined by ¹H NMR analysis; ^b Percentage of photo-crosslinker DMIBMA in hydrophobic section, calculated by the ratio of polymerization degree.

Here, the methylene groups in BCP were used to calculate each block length (label+ with different numbers in Figure A24-25 and A34-35, all chemical shifts of methylene groups are below 5.0 ppm). The specific analysis process is consistent with the analysis process in the previous chapter. For the BCPs with photo-crosslinker DMIBMA (BCP-DA-Azo (+) and BCP-Azo (+)), the crosslinker ratio in the hydrophobic part is around 20%, which is an essential ratio to crosslink polymersomes under UV irradiation.

In addition, the characteristic peaks of azobenzene can be seen from the ¹H NMR spectra of PEG-DA-Azo macroinitiator and BCP-DA-Azo in Figure 7.3, the chemical shift of 4 protons of the benzene ring (labeled with number 1 and 2 in Figure 7.2) connected to the acceptor (ester bond) appears at around 7.8 ppm and the intensity of 4 protons of the benzene ring (labeled with number 3 and 4 in Figure 7.2) linked to the donor (tertiary amine) occurred at around 8.2 and 6.6 ppm, respectively. Besides, the proton integration of azobenzene unit further validates that each BCP contains one azobenzene unit, which indicates the whole membrane of polymersomes could be participate in the process of light-induced membrane perturbation (Figure A24-A25).

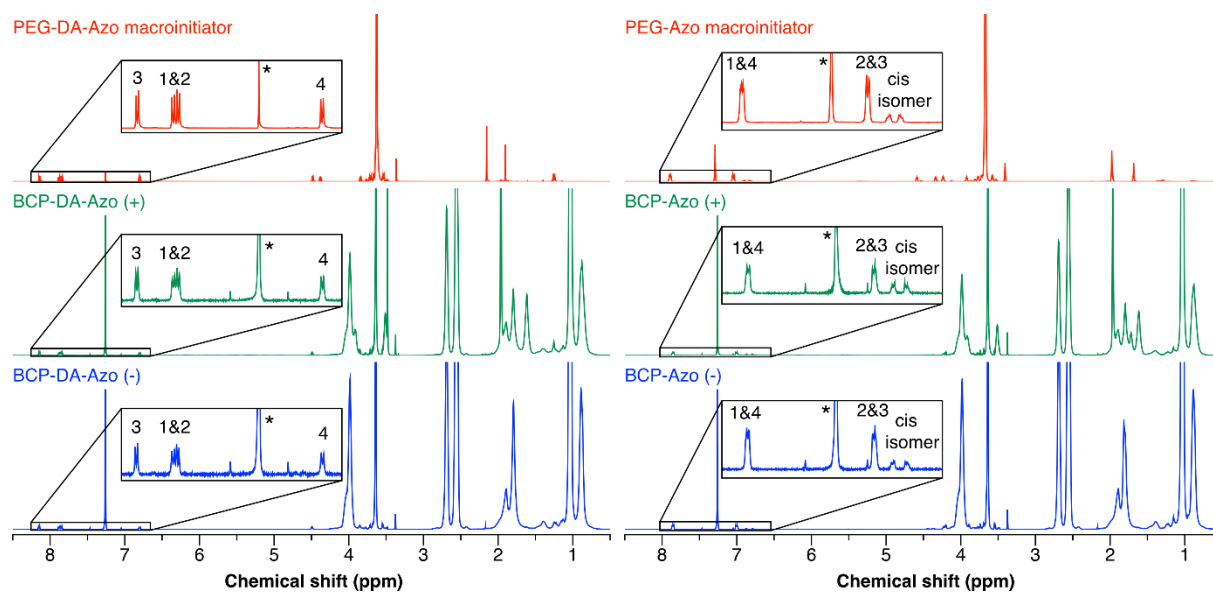


Figure 7.3 ^1H NMR spectra of macroinitiator and BCPs with donor-acceptor-substituted azobenzene linkage and ether substituted azobenzene linkage. The asterisk in the magnified view represents solvent peak of chloroform.

For the characteristic peaks of ether substituted azobenzene in the PEG-Azo macroinitiator and BCP-Azo (Figure 7.3), it is obvious that more cis isomer co-existed with trans isomer. The chemical shift of protons on the trans azobenzene (labeled with number 1-4 in Figure 7.2) occurred at around 7.95 and 7.05 ppm, however, the protons on the cis azobenzene occurred at around 6.85 and 6.95 ppm. Moreover, the proton integration of azobenzene unit including trans and cis isomer also proves that each BCP contains one azobenzene linkage, which is essential for the further investigation of light-enhanced membrane permeability (Figure A34-A35).

Table 7.2 Molar mass characteristics of BCPs with different azobenzene linkages.

Polymer	M_n^a (g/mol)	M_n^b (g/mol)	M_w^b (g/mol)	\bar{D}^b (M_w/M_n)
BCP-DA-Azo (+)	24524	37600	47700	1.27
BCP-DA-Azo (-)	26914	44300	51900	1.17
BCP-Azo (+)	20814	38900	66000	1.70
BCP-Azo (-)	21857	41800	53200	1.27

(+) With or (-) without copolymerization of photo-crosslinker DMIBMA; ^a Calculated by ^1H NMR; ^b Measured by GPC.

Moreover, molecular weight of BCPs were calculated by ^1H NMR spectra and measured by GPC (Table 7.2). The GPC results showed that the three BCPs (BCP-DA-Azo (+), BCP-DA-

Azo (-) and BCP-Azo (-) have a narrow molar mass distribution (\mathcal{D}) from 1.17 to 1.27, suggesting an almost controllable polymerization process. However, the BCP-Azo (+) show a relative broad molar mass distribution ($\mathcal{D} = 1.70$), which could be attributed to the influence of different polarity of co-existing isomerized macroinitiator in the polymerization process.

7.2.2 Self-Assembly and Photo-Crosslinking of Light-Responsive Polymersomes

Polymersomes were self-assembled by pH switch method.¹²³ Specifically, BCP was dissolved in 0.01 M HCl solution to make the fully protonation of the tertiary amine in the pDEAEMA segment. Then, to initiate the self-assembly process, deprotonation process was carried out through increasing the pH value to a basic condition ($\text{pH} \leq 9.0$). After 1 day of stirring under dark conditions, the final polymersomes were formed with a bilayer membrane and aqueous lumen. The bilayer membrane is composed by central hydrophobic part based on copolymerized DEAEMA and DMIBMA units, where the hydrophilic inner and outer corona is equipped with PEG chains. After the formation of polymersomes, the DMIBMA moieties in hydrophobic block were used to crosslink the polymersome membrane under UV irradiation. This makes the polymersomes robust and mechanically stable at various pH values.

Considering the photo-driven isomerization process of azobenzene with energy consumption, it is necessary to understand the wavelength range of photo-crosslinking, so that it is possible to better use specific wavelengths for studying membrane permeability. For previous work in Chapter 6, the used lamp for crosslinking is a high-pressure mercury lamp which has broad waveband from 250 to 650 nm. Therefore, an external filter was chosen to obtain the light beam with specific wavelength or waveband. Firstly, using blue light (the bandpass filter 400-500 nm was used) or UV light (the bandpass filter 365 nm was used) the membrane of polymersomes cannot crosslinked even for 10 min for 1 mL solution (1 mg/mL). Thus, the UV lamp equipped with shorter waveband filter (320-390 nm) was selected to crosslink the membrane of polymersomes, because it has higher energy and is well absorbed by polymersomes. For acquiring suitable crosslinked membrane, it is necessary to track the crosslinking degree with different photo-crosslinking time.

To determine the optimal crosslinking time, the volume distribution of light-responsive polymersomes at pH 5 was studied after different irradiation times. Next, once stable polymeric vesicles were obtained, the effect of crosslinking time on the swelling properties was studied.

For this purpose, the hydrodynamic size was measured by DLS at pH 8 and pH 5 for several cycles (Figure 7.4).

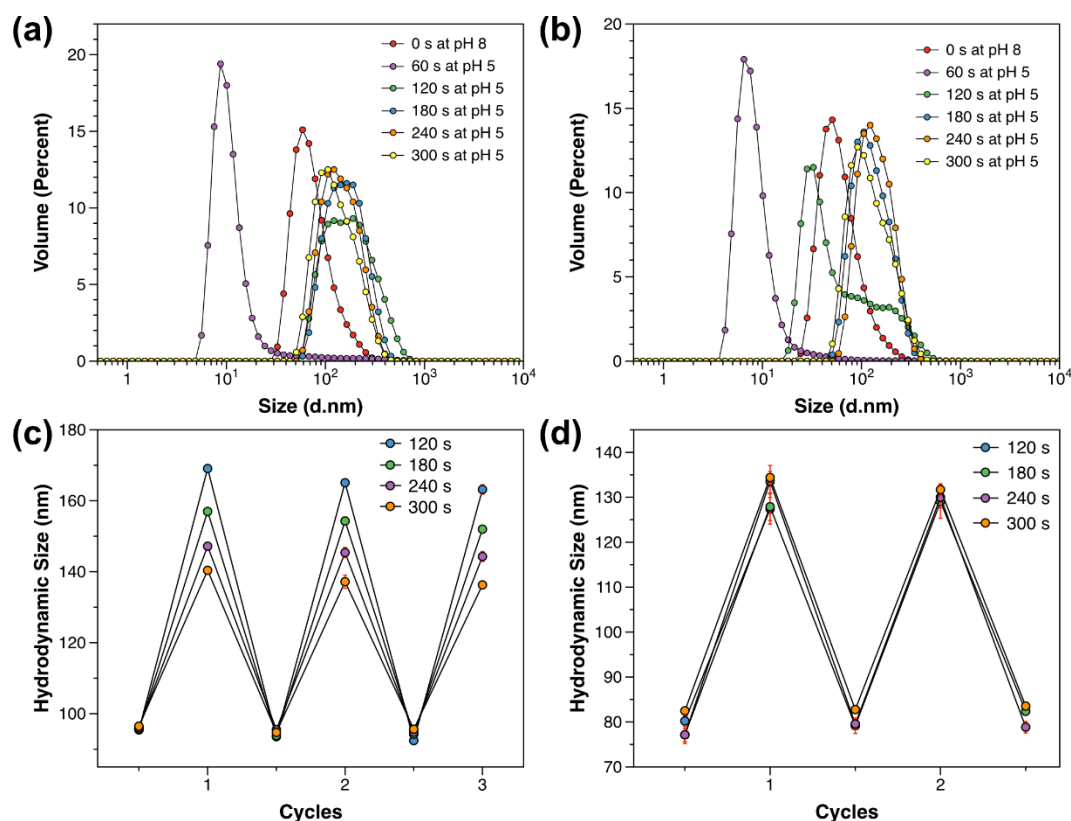


Figure 7.4 DLS study on size distribution of Psomes-DA-Azo (+) (a) and Psomes-Azo (+) (b) as well as corresponding cyclic pH-switches of Psomes-DA-Azo (+) (c) and Psomes-Azo (+) (d) after different time of photo-crosslinking upon UV irradiation (320-390 nm).

The peak at around 10 nm indicates that Psomes-DA-Azo (+) and Psomes-Azo (+) after 60 s photo-crosslinking under UV irradiation (320-390 nm, 1.34 W, 6.8 W/cm²) were dissociated into BCP chains under acidic conditions (Figure 7.4a&b). After 120 s to 300 s of photo-crosslinking, Psomes-DA-Azo (+) showed uniform volume distribution, narrow polydispersity (PDI: 0.118-0.181) and stable swelling-shrinking ability (Figure 7.4c). Although the swelling-shrinking ratio decreased from 1.77 to 1.46 with the extension of the photo-crosslinking time from 120 s to 300 s, all of them formed stable and compact membrane structure. However, Psomes-Azo (+) after 120 s photo-crosslinking showed 2 peaks in volume distribution (one for micelles around 30 nm, another for polymersomes around 200 nm) and a relative broad PDI (0.349). But after 180 s or even longer photo-crosslinking time, Psomes-Azo (+) also showed uniform volume distribution, narrow polydispersity (PDI: 0.150-0.189) and stable swelling-shrinking ability (Figure 7.4d). The swelling-shrinking ratio slightly decreased from 1.66 to

1.63 with the prolonged photo-crosslinking time from 180 s to 300 s. To sum up, 180 s was selected as optimal photo-crosslinking time to obtain robust and compact polymersomes for further experiments.

7.2.3 Characterization of Photo-Crosslinked Light-Responsive Polymersomes

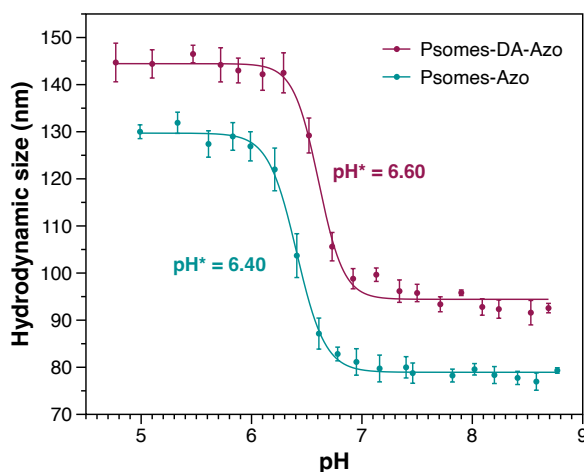


Figure 7.5 DLS study on pH titration of Psomes-DA-Azo (+) and Psomes-Azo (+). Conditions: 0.5 mg/mL Psomes-DA-Azo (+) or 0.5 mg/mL Psomes-Azo (+) in 1 mM PBS buffer.

pH titration was used to check the state of light-responsive polymersomes at different pH values by DLS measurement. As shown in Figure 7.5, the pH* of Psomes-DA-Azo (+) and Psomes-Azo (+) after 180 s photo-crosslinking under UV irradiation (320-390 nm) were 6.6 and 6.4, respectively. Additionally, Psomes-DA-Azo (+) and Psomes-Azo (+) were in the fully swollen state when the pH value is lower than 5.8 and in the collapsed state when the pH value is more than 7.2. The results indicate photo-crosslinked polymersomes with junction azobenzene are in the collapsed state at physiological pH value (pH 7.4) and probably had an impermeable membrane.

To further study the morphology, size and membrane thickness of the photo-crosslinked polymersomes with different types of azobenzene linkage, cryo-TEM was used to visualize their shape and to prove their hollow structure (Figure 7.6a&d). The spherical vesicle structure with a certain membrane thickness proves the successful assembly of Psomes-DA-Azo (+) and Psomes-Azo (+). Moreover, the histograms show that the average sizes of Psomes-DA-Azo (+) and Psomes-Azo (+) are 85 nm and 73 nm (Figure 7.6b&e), while the corresponding membrane thicknesses are 21 nm and 17 nm, respectively (Figure 7.6c&f). Their thicker membrane than typical “standard” polymersomes could be attributed to hydrophobicity and π - π stacking of

azobenzene units. The sizes measured by cryo-TEM are slightly smaller than the sizes measured by DLS (96 nm for Psomes-DA-Azo (+) and 77 nm for Psomes-Azo (+)), which is consistent with previous studies using conventional photo-crosslinked and pH-responsive polymersomes.

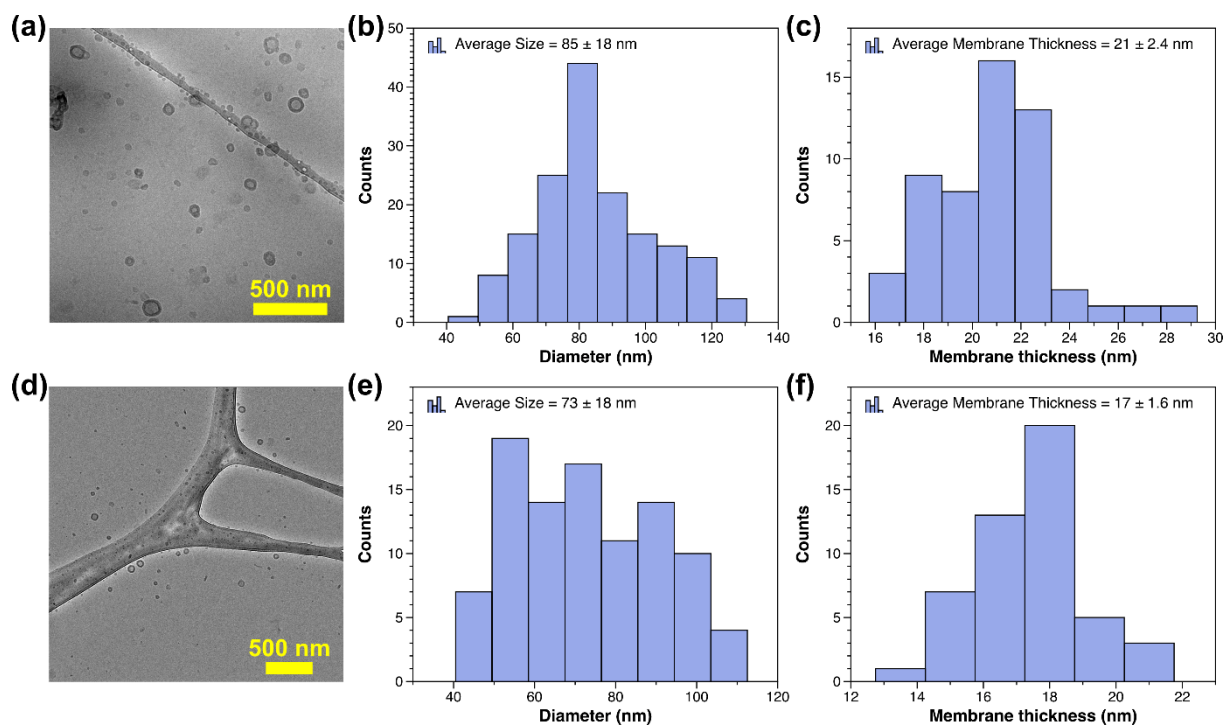


Figure 7.6 Cryo-TEM (a&d), size histograms (b&e) and membrane thickness histograms (c&f) of Psomes-DA-Azo (+) (a-c) and Psomes-Azo (+) (d-f) after 180 s photo-crosslinking under UV irradiation (320-390 nm). The average diameter and membrane thickness of polymersomes were calculated by analyzing more than 100 particles and 50 particles, respectively.

7.3 Photo-Isomerization of Azobenzene Containing Polymeric Macromolecules and Vesicles

Although the energy input as only factor leading to membrane perturbation is discussed in the literature, whether cis-to-trans or trans-to-cis isomerization responsible for the membrane disturbance is still unclear.¹⁵ Coincidentally, the wavelengths of used light sources (360 nm and 450 nm) are located in the absorption zone of azobenzene.¹⁵ Therefore, it is reasonable to assume that only wavelengths in the absorption region can affect membrane permeability. To confirm these assumptions, the absorption region and photo-induced isomerization behavior of all synthesized materials, including macroinitiators, BCPs and polymersomes with azobenzene, were investigated through UV-Vis spectroscopy.

7.3.1 Photo-Isomerization of Azobenzene Containing PEG Macroinitiators

To understand the photo-isomerization behavior of different types of azobenzene initiators, the aqueous solution of PEG-DA-Azo and PEG-Azo macroinitiators (1 mL, 0.1 mg/mL) were moved to quartz cuvette and put under UV irradiation (365 nm, 0.968 W, 4.93 W/cm²) and/or blue light irradiation (400-500 nm, 1.52 W, 7.74 W/cm²). Except for photo-crosslinking by the high-pressure mercury light equipped with external bandpass filter of 320-390 nm (high-energy UV), all further experiments used the same light equipped with external filter of 365 nm (UV) and 400-500 nm (blue light) to avoid the effects of photodamage caused by short wavelength UV light.

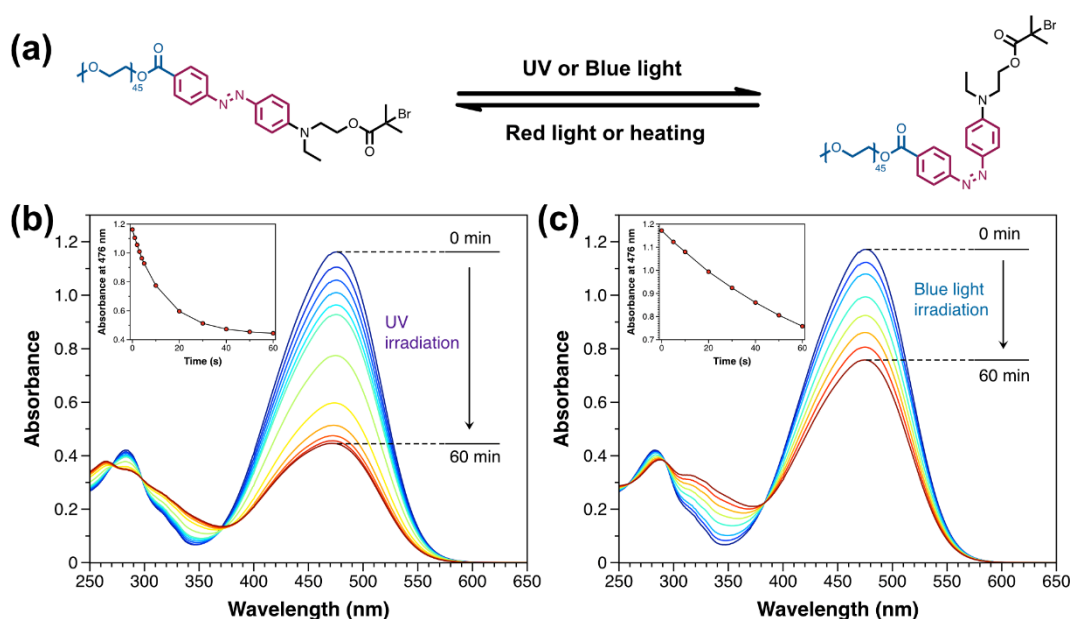


Figure 7.7 (a) Scheme of photo-isomerization of PEG-DA-Azo macroinitiator under light stimuli. (b) Photo-isomerization of PEG-DA-Azo macroinitiator under UV irradiation (365 nm). The inset shows the corresponding curve of absorption value change at 476 nm. (c) Photo-isomerization of PEG-DA-Azo macroinitiator under blue light irradiation (400-500 nm). The inset shows the corresponding curve of maximum absorption value change at 476 nm. Conditions: 0.1 mg/mL PEG-DA-Azo macroinitiator aqueous solution.

For PEG macroinitiator with donor-acceptor-substituted azobenzene, the above-mentioned two different light sources were used to isomerize the structure from trans state to cis state (Figure 7.7a). As red light-triggered cis-to-trans isomerization or thermal recovery process (even above the glass transition temperature of hydrophobic block) cannot change the mobility of cargo through the membrane in the literature, the cis-to-trans isomerization of donor-acceptor-substituted azobenzene containing macromolecules and vesicles was not studied in this work.¹⁵

The donor-acceptor substitution not only lowers the energy of the $\pi\pi^*$ state but also brings a strong charge transfer character into the $\pi\pi^*$ electronic transition. The former makes the quantum yield of trans-to-cis photo-isomerization significantly lower than the reverse process.¹⁸⁵ The latter leads to a large red-shift of the $\pi\pi^*$ absorption band from UV into visible spectral region, consequently, these spectral bands ($\pi\pi^*$ and $n\pi^*$ transitions) are overlapped.¹⁸⁴ It can be calculated that the absorbance at λ_{\max} (476 nm) decreases 61.8% and 35.3% after 60 min UV irradiation or blue light irradiation, respectively (Figure 7.7b&c). The decrease of maximum absorption indicates the successful photo-induced trans-to-cis isomerization. Although blue light has a higher power than the UV light (7.74 W/cm² vs 4.93 W/cm²), the efficiency of isomerization under UV irradiation is significantly higher than under blue light irradiation. But in general, this result proves that both light sources could be used to initiate photo-isomerization of donor-acceptor-substituted azobenzene.

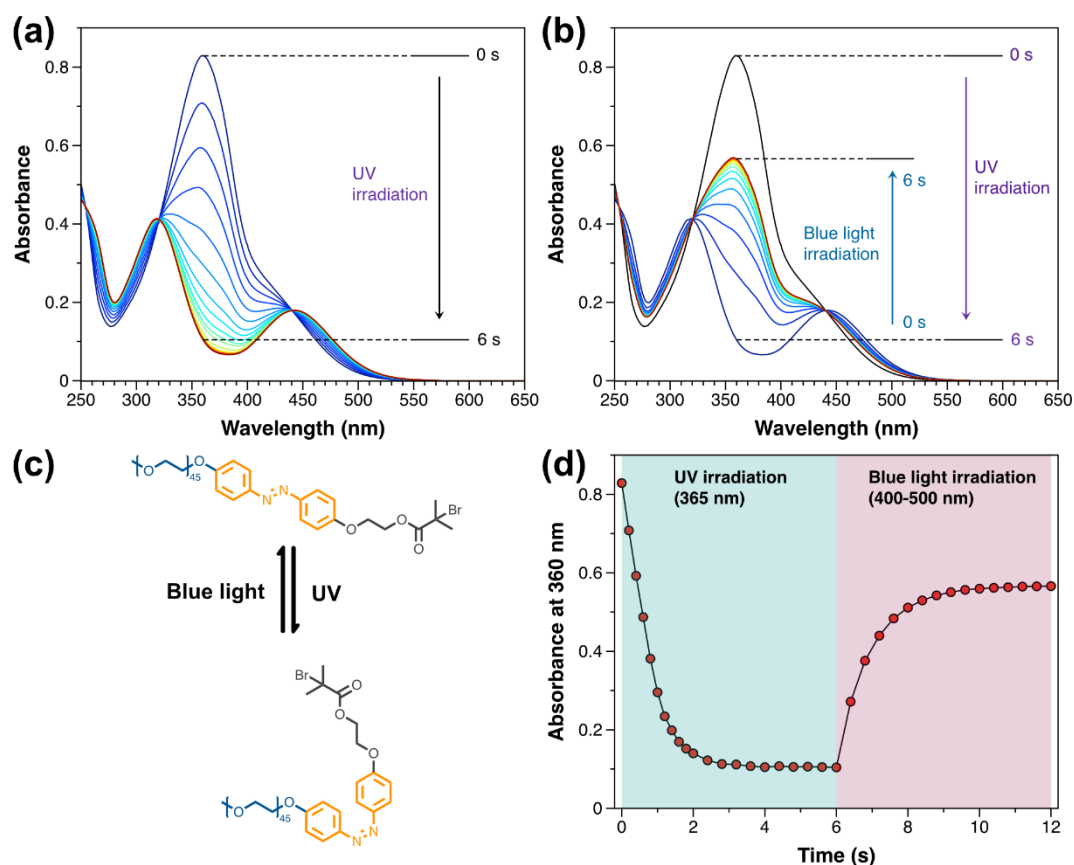


Figure 7.8 (a) Photo-isomerization of PEG-Azo macroinitiator under UV irradiation (365 nm). (b) Photo-isomerization of PEG-Azo macroinitiator under blue light irradiation (400-500 nm). (c) Scheme of photo-isomerization of PEG-Azo macroinitiator under light stimuli. (d) Curve of absorption value change at 360 nm of PEG-Azo macroinitiator undergoing light stimuli. Conditions: 0.1 mg/mL PEG-Azo macroinitiator aqueous solution.

The photo-isomerization of PEG-Azo macroinitiator was correspondingly carried out. The maximum absorption of ether-substituted azobenzene is centred around 359 nm for the trans isomer and around 442 nm for the cis form, which is attributed to their π - π^* and n - π^* transitions, respectively. Besides, the most obvious difference compared with PEG-DA-Azo macroinitiator is the very short heterogeneous equilibrium time whether trans-to-cis isomerization or cis-to-trans isomerization (Figure 7.8). Besides, the UV light leads to the trans-to-cis isomerization, however, blue light triggered the cis-to-trans isomerization. Both processes reached equilibrium within 4 s, but the second process cannot achieve complete recovery due to photobleaching upon the UV irradiation (68.3% absorbance compared with original state). From this result and referring to above-mentioned mechanism in the literature, both light sources can stimulate photo-isomerization of azobenzene unit, thereby could change the original membrane characteristics of Psomes-Azo.¹⁵

7.3.2 Photo-Isomerization of Azobenzene Containing BCPs and Polymersomes

To further study the photo-isomerization behavior of BCP and the most practical polymersomes with different types of azobenzene, the aqueous solution of BCP-(DA-)Azo without photo-crosslinker DMIBMA (BCP-DA-Azo (-) and BCP-Azo (-), 1 mL, 1 mg/mL, pH 6) and corresponding Psomes-(DA-)Azo without photo-crosslinker DMIBMA (Psoemes-DA-Azo (-) and Psomes-Azo (-), 1 mL, 1 mg/mL, pH 8) were moved to quartz cuvette and put under UV irradiation and/or blue light irradiation.

For UV-Vis spectra of BCP-DA-Azo (-), it can be figured out that the absorbance at λ_{\max} (483 nm) after 60 min blue light irradiation and UV irradiation only decrease 2.1% and 1.8%, respectively (Figure 7.9a&b). For UV-Vis spectra of Psomes-DA-Azo (-), the absorbance at λ_{\max} (435 nm) after 30 min blue light irradiation and UV irradiation only decrease 0.2% and 3.1%, respectively (Figure 7.9c&d). The blue-shift of maximum absorption from 483 nm to 435 nm is attributed to the deprotonation of donor-acceptor-substituted azobenzene (Figure A44).

Besides, a reasonable explanation for markedly decrease of isomerization degree compared with PEG-DA-Azo macroinitiator is that the push-pull azobenzene as junction between hydrophilic and hydrophobic segments of BCP-DA-Azo (-) rather than end group of PEG-DA-Azo macroinitiator converges the isomerization efficiency of trans-to-cis photo-isomerization and cis-to-trans thermal relaxation. Especially for Psomes-DA-Azo (-) under blue light irradiation, it can be seen from the inset of Figure 7.9c that the absorbance at λ_{\max} (435 nm)

after 5 min blue light irradiation decreased once and then increased with the longer illumination. This recovery process was observed and the whole unchanged isomerization result is consistent with the results in the literature.¹⁵

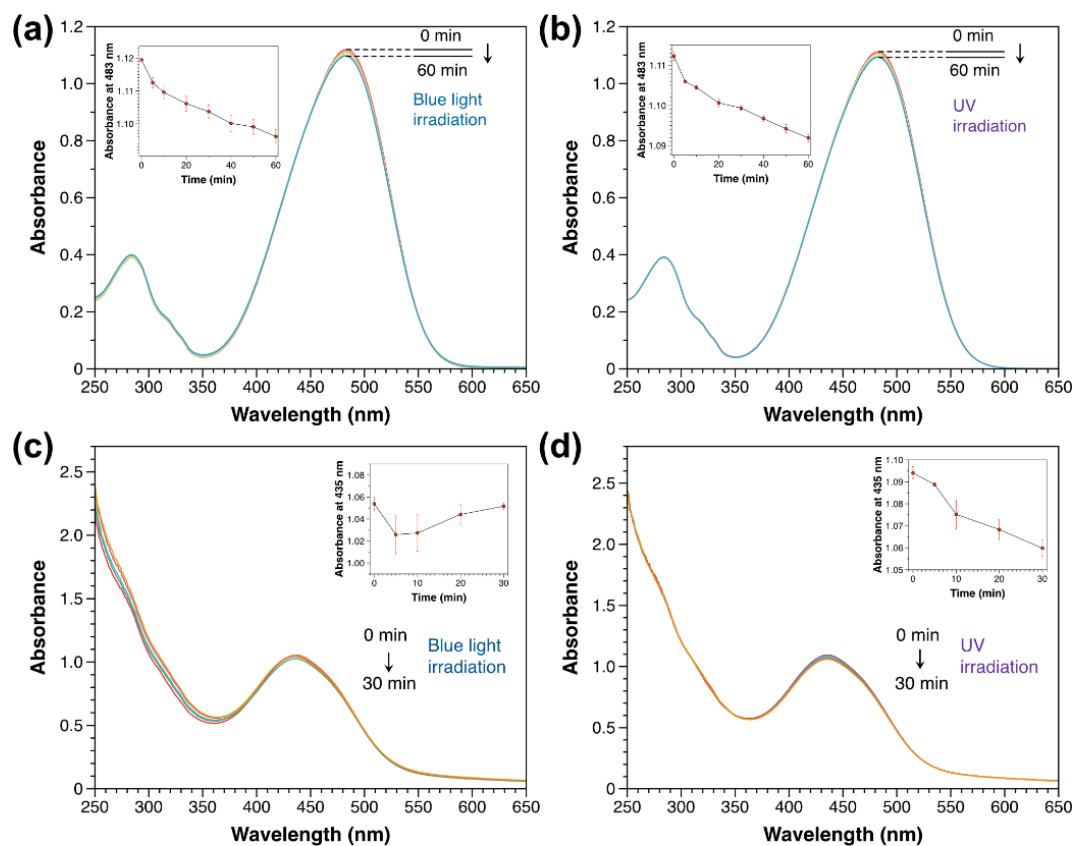


Figure 7.9 Photoisomerization of BCP-DA-Azo (-) under blue light irradiation (400-500 nm) (a) or UV irradiation (365 nm) (b). Photoisomerization of Psomes-DA-Azo (-) under blue light irradiation (400-500 nm) (c) or UV irradiation (365 nm) (d). The inset shows the corresponding curve of absorption value change at 483 nm for BCP-DA-Azo (-) and at 435 nm for Psomes-DA-Azo (-). Conditions: 1 mg/mL BCP-DA-Azo (-) dissolved in acidic solution, pH = 6; 1 mg/mL Psomes-DA-Azo (-) in basic solution, pH = 8.

However, both BCP-Azo (-) and Psomes-Azo (-) display fast photo-isomerization process (within 0.6 s) in the photo-isomerization process (Figure 7.10). These results demonstrate that the ether substituted azobenzene unit as junction in the BCP-Azo (-) remains flexible, even higher than azobenzene unit as end group of PEG-Azo macroinitiator, which may be due to the low transition barrier between two isomeric states of BCP-Azo (-) than PEG-Azo macroinitiator. Similar to photo-isomerization behavior of PEG-Azo macroinitiator, the cis-to-trans

isomerization cannot be achieved complete recovery due to the photobleaching upon to UV irradiation (72.6% for BCP-Azo (-) and 83.3% for Psomes-Azo (-)).

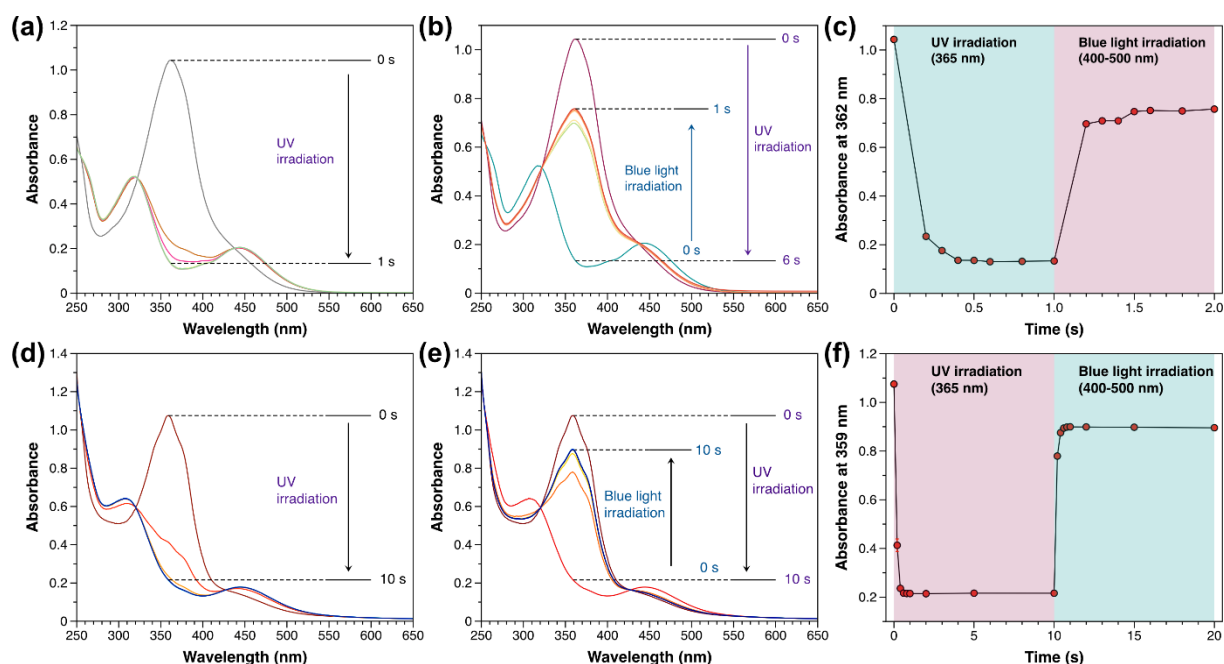


Figure 7.10 Photoisomerization of BCP-Azo (-) under UV irradiation (365 nm) (a) and then blue light irradiation (400-500 nm) (b). (c) The corresponding curve of absorption value change at 362 nm of BCP-Azo (-) undergoing light stimuli. Photoisomerization of Psomes-Azo (-) under UV irradiation (365 nm) (d) and then blue light irradiation (400-500 nm) (e). (f) The corresponding curve of absorption value change at 362 nm of Psomes-Azo (-) undergoing light stimuli. Conditions: 1 mg/mL BCP-Azo (-) dissolved in acidic solution, pH = 6; 1 mg/mL Psomes-Azo (-) in basic solution, pH = 8.

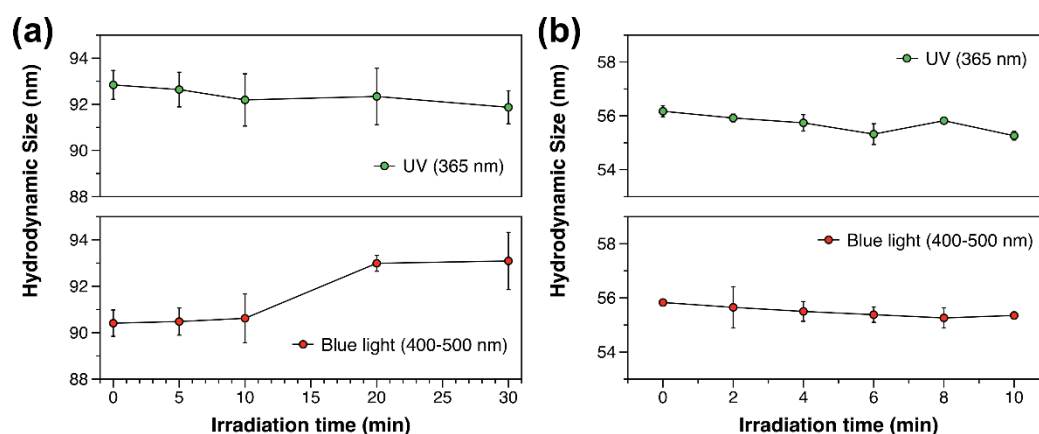


Figure 7.11 Hydrodynamic size of Psomes-DA-Azo (-) (a) and Psomes-Azo (-) (b) under light stimuli. Conditions: 1 mg/mL Psomes-DA-Azo (-) or 1 mg/mL Psomes-Azo (-) in basic solution, pH = 8.

Furthermore, the hydrodynamic size of Psomes-DA-Azo (-) and Psomes-Azo (-) after UV (365 nm) or blue light irradiation (400-500 nm) for given irradiation time has also been tested. As shown in Figure 7.11, no obvious size change was observed, which proves that single azobenzene unit for each BCP cannot significantly change the structure of polymersomes.

7.4 Light-Driven Dye Release from Polymersomes with Azobenzene at Simulated Physiological Conditions

To confirm the light-driven dye release behavior can be also achieved in the designed system, a hydrophobic dye, Nile red, was in-situ loaded into polymersomes self-assembled of BCP-DA-Azo (+) and BCP-Azo (+) (no photo-crosslinking performed because of avoidance of dye release action during photo-crosslinking process) and then used to investigate the dye release behavior through fluorescence spectroscopy.

7.4.1 Characterization of In-Situ Nile Red Loaded Polymersomes

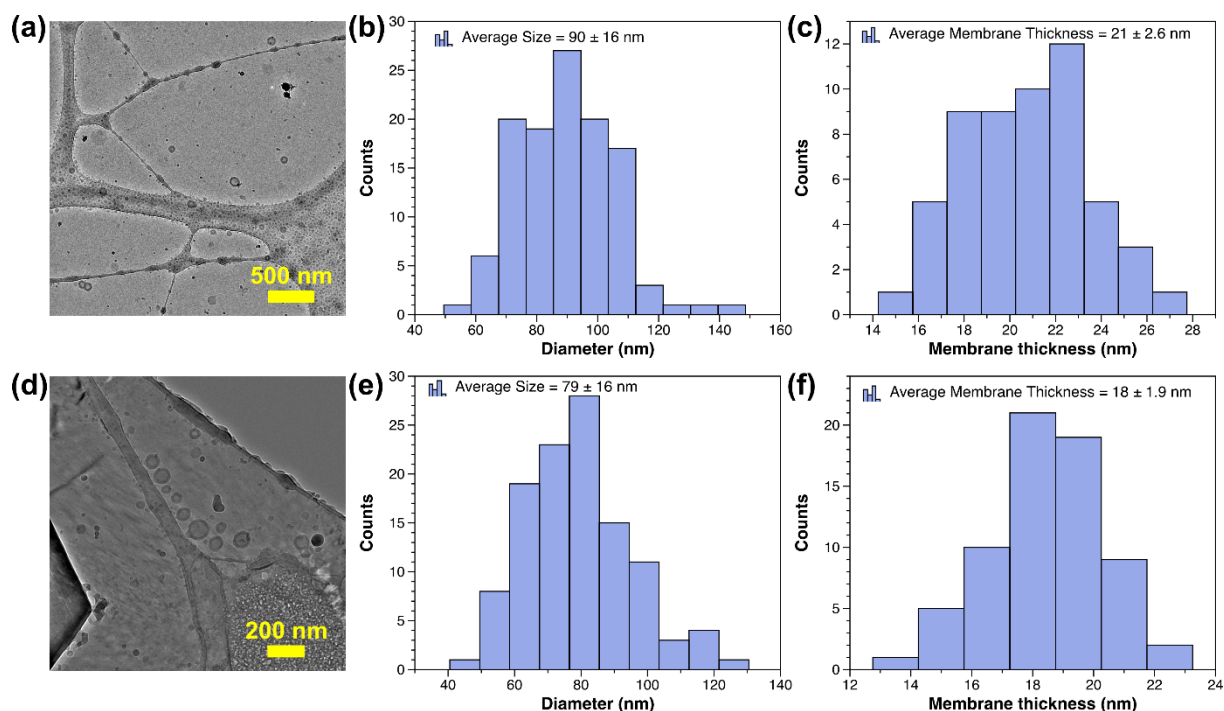


Figure 7.12 Cryo-TEM (a&d), size histograms (b&e) and membrane thickness histograms (c&f) of NR-Psomes-DA-Azo (+) (a-c) and NR-Psomes-Azo (+) (d-f) without photo-crosslinking. The average diameter and membrane thickness of polymersomes were calculated by analyzing more than 100 particles and 50 particles, respectively.

Before the dye release experiments, the morphology, size and membrane thickness of polymersomes with different types of azobenzene linkage and in-situ loaded with Nile red were checked by cryo-TEM to visualize their shape and to prove their hollow structure (Figure 7.12). The hollow sphere structure with a certain membrane thickness proves the successful assembly of NR-Psomes-DA-Azo (+) and NR-Psomes-Azo (+) (Figure 7.12a&d). In addition, the histograms show that the average sizes of NR-Psomes-DA-Azo (+) and NR-Psomes-Azo (+) are 90 nm and 79 nm (Figure 7.12b&e), while the corresponding membrane thickness is 21 nm and 18 nm, respectively (Figure 7.12c&f). The slightly increased average sizes measured by cryo-TEM compared with the empty Psomes-DA-Azo (+) (85 nm) and Psomes-Azo (+) (73 nm) (Figure 7.6) proves successful loading of Nile red.

7.4.2 Light-Driven Dye Release from Polymersomes at Simulated Physiological Conditions



Figure 7.13 Scheme of dye release from NR-Psomes-(DA-)Azo (+) at simulated physiological conditions under light stimuli. Conditions: 1 mL * 0.5 mg/mL NR-Psomes-DA-Azo (+) or NR-Psomes-Azo (+) without photo-crosslinking in 1 mM PBS buffer at pH 7.4.

To begin with, NR-Psomes-DA-Azo (+) or NR-Psomes-Azo (+) at simulated physiological conditions (pH 7.4) were moved to quartz cuvette and the fluorescence was detected before and after light stimuli for different times. The lipophilic stain, Nile red, is highly solvatochromic and its emission and excitation wavelength both shift depending on solvent polarity and in polar media will hardly fluoresce at all.^{186, 187} As a hydrophobic membrane dye, Nile red can be easily integrated in the membrane of polymersomes in the self-assembly process and shows the desired fluorescence (Figure 7.13). Once Nile red is released from the membrane to the lumen or outside environment (polar aqueous phase), the fluorescence will disappear.

To accurately calculate the release efficiency of the dye, the fluorescence quenching of Nile red under light illumination was firstly measured by fluorescence emission spectroscopy. Due to

Nile red is insoluble in water, DMF was selected as solvent to prepare Nile red solution for fluorescence measurement. After 12 min blue light irradiation or UV irradiation, the fluorescence intensity decreased by photobleaching by 4.7% and 10.9%, respectively (Figure 7.14). That is ascribed to the high power of mercury lamp, but it still can be used to perform the dye release experiments.

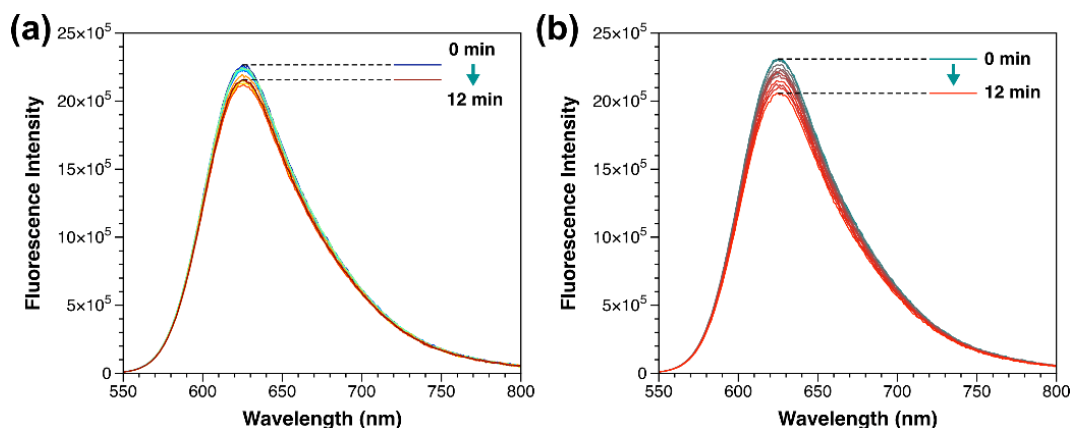


Figure 7.14 Photobleaching of Nile red under blue light irradiation (400-500 nm) (a) or UV irradiation (365 nm) (b). Conditions: 1 mL 1 $\mu\text{g}/\text{mL}$ Nile red solution, dissolved in DMF; $\lambda_{\text{ex}} = 515 \text{ nm}$, $\lambda_{\text{em}} = 626 \text{ nm}$.

Following, cyclic irradiation and relaxation in dark as well as continuous irradiation were utilized to prove the dye release behavior (Figure 7.15). It can be seen from cyclic release study that the release behavior was stopped when the light stimuli was removed (Figure 7.15a&c). Thus, light stimuli are only actuator to disturb the membrane characteristics at defined environmental conditions, which is consistent with previously mentioned mechanism.¹⁵ Moreover, the degree of dye release between cyclic irradiation-relaxation method and continuous irradiation are very close. In addition, no dye release happens without light illumination (Figure 7.15b&d). Surprisingly, the trend of dye release by NR-Psomes-DA-Azo (+) and NR-Psomes-Azo (+) is similar, that blue light irradiation has obvious higher dye release rate than UV irradiation, which could be due to the higher power density of blue light (7.74 W/cm²) than UV light (4.93 W/cm²). In specific, the percentage of dye release of NR-Psomes-DA-Azo (+) under blue light and UV light is 87.7% and 46.9%, and the percentage of dye release of NR-Psomes-Azo (+) under blue light and UV light is 94.1% and 63.8%, respectively. A reasonable explanation is that more energy input initiates stronger perturbation of original membrane characteristics, thus the dye rapidly escapes from the membrane. Concurrently, these results also rule out the influence of the ratio of cis isomer or trans isomer caused by fast

equilibrium (within 0.6 s) in the photo-isomerization for Psomes-Azo under light stimuli. As for the difference of photo-isomerization efficiency between Psomes-DA-Azo and Psomes-Azo, it is still an open point for future study.

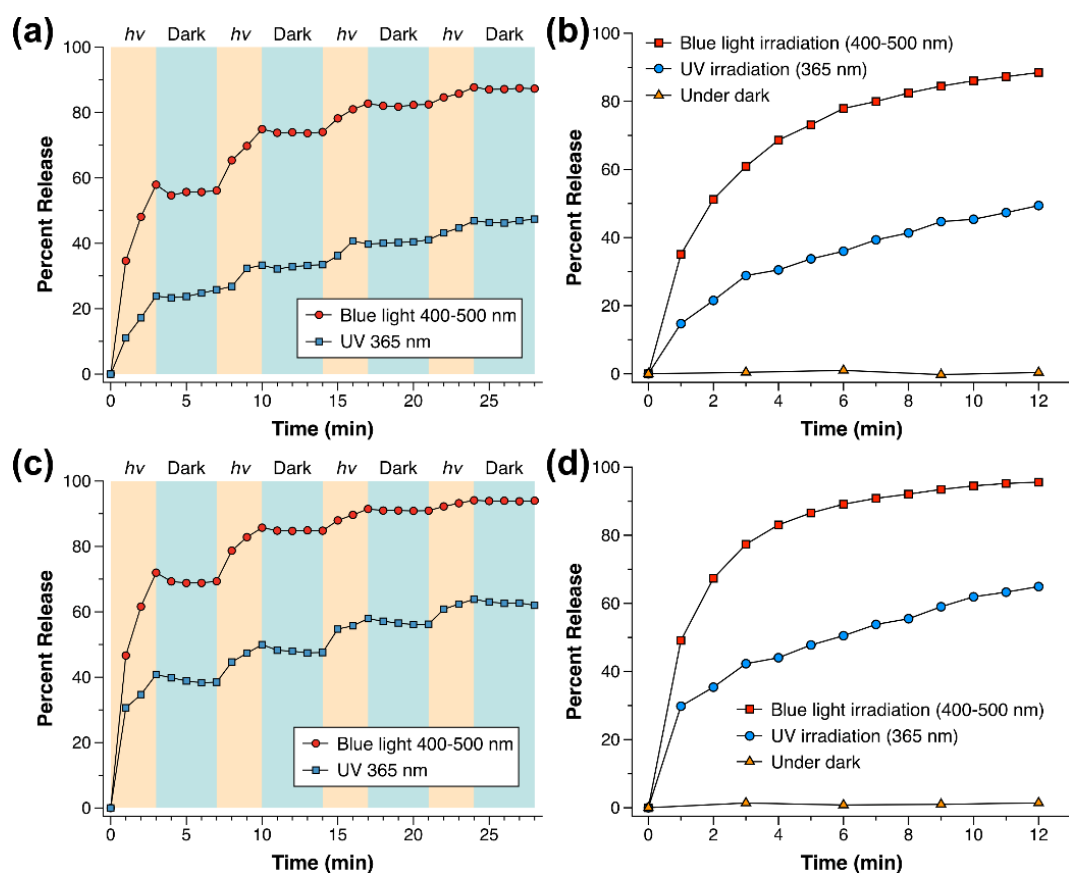


Figure 7.15 Percent release of Nile red from NR-Psores-DA-Azo (+) during the light stimuli and dark cycles (a) as well as the comparison between continuous light irradiation and under dark (b). Percent release of Nile red from NR-Psores-Azo (+) during the light stimuli and dark cycles (c) as well as the comparison between continuous light irradiation and under dark (d).

Afterwards, the average hydrodynamic size of NR-Psores-(DA-)Azo before and after light irradiation was also measured to track the dye release process (Figure 7.16). Firstly, hydrodynamic size of NR-Psores-DA-Azo (+) and NR-Psores-Azo (+) were 103 nm and 94 nm, respectively. The increased size compared with empty Psomes-DA-Azo (+) (96 nm) and Psomes-Azo (+) (77 nm) confirms successful loading of Nile red once again. It can be calculated that the average hydrodynamic diameter of NR-Psores-DA-Azo (+) and NR-Psores-Azo (+) after 12 min light stimuli decreased 10 nm and 6 nm, respectively (no matter UV irradiation or blue light irradiation). This result proves the successful dye release from the membrane of NR-Psores-(DA-)Azo (+) under light stimuli.

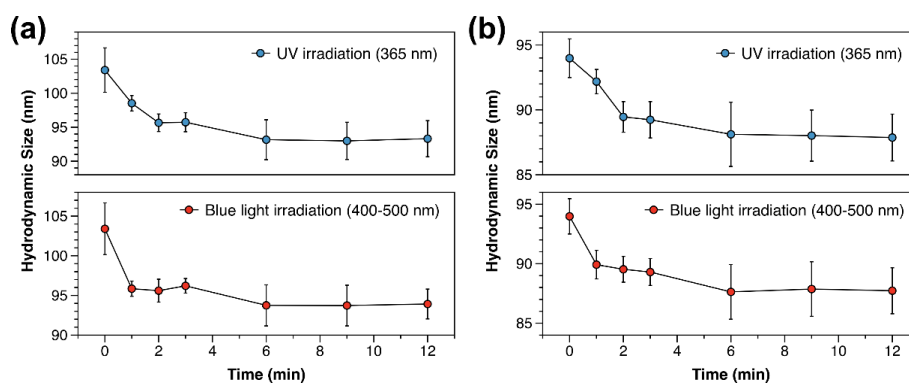


Figure 7.16 Hydrodynamic size change of NR-Psomes-DA-Azo (+) (a) and NR-Psomes-Azo (+) (b) under light stimuli.

7.5 Light-Induced Enzyme Reaction in Polymersomes with Azobenzene at Simulated Physiological Conditions

To further substantiate the light-triggered enhancement of membrane permeability, enzyme myoglobin was selected as a model for proof of concept in the enzyme assays. Firstly, myoglobin was in-situ loaded into polymersomes self-assembly of BCP-DA-Azo (+) and BCP-Azo (+) with 180 s photo-crosslinking under UV irradiation (320-390 nm) and then used to carry out the enzyme reaction and the fluorescence was tracked by microplate reader.

7.5.1 Characterization of Polymersomes in-Situ Loaded Myoglobin

Firstly, the morphology, size and membrane thickness of polymersomes with different types of azobenzene linkage and in-situ loaded with myoglobin were checked by cryo-TEM to visualize their shape and to prove their hollow structure (Figure 7.17). The hollow sphere structure with a certain membrane thickness proves the successful assembly of Myo-Psomes-DA-Azo and Myo-Psomes-Azo (Figure 7.17a&b). In addition, the size histograms show that the average diameters of Myo-Psomes-DA-Azo and Myo-Psomes-Azo are 97 nm and 88 nm, while the corresponding membrane thicknesses are 21 nm and 16 nm, respectively (Figure 7.17c&d). The average sizes measured by cryo-TEM were obviously larger than the empty Psomes-DA-Azo (85 nm) and Psomes-Azo (73 nm). The similar membrane thickness and obvious increased diameters indicate that the location of loaded myoglobin is mainly located in the lumen and the presence of myoglobin affects the assembly process which leads to bigger particles.

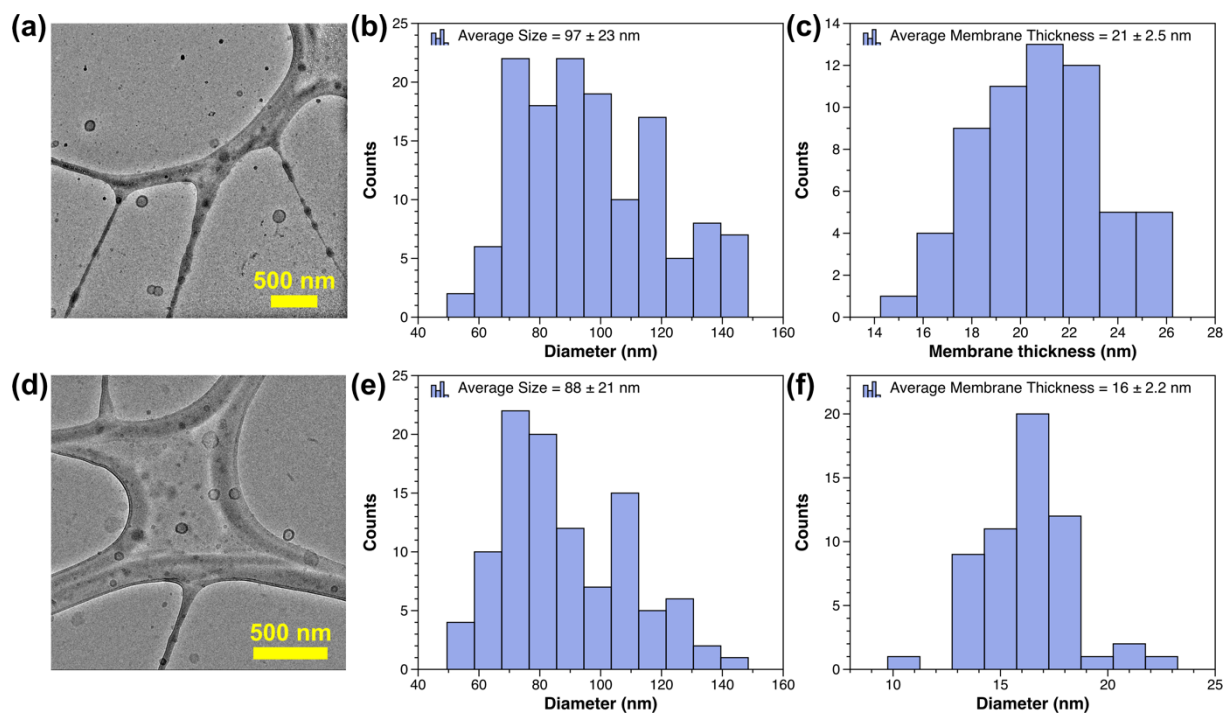


Figure 7.17 Cryo-TEM (a&d), size histograms (b&e) and membrane thickness histograms (c&f) of Myo-Posomes-DA-Azo (+) (a-c) and Myo-Posomes-Azo (+) (d-f) after 180 s photo-crosslinking under UV irradiation (320-390 nm). The average diameter and membrane thickness of polymersomes were calculated by analyzing more than 100 particles and 50 particles, respectively.

7.5.2 Light-Induced Enzyme Reaction in Polymersomes at Simulated Physiological Conditions

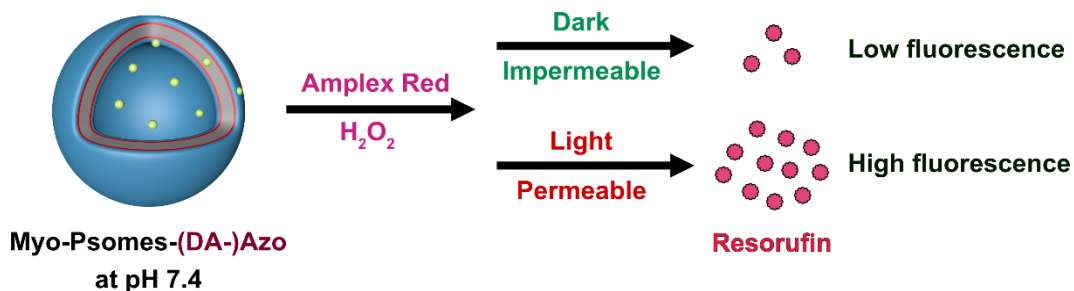


Figure 7.18 Scheme of enzymatic reaction in photo-crosslinked Myo-Posomes-(DA-)Azo (+) in the dark or upon light stimuli (UV or blue light).

To start with, substrates Amplex Red and H_2O_2 were added to Myo-Posomes-DA-Azo or Myo-Posomes-Azo at simulated physiological conditions (pH 7.4) under continuous mechanical stirring for 2 min to mix well. To initiate the enzyme assay, the solution was put under blue light irradiation (400-500 nm) or UV irradiation (365 nm). After different time of light irradiation (up to 10 min) and incubation under dark for a while for each portion (total 30 min

incubation time), fluorescence spectra were recorded. As shown in Figure 7.18, because the membrane of polymersomes is impermeable at physiological pH value (pH 7.4), the substrates can only react with individual enzyme on/in the membrane of polymersomes that HFF purification cannot remove it thoroughly.^{85, 182} Thus, low fluorescence intensity can be detected after 30 min incubation without light stimuli (Figure A45). However, once light source was used to trigger the enhancement of membrane permeability, the substrates Amplex Red and H₂O₂ can diffuse into the lumen and inside membrane to react with enzyme myoglobin, and then high fluorescence will be detected.

Next, the fluorescence intensity was normalized as shown in Figure 7.19. Both blue light and UV can trigger substrates diffusion into polymersomes lumen and then the enzyme myoglobin catalyzed the Amplex Red to resorufin in presence of H₂O₂. To keep the fluorescence signal generated by the surface enzymes consistent, the total incubation time was set to 30 min, which means the polymersomes' solution was irradiated with light for n min and then put under dark to standing for 30-n min.

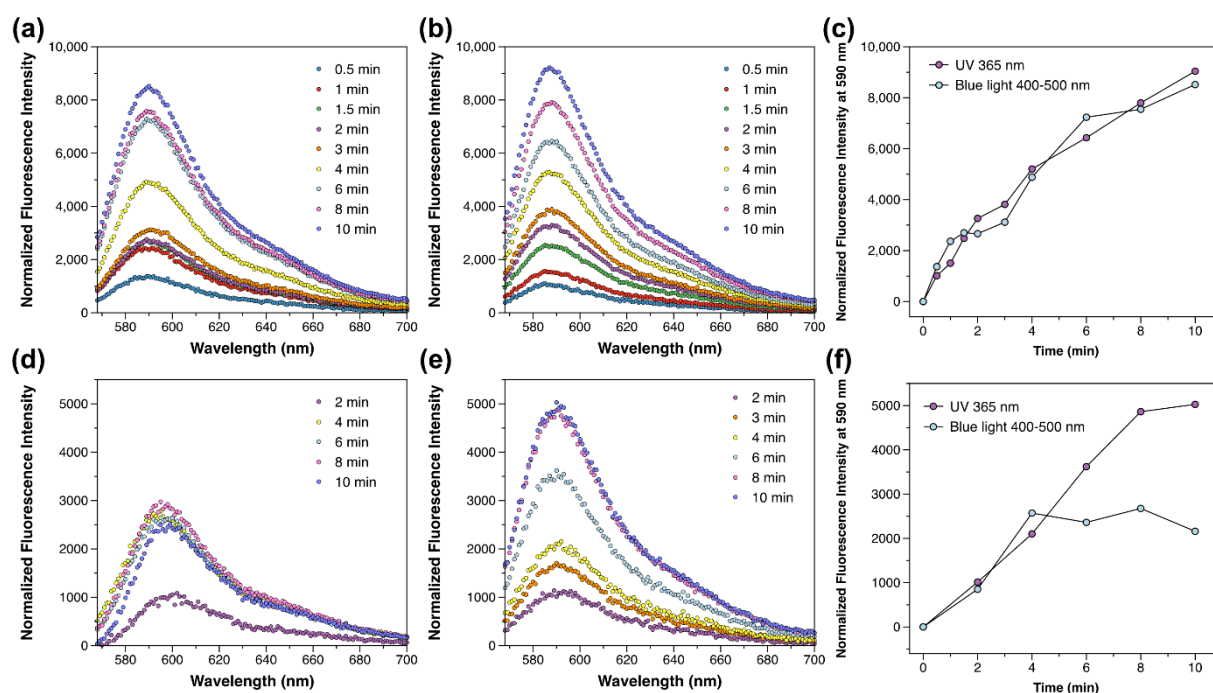


Figure 7.19 Enzymatic reaction of Myo-Psomes-DA-Azo (+) under blue light irradiation (400-500 nm) (a) and UV irradiation (365 nm) (b) at simulated physiological conditions as well as the corresponding curve of the peak value at 590 nm versus irradiation time (c). Enzymatic reaction of Myo-Psomes-Azo (+) under blue light irradiation (400-500 nm) (d) and UV irradiation (365 nm) (e) at simulated physiological conditions as well as the corresponding curve of the peak value at 590 nm versus irradiation time (f).

Due to the inherent loading difference in enzyme in different polymersomes, we cannot directly compare the efficiency of enzyme reaction between Myo-Psomes-DA-Azo (+) and Myo-Psomes-Azo (+). Besides, the fluorescence intensity increased with longer light stimuli. Although the fluorescence intensity of Myo-Psomes-Azo (+) under blue light irradiation kept no change with more than 4 min light stimuli, it is still consistent with Myo-Psomes-Azo (+) under UV irradiation within 4 min, which could be attributed to the saturation of the enzyme reaction caused by the operating error, further repeating experiments are needed (Figure 7.19f).

Moreover, the fluorescence intensity of Myo-Psomes-DA-Azo (+) keep consistent between blue light irradiation and UV irradiation in given 10 min, while the power intensity of light sources is different (Figure 7.19c). It can be concluded that both light sources, blue light and UV light, give similar degree of enhancement of membrane mobility to achieve the same diffusion rate of substrates. Thereby enzyme reaction presents the same trend and results, but with different efficiencies when only considering results of Myo-Psomes-Azo (+) and Myo-Psomes-DA-Azo (+) (Figure 7.19c&f). With this there are arising open concerns, which should be further considered with both light stimuli in the future: First, more myoglobin is loaded in the lumen of Myo-Psomes-DA-Azo (+) than in those of Myo-Psomes-Azo (+). Second, there is a similar myoglobin loading efficiency in the lumen of both polymersomes. However, twice increase in fluorescence intensity after 10 min UV light irradiation (Figure 7.19c&f) can be also explained by the greater changes in original membrane characteristics under UV light irradiation, which leads to faster diffusion rate of substrates in the Myo-Psomes-DA-Azo. As the effect of membrane permeability, caused by the irradiation of (push-pull) azobenzene linkage, is still not quantifiable, this is still an open research field and more experiments will be designed and carried out in the future.

7.6 Summary

Within this chapter, macroinitiator and BCPs with two types of azobenzene unit were synthesized and characterized, then used to assemble polymersomes with azobenzene linkage between hydrophilic and hydrophobic block (Figure 7.1 & 7.2). Following the photo-crosslinking time and pH titration of polymersomes were explored and characterized. In addition, size and membrane thickness of photo-crosslinked (and loaded) polymersomes self-assembly by BCPs with different azobenzene linkages were counted by visualization method cryo-TEM.

To confirm responsive light's wavelength for different types of azobenzene unit, the photo-isomerization of PEG macroinitiator, BCPs and polymersomes with azobenzene were further characterized by UV-Vis spectroscopy. Following, UV light (365 nm) and blue light (400-500 nm) were selected to carry out the photo-isomerization of azobenzene compounds. Besides, the hydrodynamic size of polymersomes was also measured by DLS to prove the integrity of membrane structure before and after light stimuli.

Moreover, NR-Psomes-DA-Azo (+) and NR-Psomes-Azo (+) were fabricated through in-situ loading method and followed by dialysis purification. Next the dye release was performed respective by irradiation-relaxation cycles and continuous irradiation routes under UV irradiation or blue light irradiation at physiological condition (pH 7.4). As a result, the light source proved to be the only reason for the change in membrane fluidity and thus, release of the dye.

Finally, Myo-Psomes-DA-Azo (+) and Myo-Psomes-Azo (+) were also prepared by in-situ loading and followed by HFF purification to remove unencapsulated myoglobin. Following the enzyme reaction by both polymersomes was triggered by light stimuli at simulated physiological condition (pH 7.4). Although the intensity and wavelength of light source has significant difference, the enzyme reaction rate through light-induced substrates diffusion showed consistent results whether under blue light or UV irradiation.

This strategy provides a straightforward concept for the exploitation of azobenzene as the junction molecule between hydrophilic and hydrophobic segments. Trans-cis isomerization affords the enhancement of membrane permeability to achieve not only cargo release but also small molecules diffusion at physiological condition (pH 7.4). Furthermore, dye release experiments under light irradiation with lower power density could be used to interpret the difference between NR-Psomes-DA-Azo (+) and NR-Psomes-Azo (+) as well as the differences of responsive rate between blue light and UV light. In addition, the light illumination could increase the temperature of the polymersomes solution, which is also an influencing factor of release rate of dye or substrates diffusion rate in the enzyme reaction. Therefore, monitoring and control of temperature upon light irradiation will be performed to correct the experimental results.

8 Conclusion and Outlook

Within this work, two different methods, including (i) clustering and (ii) azobenzene-containing BCPs, were developed to optimize conventional pH-responsive and photo-crosslinked polymersomes to improve the efficiency of enzyme reaction in given environments. Polymersomes as nanoreactors in the process of mimicking cellular organelles are extremely important whether it is to simulate sophisticated biological behavior or information exchange under physiological regulation. Therefore, this thesis aimed first at developing a complex artificial organelle system with co-clustered pH-responsive polymersomes in-situ loaded with different enzymes to perform enzymatic cascade reaction at neutral (pH 7.0) or slight acidic condition (pH 6.5). A second goal was fabricating selectively impermeable/permeable artificial organelles through light-responsive polymersomes with different types of azobenzene units to carry out cargo release and small molecules diffusion at physiological condition under light stimuli (pH 7.4).

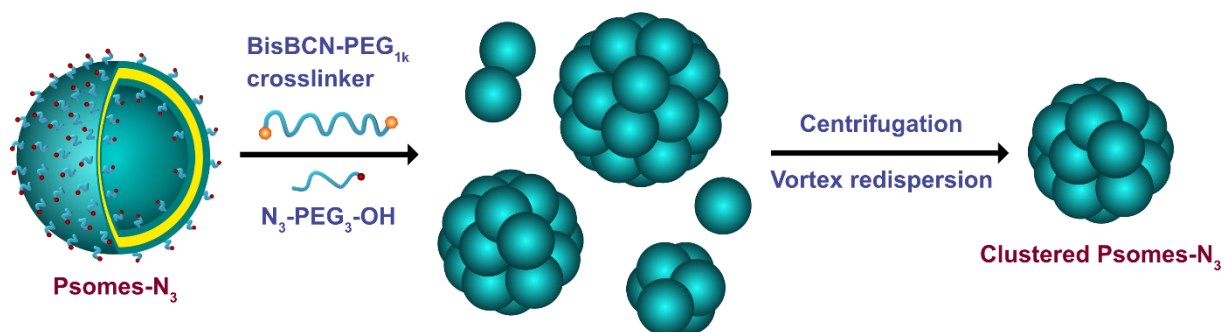


Figure 8.1 Preparation and purification routes of clustered polymersomes. The clustering process is achieved by PEG with bis-cyclooctyne end groups using copper-free click reaction. The termination step is used to control the clustering process and purification methods are utilized to obtain optimal clusters.

First, clustered pH-responsive and photo-crosslinked polymersomes based on SPAAC click chemistry were developed (see chapter 6). It is worth mentioning that most of the enzymatic cascade reaction in artificial organelles occurred through simple mixing enzyme-loaded polymersomes. However, polymersomes as nanoreactors can only achieve simple and singular function in the simulating process. In fact, a real cellular organelle is an intricate system that exhibits sophisticated biological functions. For this reason, self-assembly of artificial synthetic vesicles to clusters or to aggregates through interconnection as bionic way is a potential route to establish artificial intelligent biological systems for emergent distinct and common

properties. Until now, various bridging methods, include non-covalent bonding, DNA hybridization and click chemistry, have been used to assemble polymersomes into (large-scale) aggregates and controlled clusters. Inspired by the design of the clusters though photo-crosslinked and pH-responsive polymersomes, we decided to use bisBCN-PEG as crosslinker through a convenient and safe assembly route to form clustered polymersomes (Figure 8.1).

The resulting clustered polymersomes were expected to be pH-responsive and loaded with multiple enzymes (GOx and Myo) in single cluster to execute the enzymatic cascade reaction (Figure 8.2). Closer spatial distance between different nanoreactors (GOx-Psomes-N₃ and Myo-Psomes-N₃) could speed up the diffusion of substrates and intermediate product as well as the final enzyme reaction.

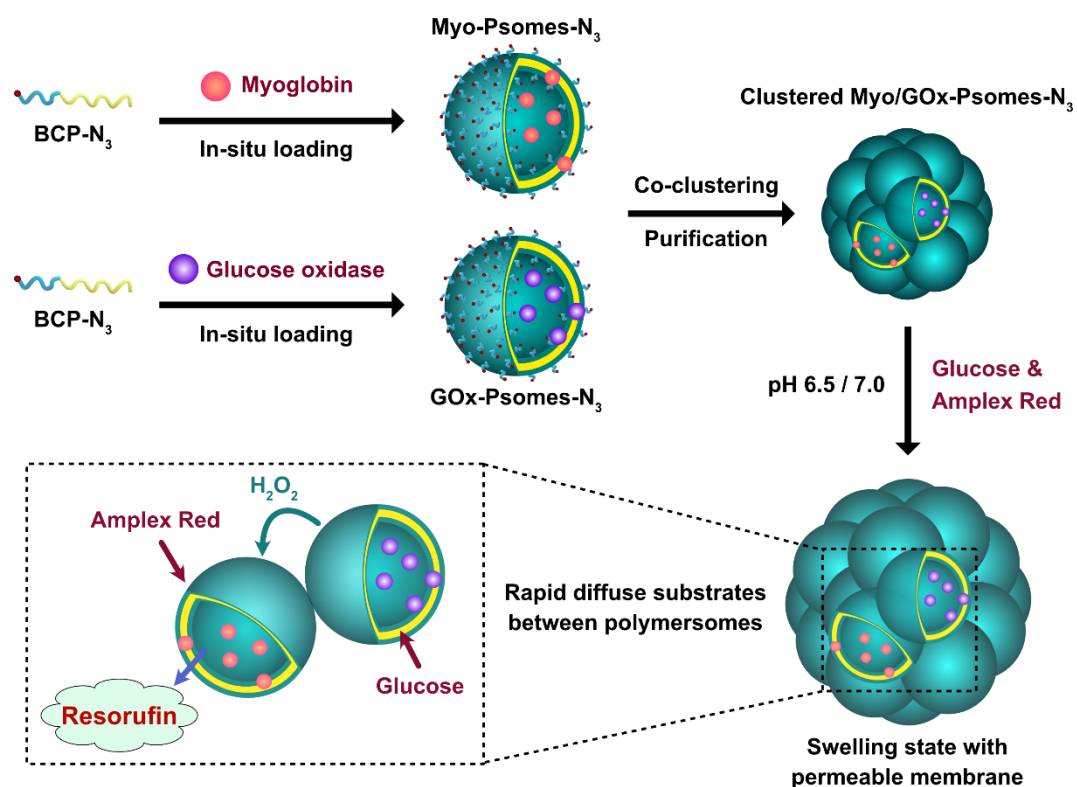


Figure 8.2 Fabrication of co-clustered enzyme-loaded polymersomes (Myo/GOx-Psomes-N₃) for enzymatic cascade reaction at neutral or slight acidic condition.

The pH-responsive BCPs with methoxy and azido end groups were synthesized through ATRP method, then used for the desired self-assembly into polymersomes and finalized by required photo-crosslinking process. Following the swelling-shrinking ability, size, and membrane thickness of polymersomes self-assembly by different BCPs were characterized. In addition,

the bisBCN-PEG crosslinker with different lengths were also prepared and then used to crosslink polymersomes with azido group to assemble pH-responsive clusters.

To obtain desirable clusters, various influencing factors in the clustering process, including temperature, proportion of BCP- N_3 , reaction time, feed ratio, crosslinker length, and concentration, were further studied. After a preliminary investigation, polymersomes (diluted to 0.5 mg/mL by PBS buffer, pH 7.4) self-assembly by 100% BCP- N_3 with same equivalent bisBCN-PEG_{1K} crosslinker (azido group: crosslinker = 1: 1) were carried out at 40 °C for 2 d to prepare clusters. Subsequently, the purification approach was optimized and finally 4 times centrifugation at 6000 rpm for 5 min and vortex redispersion method were chosen to obtain optimal clustered polymersomes. Above-mentioned clustering results were proved by size distribution measurement by DLS and many visualization methods, including TEM, cryo-TEM, in-situ AFM, CLSM and particle size and shape measurement. Except for in-situ AFM results lack sufficient samples for analysis, other approaches demonstrated the average size of clustered Psomes- N_3 as well as co-clustered Myo/GOx-Psomes- N_3 is approximately 1 μm .

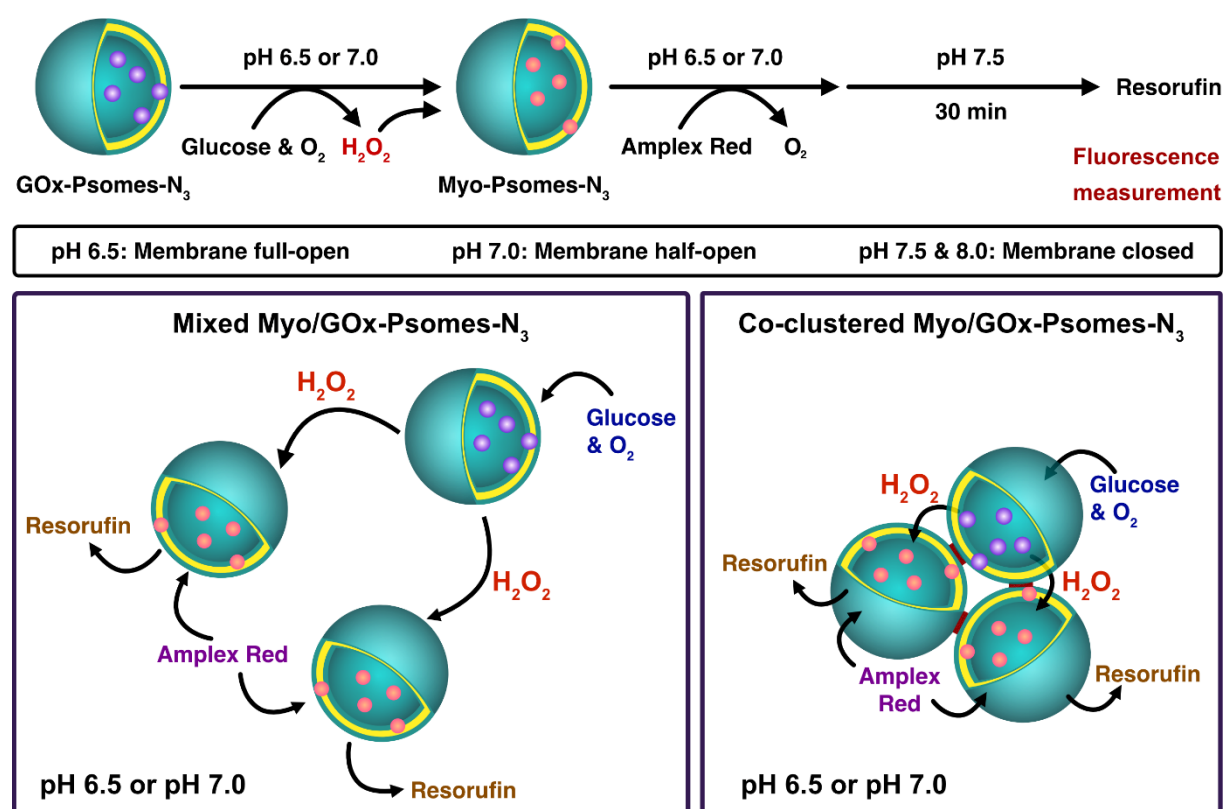


Figure 8.3 Schematic illustration of enzymatic cascade reaction mechanism (top) and substrates as well as intermediates diffusion mechanism (bottom) in mixed or co-clustered Myo/GOx-Psomes- N_3 .

Furthermore, co-clustered enzyme-loaded polymersomes (Myo/GOx-Psomes-N₃) were prepared for enzymatic cascade reaction when the membrane is open at a certain pH range (Figure 8.3). In order to realize the controllable switch-on/-off of the membrane of co-clustered Myo/GOx-Psomes-N₃ for enzymatic cascade reaction, the swelling/shrinking degree of the membrane were studied by pH titration. The results indicated that the membrane of enzyme-loaded polymersomes (Myo-Psomes-N₃ and GOx-Psomes-N₃) is semi-open at pH 7.0 (pH*) and fully open at pH 6.5.

Finally, to better compare the enzyme reaction activity between mixed Myo/GOx-Psomes-N₃ and co-clustered Myo/GOx-Psomes-N₃, the effect of enzyme activity on clustering condition was researched. The results of fluorescence spectroscopy suggested that heating does not change the activity of the enzyme Myo and GOx, even the clustered Enzyme-Psomes-N₃ with closer spatial structure only lost a little enzyme activity. At the end, compared with the conventional enzyme cascade reaction through simple mixing Myo/GOx-Psomes-N₃, the co-clustered Myo/GOx-Psomes-N₃ show higher efficiency (210.5% at incubation pH 6.5) of enzymatic cascade reaction at lower polymersomes concentration (0.3 mg Psomes-N₃/mL). Therefore, the co-clustered polymersomes loaded with different enzymes were expected to increase the efficiency of enzymatic cascade reaction and to mimic more complex biological behaviors.

For another work in chapter 7, single azobenzene was designed as junction molecule between hydrophilic and hydrophobic segment of the block copolymer and self-assembled polymersomes based on two kinds of azobenzene linkage were fabricated. With conventional pH-responsive and photo-crosslinked polymersomes enzyme reactions are performed at fully swollen, semi-open or intrinsically diffusible membrane state. The cargo (substrate, intermediate, product or metabolite) is easily to leak out from the lumen or membrane to outside environment. This leads to the polymersomes which are limited in their use as nanoreactors only under acidic conditions. However, the real organelles can not only carry but also retain biological macromolecules, even while performing biological actions preferential at physiological pH 7.4. For this reason, precision control of membrane permeability becomes particularly important in the process of mimicking signal transmission and matter production. Inspired by this, innovating a new variable in the existing system and remaining intrinsic structure but precise controlling of membrane permeability is a desirable pathway to carry out mimicking biological behaviors at physiological environment. Therefore, light-responsive azobenzene molecule as

junction molecule was used to prepare novel BCPs and self-assemble novel polymersomes with azobenzene as junction unit (Figure 8.4). The resulting polymersomes with azobenzene linkage between hydrophobic and hydrophilic segments were expected to be light-responsive and their collapsed membrane is permeable under light stimuli at pH 7.4, in which only small molecules can pass through the membrane, the macromolecules cannot be released from polymersomes (Figure 8.5).

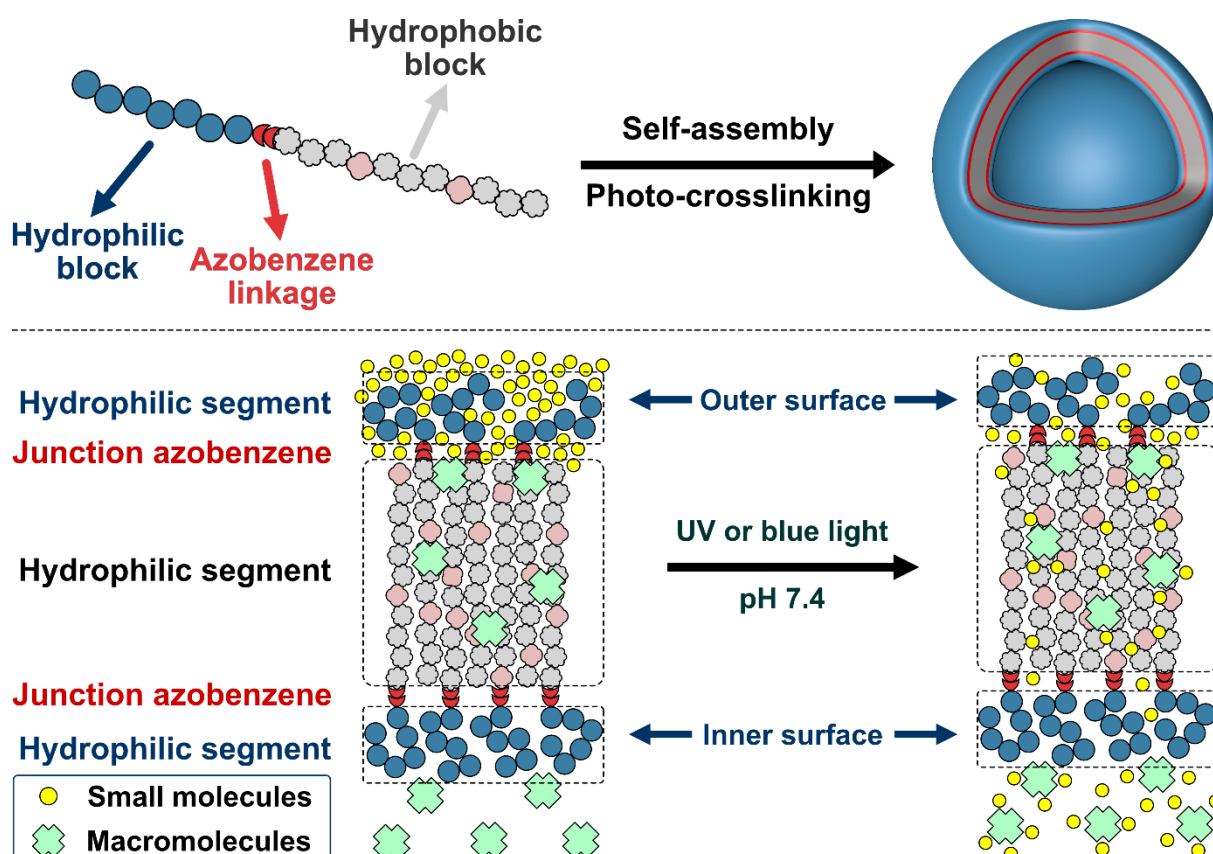


Figure 8.4 Schematic illustration of BCP structure with one-unit azobenzene and corresponding membrane structure with azobenzene as junction unit. The left bottom figure represents membrane structure, and the right bottom figure shows light-triggered transmembrane mobility of water or small molecules and retention of macromolecules.

The novel BCPs with donor-acceptor-substituted azobenzene and ether substituted azobenzene were designed and prepared. In order to achieve enough photo-crosslinking of light-responsive membrane, different photo-crosslinking time were firstly carried out under UV irradiation (320-390 nm) and the effective photo-crosslinking was proved by DLS. Short photo-crosslinking time did not lead to stable polymersomes and showed free BCP chain ($d_h = 10$ nm) and micelles ($d_h = 30$ nm), but enough photo-crosslinking time (180 s) made the self-assembly of pH-stable

vesicles ($d_h = 96$ nm for Psomes-DA-Azo and $d_h = 77$ nm for Psomes-Azo) possible. Following the pH titration confirmed that both Psomes-DA-Azo and Psomes-Azo were under collapsed state at physiological pH value (7.4) which means the membrane at pH 7.4 is compact with expected impermeable state for the no-crossing of solutes from outside to inside and vice versa. Next, the size and membrane thickness of photo-crosslinked polymersomes self-assembly by BCP-(DA-)Azo (+) were further characterized. Moreover, the size and membrane thickness of Nile red or Myo loaded polymersomes were also characterized. Besides, the cryo-TEM results also proved the successful assembly of novel polymersomes with junction azobenzene.

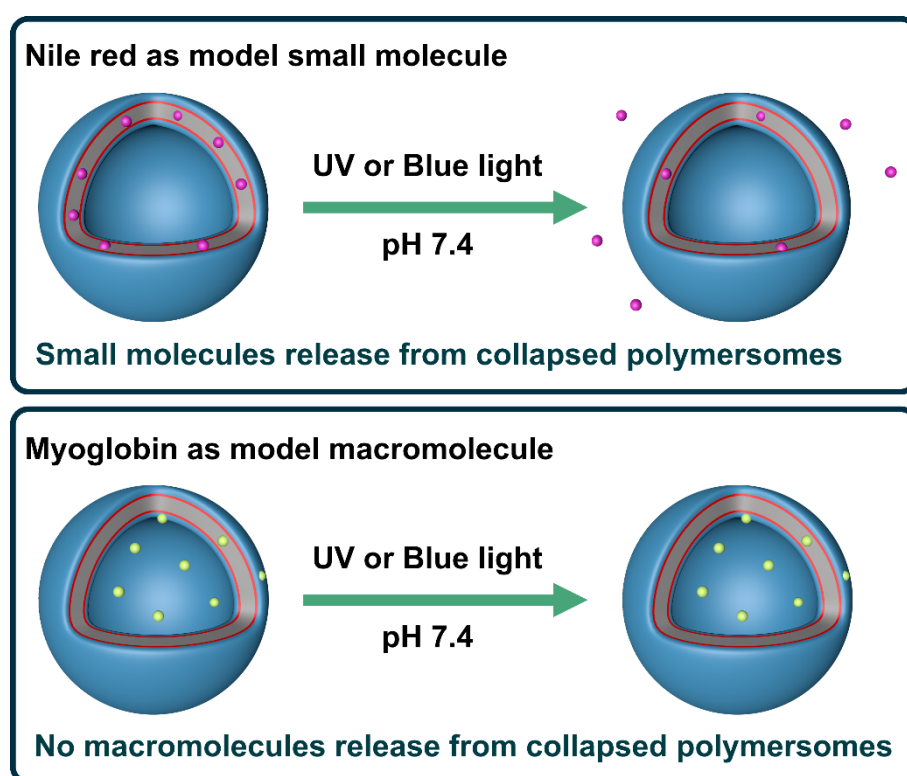


Figure 8.5 Schematic illustration of the retention of macromolecules and small molecules by the permeability of the photo-induced membrane as requirement for the establishment of complex and sophisticated artificial organelles under light stimuli.

To study the permeability of membrane at simulated physiological conditions under light stimuli, hydrophobic dye Nile red was in-situ encapsulated by Psomes-DA-Azo (+) and Psomes-Azo (+) and then the unloaded Nile red was purified by dialysis (Nile red in DMF). The dye release under irradiation by different light sources, including UV (365 nm) and blue light (400-500 nm), was detected by fluorescence spectroscopy. The results indicated the percentage of dye release from non-photo-crosslinked NR-Psomes-DA-Azo (+) under blue

light and UV light is 87.7% and 46.9%, and the percentage of dye release from non-photo-crosslinked NR-Psomes-Azo (+) under blue light and UV light is 94.1% and 63.8%, respectively. The above-mentioned results are based on ignoring effect of fluorescence quenching, although the fluorescence intensity of free Nile red after 12 min blue light irradiation and UV irradiation decreased 4.7% and 10.9%, respectively. Besides, the hydrodynamic diameter of non-photo-crosslinked NR-Psomes-DA-Azo (+) and NR-Psomes-Azo (+) was also measured and its results confirmed the successful release of Nile red from polymersomes even at physiological pH value.

In the end, enzyme-loaded and photo-crosslinked polymersomes (Myo-Psomes-DA-Azo (+) and Myo-Psomes-Azo (+)) were prepared for enzyme reaction at physiological condition (Figure 8.6). To prove controllable membrane permeability of polymersomes with junction azobenzene for enzyme reaction, the substrates Amplex Red and H₂O₂ were added to photo-crosslinked Myo-Psomes-(DA-)Azo (+) at physiological pH and the light sources were chosen to trigger the substrates diffusion and then enzyme reaction (Figure 8.6). The fluorescence of resorufin produced in the process of enzyme reaction was detected by microplate reader.

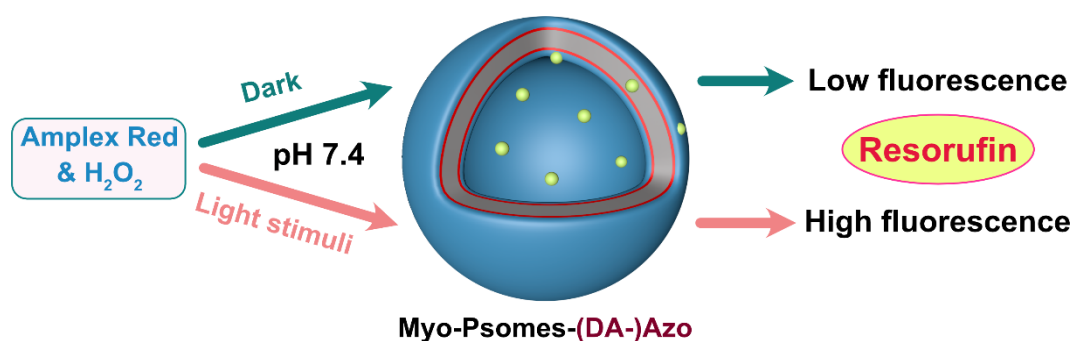


Figure 8.6 Schematic illustration of membrane permeability-driven enzyme reaction under dark and light stimuli at physiological pH value (pH 7.4) by photo-crosslinked Myo-Psomes-(DA-)Azo (+).

The results indicated that the fluorescence intensity gradually increased with the prolongation of irradiation time in a certain time range. Because of inherent loading difference of enzyme in Myo-Psomes-DA-Azo (+) and Myo-Psomes-Azo (+), the efficiency of enzyme reaction between them cannot be compared directly. Furthermore, the fluorescence intensity of Myo-Psomes-DA-Azo (+) are the same between blue light irradiation and UV irradiation in given 10 min, while the intensity of light sources is different. It means that different light sources, blue light and UV light, give a similar degree of enhanced membrane permeability to achieve the

same diffusion rate of substrates. Thereby the extent of enzyme catalysis determined by the ratio of increased fluorescence intensity and irradiation time presents the same trend. Therefore, the novel polymersomes with junction azobenzene were expected to increase the membrane permeability with temporal and marginal membrane structure changes at simulated physiological conditions (pH 7.4). This strategy provides a new idea to design artificial organelles with selective membrane permeability to perform catalysis of substrates by specific enzyme without release of encapsulated enzyme.

Considering the first work about clustered polymersomes, a promising future goal is to integrate it into artificial protocells, like proteinosome, to mimic more real biological behaviors. Meanwhile, the close spatial structure of co-clustered nanoreactors shorten the diffusion distance of substrates and intermediate product, that provides a universally applicable route to design clustered nanoreactors to carry out cascade reaction to mimic biological behaviors. Efficient clustering process and reversible clustering mechanism will be the most promising research directions. In this direction, there are two promising routes to obtain proteinosome-encapsulated bio-active clusters. The best way is to encapsulate nanoreactors into proteinosome and then the clustering process can be performed by external stimuli. For example, crosslinker could be added to proteinosome-polymersomes system to trigger clustering process, as stated in this thesis. Considering the inefficiency (long reaction time and heat) and irreversible covalent linkages of copper-free click reactions, light-induced crosslinking could be used in this system.

Firstly, BCP could be modified with a dithiolane ring as terminal group and self-assembled to polymersomes with surface dithiolane ring. Light with specific wavelength can be used to destroy the disulfide bond of dithiolane ring and could crosslink polymersomes without adding external crosslinker or other chemicals. Photo-induced cleavage of disulfide bonds in the dithiolane ring and then recombination between thiol free radicals is an efficient process that requires neither long reaction times nor heating. This crosslinking degree could be determined by UV-Vis spectroscopy. Moreover, the photo-crosslinked proteinosome-clusters system should present redox-responsive property. The addition of reducing agents, such as dithiothreitol, may disconnect the clusters in proteinosome through cleavage the disulfide bonds, whereas the addition of oxidizing agents, such as FeCl_3 , may crosslink the polymersomes in proteinosome through formation of disulfide bonds.

Except for covalent crosslinking, complex coacervation of oppositely charged polyelectrolytes in aqueous solution by a liquid-liquid phase separation could be a promising technique to achieve coacervate with encapsulated multiple nanoreactors, as substrates can freely cross the acervate to perform enzyme reaction and the pH value as most important parameters can be also kept without change in this biological mimicking process. Specifically, polymersomes and cationic polyelectrolyte diethylaminoethyl-dextran could be co-encapsulated into proteinosome. Water soluble azobenzene with multi-carboxyl groups in the trans state could be added to proteinosome-polymersomes system to trigger coacervation. Light can be used to control the configuration of azobenzene and then control the assembly or disassembly of the microdroplets inside proteinosome. Based on this research direction, the pH response range of polymersomes may need to be further optimized. Eventually, under the irradiation of UV/Vis light, the resulting proteinosome-coacervate-polymersomes system should present efficient and reversible assembly and disassembly behaviors.

For the second work, a good starting point for the future works about the system of polymersomes with trace azobenzene unit is to design enzymatic cascade reaction. Additionally, future research is also likely to be directed to the controllable delivery of hydrophobic drug in biomedical application. Firstly, through optimization the intensity and wavelength of light, Psomes-DA-Azo or Psomes-Azo with better membrane permeability could be determined. Light-triggered diffusion of substrates and intermediate product could be introduced into mixed enzyme-Psomes system to perform cascade reaction. Besides, the structure of azobenzene junction could also be designed to expand the response wavelength range from blue light to near-infrared light. Thereby, polymersomes with specific azobenzene junction could be response near-infrared light and display membrane perturbation upon near-infrared light. Furthermore, the locations of azobenzene at BCP, including azobenzene junction between hydrophilic and hydrophobic block, azobenzene as terminal group of hydrophilic block or hydrophobic block, can be optimized to obtain polymersomes that can respond to a specific wavelength and has a more efficiency on the enhancement of membrane permeability with fixed light intensity. Membrane perturbation derived on different locations of azobenzene could be determined by dye release experiment. Eventually polymersomes with trace azobenzene at specific location should present high efficiency in dye release, drug delivery and small molecules diffusion under light stimuli.

Reference

1. Discher, B. M.; Won, Y.-Y.; Ege, D. S.; Lee, J. C.-M.; Bates, F. S.; Discher, D. E.; Hammer, D. A. *Science* **1999**, 284, (5417), 1143-1146.
2. LoPresti, C.; Lomas, H.; Massignani, M.; Smart, T.; Battaglia, G. *J. Mater. Chem.* **2009**, 19, (22), 3576-3590.
3. Bermudez, H.; Brannan, A. K.; Hammer, D. A.; Bates, F. S.; Discher, D. E. *Macromolecules* **2002**, 35, (21), 8203-8208.
4. Discher, D. E.; Ahmed, F. *Annu. Rev. Biomed. Eng.* **2006**, 8, (1), 323-341.
5. Rideau, E.; Dimova, R.; Schwille, P.; Wurm, F. R.; Landfester, K. *Chem. Soc. Rev.* **2018**, 47, (23), 8572-8610.
6. Opsteen, J. A.; Brinkhuis, R. P.; Teeuwen, R. L.; Löwik, D. W.; van Hest, J. C. *Chem. Commun.* **2007**, (30), 3136-3138.
7. Rodríguez-García, R.; Mell, M.; López-Montero, I.; Netzel, J.; Hellweg, T.; Monroy, F. *Soft Matter* **2011**, 7, (4), 1532-1542.
8. Lee, J. S.; Feijen, J. *J. Controlled Release* **2012**, 161, (2), 473-483.
9. Meng, F.; Zhong, Z.; Feijen, J. *Biomacromolecules* **2009**, 10, (2), 197-209.
10. Anajafi, T.; Mallik, S. *Ther. Delivery* **2015**, 6, (4), 521-534.
11. Xu, J.-P.; Ji, J.; Chen, W.-D.; Shen, J.-C. *J. Controlled Release* **2005**, 107, (3), 502-512.
12. Kim, S.-H.; Shum, H. C.; Kim, J. W.; Cho, J.-C.; Weitz, D. A. *J. Am. Chem. Soc.* **2011**, 133, (38), 15165-15171.
13. Hu, X.; Zhang, Y.; Xie, Z.; Jing, X.; Bellotti, A.; Gu, Z. *Biomacromolecules* **2017**, 18, (3), 649-673.
14. Rifaie-Graham, O.; Ulrich, S.; Galensowske, N. F. B.; Balog, S.; Chami, M.; Rentsch, D.; Hemmer, J. R.; Read de Alaniz, J.; Boesel, L. F.; Bruns, N. *J. Am. Chem. Soc.* **2018**, 140, (25), 8027-8036.
15. Molla, M. R.; Rangadurai, P.; Antony, L.; Swaminathan, S.; de Pablo, J. J.; Thayumanavan, S. *Nat. Chem.* **2018**, 10, (6), 659-666.
16. Zhou, Y.; Chen, R.; Yang, H.; Bao, C.; Fan, J.; Wang, C.; Lin, Q.; Zhu, L. *J. Mater. Chem. B* **2020**, 8, (4), 727-735.
17. Iyisan, B.; Kluge, J. r.; Formanek, P.; Voit, B.; Appelhans, D. *Chem. Mater.* **2016**, 28, (5), 1513-1525.

18. Cabane, E.; Malinova, V.; Menon, S.; Palivan, C. G.; Meier, W. *Soft Matter* **2011**, *7*, (19), 9167-9176.
19. Wang, X.; Hu, J.; Liu, G.; Tian, J.; Wang, H.; Gong, M.; Liu, S. *J. Am. Chem. Soc.* **2015**, *137*, (48), 15262-15275.
20. Gaitzsch, J.; Appelhans, D.; Wang, L.; Battaglia, G.; Voit, B. *Angew. Chem. Int. Ed.* **2012**, *51*, (18), 4448-4451.
21. Xu, F.; Li, X.; Huang, X.; Pan, J.; Wang, Y.; Zhou, S. *Sci. Adv.* **2020**, *6*, (31), eabb8725.
22. Wang, Z.; Rutjes, F. P. J. T.; van Hest, J. C. M. *Chem. Commun.* **2014**, *50*, (93), 14550-14553.
23. Wang, L.; Liu, G.; Wang, X.; Hu, J.; Zhang, G.; Liu, S. *Macromolecules* **2015**, *48*, (19), 7262-7272.
24. Napoli, A.; Valentini, M.; Tirelli, N.; Müller, M.; Hubbell, J. A. *Nat. Mater.* **2004**, *3*, (3), 183-189.
25. Nehate, C.; Nayal, A.; Koul, V. *ACS Biomater. Sci. Eng.* **2019**, *5*, (1), 70-80.
26. de Vries, W. C.; Kudruk, S.; Grill, D.; Niehues, M.; Matos, A. L. L.; Wissing, M.; Studer, A.; Gerke, V.; Ravoo, B. J. *Adv. Sci.* **2019**, *6*, (24), 1901935.
27. Krack, M.; Hohenberg, H.; Kornowski, A.; Lindner, P.; Weller, H.; Förster, S. *J. Am. Chem. Soc.* **2008**, *130*, (23), 7315-7320.
28. Oliveira, H.; Pérez-Andrés, E.; Thevenot, J.; Sandre, O.; Berra, E.; Lecommandoux, S. *J. Controlled Release* **2013**, *169*, (3), 165-170.
29. Qin, S.; Geng, Y.; Discher, D. E.; Yang, S. *Adv. Mater.* **2006**, *18*, (21), 2905-2909.
30. Sun, Z.; Liu, G.; Hu, J.; Liu, S. *Biomacromolecules* **2018**, *19*, (6), 2071-2081.
31. Nishimura, T.; Shishi, S.; Sasaki, Y.; Akiyoshi, K. *J. Am. Chem. Soc.* **2020**, *142*, (27), 11784-11790.
32. Amstad, E.; Kim, S. H.; Weitz, D. A. *Angew. Chem. Int. Ed.* **2012**, *51*, (50), 12499-12503.
33. Liu, F.; Kozlovskaya, V.; Medipelli, S.; Xue, B.; Ahmad, F.; Saeed, M.; Cropek, D.; Kharlampieva, E. *Chem. Mater.* **2015**, *27*, (23), 7945-7956.
34. Onaca, O.; Enea, R.; Hughes, D. W.; Meier, W. *Macromol. Biosci.* **2009**, *9*, (2), 129-139.
35. Sun, J.; Mathesh, M.; Li, W.; Wilson, D. A. *ACS Nano* **2019**, *13*, (9), 10191-10200.
36. Cheng, R.; Meng, F.; Deng, C.; Klok, H.-A.; Zhong, Z. *Biomaterials* **2013**, *34*, (14), 3647-3657.

37. Jaskiewicz, K.; Larsen, A.; Schaeffel, D.; Koynov, K.; Lieberwirth, I.; Fytas, G.; Landfester, K.; Kroeger, A. *ACS Nano* **2012**, 6, (8), 7254-7262.
38. Jaskiewicz, K.; Larsen, A.; Lieberwirth, I.; Koynov, K.; Meier, W.; Fytas, G.; Kroeger, A.; Landfester, K. *Angew. Chem. Int. Ed.* **2012**, 51, (19), 4613-4617.
39. Wang, F.; Gao, J.; Xiao, J.; Du, J. *Nano Lett.* **2018**, 18, (9), 5562-5568.
40. Lomas, H.; Canton, I.; MacNeil, S.; Du, J.; Armes, S. P.; Ryan, A. J.; Lewis, A. L.; Battaglia, G. *Adv. Mater.* **2007**, 19, (23), 4238-4243.
41. Matyjaszewski, K.; Gaynor, S.; Greszta, D.; Mardare, D.; Shigemoto, T. *J. Phys. Org. Chem.* **1995**, 8, (4), 306-315.
42. Parkatzidis, K.; Wang, H. S.; Truong, N. P.; Anastasaki, A. *Chem* **2020**, 6, (7), 1575-1588.
43. Matyjaszewski, K.; Xia, J. *Chem. Rev.* **2001**, 101, (9), 2921-2990.
44. Wang, J.-S.; Matyjaszewski, K. *J. Am. Chem. Soc.* **1995**, 117, (20), 5614-5615.
45. Coessens, V.; Pintauer, T.; Matyjaszewski, K. *Prog. Polym. Sci.* **2001**, 26, (3), 337-377.
46. Tsarevsky, N. V.; Matyjaszewski, K. *Chem. Rev.* **2007**, 107, (6), 2270-2299.
47. Patten, T. E.; Matyjaszewski, K. *Adv. Mater.* **1998**, 10, (12), 901-915.
48. Matyjaszewski, K.; Nakagawa, Y.; Gaynor, S. G. *Macromol. Rapid Commun.* **1997**, 18, (12), 1057-1066.
49. Matyjaszewski, K.; Gaynor, S. G.; Müller, A. H. E. *Macromolecules* **1997**, 30, (23), 7034-7041.
50. Shipp, D. A.; Wang, J.-L.; Matyjaszewski, K. *Macromolecules* **1998**, 31, (23), 8005-8008.
51. Matyjaszewski, K.; Mu Jo, S.; Paik, H.-j.; Gaynor, S. G. *Macromolecules* **1997**, 30, (20), 6398-6400.
52. Matyjaszewski, K.; Shipp, D. A.; Wang, J.-L.; Grimaud, T.; Patten, T. E. *Macromolecules* **1998**, 31, (20), 6836-6840.
53. Matyjaszewski, K.; Wei, M.; Xia, J.; McDermott, N. E. *Macromolecules* **1997**, 30, (26), 8161-8164.
54. Plichta, A.; Li, W.; Matyjaszewski, K. *Macromolecules* **2009**, 42, (7), 2330-2332.
55. Abraham, S.; Ha, C.-S.; Kim, I. *Macromol. Rapid Commun.* **2006**, 27, (16), 1386-1392.
56. Stoffelbach, F.; Poli, R.; Richard, P. *J. Organomet. Chem.* **2002**, 663, (1), 269-276.
57. Patten, T. E.; Matyjaszewski, K. *Acc. Chem. Res.* **1999**, 32, (10), 895-903.
58. Wang, J.-S.; Matyjaszewski, K. *Macromolecules* **1995**, 28, (23), 7901-7910.

59. Tang, W.; Matyjaszewski, K. *Macromolecules* **2006**, 39, (15), 4953-4959.
60. Matyjaszewski, K.; Jo, S. M.; Paik, H.-j.; Shipp, D. A. *Macromolecules* **1999**, 32, (20), 6431-6438.
61. Golas, P. L.; Tsarevsky, N. V.; Sumerlin, B. S.; Matyjaszewski, K. *Macromolecules* **2006**, 39, (19), 6451-6457.
62. Wang, Y.; Kwak, Y.; Matyjaszewski, K. *Macromolecules* **2012**, 45, (15), 5911-5915.
63. Perrier, S. *Macromolecules* **2017**, 50, (19), 7433-7447.
64. Moad, G.; Rizzardo, E.; Thang, S. H. *Chem. - Asian J.* **2013**, 8, (8), 1634-1644.
65. Semsarilar, M.; Perrier, S. *Nat. Chem.* **2010**, 2, (10), 811-820.
66. Boyer, C.; Bulmus, V.; Davis, T. P.; Ladmiral, V.; Liu, J.; Perrier, S. *Chem. Rev.* **2009**, 109, (11), 5402-5436.
67. YK, C. J. C.; Ercole, F. *Macromolecules* **1998**, 31, 5559-5562.
68. Bleul, R.; Thiermann, R.; Maskos, M. *Macromolecules* **2015**, 48, (20), 7396-7409.
69. Israelachvili, J. N.; Mitchell, D. J.; Ninham, B. W. *J. Chem. Soc., Faraday Trans. 2* **1976**, 72, (0), 1525-1568.
70. Kita-Tokarczyk, K.; Grumelard, J.; Haefele, T.; Meier, W. *Polymer* **2005**, 46, (11), 3540-3563.
71. Thiermann, R.; Mueller, W.; Montesinos-Castellanos, A.; Metzke, D.; Löb, P.; Hessel, V.; Maskos, M. *Polymer* **2012**, 53, (11), 2205-2210.
72. Yildiz, M. E.; Prud'homme, R. K.; Robb, I.; Adamson, D. H. *Polym. Adv. Technol.* **2007**, 18, (6), 427-432.
73. Zhang, L.; Eisenberg, A. *J. Am. Chem. Soc.* **1996**, 118, (13), 3168-3181.
74. Parnell, A. J.; Tzokova, N.; Topham, P. D.; Adams, D. J.; Adams, S.; Fernyhough, C. M.; Ryan, A. J.; Jones, R. A. L. *Faraday Discuss.* **2009**, 143, (0), 29-46.
75. Robertson, J. D.; Yealland, G.; Avila-Olias, M.; Chierico, L.; Bandmann, O.; Renshaw, S. A.; Battaglia, G. *ACS Nano* **2014**, 8, (5), 4650-4661.
76. Sui, X.; Kujala, P.; Janssen, G.-J.; de Jong, E.; Zuhorn, I. S.; van Hest, J. C. M. *Polym. Chem.* **2015**, 6, (5), 691-696.
77. Kunzler, C.; Handschuh-Wang, S.; Roesener, M.; Schönherr, H. *Macromol. Biosci.* **2020**, 20, (6), 2000014.
78. Gräfe, D.; Gaitzsch, J.; Appelhans, D.; Voit, B. *Nanoscale* **2014**, 6, (18), 10752-10761.
79. Iyisan, B.; Siedel, A. C.; Gumz, H.; Yassin, M.; Kluge, J.; Gaitzsch, J.; Formanek, P.; Moreno, S.; Voit, B.; Appelhans, D. *Macromol. Rapid Commun.* **2017**, 38, (21), 1700486.

80. Gumz, H.; Lai, T. H.; Voit, B.; Appelhans, D. *Polym. Chem.* **2017**, 8, (19), 2904-2908.
81. Tong, X.; Wang, G.; Soldera, A.; Zhao, Y. *J. Phys. Chem. B* **2005**, 109, (43), 20281-20287.
82. Smith, A. E.; Xu, X.; Kirkland-York, S. E.; Savin, D. A.; McCormick, C. L. *Macromolecules* **2010**, 43, (3), 1210-1217.
83. Wolf, T.; Rheinberger, T.; Simon, J.; Wurm, F. R. *J. Am. Chem. Soc.* **2017**, 139, (32), 11064-11072.
84. Wang, X.; Moreno, S.; Boye, S.; Wang, P.; Liu, X.; Lederer, A.; Voit, B.; Appelhans, D. *Adv. Sci.* **2021**, 8, (11), 2004263.
85. Moreno, S.; Sharan, P.; Engelke, J.; Gumz, H.; Boye, S.; Oertel, U.; Wang, P.; Banerjee, S.; Klajn, R.; Voit, B.; Lederer, A.; Appelhans, D. *Small* **2020**, 16, (37), 2002135.
86. Belluati, A.; Craciun, I.; Liu, J.; Palivan, C. G. *Biomacromolecules* **2018**, 19, (10), 4023-4033.
87. Bolognesi, G.; Friddin, M. S.; Salehi-Reyhani, A.; Barlow, N. E.; Brooks, N. J.; Ces, O.; Elani, Y. *Nat. Commun.* **2018**, 9, (1), 1882.
88. Lu, A. X.; Oh, H.; Terrell, J. L.; Bentley, W. E.; Raghavan, S. R. *Chem. Sci.* **2017**, 8, (10), 6893-6903.
89. Maffei, V.; Belluati, A.; Craciun, I.; Wu, D.; Novak, S.; Schoenenberger, C.-A.; Palivan, C. G. *Chem. Sci.* **2021**, 12, (37), 12274-12285.
90. Meyer, C. E.; Liu, J.; Craciun, I.; Wu, D.; Wang, H.; Xie, M.; Fussenegger, M.; Palivan, C. G. *Small* **2020**, 16, (27), 1906492.
91. Liu, J.; Postupalenko, V.; Lorcher, S.; Wu, D.; Chami, M.; Meier, W.; Palivan, C. G. *Nano Lett.* **2016**, 16, (11), 7128-7136.
92. Jin, H.; Zheng, Y.; Liu, Y.; Cheng, H.; Zhou, Y.; Yan, D. *Angew. Chem. Int. Ed.* **2011**, 50, (44), 10352-10356.
93. Jin, H.; Liu, Y.; Zheng, Y.; Huang, W.; Zhou, Y.; Yan, D. *Langmuir* **2012**, 28, (4), 2066-2072.
94. Gobbo, P.; Patil, A. J.; Li, M.; Harniman, R.; Briscoe, W. H.; Mann, S. *Nat. Mater.* **2018**, 17, (12), 1145-1153.
95. Schneider, H.-J.; Yatsimirsky, A. K. *Chem. Soc. Rev.* **2008**, 37, (2), 263-277.
96. Zhang, M.; Xu, D.; Yan, X.; Chen, J.; Dong, S.; Zheng, B.; Huang, F. *Angew. Chem. Int. Ed.* **2012**, 124, (28), 7117-7121.
97. Li, Y.-F.; Li, Z.; Lin, Q.; Yang, Y.-W. *Nanoscale* **2020**, 12, (4), 2180-2200.

98. Kim, H. J.; Lee, M. H.; Mutihac, L.; Vicens, J.; Kim, J. S. *Chem. Soc. Rev.* **2012**, 41, (3), 1173-1190.
99. Zhang, J.; Ma, P. X. *Angew. Chem. Int. Ed.* **2009**, 121, (5), 982-986.
100. Yeung, M. C.-L.; Yam, V. W.-W. *Chem. Soc. Rev.* **2015**, 44, (13), 4192-4202.
101. Chan, A. K.-W.; Lam, W. H.; Tanaka, Y.; Wong, K. M.-C.; Yam, V. W.-W. *Proc. Natl. Acad. Sci.* **2015**, 112, (3), 690.
102. de la Rosa, V. R.; Nau, W. M.; Hoogenboom, R. *Org. Biomol. Chem.* **2015**, 13, (10), 3048-3057.
103. Szalóki, G.; Croué, V.; Carré, V.; Aubriet, F.; Alévêque, O.; Levillain, E.; Allain, M.; Aragó, J.; Ortí, E.; Goeb, S. *Angew. Chem. Int. Ed.* **2017**, 129, (51), 16490-16494.
104. Zhong, Z.; Li, X.; Zhao, Y. *J. Am. Chem. Soc.* **2011**, 133, (23), 8862-8865.
105. Yan, X.; Wang, F.; Zheng, B.; Huang, F. *Chem. Soc. Rev.* **2012**, 41, (18), 6042-6065.
106. Wankar, J.; Kotla, N. G.; Gera, S.; Rasala, S.; Pandit, A.; Rochev, Y. A. *Adv. Funct. Mater.* **2020**, 30, (44), 1909049.
107. Chen, G.; Jiang, M. *Chem. Soc. Rev.* **2011**, 40, (5), 2254-2266.
108. Chen, Y.; Liu, Y. *Chem. Soc. Rev.* **2010**, 39, (2), 495-505.
109. Liu, W.; Tagawa, M.; Xin, H. L.; Wang, T.; Emamy, H.; Li, H.; Yager, K. G.; Starr, F. W.; Tkachenko, A. V.; Gang, O. *Science* **2016**, 351, (6273), 582-586.
110. Cheng, W.; Park, N.; Walter, M. T.; Hartman, M. R.; Luo, D. *Nat. Nanotechnol.* **2008**, 3, (11), 682-690.
111. Li, Y.; Liu, Z.; Yu, G.; Jiang, W.; Mao, C. *J. Am. Chem. Soc.* **2015**, 137, (13), 4320-4323.
112. Wang, Y.; Wang, Y.; Breed, D. R.; Manoharan, V. N.; Feng, L.; Hollingsworth, A. D.; Weck, M.; Pine, D. J. *Nature* **2012**, 491, (7422), 51-55.
113. Xu, X.; Rosi, N. L.; Wang, Y.; Huo, F.; Mirkin, C. A. *J. Am. Chem. Soc.* **2006**, 128, (29), 9286-9287.
114. Xing, H.; Wang, Z.; Xu, Z.; Wong, N. Y.; Xiang, Y.; Liu, G. L.; Lu, Y. *Acs Nano* **2012**, 6, (1), 802-809.
115. Kuzyk, A.; Schreiber, R.; Fan, Z.; Pardatscher, G.; Roller, E.-M.; Högele, A.; Simmel, F. C.; Govorov, A. O.; Liedl, T. *Nature* **2012**, 483, (7389), 311-314.
116. Tian, Y.; Wang, T.; Liu, W.; Xin, H. L.; Li, H.; Ke, Y.; Shih, W. M.; Gang, O. *Nat. Nanotechnol.* **2015**, 10, (7), 637-644.

117. Zhang, T.; Neumann, A.; Lindlau, J.; Wu, Y.; Pramanik, G.; Naydenov, B.; Jelezko, F.; Schüder, F.; Huber, S.; Huber, M.; Stehr, F.; Högele, A.; Weil, T.; Liedl, T. *J. Am. Chem. Soc.* **2015**, 137, (31), 9776-9779.
118. Aldaye, F. A.; Palmer, A. L.; Sleiman, H. F. *Science* **2008**, 321, (5897), 1795-1799.
119. Zhang, Y.; Lu, F.; Yager, K. G.; Van Der Lelie, D.; Gang, O. *Nat. Nanotechnol.* **2013**, 8, (11), 865-872.
120. Agard, N. J.; Prescher, J. A.; Bertozzi, C. R. *J. Am. Chem. Soc.* **2004**, 126, (46), 15046-15047.
121. Kolb, H. C.; Finn, M. G.; Sharpless, K. B. *Angew. Chem. Int. Ed.* **2001**, 40, (11), 2004-2021.
122. Li, X.; Yang, W.; Zou, Y.; Meng, F.; Deng, C.; Zhong, Z. *J. Controlled Release* **2015**, 220, 704-714.
123. Moreno, S.; Boye, S.; Lederer, A.; Falanga, A.; Galdiero, S.; Lecommandoux, S.; Voit, B.; Appelhans, D. *Biomacromolecules* **2020**, 21, (12), 5162-5172.
124. Leong, J.; Teo, J. Y.; Aakalu, V. K.; Yang, Y. Y.; Kong, H. *Adv. Healthcare Mater.* **2018**, 7, (8), 1701276.
125. Popescu, M.-T.; Tsitsilianis, C. *ACS Macro Lett.* **2013**, 2, (3), 222-225.
126. Gillies, E. R.; Jonsson, T. B.; Fréchet, J. M. J. *J. Am. Chem. Soc.* **2004**, 126, (38), 11936-11943.
127. Gillies, E. R.; Fréchet, J. M. J. *Bioconjugate Chem.* **2005**, 16, (2), 361-368.
128. Gannimani, R.; Walvekar, P.; Naidu, V. R.; Aminabhavi, T. M.; Govender, T. *J. Controlled Release* **2020**, 328, 736-761.
129. Yassin, M. A.; Appelhans, D.; Mendes, R. G.; Rümmele, M. H.; Voit, B. *Chem. - Eur. J.* **2012**, 18, (39), 12227-12231.
130. Thibault, R. J.; Uzun, O.; Hong, R.; Rotello, V. M. *Adv. Mater.* **2006**, 18, (16), 2179-2183.
131. Wang, X.; Yao, C.; Zhang, G.; Liu, S. *Nat. Commun.* **2020**, 11, (1), 1524.
132. Wang, X.; Liu, G.; Hu, J.; Zhang, G.; Liu, S. *Angew. Chem. Int. Ed.* **2014**, 53, (12), 3138-3142.
133. Lomas, H.; Du, J.; Canton, I.; Madsen, J.; Warren, N.; Armes, S. P.; Lewis, A. L.; Battaglia, G. *Macromol. Biosci.* **2010**, 10, (5), 513-530.
134. Li, Y.; Du, J.; Armes, S. P. *Macromol. Rapid Commun.* **2009**, 30, (6), 464-468.

135. Helmy, S.; Leibfarth, F. A.; Oh, S.; Poelma, J. E.; Hawker, C. J.; Read de Alaniz, J. J. *Am. Chem. Soc.* **2014**, 136, (23), 8169-8172.
136. Klajn, R.; Bishop, K. J.; Grzybowski, B. A. *Proc. Natl. Acad. Sci.* **2007**, 104, (25), 10305-10309.
137. Zhang, F.; Wang, L.-P.; Brauner, M.; Liewald, J. F.; Kay, K.; Watzke, N.; Wood, P. G.; Bamberg, E.; Nagel, G.; Gottschalk, A. *Nature* **2007**, 446, (7136), 633-639.
138. Tsai, Y.-H.; Essig, S.; James, J. R.; Lang, K.; Chin, J. W. *Nat. Chem.* **2015**, 7, (7), 554-561.
139. Schroeder, A.; Goldberg, M. S.; Kastrup, C.; Wang, Y.; Jiang, S.; Joseph, B. J.; Levins, C. G.; Kannan, S. T.; Langer, R.; Anderson, D. G. *Nano Lett.* **2012**, 12, (6), 2685-2689.
140. Pieroni, O.; Fissi, A.; Angelini, N.; Lenci, F. *Acc. Chem. Res.* **2001**, 34, (1), 9-17.
141. Russew, M. M.; Hecht, S. *Adv. Mater.* **2010**, 22, (31), 3348-3360.
142. Baroncini, M.; d'Agostino, S.; Bergamini, G.; Ceroni, P.; Comotti, A.; Sozzani, P.; Bassanetti, I.; Grepioni, F.; Hernandez, T. M.; Silvi, S. *Nat. Chem.* **2015**, 7, (8), 634-640.
143. Klajn, R. *Chem. Soc. Rev.* **2014**, 43, (1), 148-184.
144. Pardo, R.; Zayat, M.; Levy, D. *Chem. Soc. Rev.* **2011**, 40, (2), 672-687.
145. Stoll, R. S.; Hecht, S. *Angew. Chem. Int. Ed.* **2010**, 49, (30), 5054-5075.
146. Qu, D.-H.; Wang, Q.-C.; Zhang, Q.-W.; Ma, X.; Tian, H. *Chem. Rev.* **2015**, 115, (15), 7543-7588.
147. Szymanski, W.; Beierle, J. M.; Kistemaker, H. A.; Velema, W. A.; Feringa, B. L. *Chem. Rev.* **2013**, 113, (8), 6114-6178.
148. Beharry, A. A.; Woolley, G. A. *Chem. Soc. Rev.* **2011**, 40, (8), 4422-4437.
149. Cheng, G.; Pérez-Mercader, J. *Chem. Mater.* **2019**, 31, (15), 5691-5698.
150. Senthilkumar, T.; Zhou, L.; Gu, Q.; Liu, L.; Lv, F.; Wang, S. *Angew. Chem. Int. Ed.* **2018**, 57, (40), 13114-13119.
151. Zhong, D.; Cao, Z.; Wu, B.; Zhang, Q.; Wang, G. *Sens. Actuators, B* **2018**, 254, 385-392.
152. Wu, B.; Xue, T.; Wang, W.; Li, S.; Shen, J.; He, Y. *J. Mater. Chem. C* **2018**, 6, (31), 8538-8545.
153. Jia, S.; Tan, A.; Hawley, A.; Graham, B.; Boyd, B. J. *J. Colloid Interface Sci.* **2019**, 548, 151-159.
154. Lerch, M. M.; Szymański, W.; Feringa, B. L. *Chem. Soc. Rev.* **2018**, 47, (6), 1910-1937.

155. Noirbent, G.; Xu, Y.; Bonardi, A.-H.; Duval, S.; Gimes, D.; Lalevée, J.; Dumur, F. *Molecules* **2020**, *25*, (10), 2317.
156. Kiser, P. D.; Golczak, M.; Palczewski, K. *Chem. Rev.* **2014**, *114*, (1), 194-232.
157. Helmy, S.; Oh, S.; Leibfarth, F. A.; Hawker, C. J.; Read de Alaniz, J. J. *Org. Chem* **2014**, *79*, (23), 11316-11329.
158. Ali, A. A.; Kharbash, R.; Kim, Y. *Anal. Chim. Acta* **2020**, *1110*, 199-223.
159. Zhang, H.; Wang, C.; Jiang, T.; Guo, H.; Wang, G.; Cai, X.; Yang, L.; Zhang, Y.; Yu, H.; Wang, H. *Anal. Chem.* **2015**, *87*, (10), 5216-5222.
160. Irie, M.; Fukaminato, T.; Sasaki, T.; Tamai, N.; Kawai, T. *Nature* **2002**, *420*, (6917), 759-760.
161. Xie, X.; Crespo, G. A.; Mistlberger, G.; Bakker, E. *Nat. Chem.* **2014**, *6*, (3), 202-207.
162. Davis, D. A.; Hamilton, A.; Yang, J.; Cremar, L. D.; Van Gough, D.; Potisek, S. L.; Ong, M. T.; Braun, P. V.; Martínez, T. J.; White, S. R. *Nature* **2009**, *459*, (7243), 68-72.
163. Tong, R.; Chiang, H. H.; Kohane, D. S. *Proc. Natl. Acad. Sci.* **2013**, *110*, (47), 19048-19053.
164. Sheng, L.; Li, M.; Zhu, S.; Li, H.; Xi, G.; Li, Y.-G.; Wang, Y.; Li, Q.; Liang, S.; Zhong, K. *Nat. Commun.* **2014**, *5*, (1), 1-8.
165. Yan, J.; Zhao, L.-X.; Li, C.; Hu, Z.; Zhang, G.-F.; Chen, Z.-Q.; Chen, T.; Huang, Z.-L.; Zhu, J.; Zhu, M.-Q. *J. Am. Chem. Soc.* **2015**, *137*, (7), 2436-2439.
166. Natansohn, A.; Rochon, P. *Adv. Mater.* **1999**, *11*, (16), 1387-1391.
167. Yamada, M.; Kondo, M.; Mamiya, J. i.; Yu, Y.; Kinoshita, M.; Barrett, C. J.; Ikeda, T. *Angew. Chem. Int. Ed.* **2008**, *120*, (27), 5064-5066.
168. Swallen, S. F.; Kearns, K. L.; Mapes, M. K.; Kim, Y. S.; McMahon, R. J.; Ediger, M. D.; Wu, T.; Yu, L.; Satija, S. *Science* **2007**, *315*, (5810), 353-356.
169. Singh, S.; Ediger, M. D.; De Pablo, J. J. *Nat. Mater.* **2013**, *12*, (2), 139-144.
170. Dalal, S. S.; Walters, D. M.; Lyubimov, I.; de Pablo, J. J.; Ediger, M. *Proc. Natl. Acad. Sci.* **2015**, *112*, (14), 4227-4232.
171. Martino, C.; Kim, S. H.; Horsfall, L.; Abbaspourrad, A.; Rosser, S. J.; Cooper, J.; Weitz, D. A. *Angew. Chem. Int. Ed.* **2012**, *124*, (26), 6522-6526.
172. Miller, A. J.; Pearce, A. K.; Foster, J. C.; O'Reilly, R. K. *ACS Cent. Sci.* **2021**, *7*, (1), 30-38.
173. Jain, A.; Liu, R.; Xiang, Y. K.; Ha, T. *Nat. Protoc.* **2012**, *7*, (3), 445-452.

174. Kannan, B.; Castelino, K.; Chen, F. F.; Majumdar, A. *Biosens. Bioelectron.* **2006**, 21, (10), 1960-1967.
175. Karsenti, E. *Nat. Rev. Mol. Cell Biol.* **2008**, 9, (3), 255-262.
176. Mantri, S.; Sapra, K. T. *Biochem. Soc. Trans.* **2013**, 41, (5), 1159-1165.
177. Codelli, J. A.; Baskin, J. M.; Agard, N. J.; Bertozzi, C. R. *J. Am. Chem. Soc.* **2008**, 130, (34), 11486-11493.
178. Ning, X.; Guo, J.; Wolfert, M. A.; Boons, G.-J. *Angew. Chem. Int. Ed.* **2008**, 47, (12), 2253-2255.
179. Leunissen, E. H. P.; Meuleners, M. H. L.; Verkade, J. M. M.; Dommerholt, J.; Hoenderop, J. G. J.; van Delft, F. L. *ChemBioChem* **2014**, 15, (10), 1446-1451.
180. Gordon, C. G.; Mackey, J. L.; Jewett, J. C.; Sletten, E. M.; Houk, K. N.; Bertozzi, C. R. *J. Am. Chem. Soc.* **2012**, 134, (22), 9199-9208.
181. Ma, Z.; LeBard, D. N.; Loverde, S. M.; Sharp, K. A.; Klein, M. L.; Discher, D. E.; Finkel, T. H. *PLoS One* **2014**, 9, (11), e112292.
182. Gumz, H.; Boye, S.; Iyisan, B.; Krönert, V.; Formanek, P.; Voit, B.; Lederer, A.; Appelhans, D. *Adv. Sci.* **2019**, 6, (7), 1801299.
183. Gelebart, A. H.; Jan Mulder, D.; Varga, M.; Konya, A.; Vantomme, G.; Meijer, E. W.; Selinger, R. L. B.; Broer, D. J. *Nature* **2017**, 546, (7660), 632-636.
184. Bahrenburg, J.; Röttger, K.; Siewertsen, R.; Renth, F.; Temps, F. *Photochem. Photobiol. Sci.* **2012**, 11, (7), 1210-1219.
185. Bandara, H. M. D.; Burdette, S. C. *Chem. Soc. Rev.* **2012**, 41, (5), 1809-1825.
186. Greenspan, P.; Mayer, E. P.; Fowler, S. D. *J Cell Biol* **1985**, 100, (3), 965-973.
187. Plenderleith, R.; Swift, T.; Rimmer, S. *RSC Adv.* **2014**, 4, (92), 50932-50937.

List of Figures

Figure 1.1 The mechanism of the transition metal catalyzed ATRP. The active radicals form at a rate constant of activation (k_{act}), subsequently propagate with a rate constant (k_p) and reversibly deactivate (k_{deact}), but also terminate (k_t). ⁴³ (Reproduced with permission from ref. 43. Copyright (2001) American Chemical Society).....	3
Figure 1.2 General mechanism of the RAFT polymerization. ⁶³ (Reproduced with permission from ref. 63. Copyright (2017) American Chemical Society).	4
Figure 1.3 The critical packing parameter P_c and the resulting morphologies of self-assembled amphiphilic BCPs. v : volume of the hydrophobic chain; a_0 : area occupied by the hydrophilic headgroup; l_c : length of the molecule. ⁶⁸ (Reproduced with permission from ref. 68. Copyright (2015) American Chemical Society).....	5
Figure 1.4 (a) Reversible aggregation of polymeric vesicles self-assembly by amphiphilic hyperbranched multiarm copolymers. (b) Light-responsive host-guest recognition between β -cyclodextrin and azobenzene that triggers the aggregation. ⁹² (Reproduced with permission from ref. 92. Copyright (2011) John Wiley and Sons)	10
Figure 1.5 Self-organization of complementary ssDNA-polymersomes. (a) Schematic representation of distinct spatial topology resulting from mixing differently sized complementary ssDNA-polymersomes. TEM and CLSM micrographs of chain-like (b, c) and satellite-like polymersome clusters (d, e). The scale bar for TEM micrographs is 1000 and 200 nm in the inset; in CLSM micrographs it is 2000 and 1000 nm in the inset. ⁹¹ (Reproduced with permission from ref. 91. Copyright (2016) American Chemical Society).....	12
Figure 1.6 Concepts of a GOx-LPO cascade between two clustered catalytic nanocompartments, tethered via complementary single stranded DNA, in order to facilitate the diffusion of H_2O_2 and thus improve the overall reaction efficiency. Similarly, an AMG-GOx-LPO cascade achieves an improved diffusion of the glucose derived from amylose, and the enzyme on the surface allows the access to bulky substrates that would otherwise be out of reach for encapsulated enzymes. ⁸⁹ (Reproduced with permission from ref. 89. Copyright (2021) Royal Society of Chemistry).	13
Figure 1.7 Schematic overview of SPAAC reaction. ¹²⁰ (Reproduced with permission from ref. 120. Copyright (2004) American Chemical Society).....	13
Figure 1.8 Programmed assembly of proteinosomes into synthetic prototissue spheroids. (a) Synthesis pathway for the preparation of amphiphilic thermoresponsive protein-polymer	

nanoconjugates with bio-orthogonal functionalities. (b) Molecular structures of the activated copolymer poly(N-isopropylacrylamide-co-methacrylic acid) (PNIPAM-co-MAA) and bio-orthogonal prosthetic groups (azide-amine and bicyclo[6.1.0]nonyne-amine). (c) Scheme showing experimental procedure for the preparation of proteinosome-based prototissue spheroids.⁹⁴ (Reproduced with permission from ref. 94. Copyright (2018) Springer Nature). 15

Figure 1.9 Schematic representation of pH-responsive polymersomes self-assembled from PEO-b-PTTAMA amphiphilic diblock copolymers containing acid-cleavable cyclic acetal side linkages in the hydrophobic block.²³ (Reproduced with permission from ref. 23. Copyright (2015) American Chemical Society)..... 17

Figure 1.10 (a) Chemical structure of amphiphilic block copolymers with an ethyl (C2) and butyl (C4) spacer in the cross-linking units DMIEMA and DMIBMA, which are used in 10 or 20 mol%, respectively (resulting in C2-10, C2-20, C4-10, and C4-20 nomenclature) and (b) the crosslinking reaction occurring within the membrane.²⁰ (Reproduced with permission from ref. 20. Copyright (2012) John Wiley and Sons)..... 18

Figure 1.11 General structures of the open/closed forms of the donor-acceptor Stenhouse adducts (DASAs) based on Meldrum's acid.¹⁵⁵ (Reproduced with permission from ref. 155. Copyright (2020) MDPI)..... 19

Figure 1.12 DASA-functionalized visible light-responsive nanoreactors. Two sets of enzyme-loaded polymersomes with different DASAs respond to irradiation with lower wavelength (green) or higher wavelength (red) light. The light stimuli switch the DASAs in the hydrophobic leaflet of the polymersome membrane, resulting in an increased permeability of the polymersome membrane and the activation of the enzyme nanoreactor. The polymersomes self-revert to their impermeable state in the dark at room temperature.¹⁴ (Reproduced with permission from ref. 14. Copyright (2018) American Chemical Society)..... 20

Figure 1.13 Schematic illustration of photoswitch between spiropyran and merocyanine.¹⁵⁸ (Reproduced with permission from ref. 158. Copyright (2020) Elsevier). 21

Figure 1.14 Photochromic polymersomes exhibiting photoswitchable and reversible bilayer permeability. Spiropyran-based polymersomes (SP Polymersomes) and merocyanine-based polymersomes (MC Polymersomes).¹⁹ (Reproduced with permission from ref. 19. Copyright (2015) American Chemical Society)..... 22

Figure 1.15 The photo-isomerization of azobenzene. 23

Figure 1.16 (a) Chemical structure and self-assembly of block copolymer. The cartoon representation of the vesicle with magnified region representing bilayer assembly. (b)

Schematic representation of hydrophilic and hydrophobic guest encapsulation and release from the polymersomes upon the UV ($\lambda = 365$ nm) or blue light ($\lambda = 450$ nm) irradiation. Stars indicate hydrophilic guests and squares hydrophobic guests.¹⁵ (Reproduced with permission from ref. 15. Copyright (2018) Springer Nature)..... 24

Figure 2.1 The aims of this work: i) Fabrication of photo-crosslinked pH-responsive and clustered polymersomes through copper-free click chemistry; Study of enzyme activity of co-clustered enzyme-loaded polymersomes at different pH values to enhance the enzymatic cascade reaction; ii) Construction of two novel light-responsive polymersomes with one donor-acceptor substituted azobenzene unit or one ether substituted azobenzene unit as junction between hydrophilic and hydrophobic segments of BCP; Investigation of enzyme reaction of enzyme-loaded polymersomes at physiological conditions (pH 7.4). 26

Figure 6.1 Schematic illustration shows the assembly mechanism and the application in enzymatic cascade reaction of pH-responsive clustered Enzyme-Psomes-N₃. The top inset displays the clustering mechanism based on divalent click and bridging reaction and the termination reaction mechanism based on non-reactive short PEG end-capping. The right bottom inset shows the mechanism of enzymatic cascade reaction at the swollen state based on co-clustered Myo/GOx-Psomes-N₃. 69

Figure 6.2 ATRP polymerization to synthesize BCPs with methoxy or azido end groups. ... 70

Figure 6.3 ¹H NMR spectra of BCP-OCH₃, BCP-N₃-1, and BCP-N₃-2. 71

Figure 6.4 Hydrodynamic size of Psomes-N₃ assembled with 30% (a), 40% (b) and 100% (c) BCP-N₃ with cyclic pH switches between pH 8 and pH 5. Conditions: 0.25 mg/mL Psomes in 10 mM PBS buffer; measured by DLS. 73

Figure 6.5 Cryo-TEM images of Psomes-N₃ assembled with 30% (a), 40% (b) and 100% (c) BCP-N₃ at pH 8 and diameter distribution histograms of Psomes-N₃ assembled with 30% (d), 40% (e) and 100% (f) BCP-N₃. The average diameter and membrane thickness of polymersomes were calculated by analyzing no less than 118 particles and 13 particles, respectively..... 74

Figure 6.6 (a) Synthetic route of bisPEG-BCN crosslinker. (b) Click reaction in the clustering process of Psomes-X%N₃, including monovalent click, divalent click and crosslinking reaction. 75

Figure 6.7 (a) Size distribution of the Psomes-30%N₃ mixed without and with 5 eq. bisBCN-PEG_{1k} crosslinker stirred 2 days at different temperatures; initial addition of excess crosslinker aims to speed up the clustering process. (b) The possible mechanism triggered by temperature

changes for clustered Psomes-N₃ formation shows that the higher temperature (50 or 60 °C) could hinder the click reaction between Psomes-N₃ due to self-sacrificing event..... 76

Figure 6.8 Size distribution of the Psomes-X%N₃ mixed with 1 eq. bisBCN-PEG_{1k} (a) and bisBCN-PEG_{2k} (b) crosslinker at 40 °C for 2 days. (c) The possible mechanism caused by the proportion of BCP-N₃ in Psomes-N₃ for clustered Psomes-N₃ formation indicates that increasing the proportion of BCP-N₃ in the final Psomes-N₃ with 100 % BCP-N₃ can drastically boost the clustering process..... 78

Figure 6.9 Size distribution of the Psomes-10%N₃ mixed with 1 eq. crosslinker bisBCN-PEG_{1k} (a) and bisBCN-PEG_{2k} (b) after different reaction times. Size distribution of the Psomes-30%N₃ mixed with 1 eq. crosslinker bisBCN-PEG_{1k} (c) and bisBCN-PEG_{2k} (d) at 40 °C after different reaction times. 79

Figure 6.10 Size distribution of the Psomes-30%N₃ mixed with different ratios of crosslinker bisBCN-PEG_{1k} (a) at 40 °C for 2 days as well as possible mechanisms based on excess crosslinker (b) and defined Psomes: crosslinker ratio (c) for clustered Psomes-N₃ formation. 81

Figure 6.11 Size distribution of the Psomes-X%N₃ with 30% (a), 40% (b) and 100% (c) BCP-N₃ mixed with 1 eq. bisBCN-PEG crosslinker with different chain lengths at 40 °C for 4 days. 82

Figure 6.12 Size distribution of the Psomes-N₃ at different concentrations (from 0.1 to 1 mg/mL) mixed with 1 eq. bisBCN-PEG_{1k} crosslinker at 40 °C for 1 day. (Solvent of 1 mg/mL Psomes-N₃ is 10 mM NaCl solution, pH = 7.4; solvent of both 0.1 and 0.5 mg/mL Psomes-N₃ is PBS buffer without NaCl, 10 mM, pH = 7.4)..... 83

Figure 6.13 The influence of different parameters on the clustering reaction. Blue indicates a positive effect and red indicates a negative effect on the clustering reaction. 86

Figure 6.14 Schematic illustration shows the optimal process for the formation of pH-responsive clustered Psomes-N₃..... 86

Figure 6.15 Schematic illustration shows the three different protocols for purification of clustered Psomes-N₃..... 87

Figure 6.16 (a) Hydrodynamic size of Psomes-N₃ with cyclic pH switches between pH 8 and pH 5, obtained from the supernatant (clustered Psomes-N₃ after one centrifugation at protocol 3; Figure 6.15). Conditions: 10 mM PBS buffer. (b) Hypothetical structure of unclustered polymersomes monovalent or divalent click with crosslinker (Psoemes-N₃-BCN-PEG_{1k}-BCN). 88

Figure 6.17 Fluorescence intensity of clustered BSA-Cy5-Psomes-N₃ solution before and after purification by Protocol 1 (a), Protocol 2 (b) and Protocol 3 (c). Percentage of remaining (clustered) BSA-Cy5-Psomes-N₃ in the residue solution (d) after different times centrifugation, compared with the original solution before centrifugation and calculated by fluorescence intensity. The inset is an enlarged view of the plots. Conditions: 0.5 mg/mL BSA-Cy5-Psomes-N₃ for clustering process in 1 mM PBS buffer (pH 8.0). 89

Figure 6.18 Schematic illustration shows the process for the formation and purification of Psomes-N₃ with in-situ encapsulated enzymes, Myo and GOx (Myo-Psomes-N₃ and GOx-Psomes-N₃). 90

Figure 6.19 Fluorescence intensity of Myo-Psomes-N₃ (a) and GOx-Psomes-N₃ (b) before and after HFF purification. The insets are enlarged views of the fluorescence spectra after HFF purification. 90

Figure 6.20 Hydrodynamic size of Empty-Psomes-N₃ (a), Myo-Psomes-N₃ (b) and GOx-Psomes-N₃ (c) after HFF purification followed by cyclic pH switches between pH 8 and pH 5. (d) Hydrodynamic size of Empty-Psomes-N₃, Myo-Psomes-N₃ and GOx-Psomes-N₃ through pH titration from pH 8 to pH 5. Condition: 0.25 mg/mL Psomes-N₃ in 10 mM PBS buffer. . 91

Figure 6.21 Cryo-TEM (a-c), size histograms (d-f) and membrane thickness histograms (g-i) of Empty-Psomes-N₃ (left), Myo-Psomes-N₃ (center) and GOx-Psomes-N₃ (right) after HFF purification. Condition: 1 mg/mL Psomes-N₃ in 1 mM PBS buffer (pH 7.4) for cryo-TEM. . 92

Figure 6.22 Conformation properties of polymersomes studied by AF4-LS analysis at pH 7.4. Conditions: 0.5 mg/mL polymersomes (+ 0.1 mg/mL enzyme) for preparing Empty-Psomes-N₃ and Enzyme-Psomes-N₃. Dependence of the radius of gyration (R_g) (a) and apparent density (b) on the molar mass calculated for polymersomes: Empty-Psomes-N₃, Myo-Psomes-N₃, GOx-Psomes-N₃ after HFF purification. 94

Figure 6.23 AF4 fractograms with light scattering detector signals (lines) and ρ parameter (R_g/R_h, circles) for Empty-Psomes-N₃ (a&b), Myo-Psomes-N₃ (a), and GOx-Psomes-N₃ (b) before and after HFF purification. Conditions: 1 mg/mL Psomes-N₃ in 1 mM PBS buffer (pH 7.4). 94

Figure 6.24 Cryo-TEM images (a-d) and TEM images (e-h) of clustered Empty-Psomes-N₃ at pH 8.0 before and after purification by different protocols. (a&e): Without purification. (b&f): Purified by Protocol 1. (c&g): Purified by Protocol 2. (d&h): Purified by Protocol 3. (e&g): Stained by PTA (2% w/w) water solution. (h): Prepared by freeze-drying method. 95

Figure 6.25 Cryo-TEM histograms of clustered Empty-Psomes-N ₃ before (a) and after purification by Protocol 1 (b), Protocol 2 (c) and Protocol 3 (d).	96
Figure 6.26 TEM Histograms of clustered Empty-Psomes-N ₃ before (a) and after purification by Protocol 1 (b), Protocol 2 (c) and Protocol 3 (d).....	98
Figure 6.27 TEM images of in-situ freeze-dried clustered Psomes-N ₃ at pH 8.0 (a) without and (b) with acidification process after purification. Co-clustered Myo/GOx-Psomes-N ₃ at pH 8.0 (c) without and (d) with acidification process after purification by Protocol 3. The inset shows the magnified polymersome in the cluster (yellow box) and isolated polymersome (red box).	99
Figure 6.28 Schematic illustration (a) and TEM Histograms (b) of co-clustered Myo/GOx-Psomes-N ₃ at pH 8.0 after purification by Protocol 3 in Figure 6.15.	100
Figure 6.29 In-situ AFM images of clustered Psomes-N ₃ purified by Protocol 1 (a-b) and Protocol 2 (c-d) at pH 8.0 (a&c) and pH 6.0 (b&d).	101
Figure 6.30 In-situ AFM images of clustered Empty-Psomes-N ₃ (a-c) and co-clustered Myo/GOx-Psomes-N ₃ (d-f) purified by Protocol 3 at pH 8.0 (a&d), pH 7.0 (b&e) and pH 6.5 (c&f).	102
Figure 6.31 Depth histograms of Psomes-N ₃ layer from in-situ AFM images: (a-c) Clustered Psomes-N ₃ purified by (a) Protocol 1 at pH 6.0 (Figure 6.29b), (b) Protocol 2 at pH 6.0 (Figure 6.29d) and (c) Protocol 3 at pH 6.5 (Figure 6.30c); (d) co-clustered Myo/GOx-Psomes-N ₃ purified by Protocol 3 at pH 6.5 (Figure 6.30f).	103
Figure 6.32 CLSM images and size histograms of co-clustered Myo-RhB/GOx-Cy5-Psomes-N ₃ after purification by Protocol 3 at different pH values.....	104
Figure 6.33 (a) Number distribution of clustered Psomes-N ₃ before and after 4 times centrifugation as well as redispersed by stirring and vortex, respectively. (b) Number distribution of co-clustered Myo/GOx-Psomes-N ₃ purified by Protocol 3 at different pH values. (Particle size is based on an ideal sphere.)	104
Figure 6.34 Histogram of clustered Psomes-N ₃ at pH 7.4 before (a) and at pH 8.0 after one centrifugation redispersed by stirring (b) or vortex (c) as well as after 4 times centrifugation redispersed by stirring (d) or vortex (e), and at pH 6.5 after 4 times centrifugation redispersed by vortex (f).....	105
Figure 6.35 Histogram of co-clustered Myo/GOx-Psomes-N ₃ at pH 8.0 (a&b), pH 7.0 (c&d) and pH 6.5 (e&f) purified by Protocol 3. Classification: 0.5-1 μm (a, c, e); 1-5 μm (b, d, f).	107

Figure 6.36 Schematic illustration of enzyme reaction of (a) Myo-Psomes-N₃ and (b) GOx-Psomes-N₃. (c) Fluorescence intensity at 585 nm of Myo-Psomes-N₃, Myo-Psomes-N₃ after heating 2 days at 40 °C and clustered Myo-Psomes-N₃ after adding Amplex Red and H₂O₂ at pH 6.5 with different times, and then adjusting the pH value back to pH 7.5 through 0.1 M PBS buffer. (d) Fluorescence intensity at 585 nm of GOx-Psomes-N₃, GOx-Psomes-N₃ after heating 2 days at 40 °C and clustered GOx-Psomes-N₃ after adding Amplex Red, glucose and Myo at pH 5.5 with different times, and then adjusting the pH value back to pH 7.5 through 0.1 M PBS buffer. 109

Figure 6.37 Schematic illustration of enzymatic cascade reaction in mixed or co-clustered Myo/GOx-Psomes-N₃. 110

Figure 6.38 Fluorescence intensity at 585 nm of mixed Myo/GOx-Psomes-N₃ at RT and 40 °C for 2 days after adding Amplex Red and glucose at different pH 6.5 (a), pH 7.0 (b), pH 7.5 (c) and pH 8.0 (d) with different reaction times, and then adjusting the pH value back to pH 7.5. Condition: 0.15 mg/mL Myo-Psomes-N₃ and 0.15 mg/mL GOx-Psomes-N₃. 111

Figure 6.39 Fluorescence intensity at 585 nm of mixed Myo/GOx-Psomes-N₃ after heating 2 days at 40 °C and co-clustered Myo/GOx-Psomes-N₃ after adding Amplex Red and glucose at different pH 6.5 (c), pH 7.0 (d), pH 7.5 (e) and pH 8.0 (f) with different times, and then adjusting the pH value back to pH 7.5. 112

Figure 6.40 Schematic illustration of intermediates diffusion mechanism of mixed Myo/GOx-Psomes-N₃ and co-clustered Myo/GOx-Psomes-N₃. 113

Figure 7.1 Schematic illustration shows the bilayer structure of polymersomes with azobenzene linkage between hydrophilic and hydrophobic segments as well as light-initiated membrane permeability for enzyme reaction at physiological pH value (pH 7.4). Light source that induces membrane perturbation depends on absorption wavelength, rather than the light from non-absorption zone or thermal-induced relaxation. 115

Figure 7.2 ATRP polymerization of monomers for synthesizing BCPs with donor-acceptor-substituted azobenzene linkage and ether substituted azobenzene linkage. (+) indicates copolymerization of pH-responsive monomer DEAEMA and photo-crosslinker DMIBMA, and (-) indicates only polymerization of pH-responsive monomer DEAEMA. 118

Figure 7.3 ¹H NMR spectra of macroinitiator and BCPs with donor-acceptor-substituted azobenzene linkage and ether substituted azobenzene linkage. The asterisk in the magnified view represents solvent peak of chloroform. 120

Figure 7.4 DLS study on size distribution of Psomes-DA-Azo (+) (a) and Psomes-Azo (+) (b) as well as corresponding cyclic pH-switches of Psomes-DA-Azo (+) (c) and Psomes-Azo (+) (d) after different time of photo-crosslinking upon UV irradiation (320-390 nm). 122

Figure 7.5 DLS study on pH titration of Psomes-DA-Azo (+) and Psomes-Azo (+). Conditions: 0.5 mg/mL Psomes-DA-Azo (+) or 0.5 mg/mL Psomes-Azo (+) in 1 mM PBS buffer. 123

Figure 7.6 Cryo-TEM (a&d), size histograms (b&e) and membrane thickness histograms (c&f) of Psomes-DA-Azo (+) (a-c) and Psomes-Azo (+) (d-f) after 180 s photo-crosslinking under UV irradiation (320-390 nm). The average diameter and membrane thickness of polymersomes were calculated by analyzing more than 100 particles and 50 particles, respectively. 124

Figure 7.7 (a) Scheme of photo-isomerization of PEG-DA-Azo macroinitiator under light stimuli. (b) Photo-isomerization of PEG-DA-Azo macroinitiator under UV irradiation (365 nm). The inset shows the corresponding curve of absorption value change at 476 nm. (c) Photo-isomerization of PEG-DA-Azo macroinitiator under blue light irradiation (400-500 nm). The inset shows the corresponding curve of maximum absorption value change at 476 nm. Conditions: 0.1 mg/mL PEG-DA-Azo macroinitiator aqueous solution. 125

Figure 7.8 (a) Photo-isomerization of PEG-Azo macroinitiator under UV irradiation (365 nm). (b) Photo-isomerization of PEG-Azo macroinitiator under blue light irradiation (400-500 nm). (c) Scheme of photo-isomerization of PEG-Azo macroinitiator under light stimuli. (d) Curve of absorption value change at 360 nm of PEG-Azo macroinitiator undergoing light stimuli. Conditions: 0.1 mg/mL PEG-Azo macroinitiator aqueous solution. 126

Figure 7.9 Photoisomerization of BCP-DA-Azo (-) under blue light irradiation (400-500 nm) (a) or UV irradiation (365 nm) (b). Photoisomerization of Psomes-DA-Azo (-) under blue light irradiation (400-500 nm) (c) or UV irradiation (365 nm) (d). The inset shows the corresponding curve of absorption value change at 483 nm for BCP-DA-Azo (-) and at 435 nm for Psomes-DA-Azo (-). Conditions: 1 mg/mL BCP-DA-Azo (-) dissolved in acidic solution, pH = 6; 1 mg/mL Psomes-DA-Azo (-) in basic solution, pH = 8. 128

Figure 7.10 Photoisomerization of BCP-Azo (-) under UV irradiation (365 nm) (a) and then blue light irradiation (400-500 nm) (b). (c) The corresponding curve of absorption value change at 362 nm of BCP-Azo (-) undergoing light stimuli. Photoisomerization of Psomes-Azo (-) under UV irradiation (365 nm) (d) and then blue light irradiation (400-500 nm) (e). (f) The corresponding curve of absorption value change at 362 nm of Psomes-Azo (-) undergoing light stimuli. Conditions: 1 mg/mL BCP-Azo (-) dissolved in acidic solution, pH = 6; 1 mg/mL Psomes-Azo (-) in basic solution, pH = 8. 129

Figure 7.11 Hydrodynamic size of Psomes-DA-Azo (-) (a) and Psomes-Azo (-) (b) under light stimuli. Conditions: 1 mg/mL Psomes-DA-Azo (-) or 1 mg/mL Psomes-Azo (-) in basic solution, pH = 8.....	129
Figure 7.12 Cryo-TEM (a&d), size histograms (b&e) and membrane thickness histograms (c&f) of NR-Psomes-DA-Azo (+) (a-c) and NR-Psomes-Azo (+) (d-f) without photo-crosslinking. The average diameter and membrane thickness of polymersomes were calculated by analyzing more than 100 particles and 50 particles, respectively.	130
Figure 7.13 Scheme of dye release from NR-Psomes-(DA-)Azo (+) at simulated physiological conditions under light stimuli. Conditions: 1 mL * 0.5 mg/mL NR-Psomes-DA-Azo (+) or NR-Psomes-Azo (+) without photo-crosslinking in 1 mM PBS buffer at pH 7.4.....	131
Figure 7.14 Photobleaching of Nile red under blue light irradiation (400-500 nm) (a) or UV irradiation (365 nm) (b). Conditions: 1 mL 1 µg/mL Nile red solution, dissolved in DMF; $\lambda_{ex} = 515$ nm, $\lambda_{em} = 626$ nm.	132
Figure 7.15 Percent release of Nile red from NR-Psomes-DA-Azo (+) during the light stimuli and dark cycles (a) as well as the comparison between continuous light irradiation and under dark (b). Percent release of Nile red from NR-Psomes-Azo (+) during the light stimuli and dark cycles (c) as well as the comparison between continuous light irradiation and under dark (d).	133
Figure 7.16 Hydrodynamic size change of NR-Psomes-DA-Azo (+) (a) and NR-Psomes-Azo (+) (b) under light stimuli.....	134
Figure 7.17 Cryo-TEM (a&d), size histograms (b&e) and membrane thickness histograms (c&f) of Myo-Psomes-DA-Azo (+) (a-c) and Myo-Psomes-Azo (+) (d-f) after 180 s photo-crosslinking under UV irradiation (320-390 nm). The average diameter and membrane thickness of polymersomes were calculated by analyzing more than 100 particles and 50 particles, respectively.	135
Figure 7.18 Scheme of enzymatic reaction in photo-crosslinked Myo-Psomes-(DA-)Azo (+) in the dark or upon light stimuli (UV or blue light).	135
Figure 7.19 Enzymatic reaction of Myo-Psomes-DA-Azo (+) under blue light irradiation (400-500 nm) (a) and UV irradiation (365 nm) (b) at simulated physiological conditions as well as the corresponding curve of the peak value at 590 nm versus irradiation time (c). Enzymatic reaction of Myo-Psomes-Azo (+) under blue light irradiation (400-500 nm) (d) and UV irradiation (365 nm) (e) at simulated physiological conditions as well as the corresponding curve of the peak value at 590 nm versus irradiation time (f).....	136

Figure 8.1 Preparation and purification routes of clustered polymersomes. The clustering process is achieved by PEG with bis-cyclooctyne end groups using copper-free click reaction. The termination step is used to control the clustering process and purification methods are utilized to obtain optimal clusters.	139
Figure 8.2 Fabrication of co-clustered enzyme-loaded polymersomes (Myo/GOx-Psomes-N ₃) for enzymatic cascade reaction at neutral or slight acidic condition.....	140
Figure 8.3 Schematic illustration of enzymatic cascade reaction mechanism (top) and substrates as well as intermediates diffusion mechanism (bottom) in mixed or co-clustered Myo/GOx-Psomes-N ₃	141
Figure 8.4 Schematic illustration of BCP structure with one-unit azobenzene and corresponding membrane structure with azobenzene as junction unit. The left bottom figure represents membrane structure, and the right bottom figure shows light-triggered transmembrane mobility of water or small molecules and retention of macromolecules.....	143
Figure 8.5 Schematic illustration of the retention of macromolecules and small molecules by the permeability of the photo-induced membrane as requirement for the establishment of complex and sophisticated artificial organelles under light stimuli.	144
Figure 8.6 Schematic illustration of membrane permeability-driven enzyme reaction under dark and light stimuli at physiological pH value (pH 7.4) by photo-crosslinked Myo-Psomes-(DA-)Azo (+).....	145
Figure A1 ¹ H NMR spectrum of CH ₃ O-PEG-Br macroinitiator in DMSO- <i>d</i> ₆	175
Figure A2 ¹ H NMR spectrum of N ₃ -PEG ₆₀ -Br macroinitiator in DMSO- <i>d</i> ₆	175
Figure A3 ¹ H NMR spectrum of N ₃ -PEG _{77.5} -Br macroinitiator in DMSO- <i>d</i> ₆	176
Figure A4 ¹ H NMR spectrum of intermediate 3,4-dimethyl maleic imidobutanol in DMSO- <i>d</i> ₆	176
Figure A5 ¹³ C NMR spectrum of intermediate 3,4-dimethyl maleic imidobutanol in DMSO- <i>d</i> ₆	177
Figure A6 ¹ H NMR spectrum of photo-crosslinker DMIBMA in DMSO- <i>d</i> ₆	177
Figure A7 ¹³ C NMR spectrum of photo-crosslinker DMIBMA in DMSO- <i>d</i> ₆	178
Figure A8 ¹ H NMR spectrum of BCP-OCH ₃ in CDCl ₃	178
Figure A9 ¹ H NMR spectrum of BCP-N ₃ -1 in CDCl ₃	179
Figure A10 ¹ H NMR spectrum of BCP-N ₃ -2 in CDCl ₃	179
Figure A11 ¹ H NMR spectrum of bisBCN-PEG _{2k} crosslinker in DMSO- <i>d</i> ₆	180

Figure A12	^{13}C NMR spectrum of bisBCN-PEG _{2k} crosslinker in DMSO- <i>d</i> ₆	180
Figure A13	^1H NMR spectrum of bisBCN-PEG _{1k} crosslinker in DMSO- <i>d</i> ₆	181
Figure A14	^1H NMR spectrum of bisBCN-PEG _{0.1k} crosslinker in CDCl ₃	181
Figure A15	^1H NMR spectrum of Compound 1 in DMSO- <i>d</i> ₆	182
Figure A16	^{13}C NMR spectrum of Compound 1 in DMSO- <i>d</i> ₆	182
Figure A17	^1H NMR spectrum of Compound 2 in DMSO- <i>d</i> ₆	183
Figure A18	^{13}C NMR spectrum of Compound 2 in DMSO- <i>d</i> ₆	183
Figure A19	^1H NMR spectrum of Compound 3 in DMSO- <i>d</i> ₆	184
Figure A20	^{13}C NMR spectrum of Compound 3 in DMSO- <i>d</i> ₆	184
Figure A21	^1H NMR spectrum of Compound 4 in CDCl ₃	185
Figure A22	^1H NMR spectrum of Compound 5 in CDCl ₃	185
Figure A23	^1H NMR spectrum of Compound 6 in CDCl ₃	186
Figure A24	^1H NMR spectrum of BCP-DA-Azo-1 in CDCl ₃	186
Figure A25	^1H NMR spectrum of BCP-DA-Azo-2 in CDCl ₃	187
Figure A26	^1H NMR spectrum of Compound 7 in DMSO- <i>d</i> ₆	187
Figure A27	^{13}C NMR spectrum of Compound 7 in DMSO- <i>d</i> ₆	188
Figure A28	^1H NMR spectrum of Compound 8 in DMSO- <i>d</i> ₆	188
Figure A29	^{13}C NMR spectrum of Compound 8 in DMSO- <i>d</i> ₆	189
Figure A30	^1H NMR spectrum of Compound 9 in DMSO- <i>d</i> ₆	189
Figure A31	^{13}C NMR spectrum of Compound 9 in DMSO- <i>d</i> ₆	190
Figure A32	^1H NMR spectrum of Compound 10 in CDCl ₃	190
Figure A33	^1H NMR spectrum of Compound 11 in CDCl ₃	191
Figure A34	^1H NMR spectrum of BCP-Azo-1 in CDCl ₃	191
Figure A35	^1H NMR spectrum of BCP-Azo-2 in CDCl ₃	192
Figure A36	In-situ AFM image and its cross-section of clustered Psomes-N ₃ purified by Protocol 1 at pH 8.0.....	192
Figure A37	In-situ AFM image and its cross-section of clustered Psomes-N ₃ purified by Protocol 2 at pH 8.0.....	193
Figure A38	In-situ AFM image and its cross-section of clustered Psomes-N ₃ purified by Protocol 3 at pH 8.0.....	193
Figure A39	In-situ AFM image and its cross-section of co-clustered Myo/GOx-Psomes-N ₃ purified by Protocol 3 at pH 8.0.....	193

Figure A40 In-situ AFM image and its cross-section of isolated Psomes-N ₃ in the clustering Psomes-N ₃ process purified by Protocol 3 at pH 8.0.	194
Figure A41 In-situ AFM image and its cross-section of isolated Psomes-N ₃ in the co-clustering Myo/GOx-Psomes-N ₃ process purified by Protocol 3 at pH 8.0.	194
Figure A42 In-situ AFM image and its cross-section of isolated Psomes-N ₃ in the clustering Psomes-N ₃ process purified by Protocol 3 at pH 6.5.	194
Figure A43 In-situ AFM image and its cross-section of isolated Psomes-N ₃ in the co-clustering Myo/GOx-Psomes-N ₃ process purified by Protocol 3 at pH 6.5.	195
Figure A44 Microscopic images of clustered Psomes-N ₃ before (a-b) and after one time centrifugation and redispersion by mechanical stirring (c-d) and vortex (e-f) at pH 8.0. Classification: 0.5-1 μm (left) and 1-5 μm (right).	195
Figure A45 Microscopic images of clustered Psomes-N ₃ after four times centrifugation and redispersion by mechanical stirring (a-b) and vortex (c-f) at pH 8.0 (c-d) as well as pH 6.5 (e-f). Classification: 0.5-1 μm (left) and 1-5 μm (right).....	196
Figure A46 Microscopic images of co-clustered Myo/GOx-Psomes-N ₃ at pH 8.0 (a-b), pH 7.0 (c-d) and pH 6.5 (e-f) purified by Protocol 3. Classification: 0.5-1 μm (left) and 1-5 μm (right).	197
Figure A47 UV-Vis spectrum of BCP-DA-Azo (-) aqueous solution at different pH values. At pH 7.0 and pH 9.3, BCP-DA-Azo (-) were self-assembled to polymersomes.....	198
Figure A48 Fluorescence intensity of photo-crosslinked Myo-Psomes-DA-Azo (+) after blue light irradiation (400-500 nm) (a) and UV irradiation (365 nm) (b) for different times at pH 7.4. Fluorescence intensity of photo-crosslinked Myo-Psomes-Azo (+) under blue light irradiation (400-500 nm) (c) and UV irradiation (365 nm) (d) at pH 7.4 for different times.....	198

List of Tables

Table 3.1 List of chemicals.....	29
Table 3.2 List of materials.....	32
Table 6.1 Block composition of BCPs with methoxy and azido end groups.....	71
Table 6.2 Molar mass characteristics of BCPs with methoxy and azido end groups.....	72
Table 6.3 Hydrodynamic size of the Psomes-30%N ₃ mixed with 5 eq. bisBCN-PEG _{1k} crosslinker stir 2 days at different temperatures investigated by DLS study.....	76
Table 6.4 Hydrodynamic size of different Psomes-X%N ₃ mixed with 1 eq. crosslinker both bisBCN-PEG _{1k} and bisBCN-PEG _{2k} at 40 °C for 2 days investigated by DLS study.....	77
Table 6.5 Hydrodynamic size of the Psomes-10%N ₃ and Psomes-30%N ₃ mixed with 1 eq. crosslinker both bisBCN-PEG _{1k} and bisBCN-PEG _{2k} at 40 °C for different reaction time investigated by DLS study.....	80
Table 6.6 Hydrodynamic diameter of the Psomes-30%N ₃ mixed with different ratio of crosslinker bisBCN-PEG _{1k} at 40 °C for 2 days investigated by DLS study.....	81
Table 6.7 Hydrodynamic diameter of the Psomes-N ₃ with different proportion of BCP-N ₃ mixed with 1 eq. bisBCN-PEG crosslinker with different length at 40 °C for 4 days.....	82
Table 6.8 Hydrodynamic size of the Psomes-N ₃ at different concentrations (from 0.1 to 1 mg/mL) mixed with 1 eq. crosslinker bisBCN-PEG _{1k} at 40 °C for 1 day.....	83
Table 6.9 Summary of optimal reaction conditions based on the percentage of Psomes-X%N ₃ clusters in the clustering reaction.....	84
Table 6.10 Size of clustered Psomes-N ₃ at pH 8.0 before and after purification by different protocols, characterized by TEM and cryo-TEM.....	97
Table 6.11 Size measurement of clustered Psomes-N ₃ before and after different times centrifugation and redispersion by different purification steps.....	106
Table 6.12 Size measurement of co-clustered Myo/GOx-Psomes-N ₃ at different pH values based on purification by Protocol 3.....	107
Table 7.1 Block composition of BCPs with different azobenzene linkages.....	119
Table 7.2 Molar mass characteristics of BCPs with different azobenzene linkages.....	120

List of Abbreviations and Symbols

AFM	Atomic force microscopy
AF4	Asymmetrical flow field flow fractionation
AMG	Amyloglucosidase
ATRP	Atom transfer radical polymerization
Azo	Azobenzene
BCN	Bicyclo[6.1.0]non-4-yn-9-ylmethyl
BCP	Block copolymer
BCP-Azo	Ether substituted azobenzene functionalized BCP
BCP-DA-Azo	Donor-acceptor substituted azobenzene functionalized BCP
BCP-N₃	Azido group functionalized BCP
BCP-OCH₃	Methoxy group functionalized BCP
BHT	Butylated hydroxytoluene
BisBCN-PEG	PEG functionalized with BCN group at both ends
BSA	Bovine serum albumin
BSA-Cy5	Cyanine5 labeled BSA
°C	Degree Celsius
CLSM	Confocal Laser Scanning Microscopy
CRP	Controlled radical polymerization
Cryo-TEM	Cryogenic transmission electron microscopy
CTA	Chain transfer agent
CuAAC	Copper-catalyzed alkyne-azide cycloaddition
Cu(I)Br	Copper bromide
Cy5-NHS	Cyanine5 NHS ester
d	Day
DA-Azo	Donor-acceptor substituted azobenzene
DAD	Diode array detector
DASAs	Donor-acceptor Stenhouse adducts
DCM	Dichloromethane

DEAEMA	2-(Diethylamino)ethyl methacrylate
DiI	1,1'-Dioctadecyl-3,3,3',3'-tetramethylindocarbo-cyanine perchlorate
DIPEA	<i>N,N</i> -Diisopropylethylamine
DLS	Dynamic light scattering
DMAc	<i>N,N</i> -Dimethylacetamide
DMAEMA	2-(Dimethylamino)ethyl methacrylate
DMF	<i>N,N</i> -Dimethylformamide
DMIBMA	3,4-Dimethyl maleic imidobuthyl methacrylate
DMIEMA	3,4-Dimethyl maleic imidoethyl methacrylate
DMSO	Dimethyl sulfoxide
DNA	Deoxyribonucleic acid
d. nm	Diameter values in nanometers
DPAEMA	2-(Diisopropylamino)ethyl methacrylate
EA	Ethyl acetate
Enzyme-Psomes-N₃	Enzyme in-situ loaded Psomes-N ₃
g	Gram
GOx	Glucose oxidase
GOx-Cy5	Cyanine5 labeled GOx
GOx-Psomes-N₃	GOx in-situ loaded Psomes-N ₃
GPC	Gel permeation chromatography
h	Hour
HCl	Hydrochloric acid
HFF	Hollow fiber filtration
H₂O₂	Hydrogen peroxide
H₂SO₄	Sulfuric acid
K₂CO₃	Potassium carbonate
KI	Potassium iodide
L	Liter
LPO	Lactoperoxidase
MAA	Methacrylic acid

MALLS	Multi-angle laser light scattering
MC	Merocyanine
MgSO₄	Magnesium sulfate
min	Minute
M_n	Number average molar mass
mol	Mole
mol%	Molar percent
M_w	Mass average molar mass
MWCO	Molecular weight cut-off
Myo	Myoglobin
Myo-Psomes-N₃	Myo in-situ loaded Psomes-N ₃
Myo-RhB	Rhodamine B labeled Myo
NaBH₄	Sodium borohydride
NaCl	Sodium chloride
Na₂CO₃	Sodium carbonate
NaHCO₃	Sodium bicarbonate
NaN₃	Sodium azide
NaNO₂	Sodium nitrite
NaOH	Sodium hydroxide
Na₂SO₄	Sodium sulfate
NH₄Cl	Ammonium chloride
NHS	<i>N</i> -Hydroxysuccinimide
nm	Nanometer
NMR	Nuclear magnetic resonance
NR	Nile red
PBS	Phosphate buffered saline
P_c	Packing parameter
PDI	Polydispersity index
PEG	Poly(ethylene glycol)
PEG-Azo	Ether substituted azobenzene functionalized PEG

PEG-DA-Azo	Donor-acceptor substituted azobenzene functionalized PEG
PEO	Poly(ethylene oxide)
PNIPAM	Poly(<i>N</i> -isopropylacrylamide)
Psomes-N₃	Azido group functional polymersomes
Psomes-Azo	Polymersomes self-assembled by BCP-Azo
Psomes-DA-Azo	Polymersomes self-assembled by BCP-DA-Azo
PTA	Phosphotungstic acid
RAFT	Reversible addition/fragmentation chain transfer
RhB-ITC	Rhodamine B isothiocyanate
RI	Refractive index
RT	Room temperature
SEC	Size exclusion chromatography
SP	Spiropyran
SPAAC	Strain promoted azide-alkyne cycloaddition
SPANC	Strain-promoted alkyne-nitrone cycloaddition
ssDNA	Single stranded DNA
TEA	Triethylamine
TEM	Transmission electron microscopy
THF	Tetrahydrofuran
TMP	Transmembrane pressure
UV-Vis	Ultraviolet-visible
ν	Scaling parameter for AF4 measurement
vol/vol	Volume ratio
\bar{M}	Molar mass distributions
f	Hydrophilic weight fraction
λ	Wavelength
δ	Chemical shift
μm	Micrometer
ρ	Parameter (R_g/R_h) for AF4 measurement

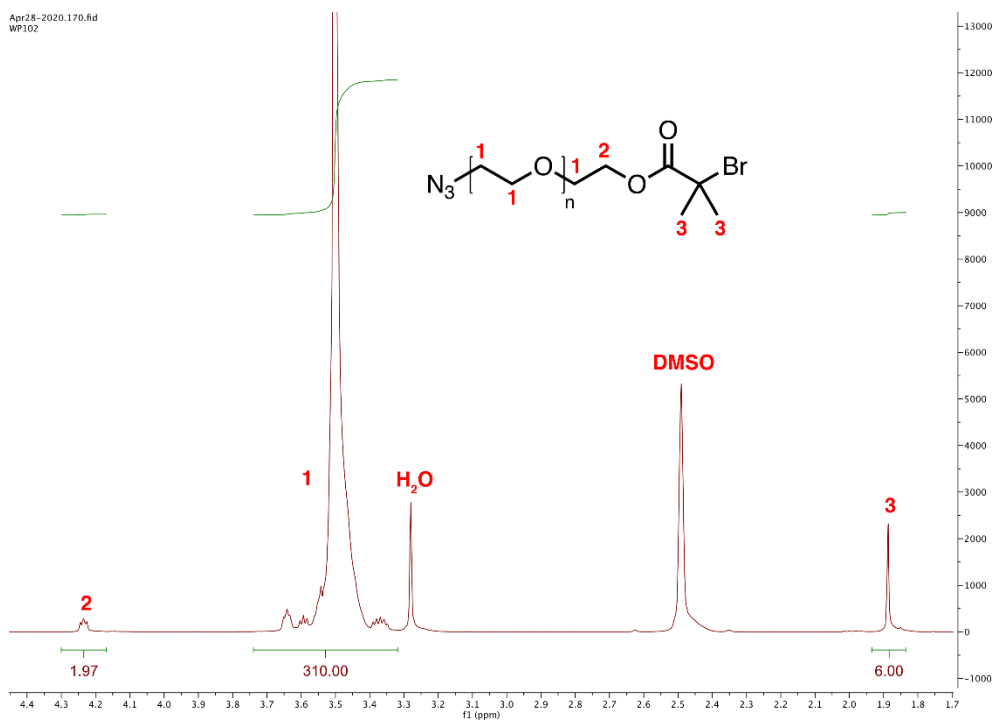


Figure A3 ¹H NMR spectrum of N₃-PEG_{77.5}-Br macroinitiator in DMSO-*d*₆.

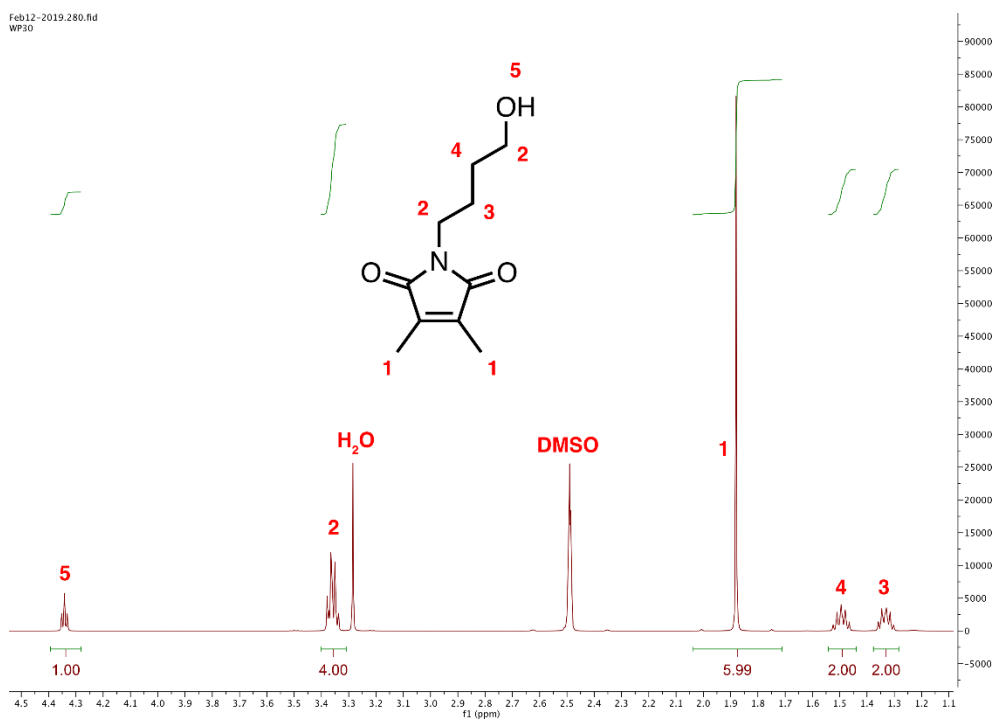


Figure A4 ¹H NMR spectrum of intermediate 3,4-dimethyl maleic imidobutanol in DMSO-*d*₆.

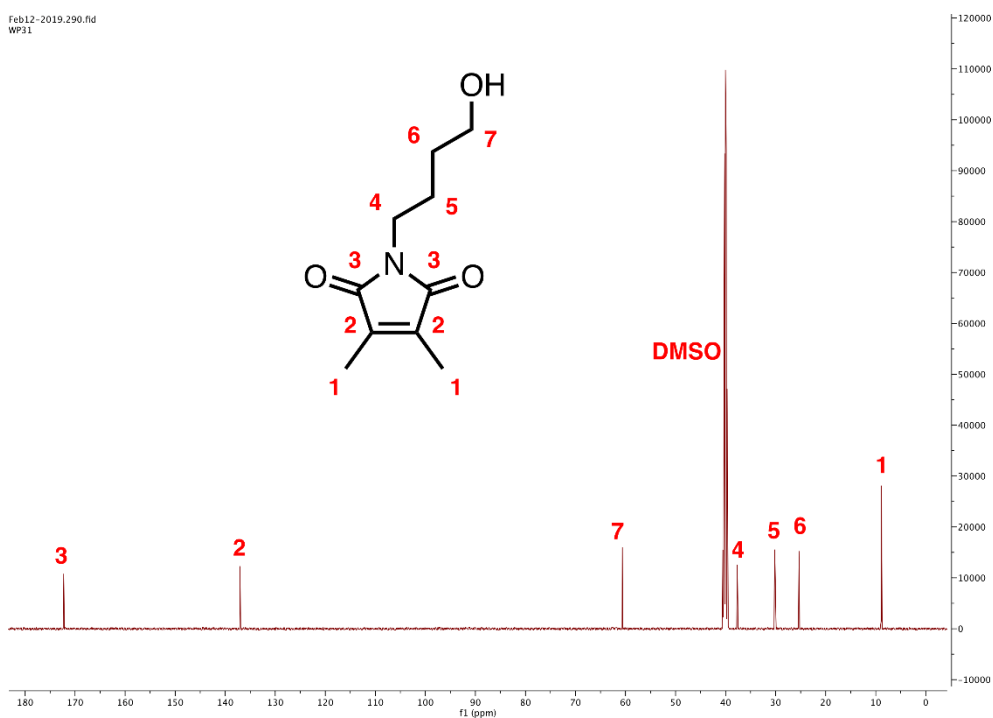


Figure A5 ^{13}C NMR spectrum of intermediate 3,4-dimethyl maleic imidobutanol in $\text{DMSO-}d_6$.

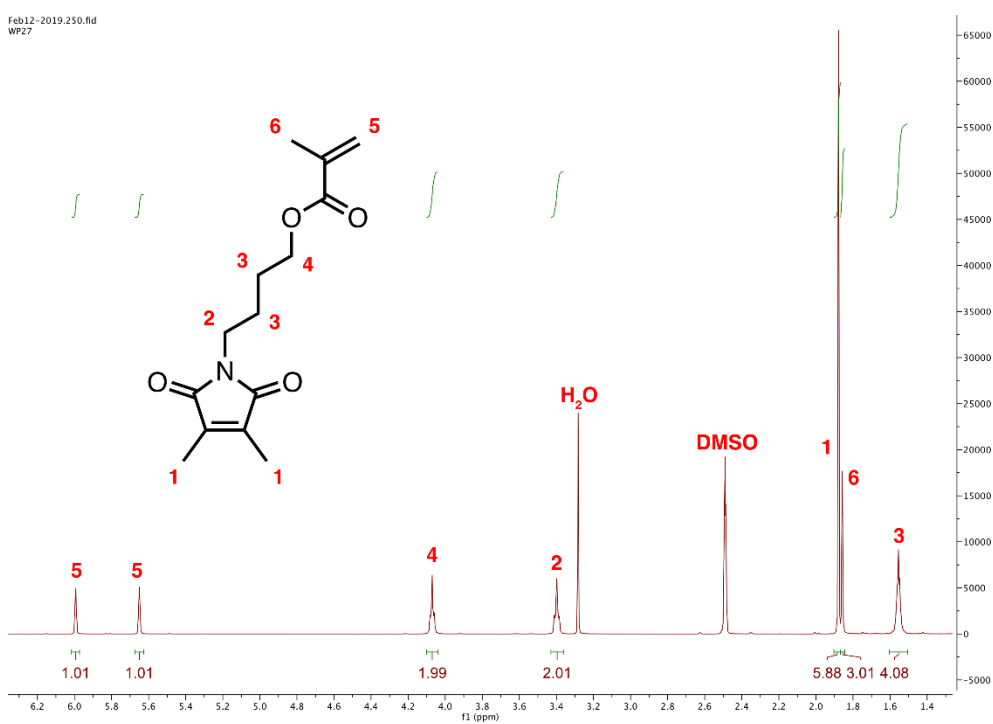


Figure A6 ^1H NMR spectrum of photo-crosslinker DMIBMA in $\text{DMSO-}d_6$.

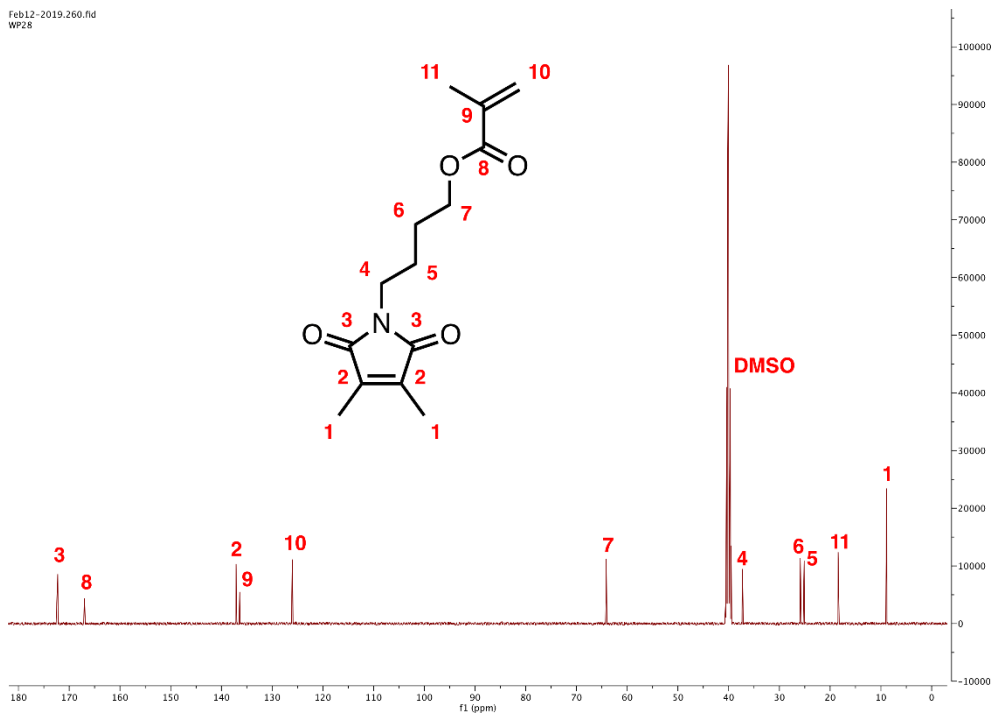


Figure A7 ^{13}C NMR spectrum of photo-crosslinker DMIBMA in $\text{DMSO-}d_6$.

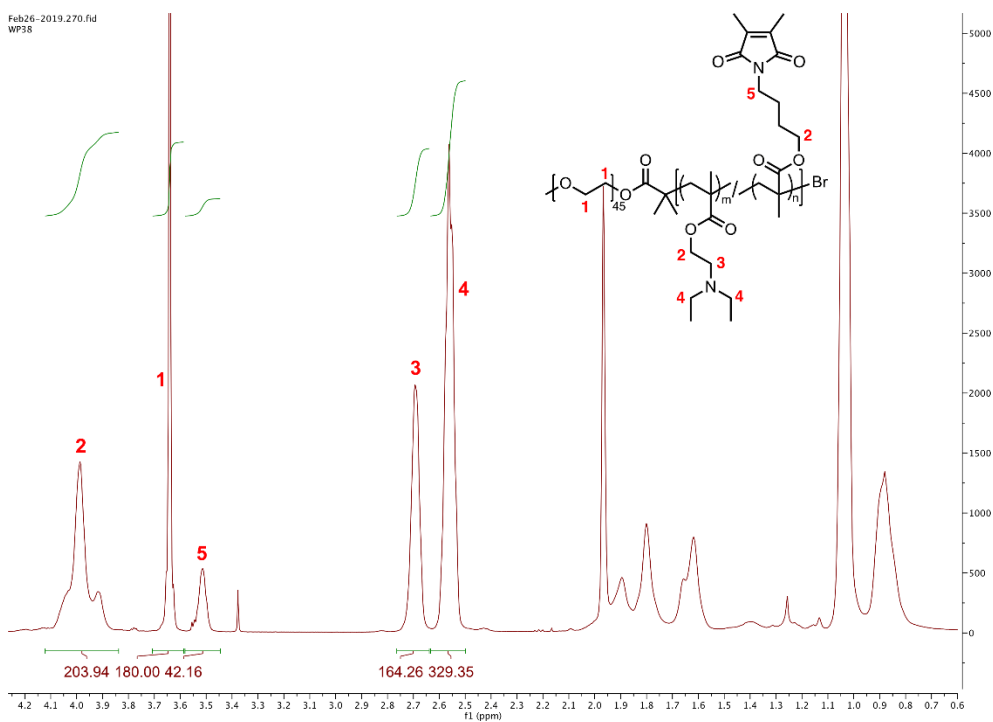


Figure A8 ^1H NMR spectrum of BCP-OCH₃ in CDCl_3 .

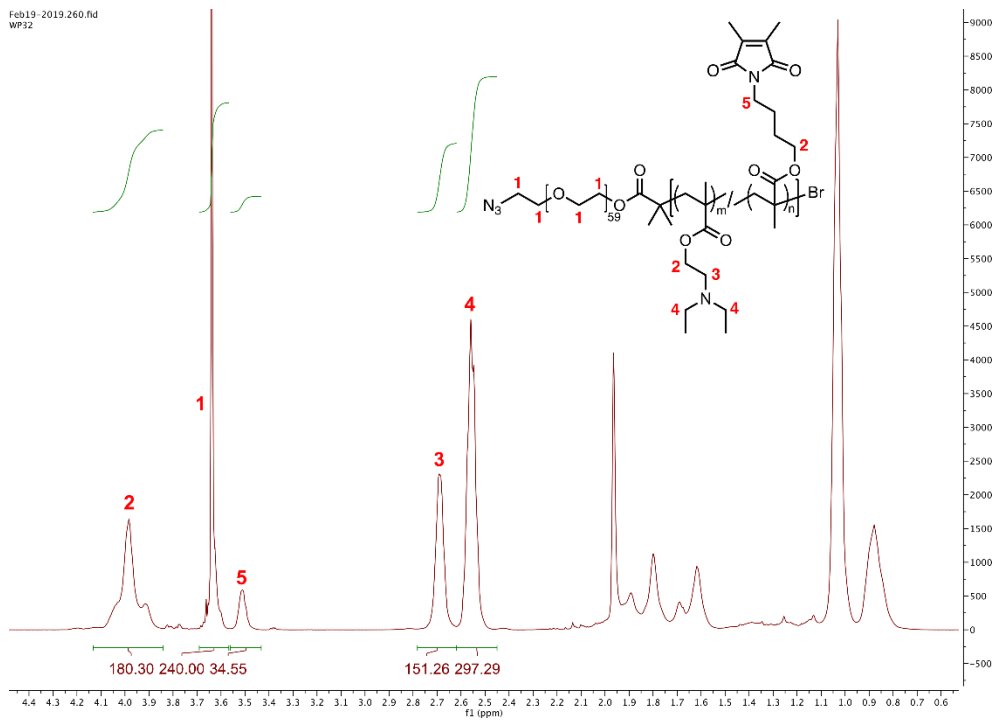


Figure A9 ¹H NMR spectrum of BCP-N₃-1 in CDCl₃.

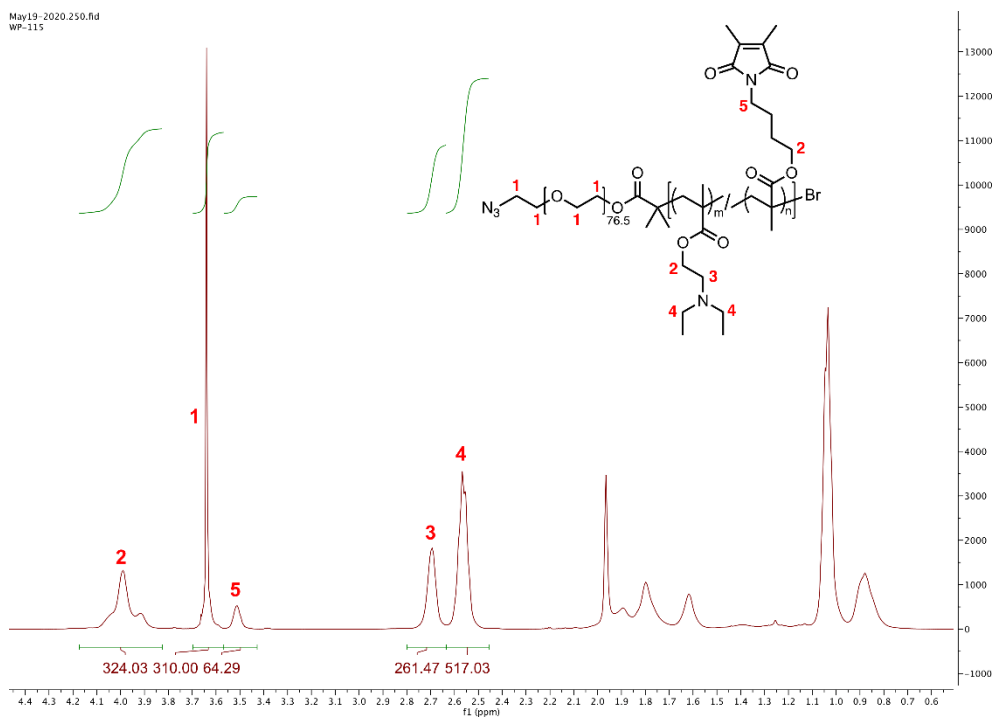


Figure A10 ¹H NMR spectrum of BCP-N₃-2 in CDCl₃.

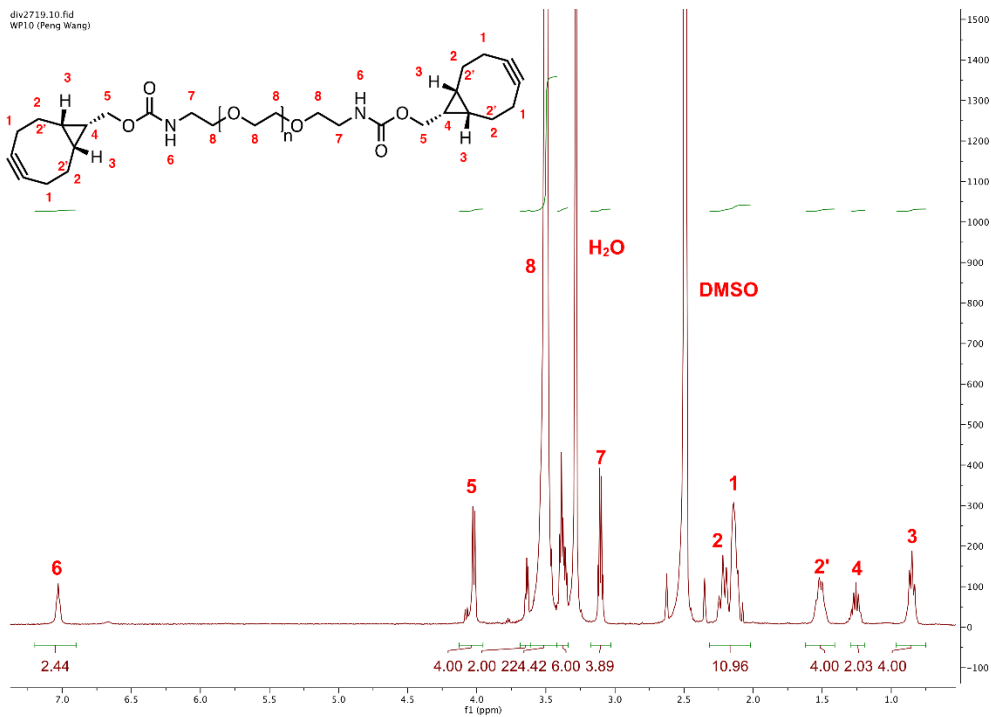


Figure A11 ^1H NMR spectrum of bisBCN-PEG_{2k} crosslinker in DMSO-*d*₆.

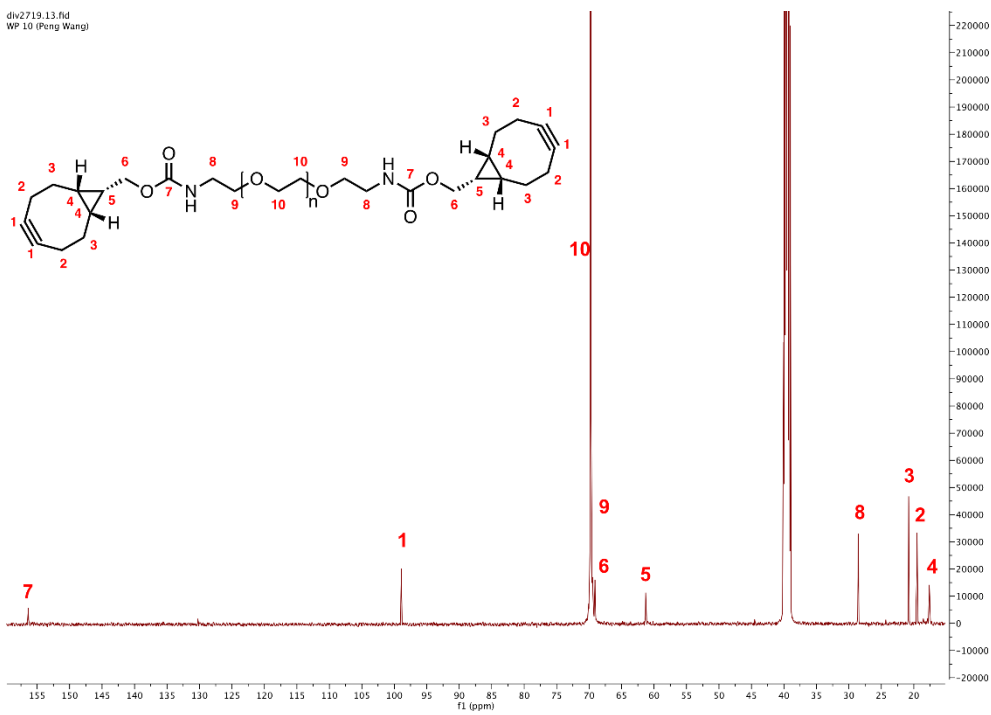


Figure A12 ^{13}C NMR spectrum of bisBCN-PEG_{2k} crosslinker in DMSO-*d*₆.

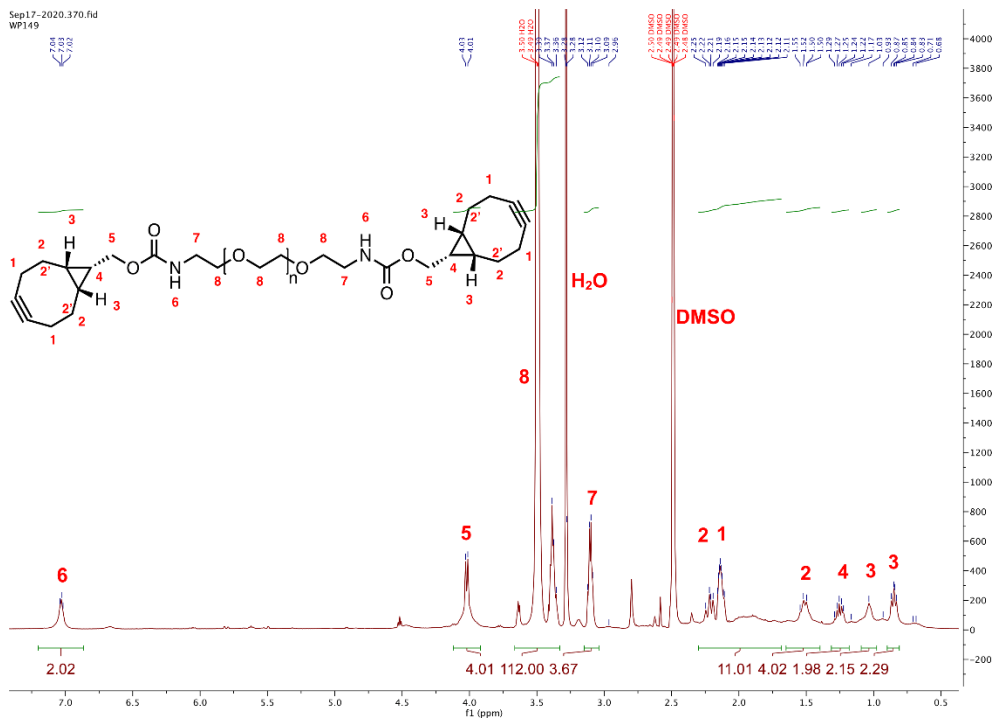


Figure A 13 ¹H NMR spectrum of bisBCN-PEG_{1k} crosslinker in DMSO-*d*₆.

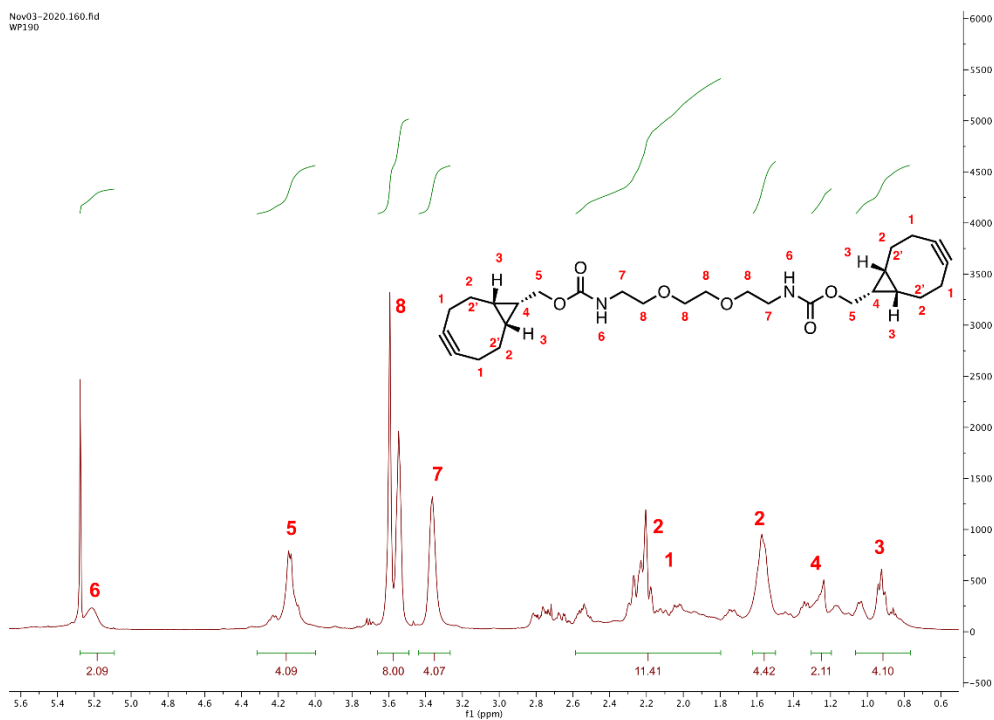


Figure A14 ¹H NMR spectrum of bisBCN-PEG_{0.1k} crosslinker in CDCl₃.

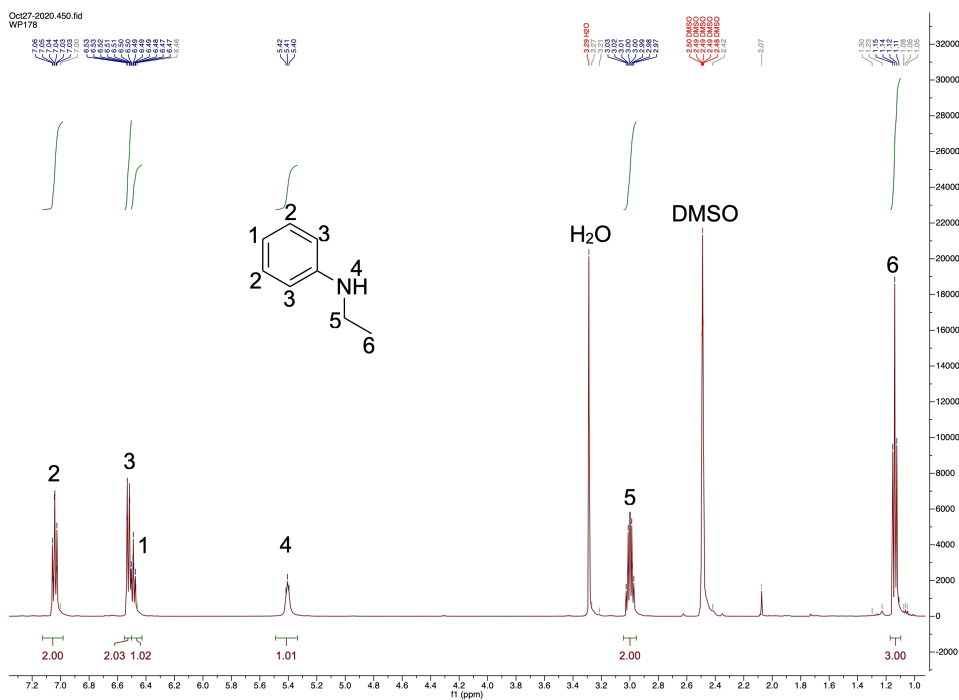


Figure A15 ¹H NMR spectrum of Compound 1 in DMSO-*d*₆.

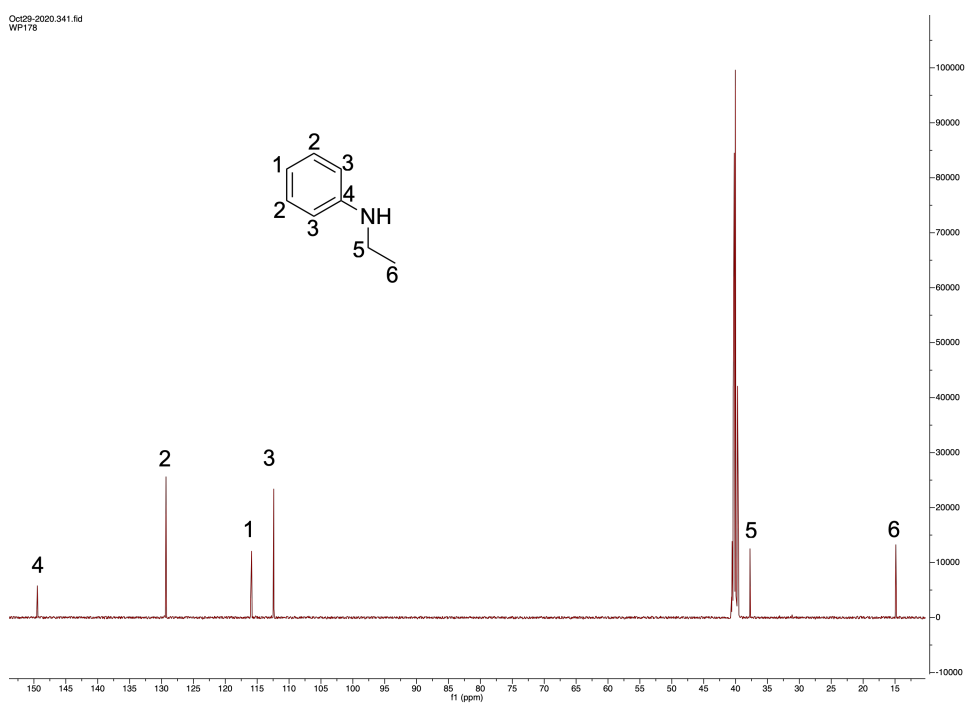


Figure A16 ¹³C NMR spectrum of Compound 1 in DMSO-*d*₆.

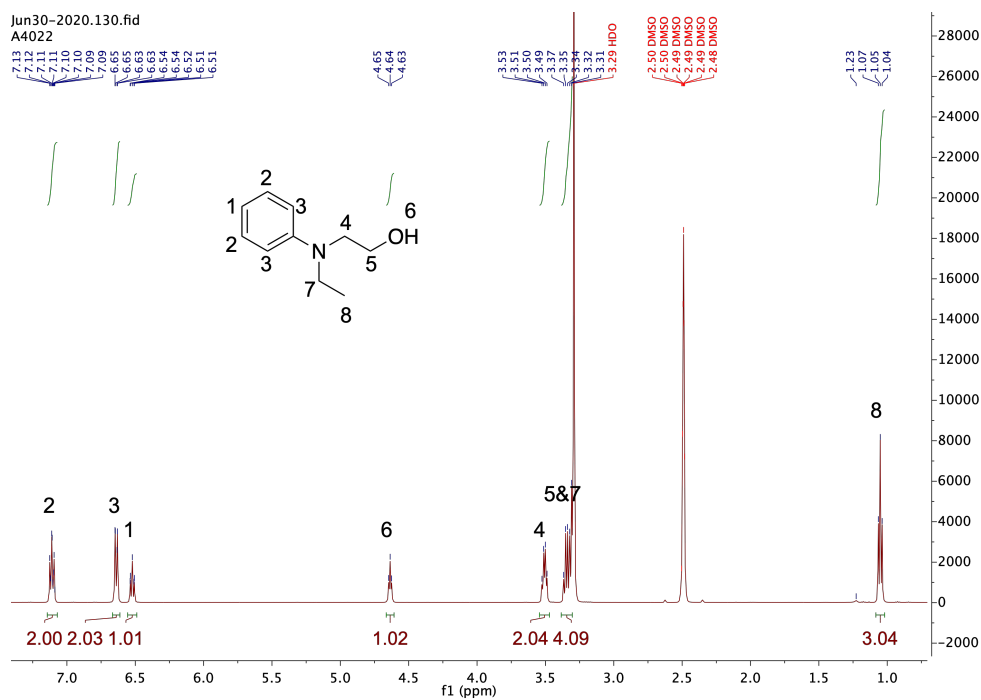


Figure A17 ^1H NMR spectrum of Compound 2 in $\text{DMSO-}d_6$.

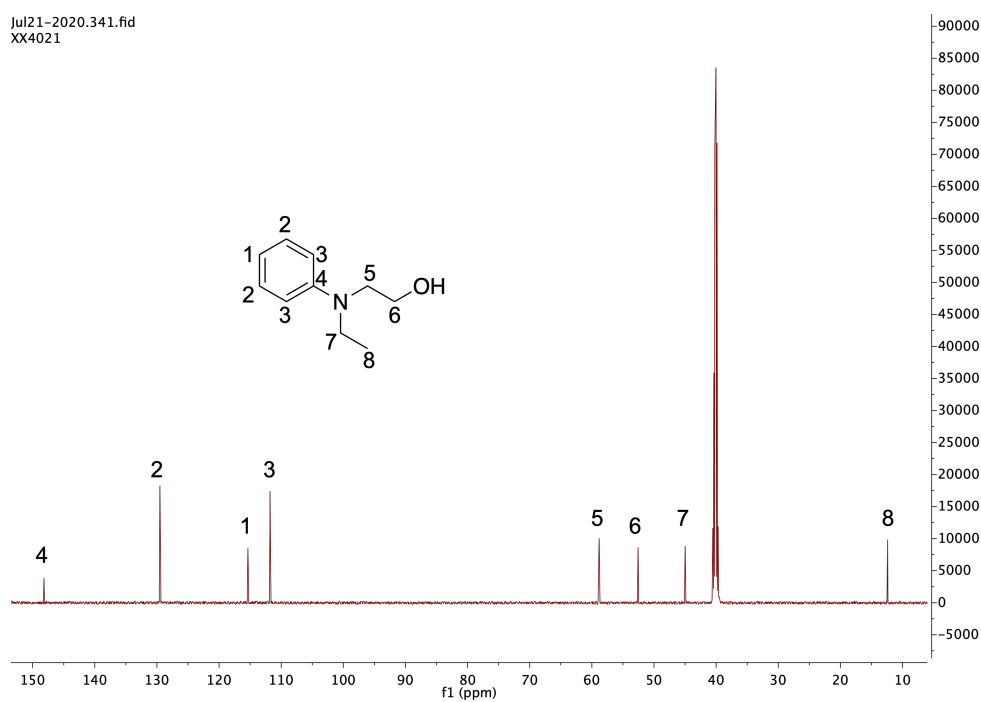


Figure A18 ^{13}C NMR spectrum of Compound 2 in $\text{DMSO-}d_6$.

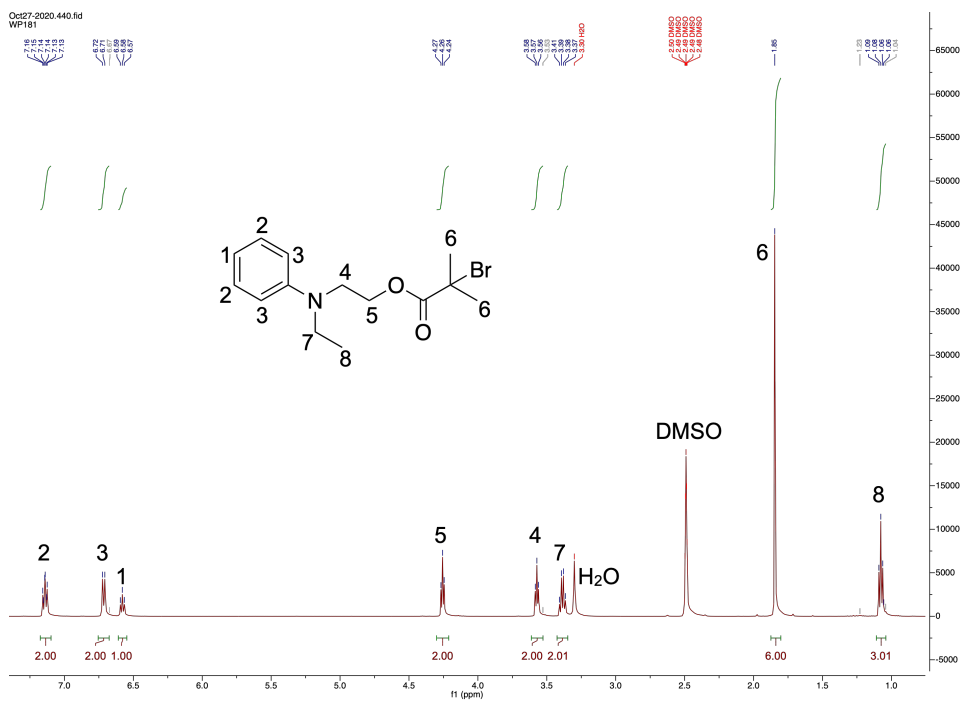


Figure A19 ^1H NMR spectrum of Compound 3 in $\text{DMSO-}d_6$.

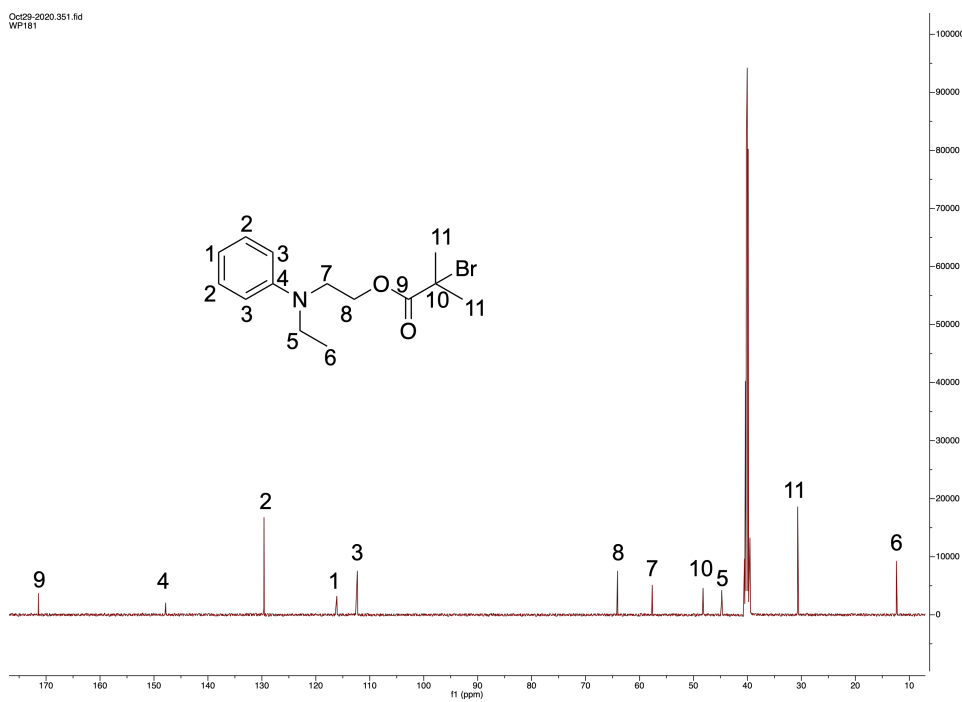


Figure A20 ^{13}C NMR spectrum of Compound 3 in $\text{DMSO-}d_6$.

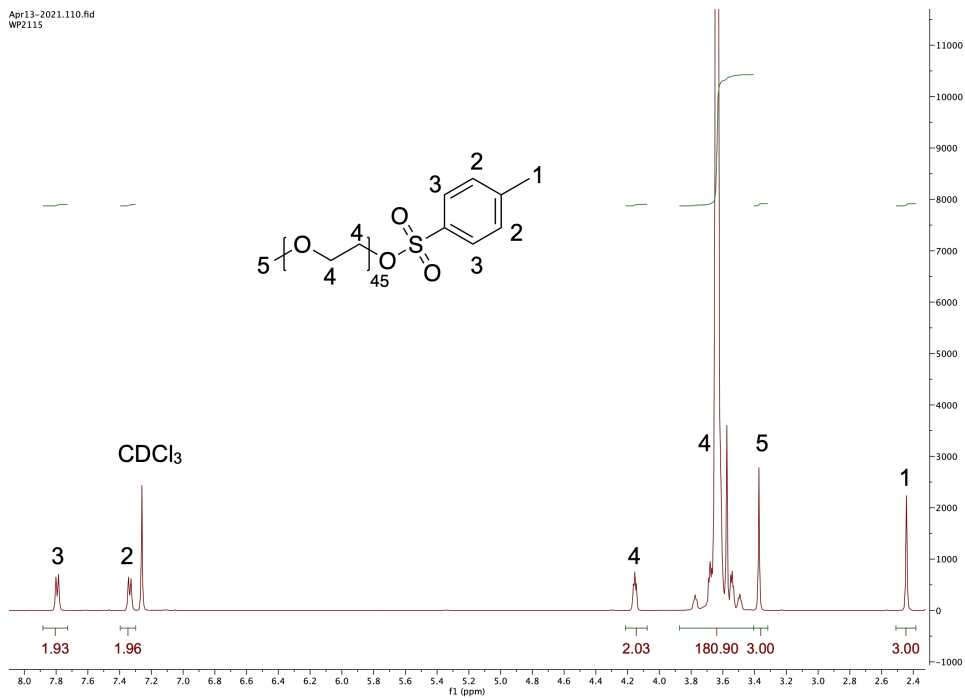


Figure A21 ^1H NMR spectrum of Compound 4 in CDCl_3 .

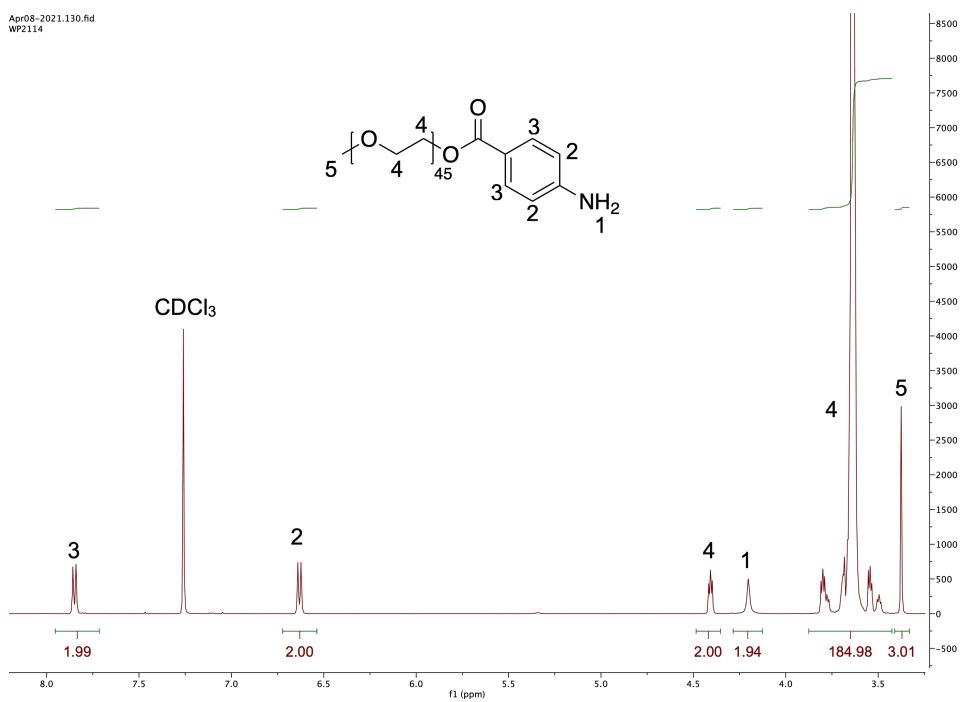


Figure A22 ^1H NMR spectrum of Compound 5 in CDCl_3 .

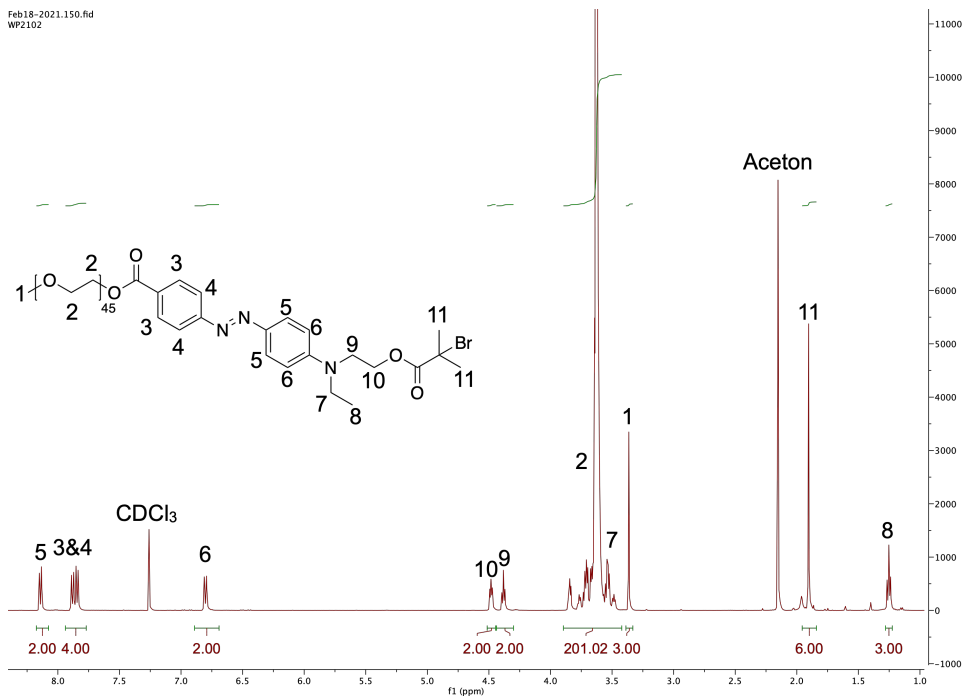


Figure A23 ^1H NMR spectrum of Compound 6 in CDCl_3 .

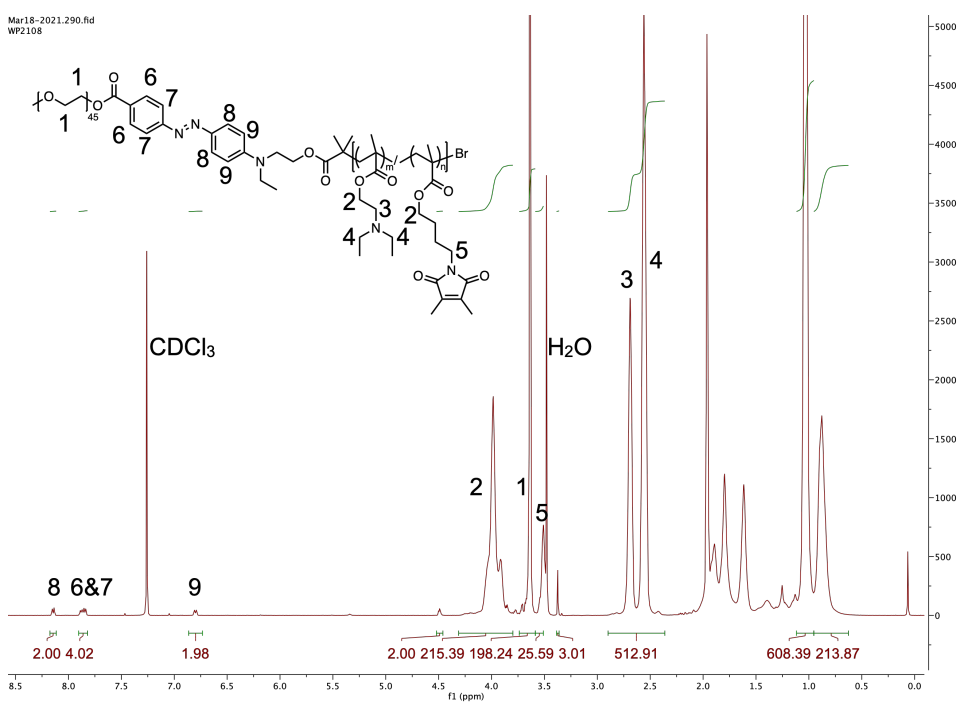


Figure A24 ^1H NMR spectrum of BCP-DA-Azo-1 in CDCl_3 .

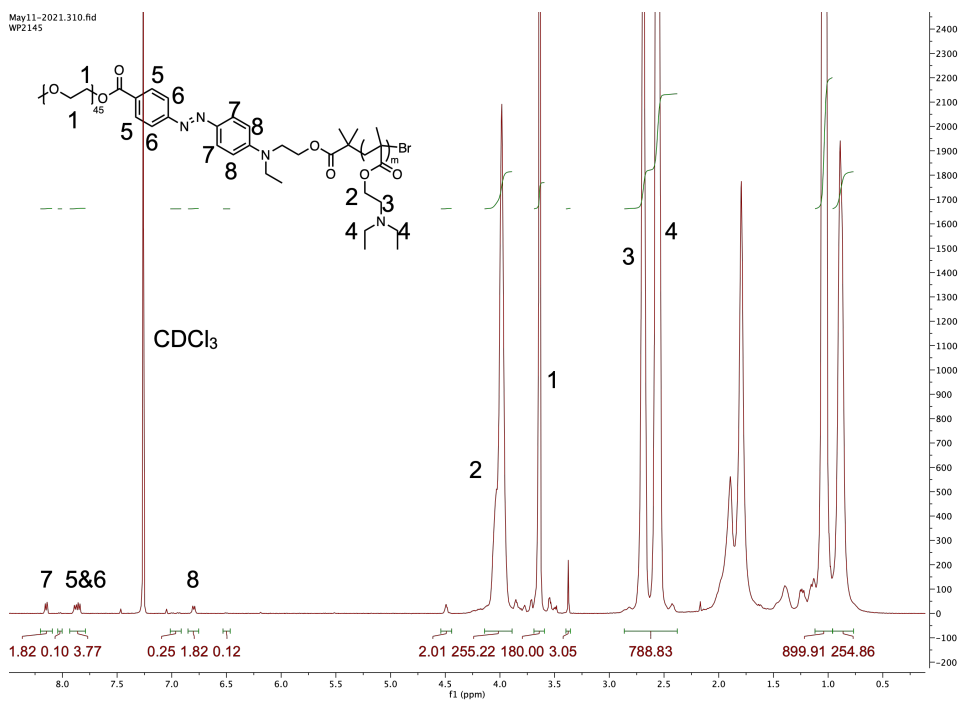


Figure A25 ¹H NMR spectrum of BCP-DA-Azo-2 in CDCl₃.

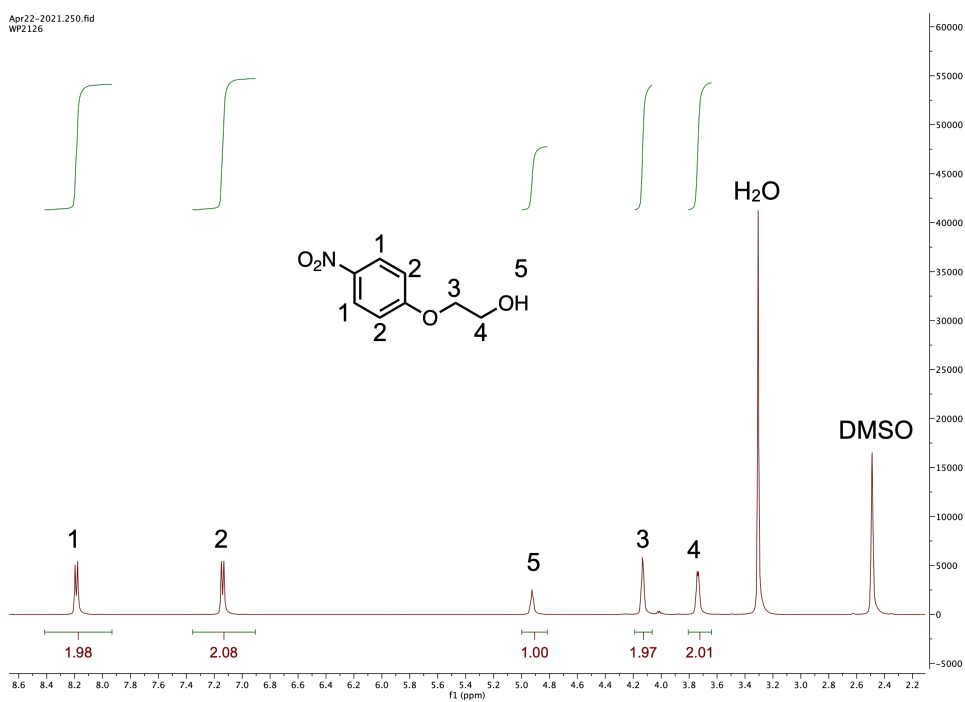


Figure A26 ¹H NMR spectrum of Compound 7 in DMSO-*d*₆.

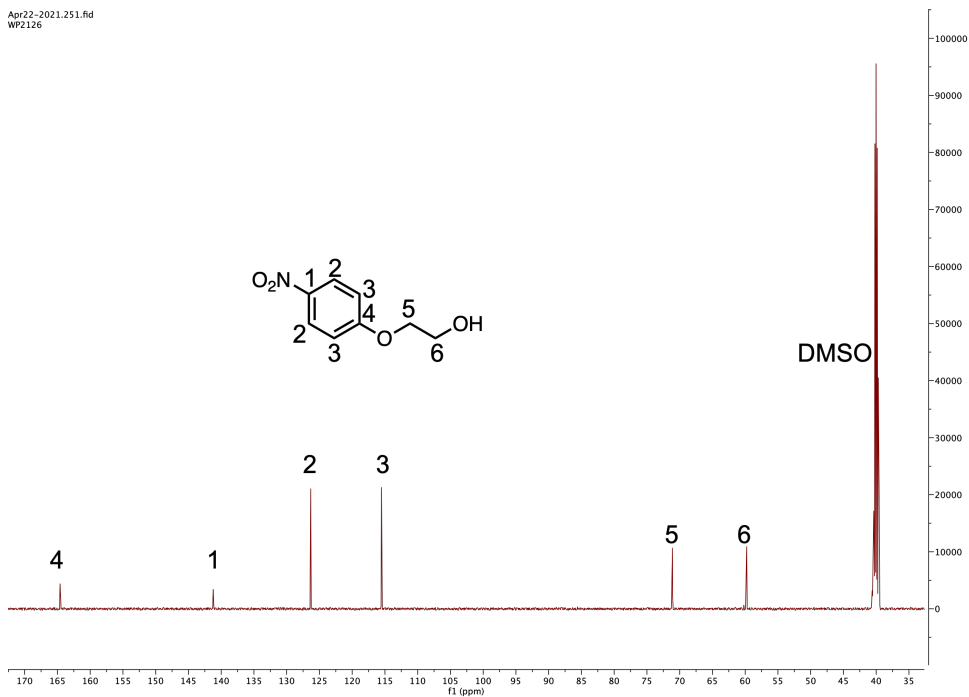


Figure A27 ¹³C NMR spectrum of Compound 7 in DMSO-*d*₆.

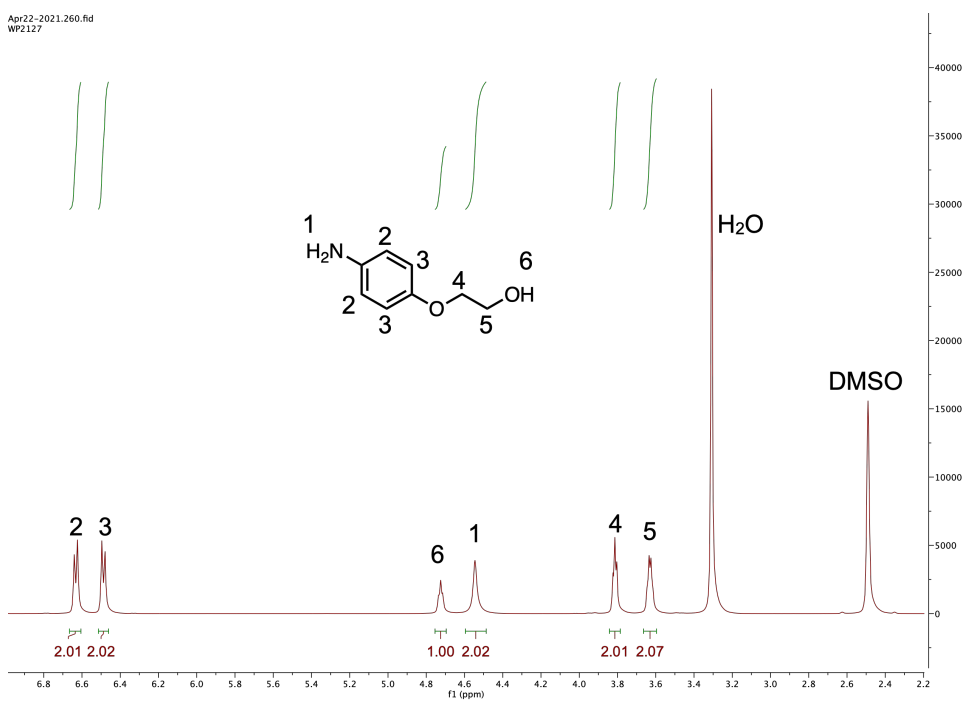


Figure A28 ¹H NMR spectrum of Compound 8 in DMSO-*d*₆.

Apr22-2021.261.fid
WP2127

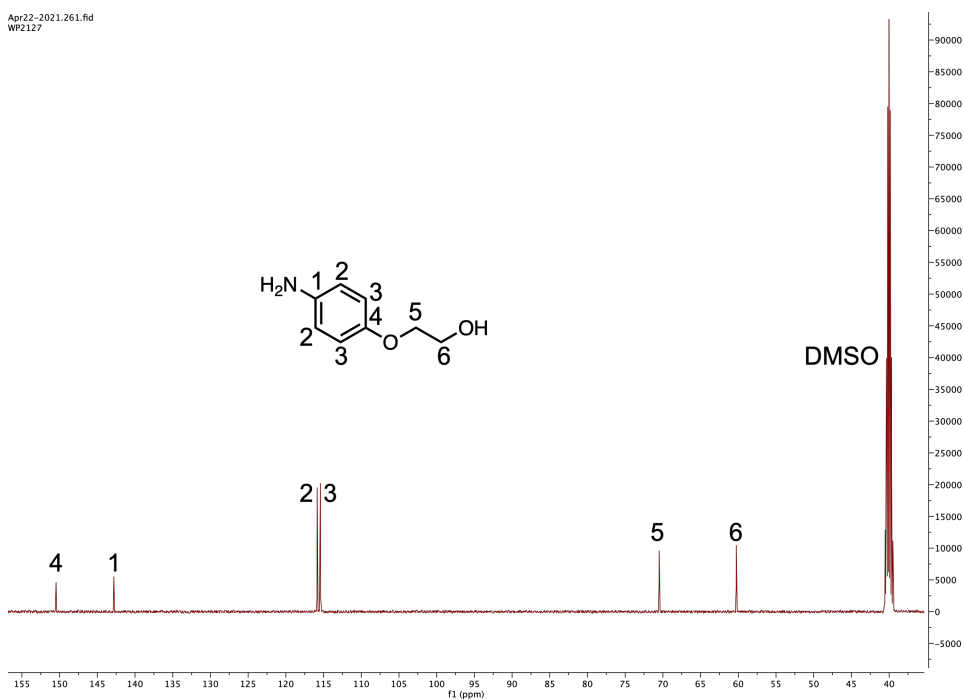


Figure A29 ^{13}C NMR spectrum of Compound 8 in $\text{DMSO-}d_6$.

Apr20-2021.290.fid
WP2123

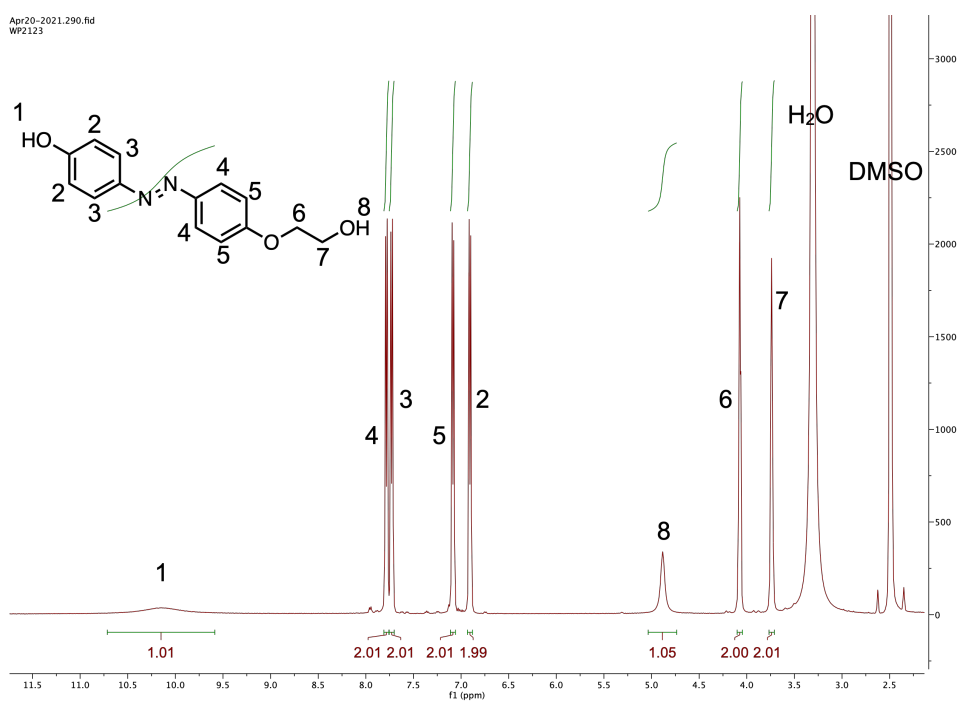


Figure A30 ^1H NMR spectrum of Compound 9 in $\text{DMSO-}d_6$.

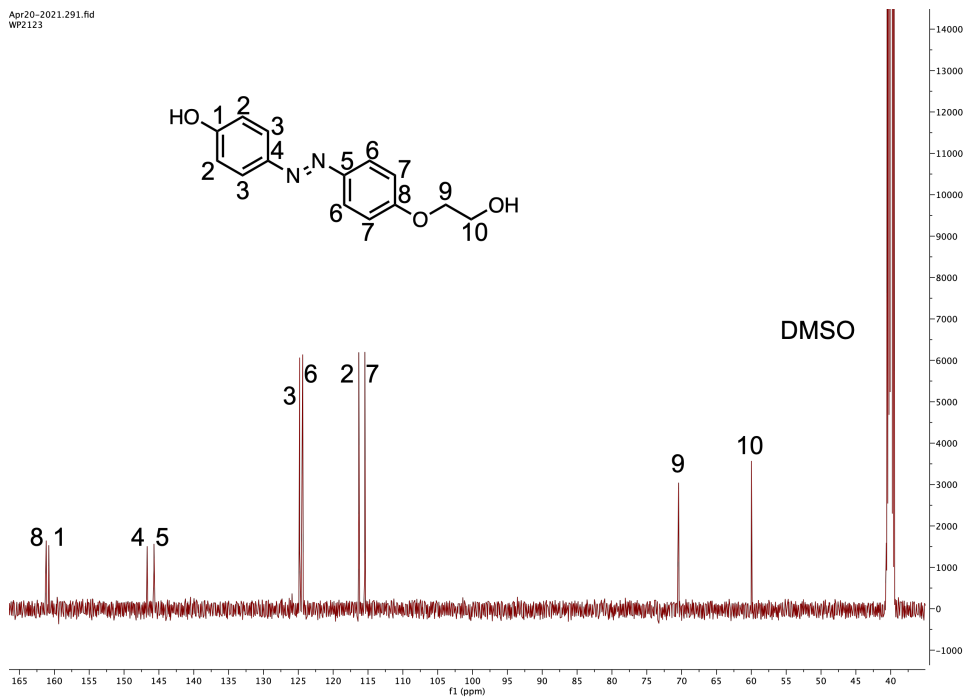


Figure A31 ^{13}C NMR spectrum of Compound 9 in $\text{DMSO-}d_6$.

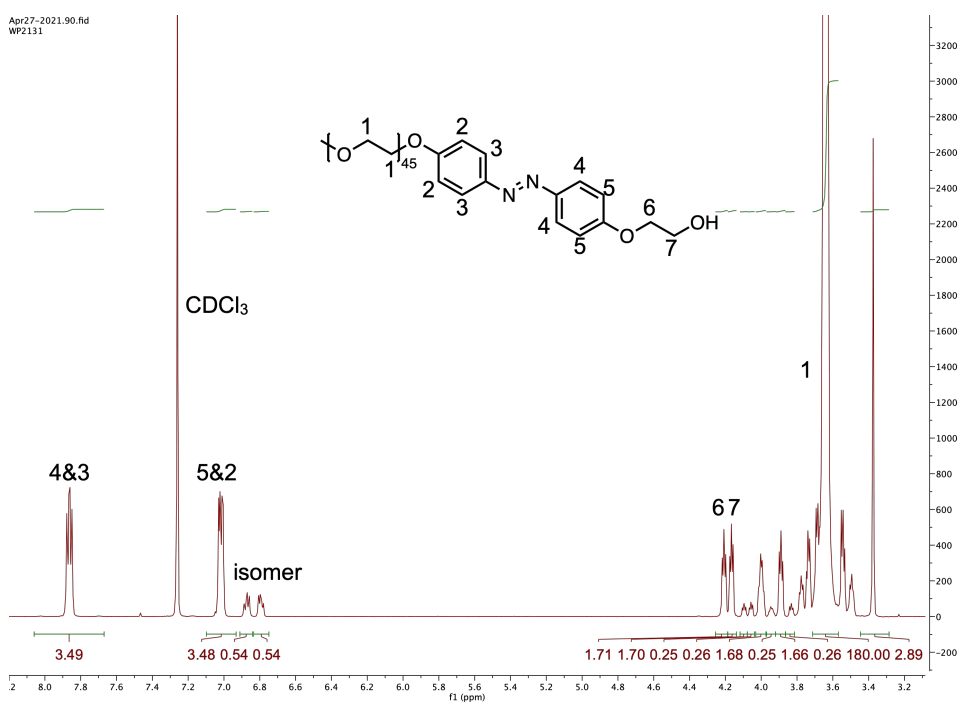


Figure A32 ^1H NMR spectrum of Compound 10 in CDCl_3 .

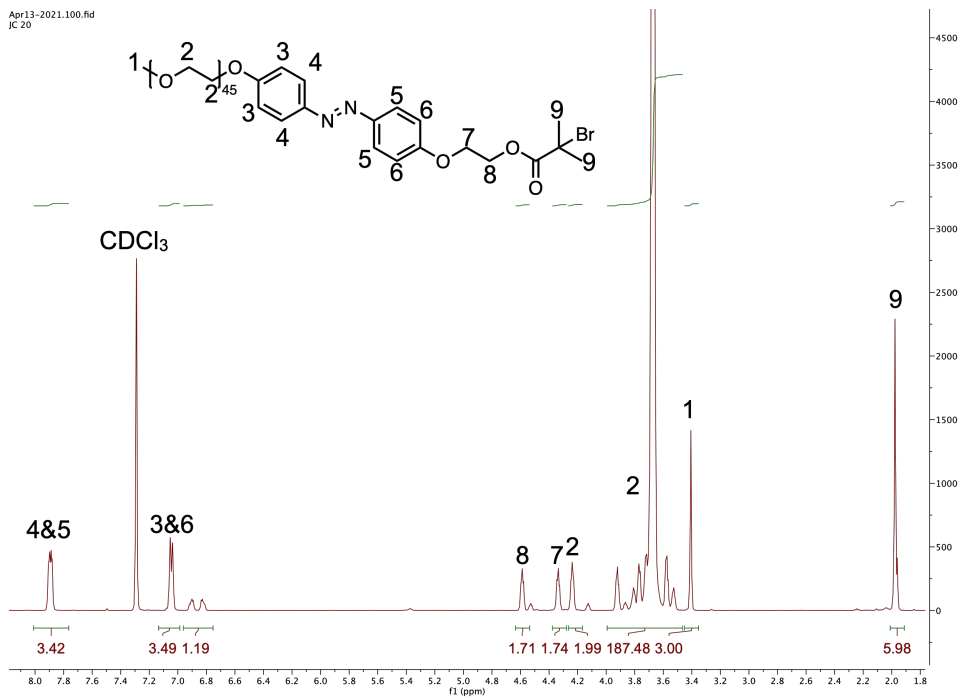


Figure A33 ¹H NMR spectrum of Compound 11 in CDCl₃.

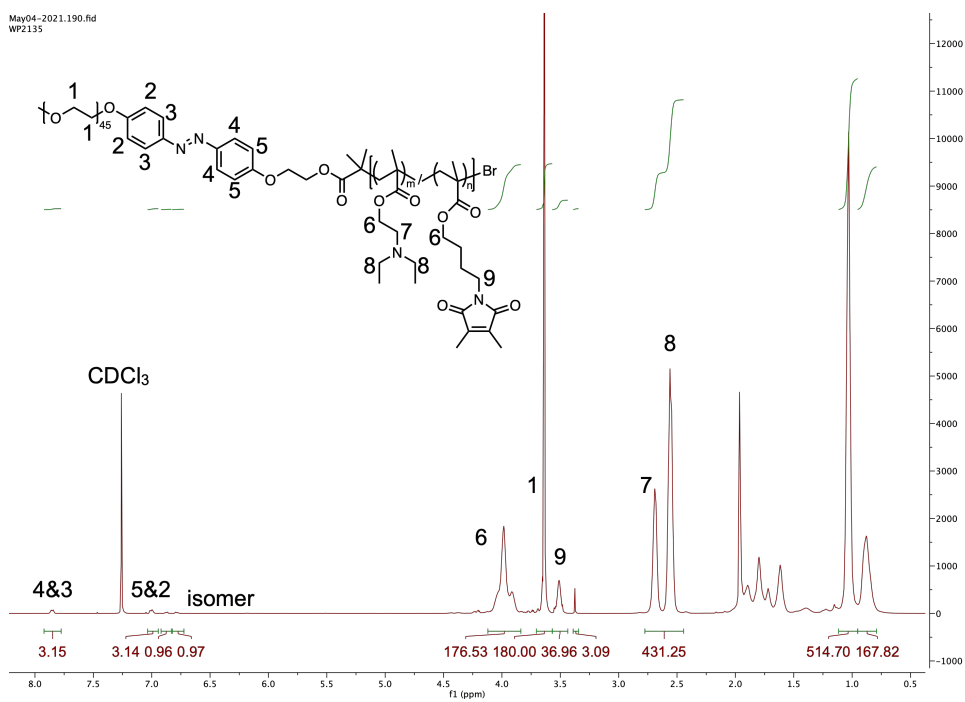


Figure A34 ¹H NMR spectrum of BCP-Azo-1 in CDCl₃.

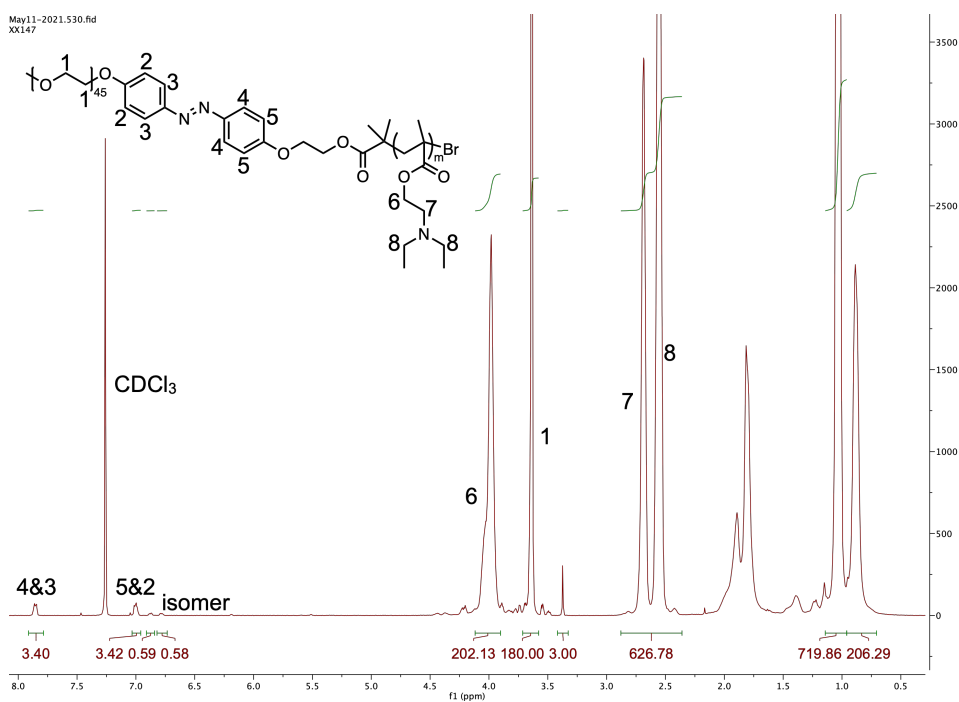


Figure A35 ¹H NMR spectrum of BCP-Azo-2 in CDCl₃.

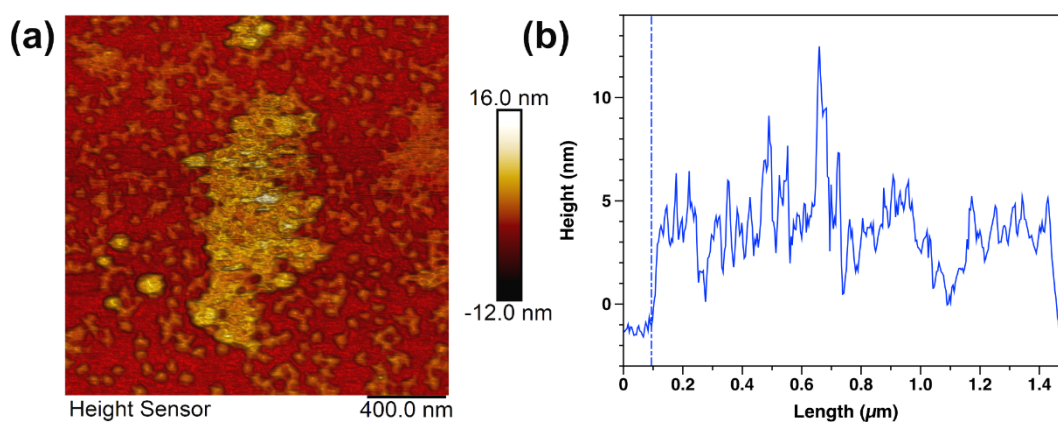


Figure A36 In-situ AFM image and its cross-section of clustered Psomes-N₃ purified by Protocol 1 at pH 8.0.

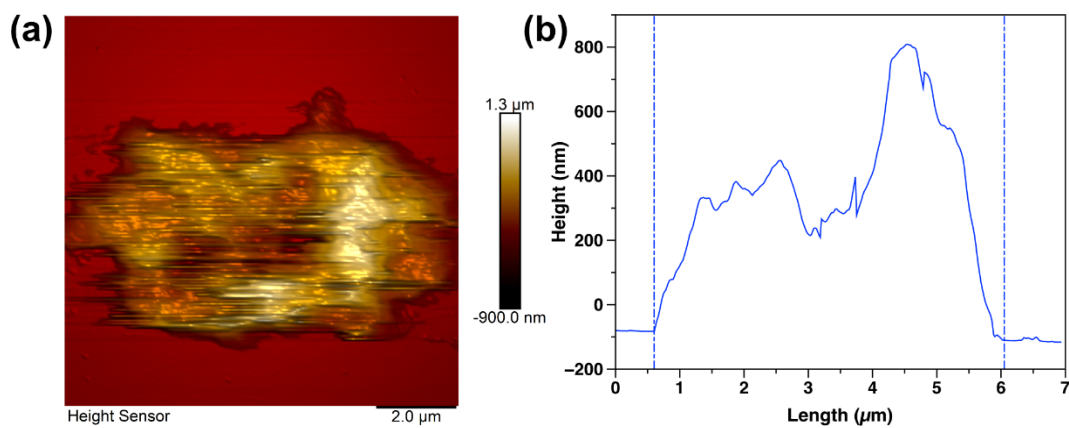


Figure A37 In-situ AFM image and its cross-section of clustered Psomes-N₃ purified by Protocol 2 at pH 8.0.

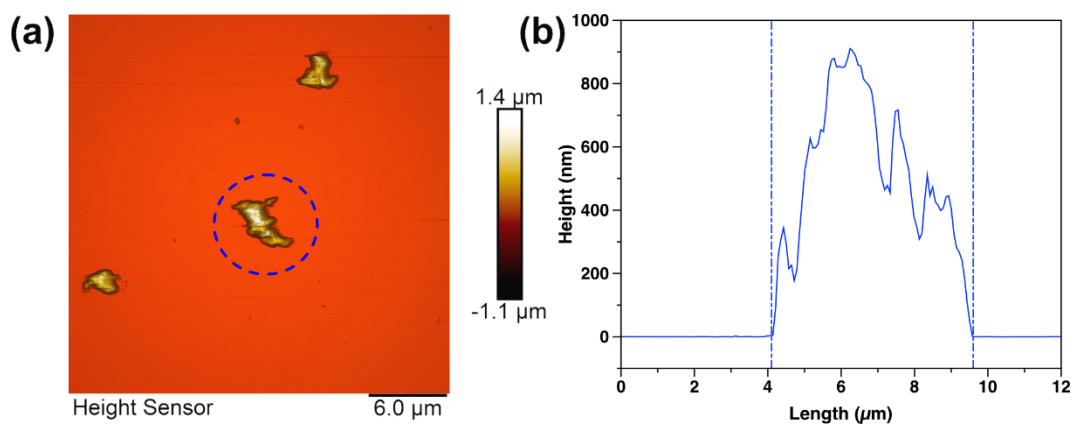


Figure A38 In-situ AFM image and its cross-section of clustered Psomes-N₃ purified by Protocol 3 at pH 8.0.

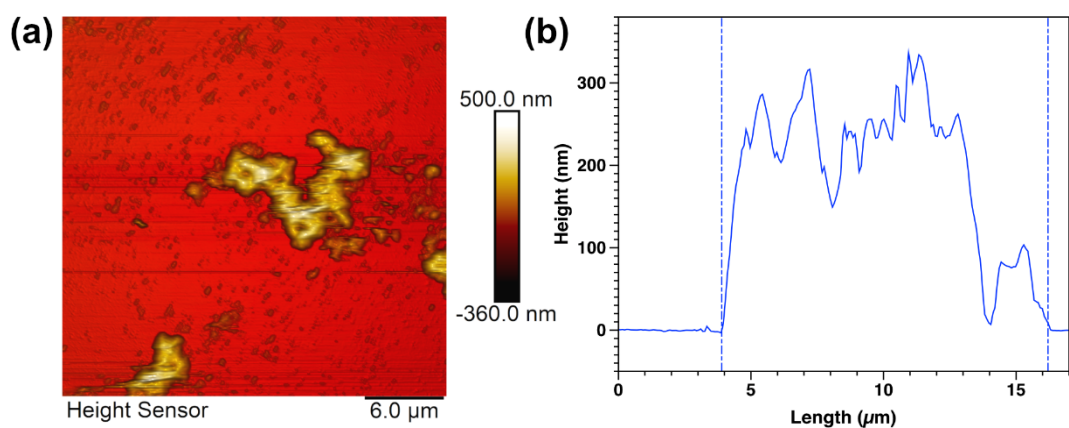


Figure A39 In-situ AFM image and its cross-section of co-clustered Myo/GOx-Psomes-N₃ purified by Protocol 3 at pH 8.0.

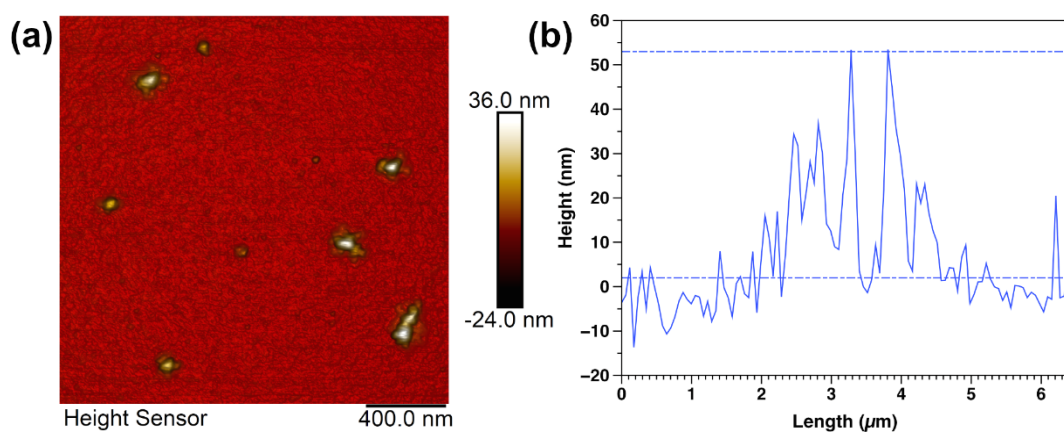


Figure A40 In-situ AFM image and its cross-section of isolated Psomes-N₃ in the clustering Psomes-N₃ process purified by Protocol 3 at pH 8.0.

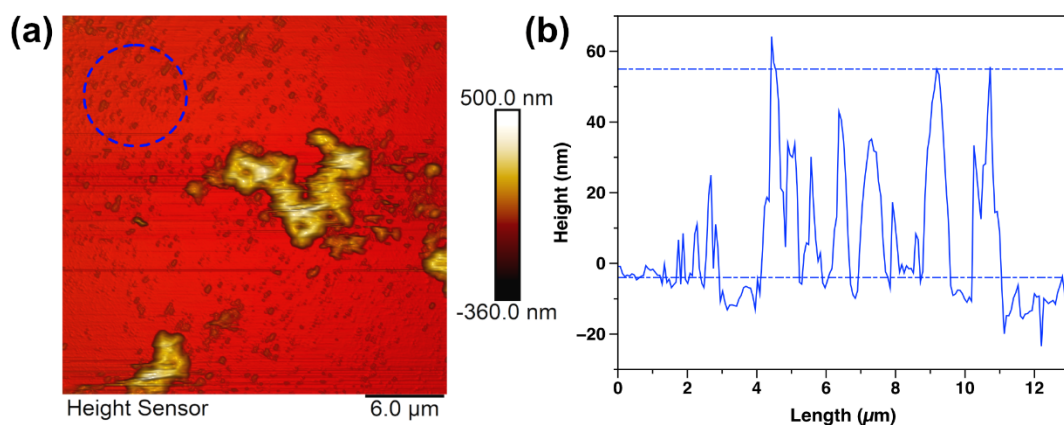


Figure A41 In-situ AFM image and its cross-section of isolated Psomes-N₃ in the co-clustering Myo/GOx-Psomes-N₃ process purified by Protocol 3 at pH 8.0.

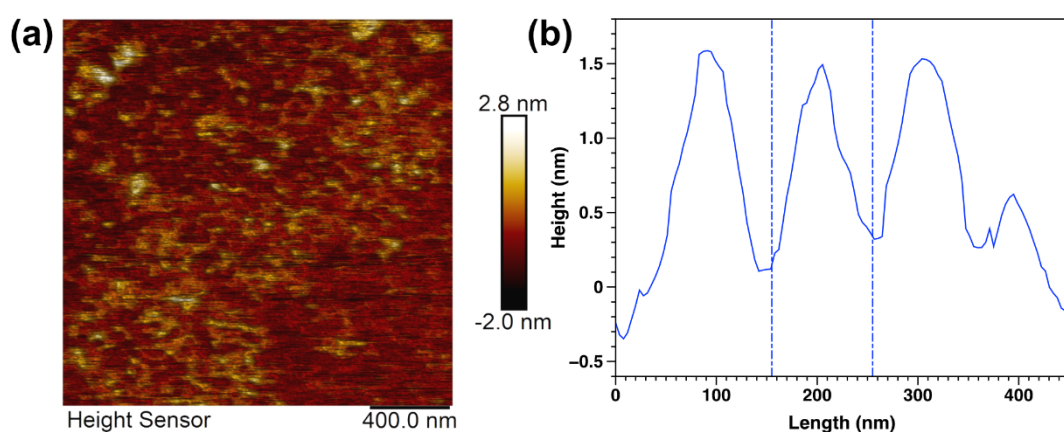


Figure A42 In-situ AFM image and its cross-section of isolated Psomes-N₃ in the clustering Psomes-N₃ process purified by Protocol 3 at pH 6.5.

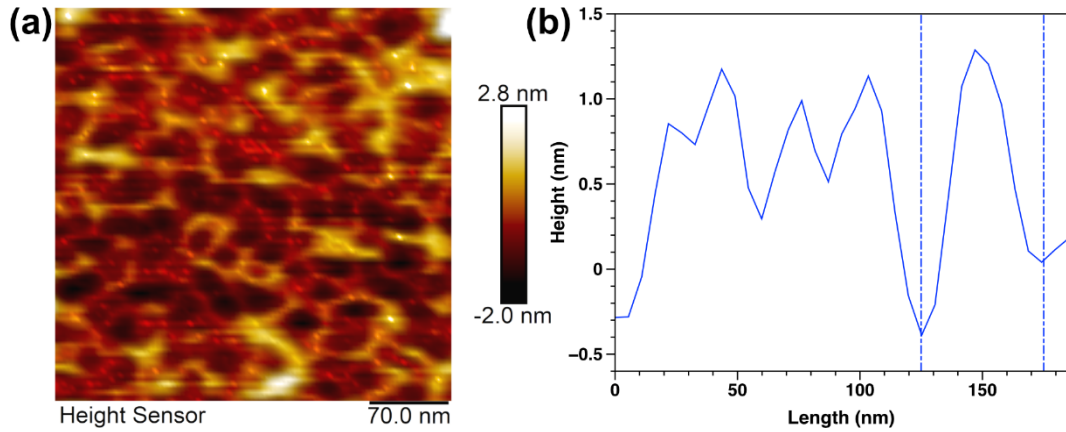


Figure A43 In-situ AFM image and its cross-section of isolated Psomes-N₃ in the co-clustering Myo/GOx-Psomes-N₃ process purified by Protocol 3 at pH 6.5.

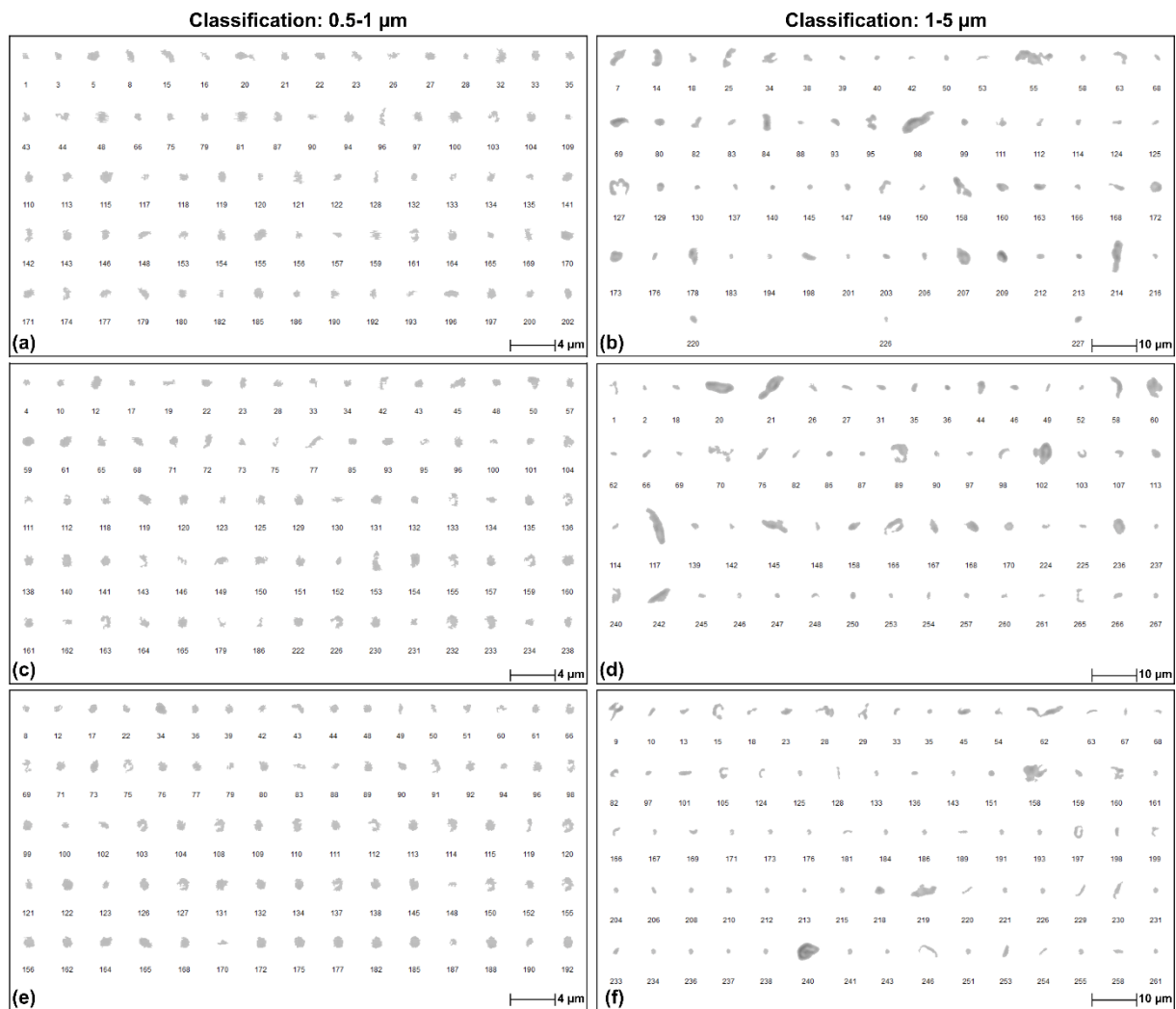


Figure A44 Microscopic images of clustered Psomes-N₃ before (a-b) and after one time centrifugation and redispersion by mechanical stirring (c-d) and vortex (e-f) at pH 8.0. Classification: 0.5-1 μm (left) and 1-5 μm (right).

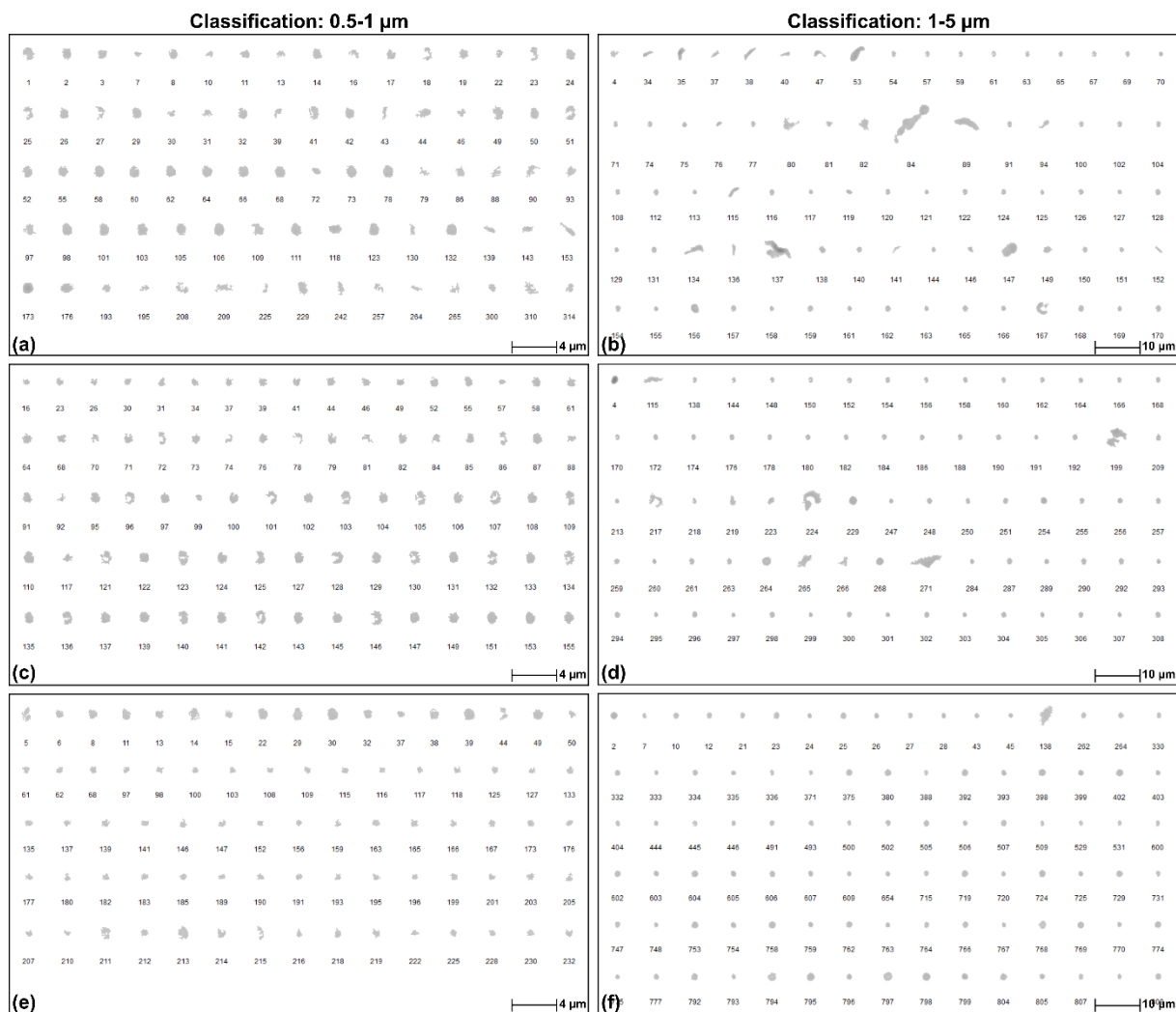


Figure A45 Microscopic images of clustered Psomes-N₃ after four times centrifugation and redispersion by mechanical stirring (a-b) and vortex (c-f) at pH 8.0 (c-d) as well as pH 6.5 (e-f). Classification: 0.5-1 μm (left) and 1-5 μm (right).

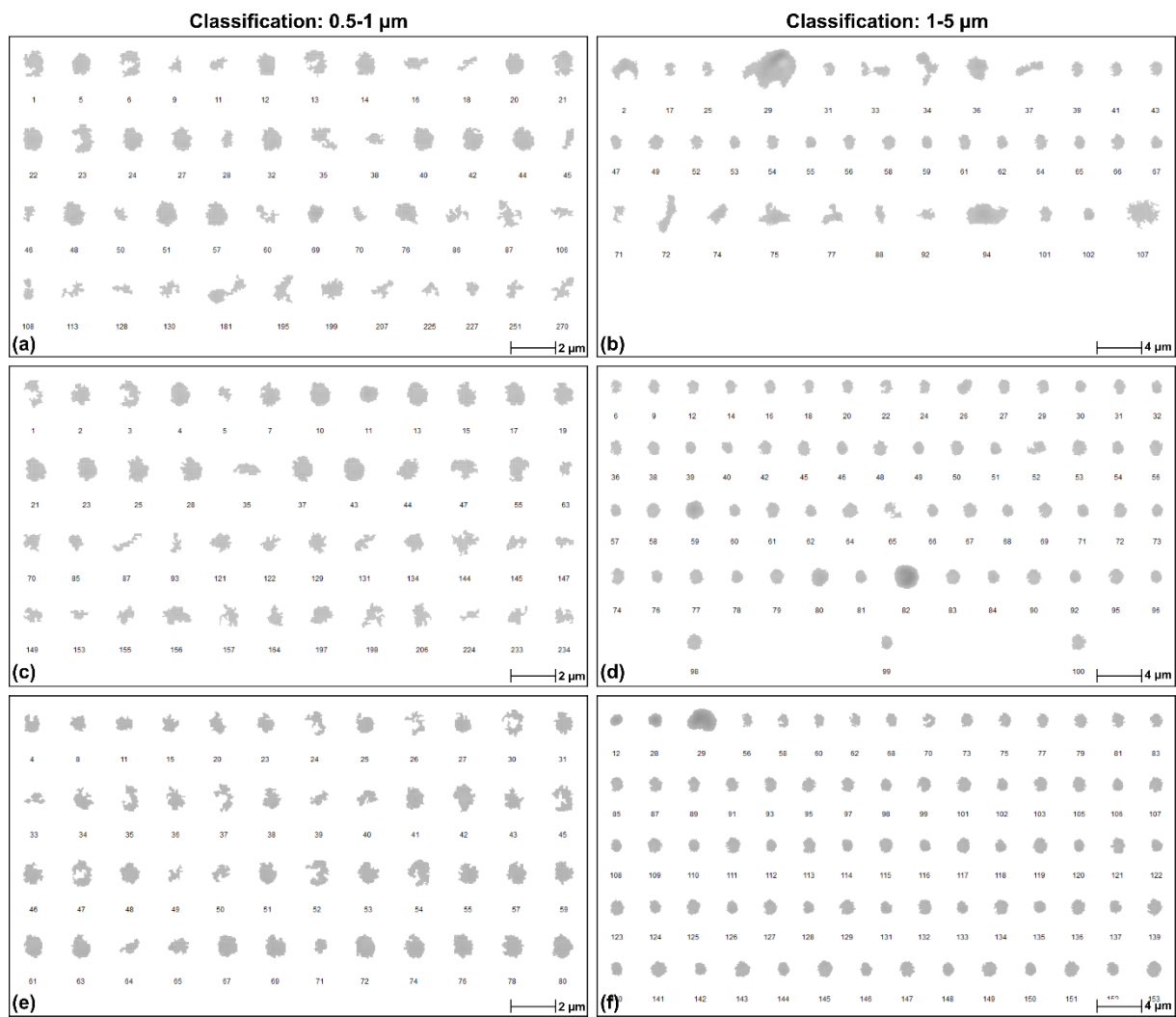


Figure A46 Microscopic images of co-clustered Myo/GOx-Psomes-N₃ at pH 8.0 (a-b), pH 7.0 (c-d) and pH 6.5 (e-f) purified by Protocol 3. Classification: 0.5-1 μm (left) and 1-5 μm (right).

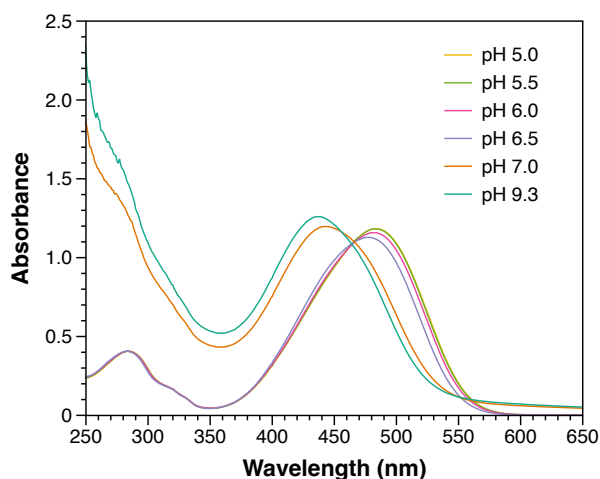


Figure A47 UV-Vis spectrum of BCP-DA-Azo (-) aqueous solution at different pH values. At pH 7.0 and pH 9.3, BCP-DA-Azo (-) were self-assembled to polymersomes.

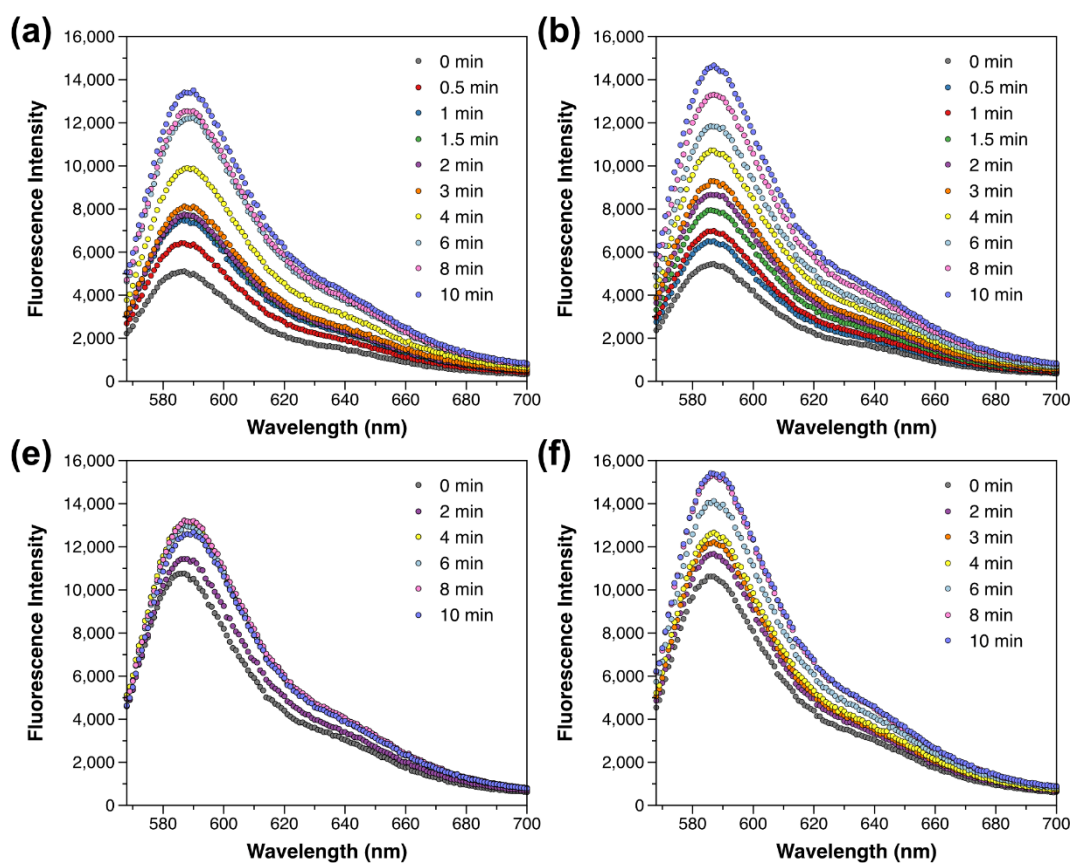


Figure A48 Fluorescence intensity of photo-crosslinked Myo-Psomes-DA-Azo (+) after blue light irradiation (400-500 nm) (a) and UV irradiation (365 nm) (b) for different times at pH 7.4. Fluorescence intensity of photo-crosslinked Myo-Psomes-Azo (+) under blue light irradiation (400-500 nm) (c) and UV irradiation (365 nm) (d) at pH 7.4 for different times.

Acknowledgements

At this point, it means that my PhD career has come to an end. Looking back on my life in Germany for more than four years, a myriad of thoughts and ideas fill my mind. Life is always ups and downs, everyone inevitably hits the rock bottom. Because of this, I would like to thank all the people who helped me during my doctoral studies.

First of all, I would like to express my sincere gratitude to my supervisor Prof. Dr. Brigitte Voit for giving me the opportunity to pursue my PhD at IPF. I do appreciate her guidance, encouragement and professional instructions throughout my research. I am also thankful for her willingness to provide funding and facilities toward the completion of my projects as well as the opportunities to attend local and international conferences.

Secondly, I would like to extend my heartfelt appreciation to my co-supervisor Dr. Dietmar Appelhans for his support, guidance and encouragement in every stage of this work. I am also very grateful to him for constructive discussions with me whenever I need them. Exactly, I have learnt a lot from those insightful comments and ideas that motivated me to think and ask more. Meanwhile, countless meetings have shaped me into a better researcher and a better communicator in science.

Besides, I am deeply grateful for the scholarship from China Scholarship Council (No. 201706630012) which realizes my dream to study in Germany. This experience has enriched my life, shaped a new outlook on life and changed my perspective on things.

Furthermore, I would like to thank Silvia Moreno Pinilla and Robin Thomas Zinke for their kindly help in my lab work. Since I stepped into the lovely laboratory L104, I can't remember how many times they helped me. As a novice in the field of organic synthesis four years ago, I can't forget the guidance and help I received from them. Moreover, the energetic music and relaxed chats also make me more motivated in my lab work.

I would like to thank all the technical staffs in IPF for their analytical investigations throughout my study, in particular Dr. Hartmut Komber (NMR); Petra Treppe, Christina Harnisch (both GPC); Dr. Susanne Boye (AF4); Dr. Andreas Janke (AFM); Christine Steinbach (Particle Size Measurement). My further special thanks go to Dr. Petr Formanek for introducing me the use of cryo-TEM which is most important tool to visualize my polymersomes and clusters. By his

warm support and guidance, I have the opportunity to meet with the fascinating world of microscopy and I am really appreciated for this. Besides, I would like to thank Franzisca Kucharczyk for the unremitting efforts in our project, she did a great job in lots of exploratory experiment and also boring but indispensable experiments.

Moreover, I am honored to make such a friend, Yunjiao Che, to discuss work, news and interesting things every lunch hour. His Chinese cooking has satisfied my stomach for countless weekends. I am also grateful to Kenan Zhang, Zheng Hua, Chen Jiao and Sai Li for our friendship. You filled me with joy and happiness during my PhD study. Besides, our travel time together was so good that I can't forget it. I also thank Kenan Zhang for teaching me the use of column chromatography, which is most important purification method to obtain pure small molecules in my research.

In addition, I would like to thank all my colleagues of the department “Bioactive and Responsive Polymers” for the help over the past years: Xueyi Wang, Christiane Effenberg, Jennifer Daeg, Franziska Obst, Bettina Keperscha, Bettina Pilch, Stefan Zschoche, Ulrich Oertel, Dishi Wang, Chen Jiao, Kehu Zhang, Nikolai Liubimtsev, Andrea Koball, Ping Wen, Jens Gaitzsch, Andreas Schurig, Julian Heinrich, Fabian Mehner, and also Christopher Schutzeichel from department “Polymer structures”. I really enjoy the outdoor activities organized by our group. Besides, many thanks are also delivered to my Chinese friends in Dresden.

At the same time, I would also like to thank Dr. Dietmar Appelhans and Dr. Silvia Moreno Pinilla for reading this dissertation and providing precious advice.

Special thanks should be given to my girlfriend, Xiaoying. Whether it is the meticulous care in life or the assistance in scientific research, it proves that my world cannot live without you. You are the best and most suitable other half in my life.

At last but above all, I would like to express my special thanks to my parents for their infinite love, support and encouragement throughout this work and my life. Thank you for raising me to be an optimistic and strong person. You will always be my favorite people.

Versicherung

Hiermit versichere ich, dass ich die vorliegende Arbeit ohne unzulässige Hilfe Dritter und ohne Benutzung anderer als der angegebenen Hilfsmittel angefertigt habe; die aus fremden Quellen direkt oder indirekt übernommenen Gedanken sind als solche kenntlich gemacht. Die Arbeit wurde bisher weder im Inland noch im Ausland in gleicher oder ähnlicher Form einer anderen Prüfungsbehörde vorgelegt.

Die Dissertation wurde vom Oktober 2017 bis Dezember 2021 am Leibniz-Institut für Polymerforschung Dresden e.V. im Rahmen des Projektes zum Thema “Optimization of pH-responsive Polymersomes for Enzyme Reactions” unter der wissenschaftlichen Betreuung von Dr. Dietmar Appelhans und Prof. Dr. Brigitte Voit (TU Dresden) angefertigt.

Frühere Promotionsverfahren haben nicht stattgefunden.

Ich erkenne die Promotionsordnung der Fakultät Chemie und Lebensmittelchemie der Technischen Universität Dresden vom 23.02.2011 in vollem Umfang an.

Datum:

Unterschrift: